Realization of Algae Potential (REAP)
Final Report

Acknowledgment: This material is based upon work supported by the Department of Energy's Office of Energy Efficiency and Renewable Energy under the Bioenergy Technologies Office, Award Number EE0006316.

Authors: Peter J. Lammers, Edward Frank, R.T. Sayre, Michael Huesemann, Wiebke Boeing, F. Omar Holguin, Eric Dunlop, Shulin Chen, Tanner Schaub

Disclaimer: This report was prepared as an account of work sponsored by an agency of the United States Government. Neither the United States Government nor any agency thereof, nor any of their employees, makes any warranty, express or implied, or assumes any legal liability or responsibility for the accuracy, completeness, or usefulness of any information, apparatus, product, or process disclosed, or represents that its use would not infringe privately owned rights. Reference herein to any specific commercial product, process, or service by trade name, trademark, manufacturer, or otherwise does not necessarily constitute or imply its endorsement, recommendation, or favoring by the United States Government or any agency thereof. The views and opinions of authors expressed herein do not necessarily state or reflect those of the United States Government or any agency thereof.

Table of Contents

1. Introduction 5
2. Summary of projected areal yield 6
2.1 Photoautotrophic productivity 6
2.1 Mixotrophic productivity 8
2.2 HTL yield 9
2.3 Areal biocrude yield 10
2.4 Cost and energy use 14
2.4.1 Cost 14
2.4.2 Energy use and emissions 15
2.4 References 16
3. REAP objectives and outcomes 16
4. Technical / Financial Table discussion ..... Error! Bookmark not defined.
5. Science and engineering summary ..... Error! Bookmark not defined.
5.1 Cultivation ..... **Error! Bookmark not defined.**
5.1.x References ..... **Error! Bookmark not defined.**
5.2 Cultivation ecology (Omar & Tanner) 17
5.2.1 Ecology 17

5.2.2 Invasive Algae 18
5.2.3 Allelopathy 18
5.2.4 Metabolite/Biochemical Analysis 21
5.2.5 Growth Media Analysis by FT-ICR Mass Spectrometry 23
5.2.6 References 24
5.3 Strain Development 26
5.3.1: Improving light harvesting efficiency and photosynthetic rates (Sangeeta Negi, Shawn Starkenberg, Srinivas Iyer, and Richard Sayre) 26
5.3.2: Transgene expression of Cellobiose transporter / β-glucosidase to enhance cellobiose metabolism (Amanda Barry, Sowmya Subramanian and Richard Sayre) 29
5.3.4: Control of pond pathogens using antimicrobial peptides (AMP) (Sathish Rajamani and Richard Sayre) 37
5.3.5: Development of biocontainment strategy for engineered algae 40
5.3.6: Thermotolerance (Angela Tonin and Richard Sayre) 44
5.4 Harvesting and dewatering (Shulin) 50
5.4.1 Flocculation performance in harvesting *Chlorella sorokiniana* UTEX 1602 51
5.4.2 High pH *Galdieria sulphuraria* induced flocculation 56
5.4.3 Scale up the High-pH flocculation process 62
5.4.4 Harvesting *Kirchneriella* sp. by low-pH and recycling the used HNO_3 66
5.4.5 References 68
5.5 Analytics (Tanner) 69
5.5.1 Proximate analysis of biomass 69
5.5.2 Elemental analysis of biomass 69
5.5.3 Compositional Analysis of *C. sorokiniana* Hydrothermal Liquefaction Bio-oils Produced at Variable Temperature 69
5.5.4 References 77
5.6 Sequential hydrothermal liquefaction (WSU) (Shulin) 79
5.6.1 Batch SEQHTL trials 82
5.6.2 Char characterization and utilization 104
5.6.3 Microalgae Growth Trials and Nutrient Recycling 105
5.6.3.1 Sugar utilization (mono sugars and polysaccharides) 107
5.6.3.2 Nitrogen utilization (NH_3 and Organic Nitrogen) 109
5.6.3.3 Phosphate recovery (PO_4^{3-}) 111
5.6.3.4 Nutrition recovery by growing yeast 113
5.6.4 Continuous Sequential Hydrothermal Liquefaction 113

5.6.5 References 119
5.7 Hydrothermal liquefaction (NMSU and ASU) (Shuguang) 124
5.7.1 HTL background 124
5.7.2 Overview of HTL work 124
5.7.3 Experimental methods 125
5.7.4 Results & Discussion 126
5.7.4a HTL of Galdieria sulphuraria, chlorella and coelastrella 126
5.7.4b HTL of C. merolae and the influence of catalysts on product fractions 129
5.7.4c Sequential HTL of Galdieria sulphuraria 132
5.7.4d Continuous HTL of chlorella 136
5.7.4e Co-liquefaction of two algal species: 137
5.7.4f HTL water process recycle to enhance biocrude oil yield 137
5.7.4g HTL of Galdieria, Chlorella and Kirchneriella grown at ASU: 138
5.7.5 ASU HTL Conclusions 139
5.7.6 ASU HTL Recommendations 140
5.7.7 ASU HTL Publications 140
5.7.8 ASU HTL Presentations 141
5.8 Life cycle analysis of energy use and GHG emissions (Ed) 143
5.8.1 Biomass and productivity 145
5.8.2 Cultivation and site model 146
5.8.3 CO_2 supply 147
5.8.4 Water supply to site 148
5.8.5 Water and algae recycle loops 151
5.8.6 Hydrothermal liquefaction 151
5.8.7 Catalytic hydrothermal gasification 153
5.8.8 Mass balance and nutrient recycling 156
5.8.9 pH management 157
5.8.10 Biochar utilization 157
5.8.12 Miscellaneous factors 157
5.8.11 LCA Results 158
5.8.12 LCA Conclusions 163
5.8.13 Other REAP LCA studies 164
5.8.14 References 166
5.9 Technoeconomic analysis 168

5.9.1 Executive Summary 168
Task Summary 168
Key results 169
Achievements 170
Future work 171
Milestone Report 171
5.9.2 Methods: An Overview 171
5.9.2.1 Software Programs used for all Tasks for Integrated System Modeling 171
5.9.2.2 Integrated Systems Modeling 172
5.9.2.3 Techno-economic Modeling Framework for REAP Process Model 173
5.9.2.4 Scenario used for TEA modeling 174
5.9.2.5 Sea water vs. fresh water 174
5.9.3 Milestone 1.3.1 – Integrated Systems Modeling 174
5.9.3.1 Unit Operations: An Overview 174
5.9.3.2 First order analysis of REAP process model using baseline data of Tech Fin Report 178
5.9.3.3 Optimized REAP process flowsheet from Aspen model 182
5.9.4 Milestone 1.3.2 – Model of Integrated Unit Operations 187
Models of individual unit operations 187
Model Assumptions: 187
5.9.4.1 Area 100: Cultivation 188
5.9.4.2 Area 400: Downstream biocrude conversion process 208
5.9.5 Milestone 1.3.3 – Techno-Economic Analysis (TEA) 217
TEA Modeling basic approach 217
5.9.5.1 Techno-Economic Analysis of Unit Operations 221
5.9.5.2 Techno-Economic Analysis of REAP Process 229
Case studies 239
Comparison of the DHTL and SEQHTL scenarios 250
5.9.7 References 252

1. Introduction

The goal of the REAP R&D program was to advance the DOE goal of demonstrating 5,000 gallons per acre per year by 2022 by developing an integrated process for producing at least 3,500 gallons of bio-fuel intermediate per acre per year. The project plan called for

- Genetic enhancement of yield traits in Chlorella sorokiniana, a microalgae identified as the top performer in a screen of over 2,000 strains conducted by the DOE-NAABB consortium
- Outdoor testing of enhanced strains in scalable, inexpensive plastic photobioreactors
- Strain-optimized flocculation-based harvesting strategies
- Wet biomass extraction using sequential hydrothermal liquefaction
- Recycling of up to 80% of the nitrogen and phosphorus in the biomass
- Use of biochar co-product from liquefaction to provide process heat energy
- Technoeconomic analysis (TEA) of projected fuel selling price and life-cycle analysis (LCA) of energy use and greenhouse gas (GHG) emissions.

The work plan called for developing a transformation system for *Chlorella* with which constructs would be developed that demonstrated a 40% increase productivity by attenuating the light harvest antennae and that provided 300% increase in lipid content. In addition, REAP would cultivate thermophilic acidophiles and would explore crop rotation strategies. The extremophile R&D hedged the risk surrounding metabolic engineering and also explored mixotrophic strains that could provide productivity boosts on organic substrates. Cultivation was to be carried out in horizontal photobioreactors developed by Algenol, one of the REAP corporate partners. The horizontal Algeonol PBRs were made from inexpensive plastic film and had low mixing energy requirements.

Thus, REAP was to test several hypotheses

- Reducing light attenuation by attenuating the photosynthetic apparatus would lead to a net increase in productivity
- Thermophillic algae can endure extreme PBR temperatures thus permitting cultivation in the arid southwestern US without cooling water consumption
- Mixotrophic growth can provide large productivity enhancements

This report will present the core REAP results in detail. A brief overview is as follows. Progress was made toward a transformation system for *Chlorella sorokiniana* 1412, but much more time and effort were required than anticipated. As a result, antenna mutants and strains with enhanced lipid accumulation were not available for outdoor testing. Thus, the hypothesis that reducing light attenuation can enhance the net productivity remains untested. Further, *Chlorella sorokiniana* was found to be more susceptible to predation and infection when grown at NMSU. Later experiments at ASU have been more successful, but culture stability for *C. sorokiniana* remains a concern. A *C. sorokiniana* (UTEX 1230) proline-overproducing strain (P5CS) was constructed that provided higher thermo-tolerance and salinity tolerance in laboratory tests. (*add field test result summary here in final version*).

The horizontal Algenol PBRs were found to be problematic. Mechanical issues were encountered (leaks, robustness of the mixing system) and, further, cultures did not thrive. Cultivation experiments switched to vertical acrylic PBRs at ASU which are comparable in height to the current Algenol production (vertical) PBRs. This switch provided robust cultivation of biomass for downstream experiments. Ultimately, it was found that aeration rates and associated mixing energy were too high to achieve target GHG emissions. Nevertheless, the core idea of growing thermophillic extremophiles without additional cooling was validated and a suite of strains was demonstrated that could be grown year round in a crop-rotation strategy.

Many additional results and experimental details will be discussed in the sequel, but we turn now to a presentation of the areal biofuel precursor yield data for REAP. The results were obtained in three PBR designs at ASU and involve five strains, namely *Chlorella sorokiniana* DOE 1412; *Chlorella sorokiniana* UTEX 1230; *Galdieria sulphuraria* 5587.1; *Kirschneriella cornutum; Cyanidioschyzon merolae*.

2. Summary of projected areal yield

2.1 Photoautotrophic productivity

Photoauthotrophic growth data from the 48' vertical acrylic 4" light path PBRs, 4' vertical acrylic 1.5" light path PBRs, and from the “hanging bag” PBRs were selected from the September 27, 2016 version of the Growth Summary file. Early data from the paddlewheel driven enclosed raceways and Algenol PBRs were excluded. The productivities were computed neglecting lag.

The 4’ vertical acrylic PBRs comprise an array of six PBRs which can be configured with respect to PBR spacing. The end PBRs receive different light exposure over the course of the day than do the central elements. Therefore, the end PBR data were dropped. There were some cases in which the array had been split to run two different growth experiments, one of which was not relevant to the current analysis, e.g., one treatment was not photoautotrophic growth. In all such cases, data from the end PBR that received direct sunlight were dropped, but data from all other PBRs were retained because the PBRs containing the second treatment provided shielding. In this way, the 4’ vertical PBR data approximately correspond to those from a scaled up array.

The 48’ PBRs were spaced so far apart that no shading occurred, but most of the 4’ PBR data were taken with 0.5m spacing. Algenol has determined that 0.38m spacing is optimal for their array of hanging bag PBRs. Their PBRs are approximately the same height as the ASU and have an average light path of 1.8 cm (4 cm max, pseudo-tubular). REAP scale-up analysis will assume a field with 0.38m spacing.

Figure 1 displays the REAP no-lag productivity and contains one point for each productivity period. When experiments were run in replicate (typically the case), each replicate is shown as a separate data point. The points with errors bars will be explained later in the discussion. In Figure 1, the abscissa (“Average Month”) is the month-average of the start and end dates for each productivity period. All data are thus binned by month, i.e., growth in separate years is folded together. The ordinate (productivity) is the productivity computed from the OD 750 vs.

ash free dry weight (afdw) correlation. The productivity is directly from the data and has not been corrected for PBR spacing. Different marker types and colors indicate the various strains.

The strain with highest performance was selected in each month. The selection was somewhat subjective, e.g., the selection avoided having too many strain changes for a realizable crop rotation at scale. KC has shown the highest performance in cold months and was selected for January. KC has high cold-temperature performance, but limited productivity above 32 ^{o}C (M. Huesemann, personal communication) which occurs in PBRs in mid-November and early February. *Few data were available in the fall, with none in November. New data will be acquired through calendar year 2016, but will not be available for modeling purposes.* PBR temperatures were compared between the vertical acrylic PBRs and the hanging bag PBRs. The vertical PBRs were found to be several degrees warmer than the hanging bags (Pete, please make this more specific) and, since the hanging bags are more representative of a scaled up reactor, we believe that KC growth will be possible in November and will outperform CS 1412 in December. To limit the number of strain changes, we therefore assume KC will be grown from November through January.

Spring growth was best for CS 1412, which was therefore selected for February through April. GS shows comparable performance in April, but CS was selected in order to reduce the number of strain rotations. It is actually encouraging to have two strains growing with comparable performance during a changeover, since it promises a smoother changeover. CS 1230 was selected for May, but we envision only one strain of CS being pursued. GS was selected for the hotter months of May through October. Few data were available in the fall months. We hope to have additional data before the close of the experiment for this period.

The mean and standard deviation (N-1) were computed for the selected strains (excluding all other strains). The results are plotted month by month in Figure 1 offset by 0.25 along the abscissa for clarity. The data point is plotted at the mean and the whiskers show one standard deviation. For example, KC was selected for November through January. The mean and standard deviation of the KC data are plotted at 11.25, 12.25, and 1.25 along the X-axis for November, December, and January. When necessary, data were averaged the rotation period, but in May through September there were enough data to compute results month by month and to compute the standard deviation. The September and October standard deviations were arbitrarily set equal to that from August.

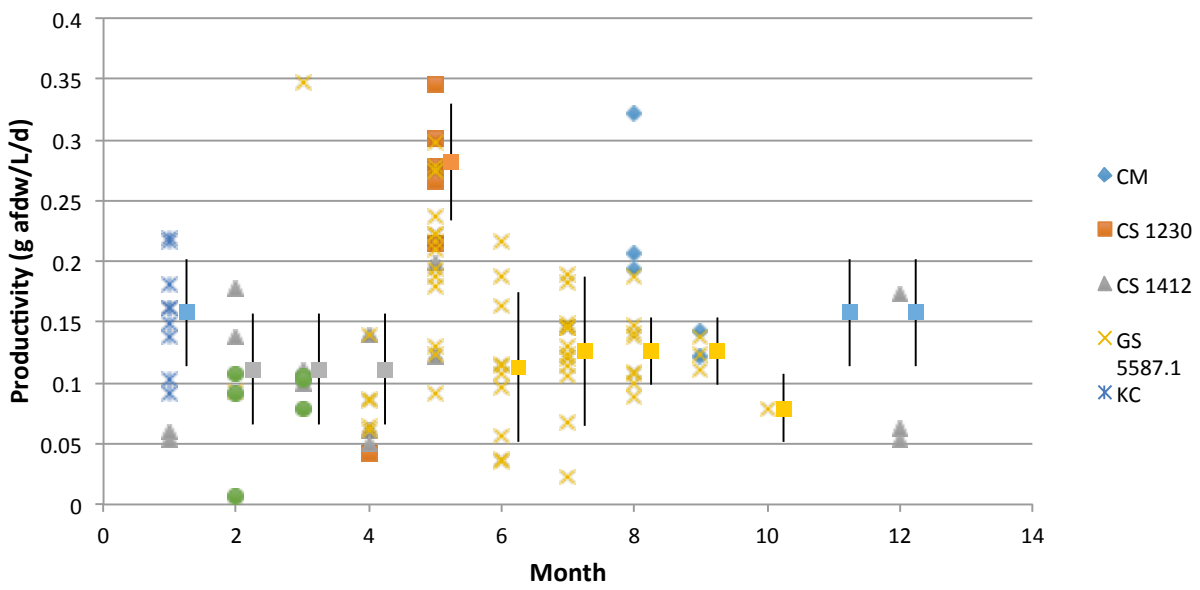

Figure 1: REAP photautotrophic growth data in vertical ASU PBRs. The abscissa ("Average Month") reports the average of the start and end date of each run. CM- *C. merolae;* GS- *G. sulphuraria;* KC- *Kirschneriella cornutum;* CS- *C. sorokiniana*.

Table 1: Selected strains by month and assigned productivities.

Month	Selected	Basis	g afdw/L/d	Std. Dev.
January	KC	Avg Jan	0.16	0.044
February	CS	Avg Feb-Apr	0.11	0.045
March	CS	Avg Feb-Apr	0.11	0.045
April	CS	Avg Feb-Apr	0.11	0.045
May	CS	May	0.28	0.048
June	GS	Avg Jun	0.11	0.061
July	GS	Avg Jul	0.13	0.061
August	GS	Avg Aug-Sep	0.13	0.028
September	GS	Avg Aug-Sep	0.13	0.028
October	GS	Oct	0.08	0.028
November	KC	Avg Jan	0.16	0.044
December	KC	Avg Jan	0.16	0.044

2.1 Mixotrophic productivity

The red mircoalga *Galdieria sulphuraria* 5587.1 grows at temperatures between 25 and 56 ^{o}C and pH values between 0.5 and 5.0. It is also the most versatile alga known with respect to growth on organic carbon sources. The extreme growth conditions afforded the opportunity to

determine productivities on organic carbon sources. Fifty liter outdoor cultures were provided 25 mM sucrose as a test of the concept which yielded a volumetric productivity of 1.0 g/L/day at 0.5 m PBR spacing. The same reactor set up yielded 0.49 g/L/day productivity in fed-batch mode using 6 mM glycerol added once each day as a carbon source. The sucrose experiment was run in July yielding an areal productivity of 82 g/m^2/day while the glycerol experiment was run in August yielding an areal productivity of 40 g/m^2/day. These results led to a new BETO-funded project to evaluate *G. sulphuraria* mixotrophic productivity using cellulosic sugars as a substrate.

2.2 HTL yield

Over the course of the REAP experiment, sequential hydrothermal liquefaction (SEQHTL) and direct hydrothermal liquefaction (DHTL) experiments have been performed under a number of conditions. Although further work is possible, a provisional set of processing conditions has been determined, namely first-stage processing at 180 °C and second stage processing at 300 °C for SEQHTL and single-stage processing at 300 °C for DHTL. These conditions are for batch processing. Continuous SEQHTL and DHTL reactors were constructed, but are still being commissioned. While we hope to have continuous data by the close of REAP, we proceed here with the batch data. Biomass is fed at 20 dry wt%.

Biomass samples with adequate mass were selected and were aliquoted for SEQHTL and DHTL processing. Results in Table 2 are, therefore, performed on biomass that is identical other than for any effects related to shipping and storage. Two different samples of GS were studied. The yield ratio of DHTL/SEQHTL for biocrude production was 1.6, 1.3, 0.83, and 1.8 for KC, GS, GS, and CS respectively. The average N and O content of the DHTL biocrude was 6.4 wt% and 9.1 wt% while in the SEQHTL data, the average N and O content was 5.9 and 8.2 wt%. The heteroatom content of the DHTL and SEQHTL oils are similar, as were the average molar H/C ratio, which was 1.3 for both methods.

Although SEQHTL biocrude may be slightly lower in N, the carbon yield to biocrude is higher for DHTL (50% vs. 38%) and the biocrude yield is higher by 38% on average. Given the ABY focus on areal fuel yield and the fact that DHTL is a simpler process, the analysis carries forward based upon the DHTL data.

Table 2: Summary of DHTL and SEQHTL experiments performed with 20 dw%.

Strain UID #	KIRCHNERIELLA KC_P_RW(20)_1-22_2-10-2016	GALDIERIA GS_P_MM1-5 (3.81)_7-1_7-5-2016	GALDIERIA	CHLORELLA CS1412_P_VL12(5.08)_1-1_2-16-2016
Harvest Date	2/10/16	7/6/16	10/15/15	3/23/16
Ash	6.2%	2.4%	3.1%	4.2%
FAME	13%	8.9%	5.9%	8.2%
Carbohydrates	26%	18%	8.9%	44%
Proteins	28%	43%	50%	26%
	DHTL			
Algae feed, g dw	1	1	1	1
Biocrude yield, g/g dw	41%	31%	30%	25%
Biochar yield, g/g dw	14%	4.8%	2.5%	18%
Water solubles	15%	8.2%	5.0%	10%
Gas (by difference)	30%	56%	62%	47%
C yield (oil)	61%	50%	43%	38%
H/C (molar)	1.4	1.4	1.5	0.97
N in oil, wt%	5.2%	7.8%	7.2%	6.3%
O in oil, wt%	7.8%	7.8%	7.8%	11%
	SEQHTL			
Algae feed, g dw	20	20	20	20
Biocrude oil	26.3%	23.5%	36.5%	14.5%
Biochar	11.9%	3.7%	0.54%	22.9%
Water solubles	15.6%	35.8%	41.3%	15.3%
Gas (by difference)	46.2%	36.9%	21.6%	47.3%
C yield (oil)	34%	38%	52%	23%
H/C (molar)	1.6	1.4	1.3	1.3
N in oil, wt%	4.1 wt%	6.8 wt%	7.1 wt%	5.8 wt%
O in oil, wt%	9.1 wt%	6.2 wt%	10 wt%	7.3 wt%

2.3 Areal biocrude yield

Table 3 displays the biocrude yield per month and in total for the DHTL yields under the following set of assumptions:

- Net PBR footprint of 115 L/m^2 (Current Algenol production vertical PBR)
  - PBR spacing of 0.38 m
  - 50L PBR footprint of 1.15 m^2
- 100% harvest efficiency (algae not captured are returned to the culture)
- Oil density of 0.9 kg/L

Under these assumptions the total areal yield is 2300 gal/ac/yr under for the DHTL yields. This value falls to 1800 gal/ac/yr for the SEQHTL yields. If the DHTL yields are sampled from Gaussian distributions with standard deviations as shown in Table 1, the standard deviation of the resulting distribution of annual biocrude yields is 216 gal/ac/yr. We therefore report a result of 2300 +/- 200 gal/ac/yr but note several issues. First, several of the means in Table 1 are fewer than two or three standard deviations away from zero. Therefore, the distributions cannot truly be Gaussian and the Monte Carlo computation of the uncertainty (500 samples) must include at least some cases with negative productivities. Second, the standard deviation of the data may not be an appropriate estimate of the variation in productivity since it includes both inherent variation in productivity, e.g. weather-driven, and also technological variation arising from changes in how the algae were grown run to run. One would expect that further cultivation experience would move the means upwards, even without strain improvement, and would reduce the variation; however, to be conservative, we are reporting the full variation in the data.

The results above are for an ensemble of data comprising 70% at 0.5m PBR spacing and 30% at 1m or 2.4m spacing. We did not make any corrections for spacing effects when computing results for 0.38m spacing. Slegers et al. (2011) [1] examined the effects of spacing on productivity of *Phaeodactylum tricornutum* in 1m tall vertical PBRs with 2 inch light paths using a computational model. They include results at Algiers which has a latitude comparable to Phoenix (37° N vs. 33° N). They concluded that shading effects would *increase* productivity by 8% when spacing was decreased from 0.5m to 0.4m and would increase productivity by 56% when reducing spacing from 1m down to 0.4m. Weighting by our spacing, this gives a 22% increase in productivity. The increase in productivity is understood to be the result of shading helping to control the PBR temperature. *P. tricornutum* has an optimal temperature of 23 °C. The REAP strains have higher temperature tolerances, so the Slegers result cannot be carried directly into our results, but if decreasing the spacing from 0.5m, 1.0m, and 2.4m (actual REAP data) to 0.38m improved the productivity by 9%, the REAP photoautotrophic data would achieve the ABY target of 2500 gal/ac/yr. In any case, we have applied neither a penalty nor a benefit for the design spacing of 0.38m vs. the actual growth trials spacing.

G. sulphuraria 5587.1 was grown at New Mexico State University in Solix flat-panel PBRs in the same media that was used in the vertical PBRs and was processed at PNNL in their continuous HTL reactor at 342 °C . The ash content in the PNNL sample was 7.8%, while comparable ASU *Galdieria* biomass has a 2.8% ash content. Otherwise the *Galdieria* biomass samples from NMSU and ASU are comparable. A total of 3.7 kg afdw of biomass was fed in an 8 hour run at 2 L/hr feed containing 23.4 afdw% solids. The PNNL continuous HTL reactor showed a yield of 0.33 g oil / g dw algae with N, O, and H/C (molar) levels of 7.3%, 3.7%, and 1.42 in the biocrude. Thus, the PNNL HTL oil was similar to the HTL oil produced at ASU, but with lower oxygen. The continuous reactor performance of 0.33 g/g is comparable to the small batch runs done at ASU, reported in Table 2. If the slightly higher level of HTL performance seen in the continuous reactor is used in the computations, then the total oil yield would be 2400 +/- 200 gal/ac/yr.

As noted above, *G. sulphuraria* 5587.1 is a versatile mixotrophic organism, able to utilize a wide variety of organic carbon sources. Sucrose was used as a proxy for waste carbon at 25 mM in a series of experiments conducted in July 2015. The average productivity was 1.03 g/L/day (S.D.

0.3) during the period sucrose was available (see Table 4). No contamination was observed during these trials. Analysis of continuously recorded temperatures during this period suggest a 4 month window for mixotrophic growth at the expense of waste sugars from approximately mid-May through mid-September in Phoenix AZ. When these values are used to compute annual HTL oil yields the result is a projected 6,740 gallons/acre/year.

Table 3: REAP biofuel-intermediate yield for photoautotrophic growth

Month	Selected	g/L/d	Sigma	Days	kg/ha	HTL Oil yield	gal oil /ha
Month	KC	0.158	0.044	31	5649	0.41	681
January	CS	0.111	0.045	28	3580	0.25	263
February	CS	0.111	0.045	31	3963	0.25	291
March	CS	0.111	0.045	30	3835	0.25	282
April	CS	0.281	0.048	31	10053	0.31	916
May	GS	0.113	0.061	30	3910	0.31	356
June	GS	0.126	0.061	31	4510	0.31	411
July	GS	0.126	0.028	31	4521	0.31	412
August	GS	0.126	0.028	30	4375	0.31	399
September	GS	0.079	0.028	31	2824	0.31	257
October	KC	0.158	0.044	30	5466	0.41	659
November	KC	0.158	0.044	31	5649	0.41	681
Total						gal / ha/ yr	5608
						gal / ac / yr	2270

Table 4: REAP biofuel-intermediate yield for mixotrophic growth

Month	Selected	g/L/d	Sigma	Days	kg/ha	HTL Oil yield	gal oil /ha
	KC	0.16	0.044	31	5649	0.41	681
January	CS	0.11	0.045	28	3580	0.25	263
February	CS	0.11	0.045	31	3963	0.25	291
March	CS	0.11	0.045	30	3835	0.25	282
April	CS	1.03	0.300	31	36824	0.31	3355
May	GS	1.03	0.300	30	35636	0.31	3247
June	GS	1.03	0.300	31	36824	0.31	3355
July	GS	1.03	0.028	31	36824	0.31	3355
August	GS	0.08	0.028	30	2733	0.31	249
September	GS	0.08	0.028	31	2824	0.31	257
October	KC	0.16	0.044	30	5466	0.41	659
November	KC	0.16	0.044	31	5649	0.41	681
Total						gal / ha/ yr	16677
						gal / ac / yr	6752

2.4 Cost and energy use

2.4.1 Cost

The scaled-up system used for the TEA was based upon an Algenol model of their vertical PBR system with DHTL as the downstream conversion process. It conformed to NREL standard methods and other industry standards. Table 5 shows the results of the bio-crude productivities and the minimum selling price for the three autotrophic strains in rotation in an 11-month year with October a non-growing month.

Table 5: Bio-crude productivities for REAP process strain rotation

Algal strain	*Kirschneriella*	*Chlorella*	*Galdieria*
Operating period	November to January	February to April	May to September
Wet land required for a 10-MGY biocrude facility (acre)	3,615	6,388	4,374
Bio-crude productivity (Gal/acre/yr)	2,767	1,565	2,286
Minimum Bio-crude selling price ($/gallon)	12.91	19.11	15.06

The model with strain rotation forces the use of the worst case to determine the land area required. This has a major impact on the capital cost. Two scenarios were therefore modeled for the TEA to overcome the problem. Scenario 1 was modeled using the wet land area required by the *Chlorella* case and has two DHTL facilities. Only one DHTL facility operates from February to April for the conversion of *Chlorella,* with both DHTL facilities then operating in the other months to accommodate the higher *Kirschneriella* and *Galdieria* productivity and therefore maximize the conversion of biomass to biocrude.
Scenario 2 introduced drying units to minimize land required and is in line with commercial practice elsewhere. Part of the algal biomass produced in the high seasons is dried and stored for the low season. Technical and economic results of Scenario 1 and 2 are summarized in Table 6.

Table 6: Technical and economic results of Scenario 1 and 2

	Scenario 1	Scenario 2
	2 DHTL facility	Algae drying
Biocrude output (MGY)	14.2	10.0
Area required (acre)	6,388	4,530
Biocrude productivity (Gal/acre/yr)	2,224	2,208
Energy output (MJ/acre/yr)	250	248
Total capital investment ($MM)	797.85	534.12
Operating cost ($MM /yr)	84.4	59.2
Minimum Bio-crude selling price ($/gal)	15.87	15.46

For both scenarios, the major contributor to the capital cost is the VPBR. For Scenario 1 this cost is $358.6 MM (45% total capital cost), and for Scenario 2 it is $254 MM (48% total capital cost). The major

contributor to both operating costs is fluegas which, at $10.2 MM/year for Scenario 1 and $14.3 MM/year for Scenario 2, represents 17% of the annual operating cost.
Opportunities exist to improve the results. More commercial/pilot facility data to inform the layout and piping costs would contribute to a more accurate VPBR cost estimation. Flocculation of algal slurries could be further developed once sedimentation cost estimation and energy demand are known. Pinch Analysis could also further optimize the DHTL process (optimization of the SEQHTL process using this technology produced significant results).

2.4.2 Energy use and emissions

LCA results were computed for the autotrophic growth productivities on an annual average basis for a scaled-up scenario. The scaled-up system used for the LCA was based upon an Algenol model of their vertical PBR system deployed on 2000 acres, but in a biomass-only configuration (no ethanol). This model provided the upstream energy demand for inoculum production, cultivation, and pumping of culture to central processing for dewatering and conversion. A model of the remaining operations was added to this. Details are presented in Section 5.8 and a summary of results is given here.

For the ASU operating conditions, energy use and GHG emissions on a life-cycle basis were too high for the algal biofuel to qualify as an advanced biofuel under RFS2. When the aeration rate was reduced from 0.3 vvm (ASU nominal) to 0.034 vvm (Algenol nominal) GHG emissions fell from 560 gCO_2e/MJ (6x conventional diesel) to 110 gCO_2e/MJ (1.2x conventional diesel) and fossil energy use fell from 6.7 MJ/MJ (6x petroleum diesel) down to 1.5 MJ/MJ (1.2x petroleum diesel). Excessive energy use, which drives the GHG emissions, occurred because of the high mixing energy demand for the PBRs and because of the use of NaOH for pH shifts during harvesting.

A 50% reduction in GHG emissions was only possible when the cultivation energy was reduced 20 to 60-fold and when substantial amounts of organic carbon were available in the HTL aqueous product for electricity generation. An alternative scenario was examined in which the NaOH-dependent flocculation harvesting was replaced with the Global Algae Innovations membrane filtration unit and centrifugation and in which the aeration was reduced to 0.005 vvm. This scenario achieved 41 gCO_2e/MJ and 0.68 MJ/MJ fossil energy use. The 50% GHG reduction target was satisfied even if the biochar rate fell from the assumed 0.05 g/g dw to 0.025 g/ g dw, but it was not satisfied if the membrane filtration energy demand was increased from the GAI claimed value of 0.04 kWh/L to the more typical value of 0.5 kWh/L.

Aeration at 0.005 vvm is likely too low to be realizable, but at that level the energy use for cultivation is approximately equal to the cultivation in open pond scenarios. It is also approximately equal to the energy demand for the horizontal Algenol PBRs. Thus, the scenario helps to set an energy budget for future PBR development at ASU using different methods.

High-productivity but low or moderate oil yield, which was the case in REAP, means that the energy used to grow and process the non-fuel fraction of the biomass is wasted. Future experiments should examine ways to increase the algae lipid yield guided by life-cycle analysis of tradeoffs between productivity and lipid content. One can consider supplementing the process with renewable power, but this approach must be assessed by economic analysis: Even if renewable power can be supplied at a price that matches fossil power, a high power budget will be associated with increased fuel costs. Renewable power may be free from an LCA perspective, but it is not free from a TEA perspective.

The uncertainties in this analysis are large. REAP data for mass balances are poor; thus, values assumed for the total organic carbon in the aqueous phase and for the biochar yield are uncertain yet these parameters were critical to the analysis. Even if these data were in hand, CHG is unproven, especially with regard to catalyst lifetime and robustness against poisoning, e.g., with sulfur. The HTL/CHG energy demand is from computations rather than from data. One particular concern in this regard is establishing the heat exchanger performance in the face of high-solids feeds and fouling. A thorough analysis of the realizable effectiveness vs. cost tradeoff is required.

2.4 References

[1] P.M. Slegers, R.H. Wijffels, G. van Straten, A.J.B. van Boxtel, Design scenarios for flat panel photobioreactors, Applied Energy, 88 (2011) 3342-3353.

3. REAP objectives and outcomes

1. Genetic enhancement of *Chlorella sorokiniana* is possible. We will increase biomass productivity by 40% and oil content by 300% 1.020
2. Enclosed PBR cultivation systems for EPA-exempt outdoor testing of enhanced strains will be developed. We will achieve >3 gAFDW per liter autotrophic density and 6 gAFDW per liter mixotrophic density with >50% oil content by mass and will achieve productivity exceeding 25 $g/m^2/d$.
3. Innovative Harvesting and Dewatering Systems will be developed with 5% solids at harvest and 30% solids after dewatering.
4. Sequential hydrothermal extraction technologies to produce bio-fuel intermediate with C, N and P recycle to cultivation will be explored leading to the design of a continuous reactor with bio-char production for heating.
5. A project plan will be executed that iteratively optimizes unit operations for algal cultivation and processing by deploying a baseline at NMSU followed by a technology update based

upon technology R&D performed by REAP partners.

6. A process model of a conceptual integrated process will be developed. Technoeconomic and life-cycle energy analysis will be used to guide R&D.

Figure 5.2-1. Algae cultures are influenced by different trophic levels: top-down (predators), other algae competitors, and bottom-up (water quality, bacteria, viruses).

5.2 Cultivation ecology

Biomass producers typically attempt to cultivate microalgae as monocultures, using a highly productive algae species that may be genetically modified. However, at large scales, we are unable to grow microalgae under sterile conditions and cultures will inevitably be invaded by air-borne viruses, bacteria, fungi, algae competitors and grazers (ciliates and rotifers) (**Figure 5.2-1**). Besides water quality fluctuations due to weather events, any of these invaders have the ability to cause a sharp decline or "crash" of the algae crop population (Tamiya 1957, Borowitzka 2005). Algae crashes can be caused by top-down (predation), competitive, and bottom up (disease, water quality) processes (**Figure 5.2-1**). Approaches for the mitigation of algae loses during cultivation include the use of biocides substances (Mendes & Vermelho 2013), which increase the cost in large-scale production (Klein-Marcuschamer et al., 2013). In this proposal, we will focus on algae crashes that are caused by allelopathic interactions among algae competitors and will explore mitigation strategies, which include increasing resistance to allelopathic agents by the crop species as well as engineering invasion-resistant polycultures.

5.2.1 Ecology

Crop protection strategies to control microalgae contaminates are focused on environmental pressure, separation of contaminants, chemical compounds and allelopathy. The phenomenon of allelopathy is one in which an organism produces molecules that affect the growth, reproduction and survival of other organisms. Allelochemicals are largely associated with the secondary metabolism of algae, plants, fungi, bacteria, and coral (Mendes & Vermelho 2013). Microalgae are sources of a variety of metabolites including fatty acids, sterols, carotenoids, phycocolloids, lectins, polyketides, and mycosporine like amino acids (Cardozo et al. 2007). The variety of the compounds produced by microalgae is attributed to their ability to adapt and survive diverse environmental conditions (Adarme-Vega et al. 2012). Allelopathy has been documented as a defense employed by microalgae against pathogens, competitors and predators (Cembella 2003, Solé et al. 2005). Allelopathy can have both positive and negative affects and is an important factor in determining diversity, distribution, and abundance amongst plant and plankton communities. Inhibitory modes of action of microalgal allelochemicals range from enzyme

inhibition, RNA synthesis, DNA replication and protein synthesis, photosynthesis and Toxin-assisted micropredation (Mendes and Vermelho 2013).

To maintain a healthy monoculture, it is important to be able to prevent contamination and treat invasive organisms. These experiments help to better understand the behavior and effect of allelopathic organisms such as *Coelastrella* sp. by using isolated exudomes from invading species and gramine and known allopathic compound as an allelopathic model. These results provided an estimation of how microalgae respond to alleopathic interactions.

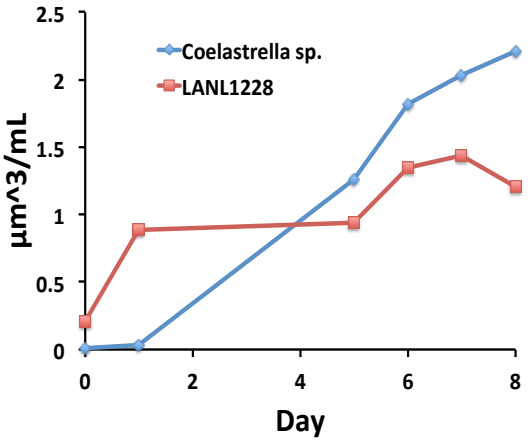

Figure 5.2-2. Halt in growth of *Chlorella sorokiniana* LANL1228 crop due to invasion and take-over by a superior competitor (*Coelastrella* sp.) in an algae production facility in Las Cruces, NM.

5.2.2 Invasive Algae

Several of the NMSU cultivation crash samples also contained an invasive algae species *Coelastrella sp*. We evaluated the mechanism by which *Coelastrella* suppresses the growth of *C. sorokiniana* via the development of high-throughput, microtiter plate-based competition assays. The figure above plots the biovolume versus time as measured by an imaging FlowCytometer and demonstrates the rapidity with *Coelastrella* can overgrow *C. sorokininana* 1412 **Figure 5.2-2**. Through a unique phenotype of the invading algae and isolation scheme, we were able to develop a procedure for the purification of the invading strain. The unique highly pigmented phenotype of the strain could be expressed through abiotic stress from decreased N and or high light exposure. Thus the microalagal species was isolated as seen in **Figure 5.2-3.**

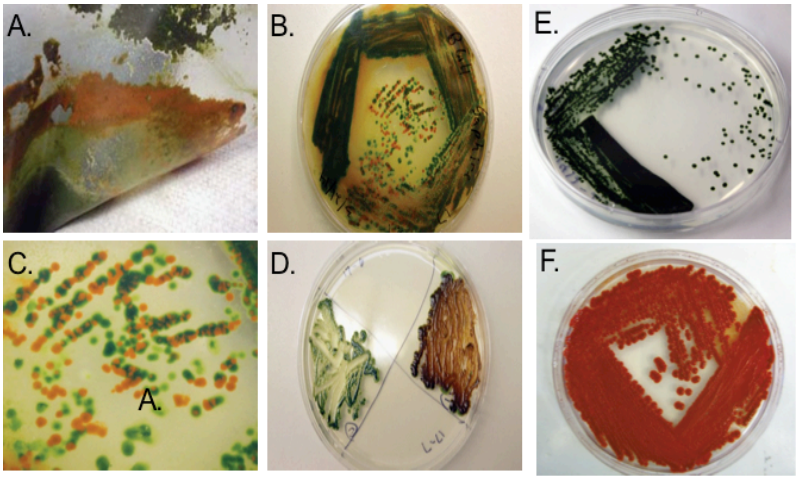

Figure 5.2-3. Images taken of cultures during the isolation/purification process: (A) Biofilm accumulation inside the enclosed outdoor PBR system; (B and C) Streak of the original sample collected from the outdoor PBR system; (D) First round of repeated streaking of isolated colonies; (E) Purified *Chlorella* culture; and (F) purified invader species (*Coelastrella*).

5.2.3 Allelopathy

Invasive algal species are a significant threat to successful cultivation of elite algal species for renewable energy production. As seen above in Figure 5.2-4 the take-over by an invasive competitor was identified as a *Coelastrella* sp. in our outdoor *Chlorella sorokiniana* production facility. *Coelastrella* was genetically identified and isolated (Genbank 18S RNA sequence accession number KP167584). After obtaining and

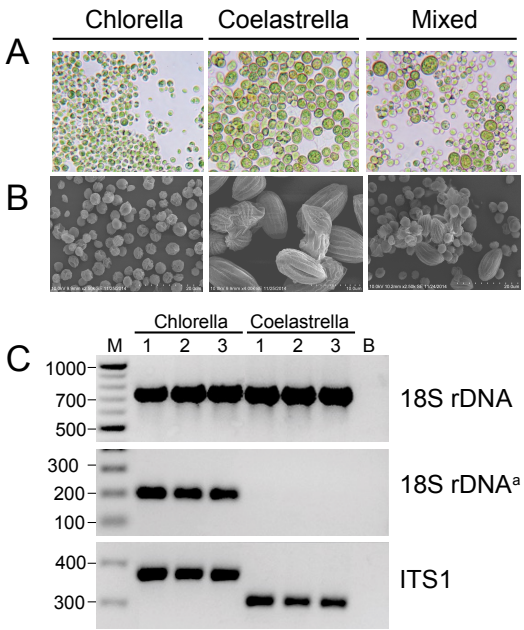

Figure 5.2-4. (A) Microscopic images of Chlorella, Coelastrella, and a mixed sample of pure cultures. (B) SEM microscopy images (C) Amplicons shown in ethidium bromide stained (1%) agarose gels

suggest is a response only present under direct competition with *Chlorella*. Furthermore, *Coelastrella* spec. and three strains of *Chlorella sorokiniana* (1228, 1230, and 1412) were co-cultured at three different temperatures (18, 25, and 32 °C). All three *Chlorella* strains were then grown in each of the 9 exudates (3 strains x 3 temperatures) at 25 °C. *Chlorella sorokiniana* 1412 responded most sensitively to the exudates and response was independent on which *Chlorella* strain was co-cultured with *Coelastrella* to derive the exudate. Exudates appeared to be stronger when algae were co-cultured at sub-optimal temperatures (18 or 32 °C). We found that *Coelastrella* will inhibit *Chlorella* when grown together, however, the allelopathic chemical is ineffective at higher temperatures (37 °C). Furthermore, we subjected *Chlorella* to culture media that previously contained *Coelastrella*, *Chlorella*, or verifying a purified culture of Coelastrella sp, we then conducted series of experiments in test tubes and 96-well plates in the laboratory.

In **Figure 5.2-5** we see the evaluation of cell-free extracts from each purified strain and a mixed culture of the two purified strains. No significant effect were seen in panels B or C, but the cell-free supernatant from the mixture inhibited *C. sorokiniana* 1412 at 50% and 100% of the concentration in the mixed culture as seen in panel D.

We were able to show that all three exodomes (*Coelastrella* spec. vs. *Chlorella sorokiniana* 1228, 1230, and 1412) are effective against each of the three *Chlorella* strains. *Coelastrella* continues to be a superior competitor with a negative allelopathic interaction against *Chlorella* strains, which we

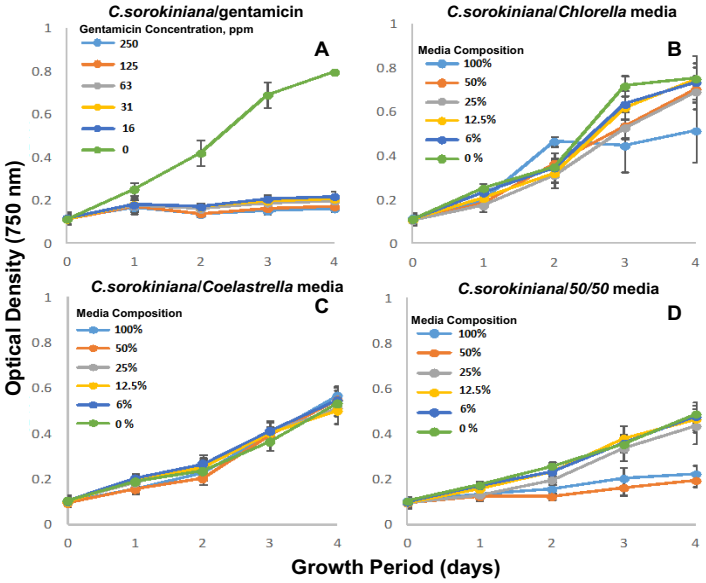

Figure 5.2-5. *Chlorella sorokiniana* 1228 and *Coelastrella sp.* growth profiles for cultures grown with the antibiotic gentamicin as well as with media obtained from prior cultures of pure *Chlorella* culture (B), pure *Coelastrella* culture (C) and a 50:50 *Chlorella*:*Coelastrella* culture (D). *C. sorokiniana* growth was also inhibited by gentamicin, as shown in panel **(A)**. Full-strength *Chlorella* media results in reduced growth after 2 culture days, indicating some self-inhibition at high *Chlorella* cell density **(B)**. Full-strength *Coelastrella* media did not impact *C. sorokiniana* growth **(C)**. However media from 50:50 *Chlorella*:*Coelastrella* culture reduced *C. sorokiniana* growth at both 50% dilution and full-strength, as shown in panel **(D)**. Thus allelopathic compounds appear to be produced by *Coelastrella* when in direct contact with *Chlorella*.

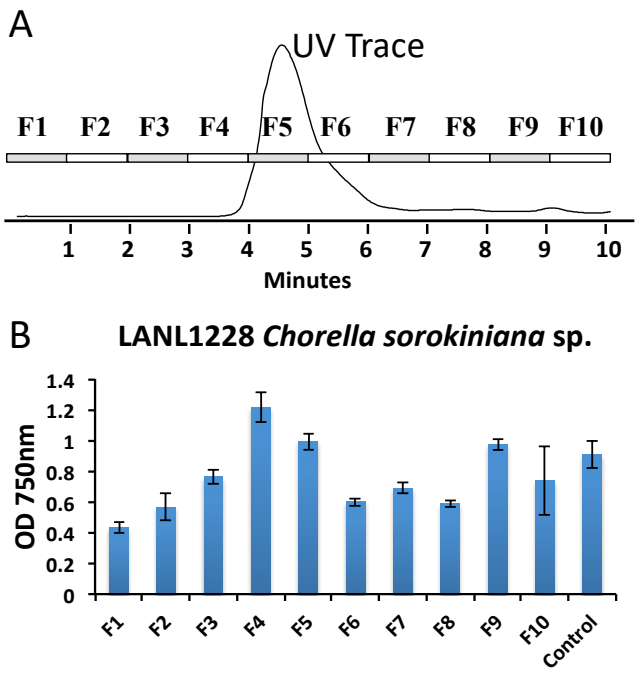

Figure 5.2-6. Purification and bioassay of exudates produced by a 50:50 *Chlorella*:*Coelastrella* culture. Semi-preparative separation and purification of exudome on C18 column with collection of 1 minute interval fractions (A). LANL1228 and *Coelastrella sp.* growth profiles for cultures grown with the individual purified fractions (B). Allelopathic compounds produced by the algal-algal interaction of *Coelastrella* and *Chlorella* are not easily distinguished by UV detection but can be followed by bioassay

both algae together. Media from *Coelastrella* cultures was did not inhibit *Chlorella*, but media from the *Coelastrella/Chlorella* co-culture did. We conclude that *Coelastrella* needs the direct contact with *Chlorella* to produce the allelopathic chemicals. We also found that *Chlorella* exhibits self-inhibition, which seems to be density dependent. The mixed strain exudate is being fractioned using the bioassay to partially purify and chemically identify the inhibitory (allelopathic) substance.

The identified bioactive extracts then underwent further processing and are separated into fractions using chromatography **Figure 5.2-6**. The fractions were reanalyzed and only those fractions that maintain the activity are further processed. We were successful in fractionating and purifying a select region from the exudome that inhibits the growth of a *Chorella sorokiniana* sp. **Figure 5.2-6**. This method narrowed down the candidates responsible for the bioactivity, and greatly enhances the likelihood of isolating biologically active compounds.

To further model allephathy in microalgal cultivation as model alleopathic compound was choose for further investigation. Gramine and indole alkaloid allelochemical that is commercial available was shown to greatly influence algal growth for both *Coelastrella* sp. and *C. sorokiniana*. However, when exposed to temperature and gramine stresses simultaneously, small volumes of algae cultures displayed varying behaviors as temperature increased. Higher temperatures resulted in a greater distinction of growth with each gramine treatment compared to lower temperatures. 18˚C growth, however, was much slower for both algae and distinctions between gramine treatments were much less, with exception to 0 mg L^{-1} and 64 mg L^{-1}. Lipid accumulation, however, was not significantly affected by the application of gramine at any concentration utilized. Overall, gramine is an effective algaecide, but unfortunately has strong effects on both algae strains (*Chorella* and *Coelastrella*) at higher concentrations. If gramine is utilized as an allelopathic control, care should be taken with dosage to ensure the biofuel algae is not completely killed. As the effects of gramine are similar to both algae, it is likely only small, low optical density invasions by *Coelastrella* sp. in the early stages of an outbreak can be treated without killing the *C.*

sorokiniana. Based on our timescale at 25˚C, gramine may have to be reapplied if a longer treatment time is required than several days.

5.2.4 Metabolite/Biochemical Analysis

Efforts are underway to chromatographically separate the exudates from the challenged cultures Figure 5.2-6. Methods were developed for the isolation and analysis by using C18 solid phase extraction cartridges to concentrate the exudates followed by LC/MS analysis. **Figure 5.2-7** represents the hydrophobic region of the chromatogram where an abundance of metabolites are found. Under negative ESI conditions only shared compounds are found among all three exudome. However using positive ionization some unique molecular features were observed similarly to that seen by the FT-ICR results. Further analysis and mass spectral analysis on structural components of the unique ions will need to be performed to aide in the identification of these novel allopathic compounds. After method development samples will be delivered to CAIL for HRMS analysis of chemical formula prediction of the differentially expressed compounds.

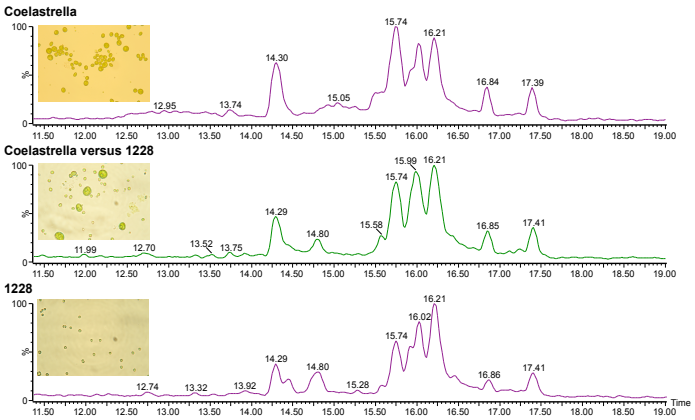

Figure 5.2-7. Negative ion chromatogram of exudates from microalgae cultures.

Chemical analysis methods were also developed to evaluate carbon portioning in *Galdieria sulphuraria* strain 5587.1 under a simulated heterotrophic boost. Cells were grown on Cyanidium media (pH 2.5) in 500 ml culture flasks in bioreactors Phenometrics photobioreactors (ePBR) under mixotrophic condition with 12/12 light/dark and CO_2 gas enrichment of 1% and 42C temperature. Cultures were inoculated with 25 mM glucose, 12.5 mM sucrose as carbon sources. For the lipids analysis, cells were harvested at three different growth conditions; log phase (Optical density at exponential (OD_{750}=0.5) and stationary phase (OD_{750}=1.6). The results are based on two replicates for each inoculation. We measured the OD using spectrophotometer to measure the growth of *Galdieria* in medium at 750 nm under mixotrophic condition supplemented with 25 mM glucose and 12.5 mM sucrose. Concentrations of the carbohydrate in the supernatant of the cultures was measured **Figure**

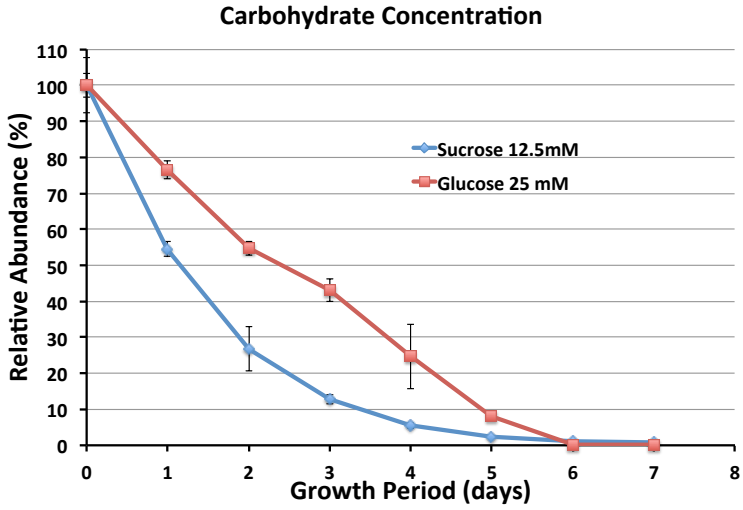

Figure 5.2-8. Concentration of supplemented carbon source in 5587.1 cultures grown under mixotrophic conditions.

5.2-8. In both cases by Day 6 greater than 95% of the carbon source was removed from the supernatant. For lipid body measurement in **Figure 5.2-9**, the Nile red staining was used to detect the lipophilic stain for intracellular TAG. The stock solution (1 mg/ml) was prepared in acetone. Upon addition of the nile red, tubes were incubated at room temperature in darkness for 30 minutes. Then after the centrifugation of the cells, microscopic images were acquired in a fluorescence microscope.

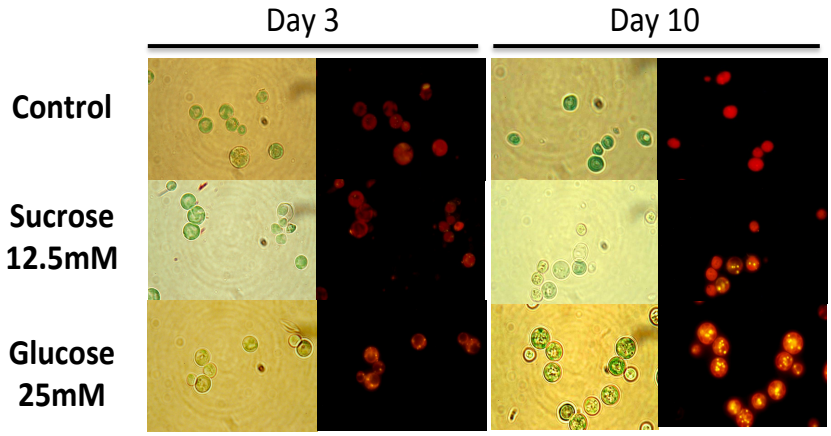

Figure 5.2-9. Nile red lipid staining in 5587.1 under mixotrophic growth with sucrose and glucose at equal C atom concentration

In summary we analyzed the biomass and lipid accumulations in the red alga *Galdieria sulphuraria* under mixotrophic conditions. Growth of *Galdieria* under such conditions supplemented with glucose and sucrose had higher biomass production compared to the media with no sugars. Based on our microscopy analysis, cells which grown on glucose produced more lipid bodies compared to control and those supplemented with sucrose. Also cells grown mixotrophically increased their laminarin starch content over 300% greater than phototrophic cultures. To further understand the regulation and fluxes of oil production we have begun to take baseline data on *G. sulphuraria's* lipid production and metabolism **Figure 5.2-10**. Ultimately we seek to answer: Does increasing C/N ratio boost lipid content in Galdieria. From the metabolic analysis we found an increase in free fatty acids, lipids and lipid

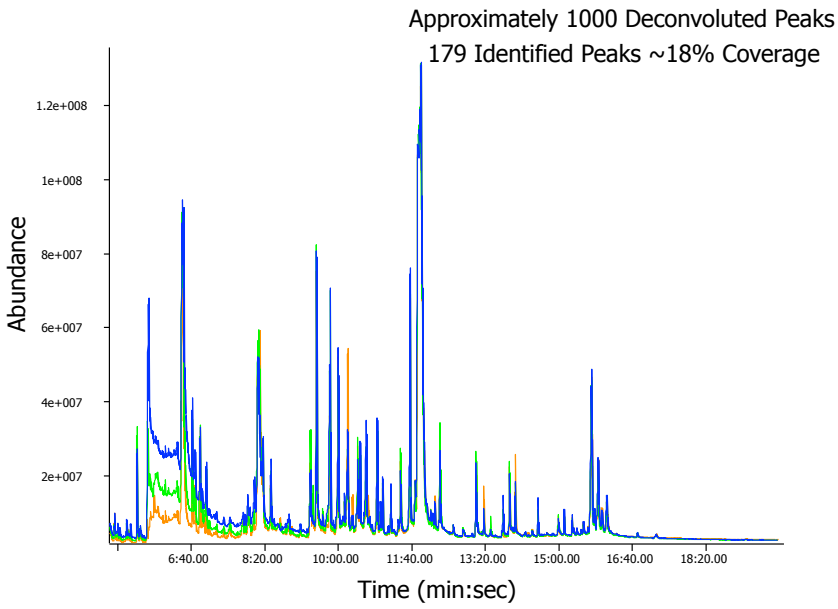

Figure 5.2-10. Replicate GC/MS metabolic profiles of a *G. sulphuraria* extract that provides the identification for many of the intracellular components. Individual components are identified by matching their mass spectra to those in the Oliver Fiehn mass spectral database. Currently we have identified a large number (>170 currently) of primary metabolites in *G. sulphuraria*.

derivatives from the increased supply of carbon to the cells. An outcome of interest is how this increased in C has an impact on photosynthetic intermediates and what role that plays in carbon partionining between lipids and increased synthesis of polysaccharides.

5.2.5 Growth Media Analysis by FT-ICR Mass Spectrometry

The Chemical Analysis and Instrumentation Laboratory at NMSU analyzed multiple ABY growth media sample sets by FT-ICR mass spectrometry to characterize potential allelopathic compounds within co-cultures of *Coelastrella/Chlorella*. Those analyses were performed for both fractionated and non-fractionated media samples and for multiple culture experiments (see discussion in section 5.2.3).

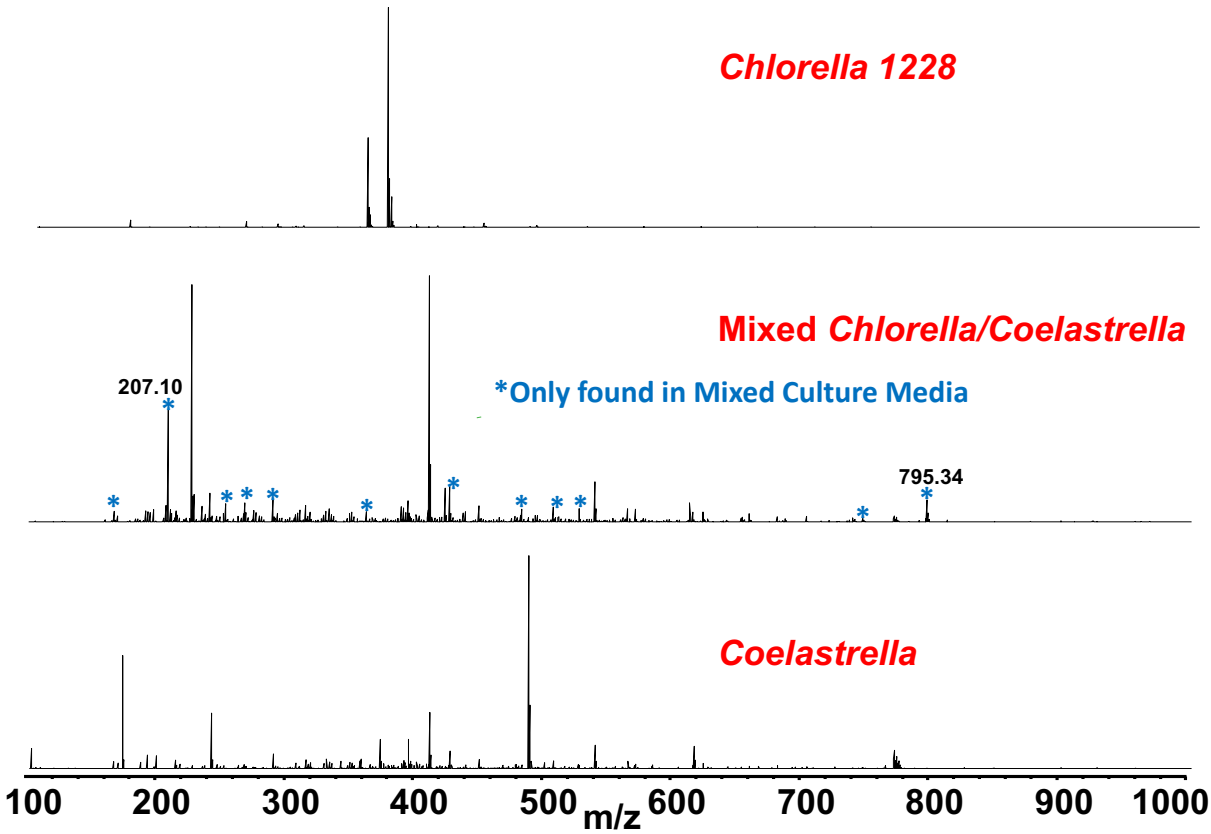

Figure 5.2-11. Molecular characterization of media dissolved organics/potential allelopathic compounds by ultrahigh resolution mass spectrometry.

Media samples were subjected to solid phase extraction to retain/concentrate dissolved aqueous organics and remove salts prior to elution and direct-infusion into a 7 tesla FT-ICR mass spectrometer. Through our measurements we produced chemical identifications at the level of elemental composition for each media extract interrogated. Those compound lists were typically

comprised of ~1500- 2000 masses which were sorted and filtered based on output from activity assays. For each of three separate culture experiments (one including fractionation) we identified lists of potential allelopathic compounds, usually 5-150 compounds that were unique to the mixed culture media samples or fractions. However, the culture experiments proved to be problematic and the magnitude of apparent allelopathic interaction between the two species (observed via bioassay) was not reproducible. In turn, no compounds were found across all experiments that could be uniquely assigned as allelopathic compounds.

For this effort, significant improvement in the reproducibility of *Coelastrella/Chlorella* co-culture is needed along with improved documentation of the allelopathic interaction. The mass spectral method presented here is shown capable of the differential analysis approach that would be needed to identify allelopathic compounds should representative media samples become available.

5.2.6 References

Adarme-Vega, T. C., Lim, D. K., Timmins, M., Vernen, F., Li, Y., & Schenk, P. M. (2012). Microalgal biofactories: a promising approach towards sustainable omega-3 fatty acid production. *Microb. Cell Fact*, *11*, 96.

Borowitzka, M. A. 2005. Culturing microalgae in outdoor ponds. *In* R. Andersen [ed.], Algal Culturing Techniques. Elsevier.

Cardozo, K. H., Guaratini, T., Barros, M. P., Falcão, V. R., Tonon, A. P., Lopes, N. P., ... & Pinto, E. (2007). Metabolites from algae with economical impact. *Comparative Biochemistry and Physiology Part C: Toxicology & Pharmacology*, *146*(1), 60-78.

Cembella, A.D. 2003. Chemical ecology of eukaryotic microalgae in marine ecosystems. Phycologia 42: 420-447.

Hegewald, E., Wolf, M., Keller, A. Friedl, T. & Krienitz, L. (2010). ITS2 sequence-structure phylogeny in the Scenedesmaceae with special reference to Coelastrum (Chlorophyta, Chlorophyceae), including the new genera Comasiella and Pectinodesmus. Phycologia 49(4): 325-335.

Iyer G., Nagle V., Gupte Y.V., Desai S., Iyer M., Moramkar N. and Sawant V. (2015). Characterization of High Carotenoid Producing Coelastrella oocystiformis and its Anti-Cancer Potential. Int.J.Curr.Microbiol.App.Sci 4(10): 527-536.

Mendes, L. B. B., & Vermelho, A. B. (2013). Allelopathy as a potential strategy to improve microalgae cultivation. *Biotechnology for biofuels*, *6*(1), 152.

Tamiya, H. 1957. Mass culture of algae. Annual Reviews 8: 309-334.

5.3 Strain Development

5.3.1: Improving light harvesting efficiency and photosynthetic rates (Sangeeta Negi, Shawn Starkenberg, Srinivas Iyer, and Richard Sayre)

Objective: Improving photosynthetic efficiency and biomass conversion in *Chlorella sorokiniana* by optimizing light harvesting antenna size.

Approach: To achieve this goal we utilized an RNA interference (RNAi) technology to knock down chlorophyll a (Chl a) oxygenase (CAO) to generate intermediate antenna size lines in *Chlorella sorokiniana*. We also assessed the impact of the knock out of we describe as a master regulatory growth control gene (phototropin) in *Chlamydomonas* on biomass yields.

Previous studies had demonstrated that optimization of the light harvesting antenna complex by down-regulating the peripheral LHCII proteins in green algae leads to increased photosynthetic energy conversion efficiency and improves biomass at high light intensities (Perrine et al., 2012). These goals were achieved by reducing Chlorophyll b (Chl b) levels, using a knock down strategy to control Chlorophyll a oxygenase (CAO) expression levels. CAO is an enzyme which is involved in conversion of chlorophyllide a into chlorophyllide b (Tanaka et al. 1998).

During the course of the REAP grant, we designed a *Chlorella sorokiniana* 1230 (Cs-1230) specific vector to perform transformation with Cs-1230 CAORNAi constructs. Cs-1230 is a diploid organism and we found 2 CAO genes in the genome, which have significantly different DNA sequences that each other. We designed 3 CAORNAi constructs covering 1. CAO A gene, 2. CAO B gene and, 3. a single construct covering both CAO genes. We were able to achieve transgenics with higher Chl a/b ratios (up to 3.2) but after growing them in liquid culture media, these putative transformants were unable to sustain the higher, more optimal Chl a/b ratios. We have previously observed lack of stable RNAi mediated suppression of gene expression in *Chlamydomonas* (Perrine et al., 2012). As a result, we explored using knock out and gene overexpression strategies to improve biomass production.

One of these options was to alter photoropin expression levels. Phototropin is a family of blue light receptors, which mediate a variety of physiological processes in plants (Christie, 2007). In contrast to plants, however, the green alga *Chlamydomonas reinhardtii* has only a single phototropin (CrPhot) gene. In *Chlamydomonas* PHOT has previously been shown to play a central role in controlling sexual life cycle, eye spot size, and light sensitivity. CrPhot has also shown to regulate chlorophyll, carotenoid, and light-harvesting chlorophyll binding protein abundance in algae (Huang and Beck 2003; Im et al. 2006; Trippens et al. 2012). During this period, we compared the growth and photosynthetic rates of C*hlamydomonas* phototropin knock-out (PHOT-KO) mutants to their parental wild-types. We observed 2-fold higher growth rates associated with substantial increases in CO_2-dependent rates of photosynthesis in PHOT-KO mutants (Fig 5.3.1.1 and 5.3.1.2). Comparative analyses of the transcriptomes of a PHOT-KO mutant to its parental wild-type (WT) demonstrated significant increases in transcript levels for genes involved in photosynthetic electron transport, carbon fixation, starch and lipid synthesis, and those regulating cell cycle and cell division control (Fig. 5.3.1.3) Our studies suggest that phototropin may be a master regulatory gene that suppresses rapid cell growth and promotes

gametogenesis and sexual recombination in wild-type strains but allows for rapid growth when inactivated in PHOT-KO mutants (Negi et al. 2016, Patent pending). We are currently working on getting PHOT gene knock out line in Cs-1230 background to improve photosynthesis and biomass yield but have been hampered by a failure to achieve transgenics. The *aphVIII* gene used for paramomycin resistance selection was not actively inactivating paramomycin, presumably due to a failure to integrate into the genome. Replacement with the *ble* gene conferring zeomycin resistance has led to substantial numbers of transgenic events confirmed by DNA sequencing. Additional efforts are now underway to enhance photosynthetic efficiency in *C. sorokiniana* on follow up projects after REAP.

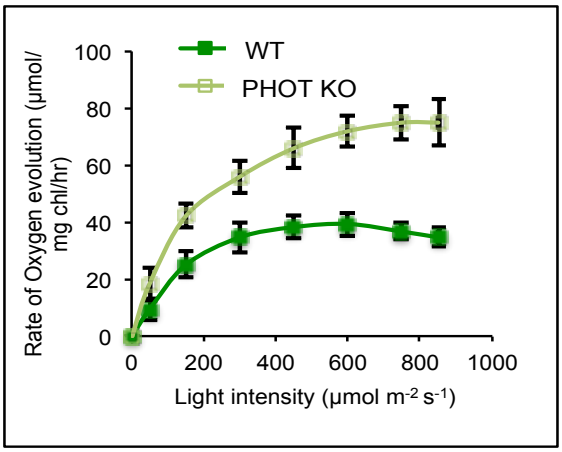

Figure 5.3.1.1: Photosynthetic efficiency is increased 2-fold in PHOT KO mutant compared to WT parent.

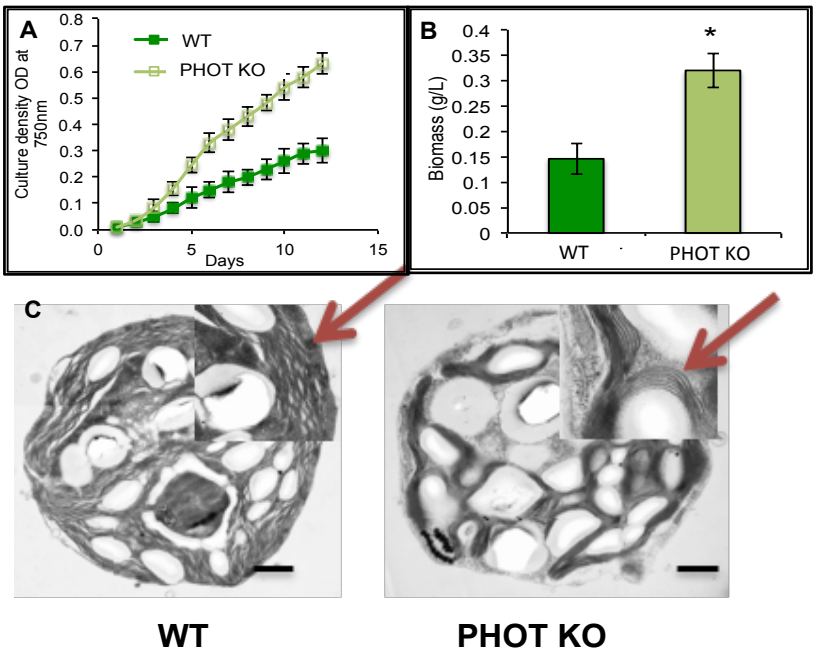

Figure 5.3.1.2: Growth biomass and TEM analysis of PHOT KO mutant. (A,B) Growth and biomass is increased 2 fold in PHOT KO mutant (C) Higher accumulation of starch and altered membrane structure in PHOT KO mutant.

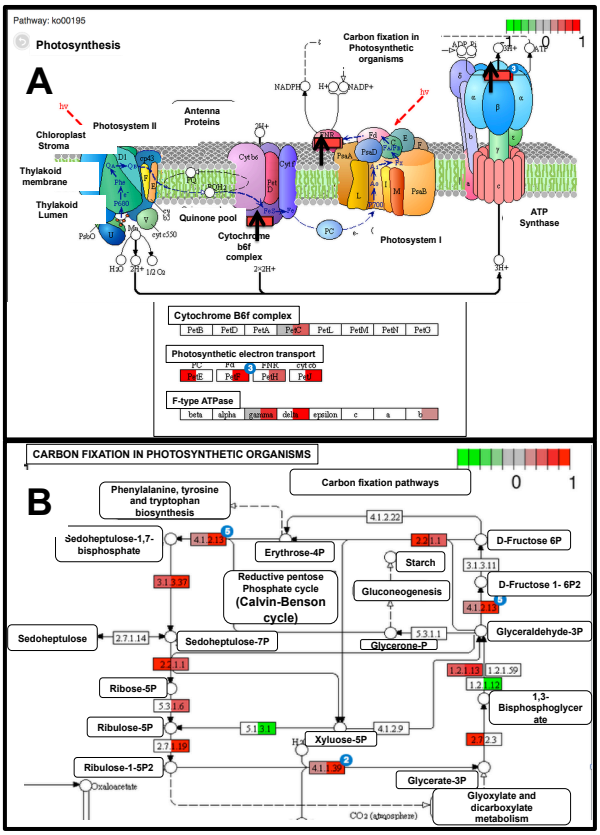

Figure 5.3.1.3: Kyoto Encyclopedia of genes and genomes (KEGG) pathway showing photosynthesis genes up-regulation in PHOT KO mutant. (A) Photosynthetic electron transport chain (PET) (B) Calvin and Benson Cycle genes. Results represent statistically significant data from average and SE of three independent measurements (pValue= >0.05).

References:

1. Perrine, Z., Negi, S. & Sayre, R.T. Optimization of photosynthetic light energy utilization by microalgae. *Algal Research* **1**, 134-142 (2012).
2. Tanaka, A. et al. Chlorophyll a oxygenase (CAO) is involved in chlorophyll b formation from chlorophyll a. *Proceedings of the National Academy of Sciences of the United States of America* **95**, 12719-12723 (1998)
3. Christie JM (2007) Phototropin Blue-Light Receptors. *Annu Rev Plant Biol* 58(1):21–45.
4. Huang KY, Beck CF (2003) Photoropin is the blue-light receptor that controls multiple steps in the sexual life cycle of the green alga Chlamydomonas reinhardtii. *Proc Natl Acad Sci U S A* 100(10):6269–6274.
5. Im C-S, Eberhard S, Huang K, Beck CF, Grossman AR (2006) Phototropin involvement in the expression of genes encoding chlorophyll and carotenoid biosynthesis enzymes and LHC apoproteins in *Chlamydomonas reinhardtii*. *Plant J* 48(1):1–16.

6. Trippens J, et al. (2012) Phototropin influence on eyespot development and regulation of phototactic behavior in Chlamydomonas reinhardtii. *Plant Cell* 24(11):4687–702.

Patent Filed: Patent Cooperation Treaty (PCT) International Application No.: PCT/US16/36077. For: *Improved Productivity and Bioproduct Formation in Phototropin Knock/Out Mutants in Microalgae.* Inventors: Sangeeta Negi, Richard Thomas Sayre, Shawn Robert Starkenburg. Applicant: NMC, INC. and Los Alamos National Security, LLC

5.3.2: Transgene expression of Cellobiose transporter / β-glucosidase to enhance cellobiose metabolism (Amanda Barry, Sowmya Subramanian and Richard Sayre)

Objective: Previous studies had demonstrated that *C. sorokiniana* rapidly assimilates glucose at 37°C and converts more than 1/3 of the carbon in the glucose to lipid. Instead of adding glucose to ponds, we proposed to utilize cellobiose as a reduced carbon substrate and to facilitate its uptake and conversion to glucose inside the cell. Cellobiose may be less metabolizable by competing organisms compared to glucose resulting in fewer pond contaminants. Furthermore, cellobiose is a product of cellulose digestion and potentially an inexpensive and abundant carbohydrate source for biological conversion into lipids. Recently, it was shown the *Chlamydomonas* had the ability to metabolize and grow on cellulose as a carbon source (Blifernez-Klassen, 2012), thus we explored the possibility that Chlorella could do the same and perhaps be enhanced in its ability to metabolize cellulosics through targeted engineering

Approach: We first screened Chlorella and other green algae for their ability to metabolize cellodextrin**.** We subsequently engineered *C. sorokiniana* to determine if we could further enhance celloulosic metabolism. Utilizing the cellodextrin transporter and β-glucosidase genes from *Neurospora crassa*, we genetically engineered C. sorokiniana 1230 to utilize cellobiose (CB)and convert it to glucose enhancing biomass yield and oil accumulation.

Methods: Transformed *Chlorella sorokiniana* strain Cs-1228 with plasmid pCSANW1

- Establish the identity of Cs-1228 transgenics with β-glucosidase/cellobiose transporter using primers designed for Cs-1228, Cs-1230 and Cs-1412.
- Carried out cellobiose boost to Cs-1412 after concentrating 20 x fold: This experiment was repeated with the simultaneous monitoring of cell counts and Bodipy (lipid) fluorescence after the addition of 0, 0.3, and 1.0 mM cellobiose

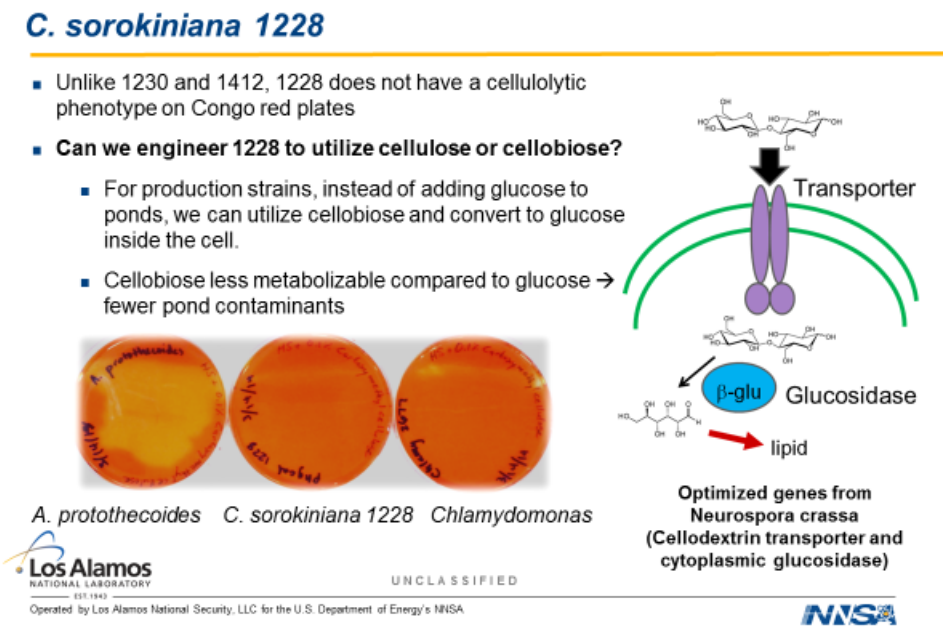

Figure 5.3.2.1: Cellodextrin digestion by various algae species and target proteins (*Neurospora* CDT transporter in purple and β-glucosidase in blue) for over-expression in algae to enhance cellodextrin uptake and metabolism.

Results: Cs-1228 transgenics having the β-glucosidase/cellobiose transporter genes were identified by PCR. The expected size of the bands for the cellobiose transporter was 300 bp.

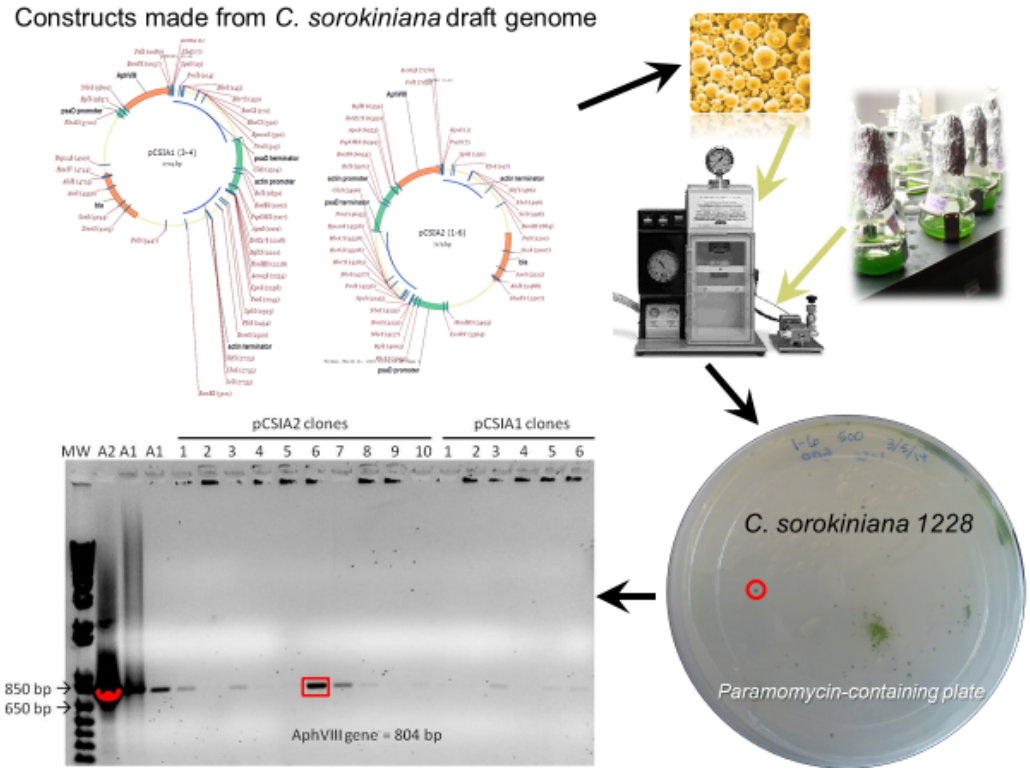

Figure 5.3.2.2: Design of transformation vectors for incorporation of CDT and β-glucosidase genes into *C. sorokiniana* and their confirmation by PCR amplification of the selectable marker gene AphVIII.

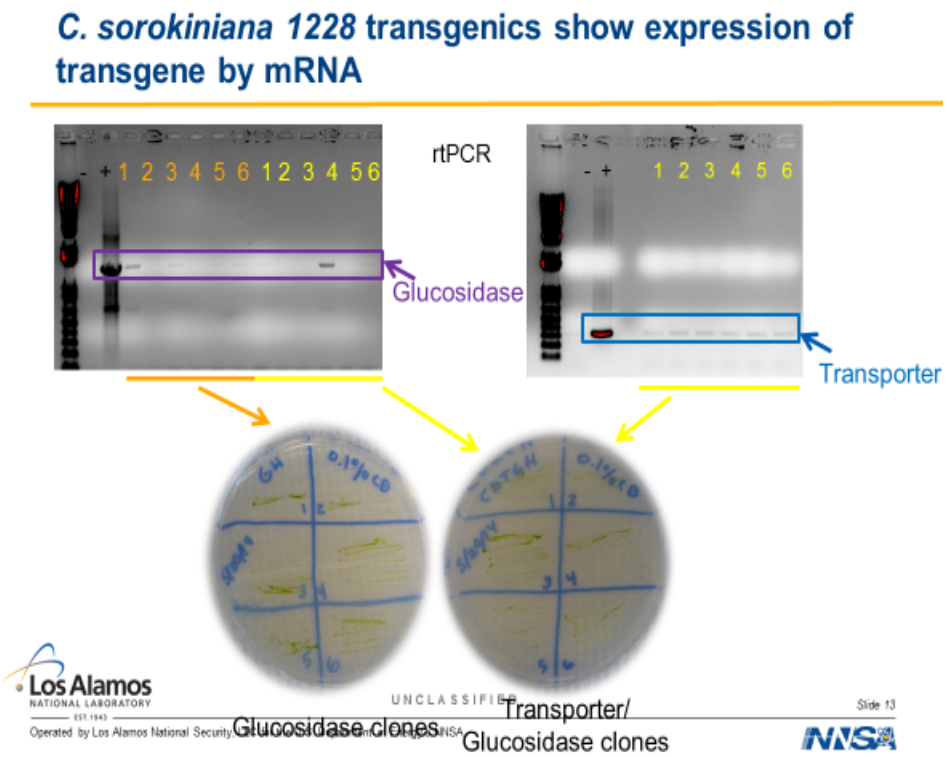

Figure 5.3.3.3: RT-PCR confirmation of CDT and β-glucosidase gene expression in transgenic *C. sorokiniana.*

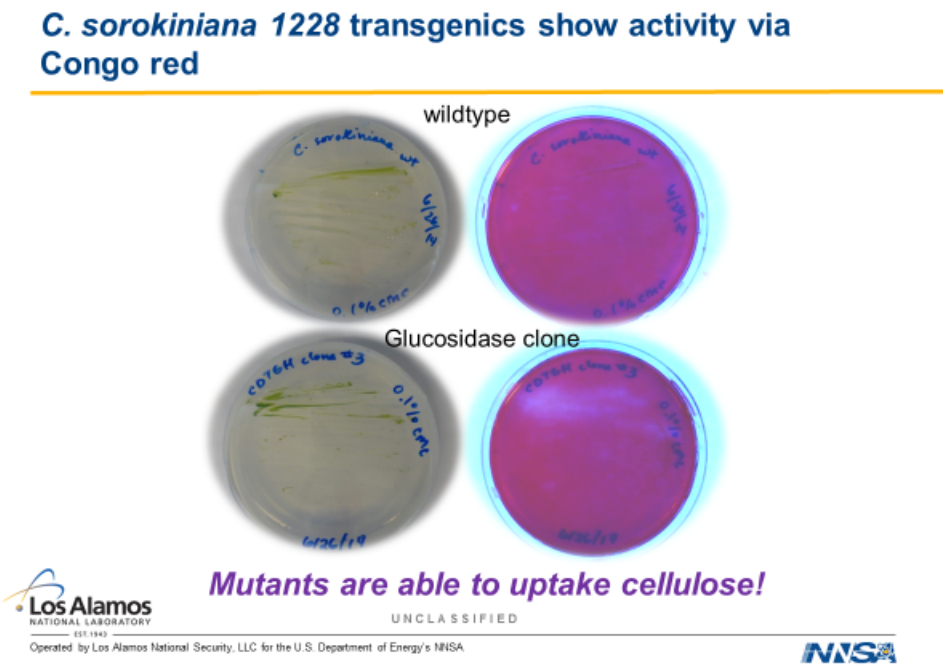

Figure 5.3.3.4: Congo Red assessment of cellodextrin digestion in wild-type and β-glucosidase expressing *C. sorokiniana*

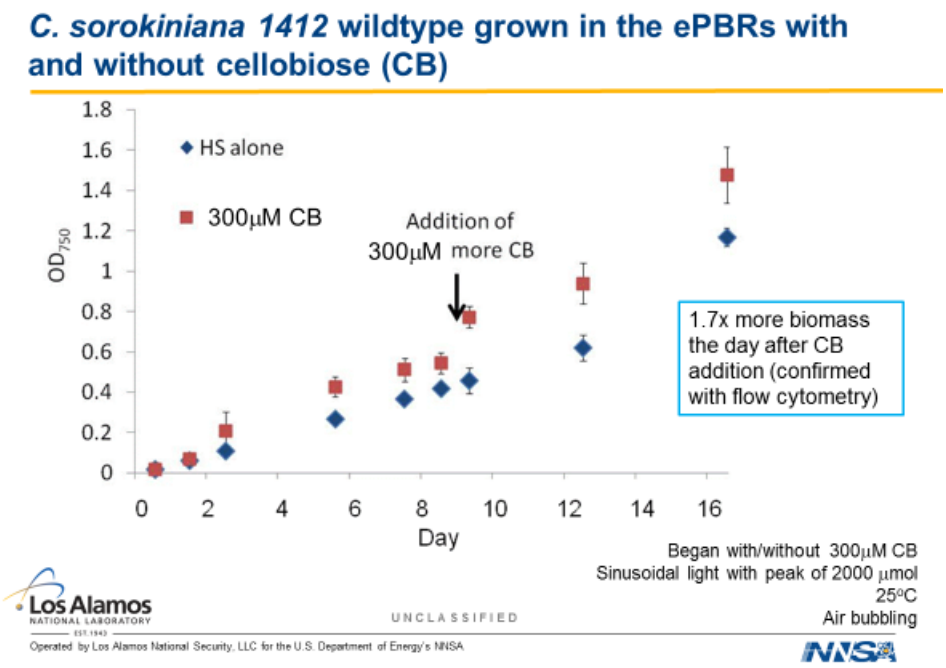

Figure 5.3.3.5: Effect of cellobiose addition on the growth of wild-type *C. sorokiniana* cultures in environmental photobioreactors (ePBRs) with 12 hr light/dark cycles.

As shown above (Figure 5.3.3.5), adding cellobiose to *C. sorokiniana* enhanced biomass yields by 70%, a substantial enhancement in biomass yield.

One concern, however, is that the addition of cellobiose to open ponds could lead to enhanced bio-contaminant loads. Thus, we explored doing a cellobiose boost post-harvest when bio-contaminant load would be limited. Transgenic algae expressing the β-glucosidase gene were first grown in e-PBRs under 12 hr sinusoidal light and dark conditions. After two weeks, the cells were harvested, concentrated and re-suspended in fresh HS media such that the algae were concentrated twenty-fold. The samples (25 mL in 125 mL Erlenmeyer flasks) were then moved to the shaker (150 rpm) with a light intensity of ~ 100 $\mu E/m^2/sec$. The hetero-boost boost was provided using 0, 0.3 and 1 mM cellobiose. Samples were collected at different time points; 0, 1, 2, 4, 6, 10, 18 and 24 hours after cellobiose addition for analysis of cell numbers and lipid content by Bodipy staining.

We observed a substantial 2.9 fold ($23/8 \times 10^4$ bodipy units) increase in relative lipid content following a heteroboost with 0.3 mM cellobiose relative to the control with no cellobiose added (Fig. 5.5.5.6). However, there was an 2.3-fold increase in lipid content in control cells as well during the first six hours following their concentration and exposure to light. We attribute this effect to the stress associated with high cell concentrations. While addition of 1 mM cellobiose resulted in the fastest initial rate of lipid accumulation, the magnitude of change observed was similar to that of control cells at 4-5 hours (Fig 5.3.3.7). The cell counts on the other hand showed an initial decline and then increased to a constant number under all the three cellobiose concentrations tested at 10 hours. The highest cell counts were observed with 0.3 mM cellobiose, the same cellobiose concentration that gave maximum lipid yields at 6 hours.

-

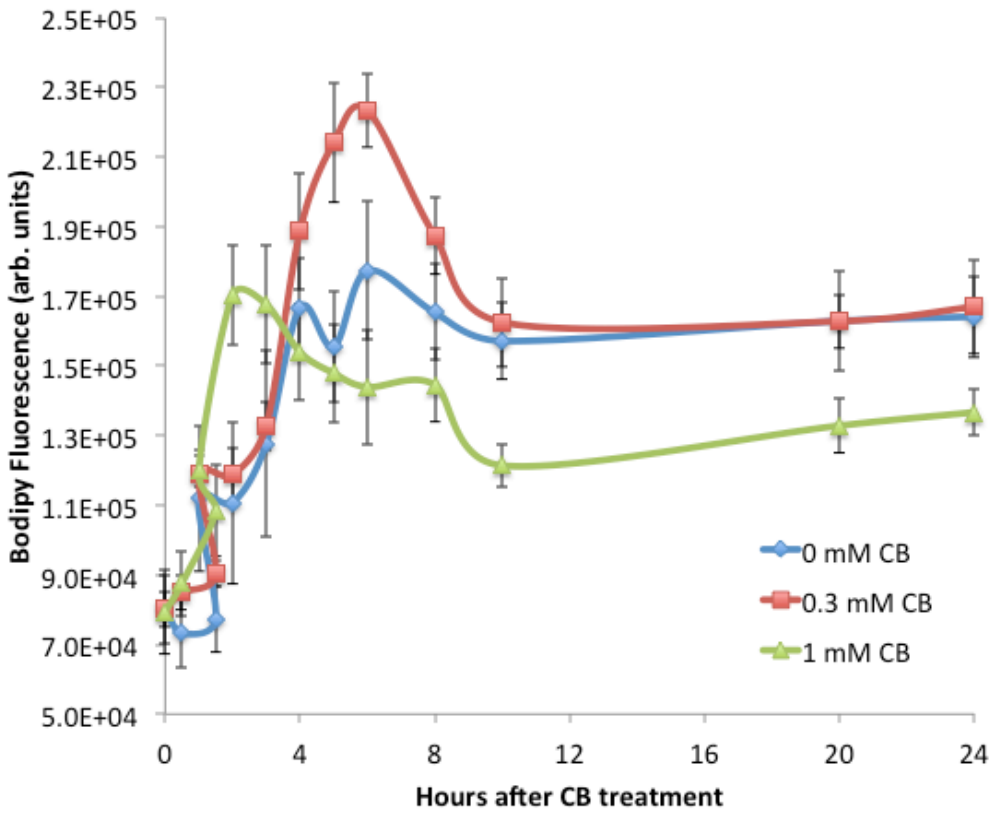

Figure 5.3.3.6: Relative lipid content of β-glucosidase expressing transgenic *C. sorokiniana* as determined using Bodipy stained cells following harvesting and concentraing algae by 20-fold and subsequent addition of cellobiose at various concentrations.

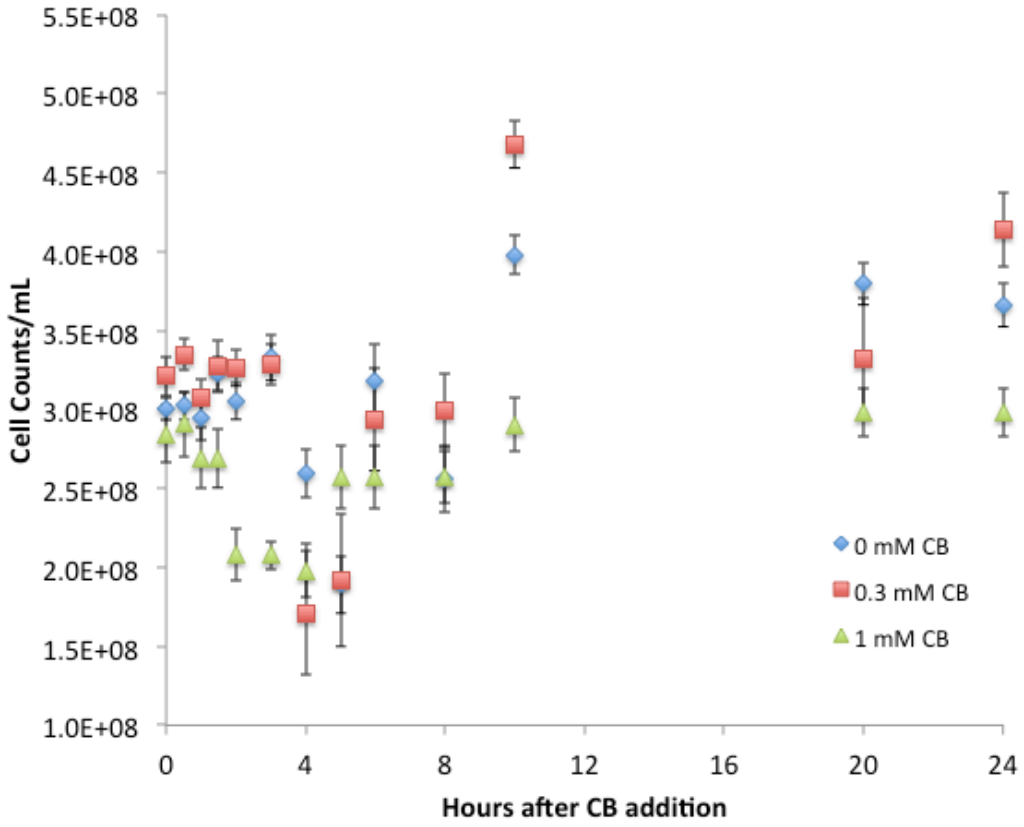

Figure 5.3.3.7: Change in cell counts during cellobiose treatment in concentrated algae

Overall, there was an approximate 45% increase in cells numbers under optimal cellobiose concentrations (0.3 mM) between 8 and 10 hr after the cellobiose heteroboost (Fig. 5.3.3.7). However, during the first six hours, when lipid levels increased (Fig. 5.3.3.6) to their highest values, there was no change in cell number. These results suggest that there is a shift after the first six hours in cellobiose from lipid accumulation to cell division consistent with the observed drop in lipid levels after the first 6 hrs of cellobiose treatment. These results indicate that there is a trade off between lipid accumulation and biomass yield when cellobiose is added to growth media.

Thermodynamically, however a 45% increase in biomass and concomitant increase in relative lipid yield of 2.3 fold results in a 75% greater total relative energy recovery in algal biomass following the cellobiose boost at 10 hrs treatment than the 2.9 fold increase in lipid content (without additional cell division) that occurs in the first six hours following cellobiose addition. Finally, boosting lipid yield in concentrated algal cells post-harvest has the advantage of reducing potential competition for cellobiose by other competing microbes.

References:

Blifernez-Klassen, O., Klassen, V., Doebbe, A., Kersting, K., Grimm, P., Wobbe, L., & Kruse, O. (2012) Cellulose degradation and assimilation by the unicellular phototrophic eukaryote *Chlamydomonas reinhardtii*. *Nat Commun* 3:1214.

5.3.4: Control of pond pathogens using antimicrobial peptides (AMP) (Sathish Rajamani and Richard Sayre)

Objective: Develop a transgenic *C. sorokiniana* expressing AMPs that confer protection against invaders such as rotifers (*Adenata Vaga, Philodina and Brachionus sp*) and the known *C. sorokiniana* bacterial pathogen *Vampirovibrio chlorellavorus.*

Strategy: To achieve this aim, we needed to identify AMP(s) that would selectively kill the aforementioned pathogens but which were innocuous to *C. sorokiniana* (Fig. 5.3.4.1). Second, we would engineer *C. sorokiniana* to express AMP against these invaders, which will be useful for crop protection. We would also need a regulated system to express AMP(s) in algae for that we will use a gene-switch system (see hammerhead nuclease control of gene expression below).

Strategy

1. Find the best AMP(s) candidate that kill both rotifers and *V. chlorellavorus*
2. Identify the lowest concentration of AMP(s) required to kill them but do not kill Cs1412.
3. Engineer *C. sorokiniana* to express AMP(s) in the cytoplasm or to be secreted out of the cell.

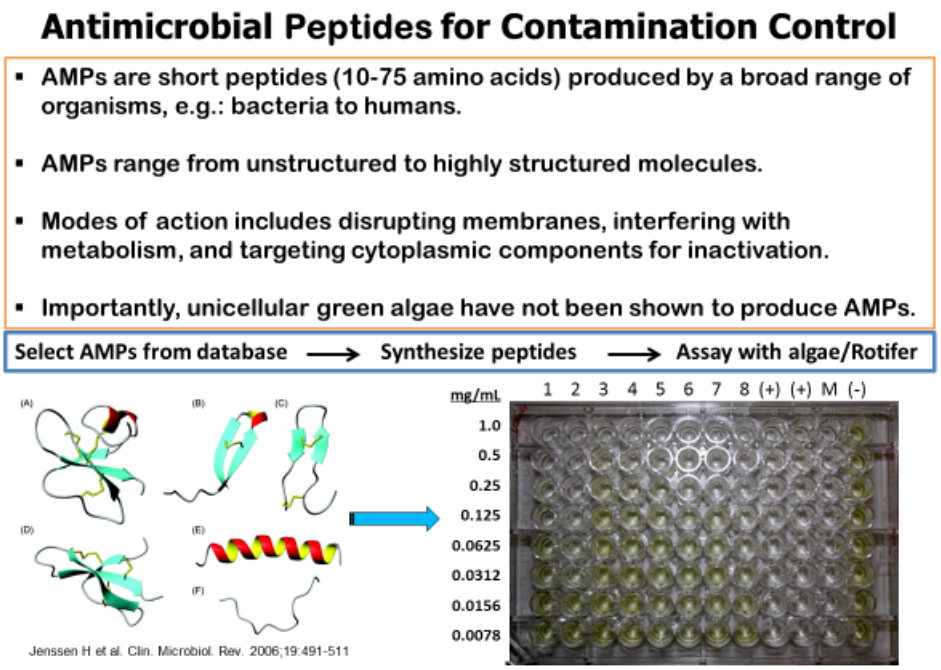

Figure 5.3.4.1: AMP mode of action and microtiter dish screening of AMPs on algal growth

The most promising AMPs from a prescreen of 40 Met-AMPs for controlling *Vampirovibrio* or rotifers

AMPs	AA	From	Against
Cecropin A	37	Insect	G(+), G(-), Virus, Parasites
MsrA (Temporin A derivative)	19	Frog	G(-) plants
Dermaseptin S1	34	Frog	G(+), G(-), Virus,Fungi,Parasites
Piscidin 1	22	Fish	G (+), G(-), Virus, Fungi
Piscidin 2	22	Fish	Virus, fungi and parasites
Piscidin 3	22	Fish	G(+), G(-), Virus, Fungi
Ponericin G1	30	Ant	G(+), G(-), insects, erythrocytes
Ponericin G4	29	Ant	G(+), G(-), insects,
Ponericin G6	18	Ant	G(+), G(-), insects,
Ponericin W6	20	Ant	G(+), G(-), insects, erythrocytes

Vampirc vibrio

Rotifers

Figure 5.3.4.2: Met-AMPs screened, source and pathogens (Vampirovibrio) and herbivores (rotifers) screened against.

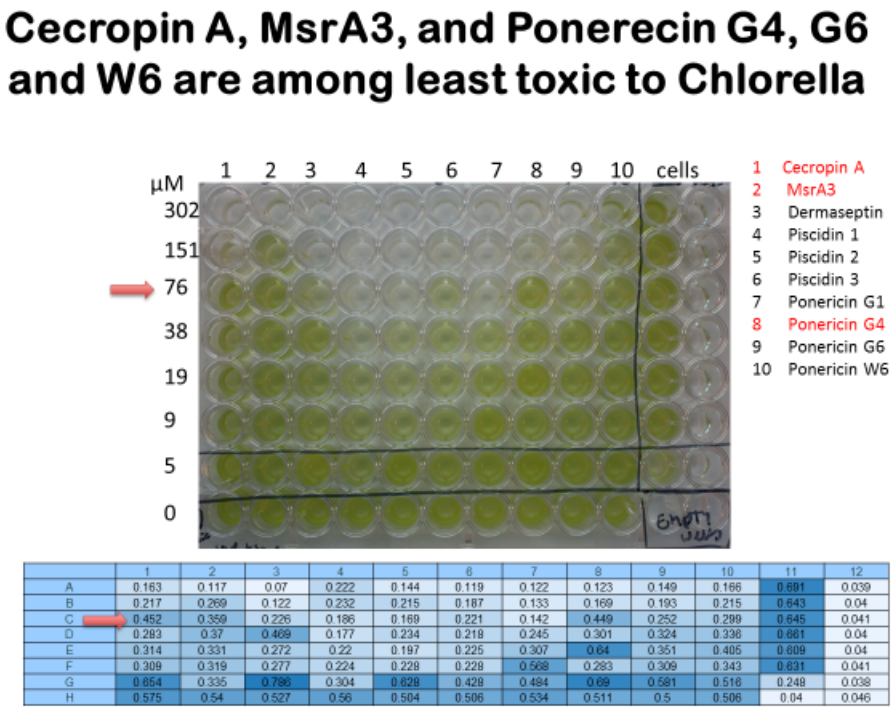

	1	2	3	4	5	6	7	8	9	10	11	12
A	0.163	0.117	0.07	0.222	0.144	0.119	0.122	0.123	0.149	0.166	0.691	0.039
B	0.217	0.269	0.122	0.232	0.215	0.187	0.133	0.169	0.193	0.215	0.643	0.04
C	0.452	0.359	0.226	0.186	0.169	0.221	0.142	0.449	0.252	0.299	0.645	0.041
D	0.283	0.37	0.469	0.177	0.234	0.219	0.245	0.301	0.324	0.336	0.661	0.04
E	0.314	0.331	0.272	0.22	0.197	0.225	0.307	0.64	0.351	0.405	0.609	0.04
F	0.309	0.319	0.277	0.224	0.228	0.228	0.568	0.283	0.309	0.343	0.631	0.041
G	0.654	0.335	0.786	0.304	0.628	0.428	0.484	0.69	0.581	0.516	0.248	0.038
H	0.575	0.54	0.527	0.56	0.504	0.506	0.534	0.511	0.5	0.506	0.04	0.046

Fig. 5.3.4.3: Screening AMPs for algal toxicity.

Results:

1. AMP(s) including Cecropin A, MsrA3, Dermaseptin S1, Piscidin 3, Ponerecin G4, were identified as the best AMP candidates to kill *V. chlorellavorus* and are less toxic to *C. sorokiniana.*
2. AMP(s) concentration at around 76 µM-38 µM and lower were non-toxic to Cs1412.
3. The lowest AMP concentrations that kills *V. chlorellavorus* were identified to be around 76 to 38 µM.
4. Rotifers were cultured with AMPs for 24 hrs at room temperature. Only Dermaseptin S1, killed rotifers at concentration around 76 µM. The other AMP(s) tested killed rotifers at concentration higher than 76 µM and 151 µM.
5. Dermaseptin S1 with signal peptide and without signal peptide was cloned between NdeI and XbaI restriction sites of the vector. The signal sequence belongs to carbonic anhydrase from C. sorokiniana.
6. The sequence of Dermaseptin S1 was codon optimized for Cs1412.
7. Transformation of Cs-1412 was not achieved

Conclusions: We have identified several AMPs that kill both rotifers and Vampirovibrio but which are not toxic to algae when externally applied (Fig. 5.3.4.3). The expression of AMP genes encoding these AMPs in *C. sorokiniana* has been delayed due to unexpected barriers encountered in achieving effective transformation. Those barriers were just recently overcome and experiments are ongoing to express AMPs in *C. sorokiniana*.

5.3.5: Development of biocontainment strategy for engineered algae

Objective: Biocontainment of genetically modified (GM) algae through development of suicide gene technology for algal growth only in defined algal cultivation ponds.

Strategy: The objective is to achieve Ribonuclease protein Barnase expression in algae in a regulated environment to induce cell death upon escape from a pond and controlled barnase inhibition by the high-affinity Barnase inhibitor Barstar in the pond environment. To achieve this we will control the expressions of Barnase (decrease) and Barstar (increase) in algae cultivation ponds using xenobiotic ligand (caffeine) that regulate a hammerhead nuclease activity controlling the expression of Barstar achieving algal growth only in the regulated algal ponds. Escape of these lines will result in Barnase mediated death of these algae.

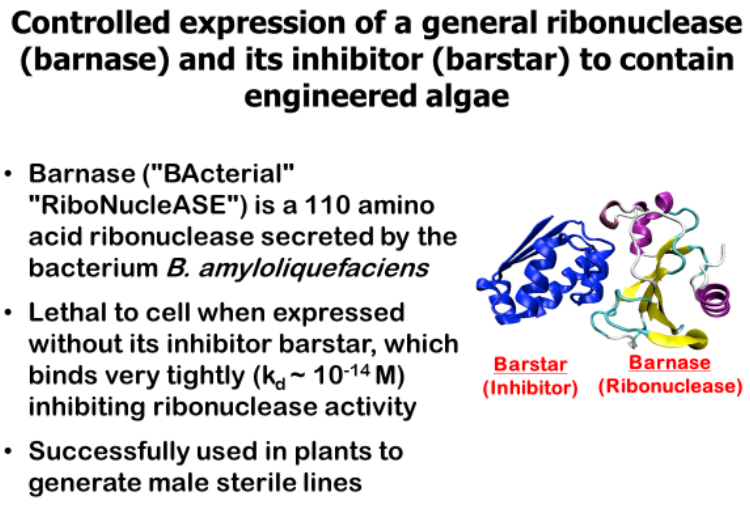

Figure 5.3.5.1: Mode of action of Barnase and its inhibitor Barstar

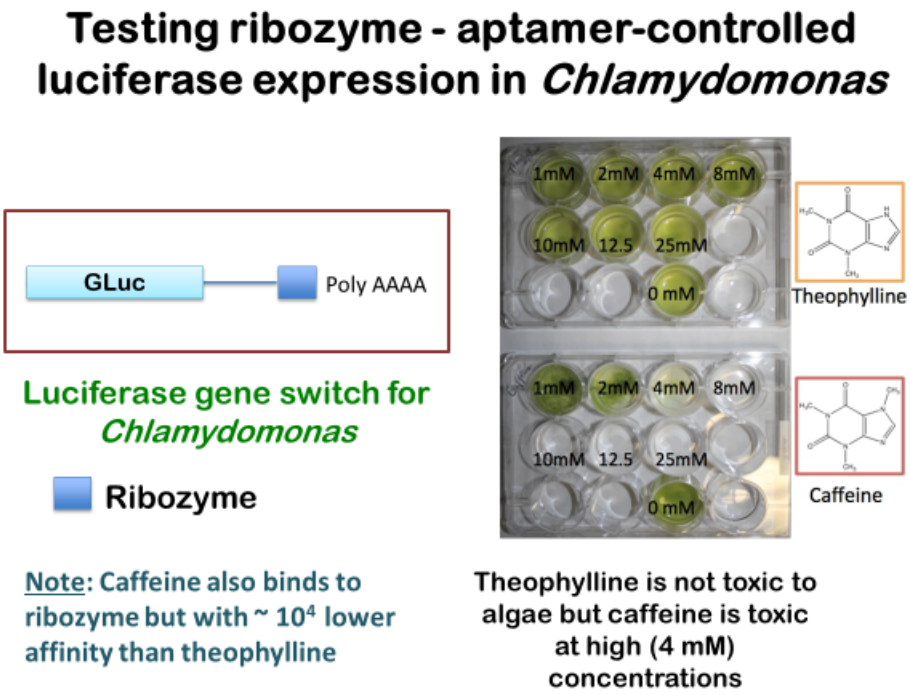

Figure 5.3.5.2: Ribozyme interruption of Gluc (luciferase) reporter gene and theophylline and caffeine toxicity to *Chlamydomnas reinhardtii.*

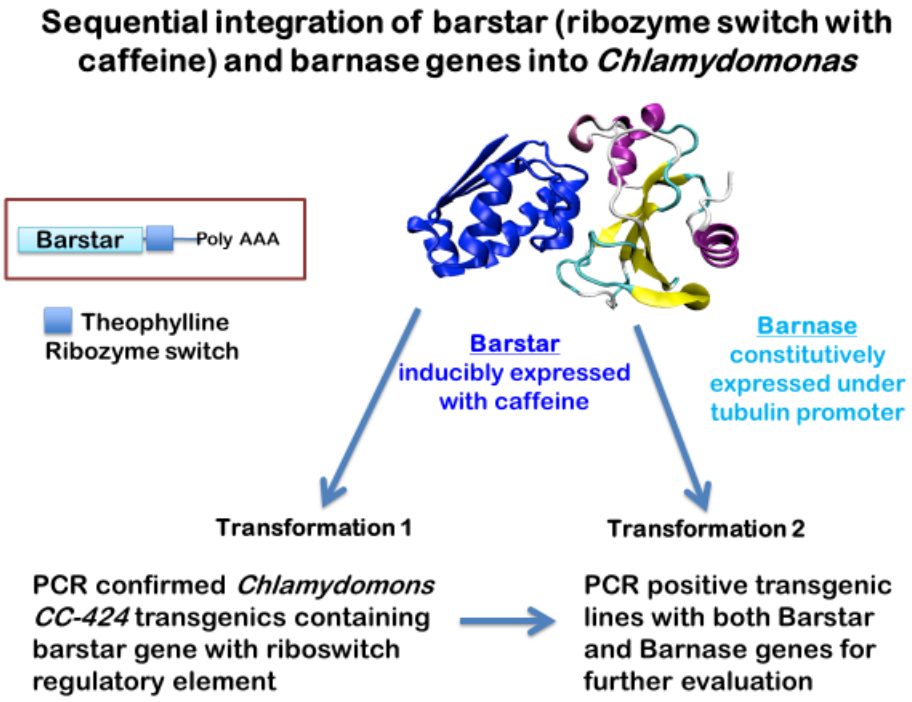

Figure 5.3.5.3: Sequential transformation strategy for integrating first Barstar inhibitor followed by Barnase ribonuclease in the presence of the ribozyme inhibitor caffeine

Results: As a model system to test the efficacy of the Barnase/Barstar system we expressed the gene constructs in *Chlamydomonas* initially due to its ease of transformation. Transgenic *Chamydomonas reinhardtii* (Fig. 5.3.5.4) lines engineered to produce Barstar regulated by caffeine/theophylline aptamer-ribozyme switch to control toxic Barnase were screened in ePBR experiments and flask experiments (Fig. 5.3.5.5) for caffeine mediated regulation of Barnase (suicide gene) activity by Barstar. We observed a 3.5-fold reduction in growth rate in the absence of caffeine relative to its optimal concentration of 1.0 mM.

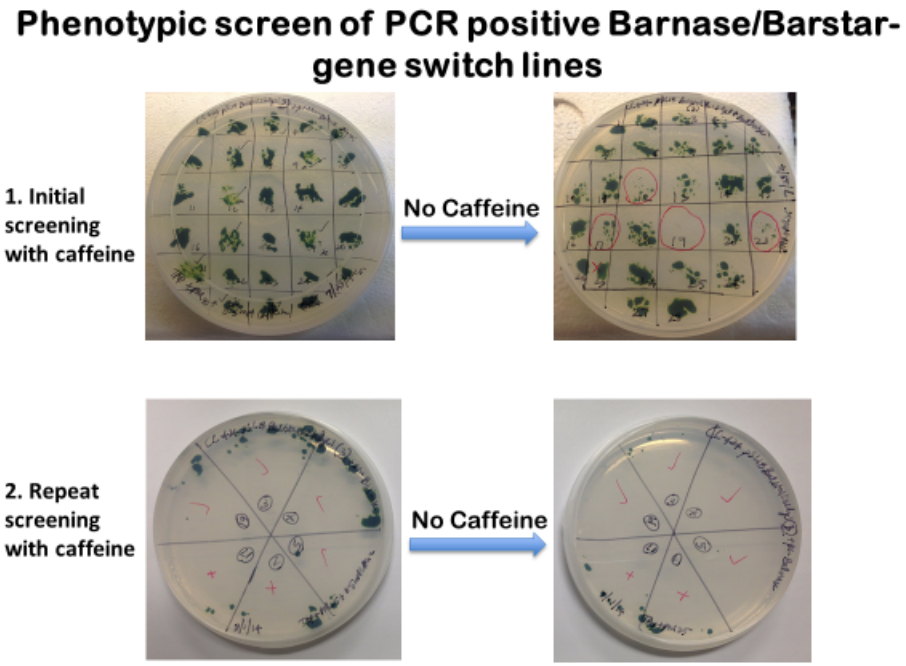

Figure 5.3.5.4: Isolation of double (Barstar then Barnase) transformants and their growth with caffeine and lack of growth in the absence of caffeine.

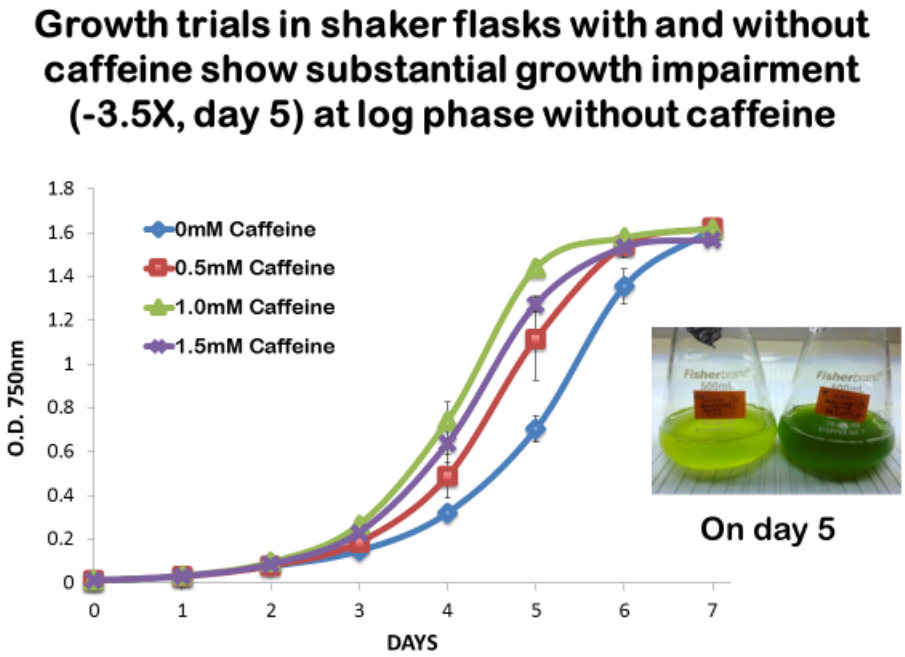

Figure 5.3.5.5: Growth curves of Barstar/Barnase transgenics at various caffeine concentrations

Conclusions: Overall, these results in *Chlamydomonas* look promising for caffeine mediated regulation of a suicide gene (Barnase) to control the escape of transgenic algae. Ongoing experiments are designed to optimize the expression levels of Barnase and Barstar in *C. sorokiniana* transgenics. Due to the recent breakthrough in Cs-1230 transformation it is now possible to test this system in *C. sorokinaiana*.

5.3.6: Thermotolerance (Angela Tonin and Richard Sayre)

Objective: Increase the heat tolerance of *C. sorokiniana* so as to grow at the high temperatures experienced in closed ponds and photobioreactors. The optimal temperature for C. sorokiniana growth is 37 C. But C sorokiniana is intolerant to temperatures above 42 C. Closed pond systems in Tuscon will reach temperatures of 55 C in the summer (P. Lammers). To reduce water loss it will be necessary for C. sorokiniana to be grown in closed and potential high temperature environments.

Research Strategy:

1) Directed Evolution Approach to Enhance Thermal Tolerance: *C. sorokiniana* was adapted to higher temperatures utilizing the ePBRs and a directed evolution strategy. We continuously selected over 6 weeks for strains that would survive in 2 C stepwise increases in growth temperature in a series of ePBRs connected by continuous flow from the permissive temperature (37 C) to higher temperatures (37, 41, 43, 45 C). The flow rate between ePBR was regulated to achieve a complete volume exchange in 24 hours. Growth in ePBRS having higher temperatures would indicate selection for heat tolerant strains. However, a net increase of only 2 C (39 C) in growth temperature was observed and so we switched to strategy 2 described below
2) Targeted sequestration of damaging Reactive Oxygen Species (ROS) Produced During Stress by Chemical Quenchers Expressed in Transgenic Cells. The second strategy was to use a transgenic approach to quench damaging reactive oxygen species(ROS), generated during stress. Previously, we had shown that proline overexpression in *Chlamydomonas*, induced by overexpressing the P5CS gene, would elevate internal proline levels leading to enhanced ROS quenching and elevated tolerance to heavy metal and salt stress (Siripornadulsil, 2002) (Fig. 5.3.6.1). Thus, we explored whether P5CS overexpression and elevated proline levels could confer generalized resistance against heat stress.

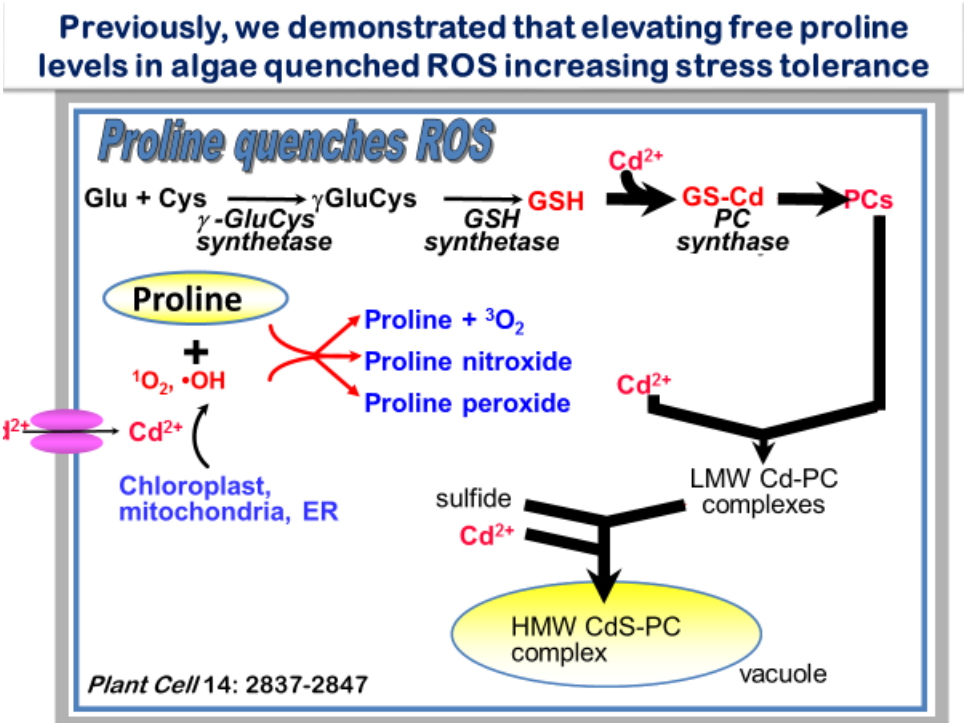

Figure 5.3.6.1: Mechanism of proline mediated ROS quenching during heavy metal stress.

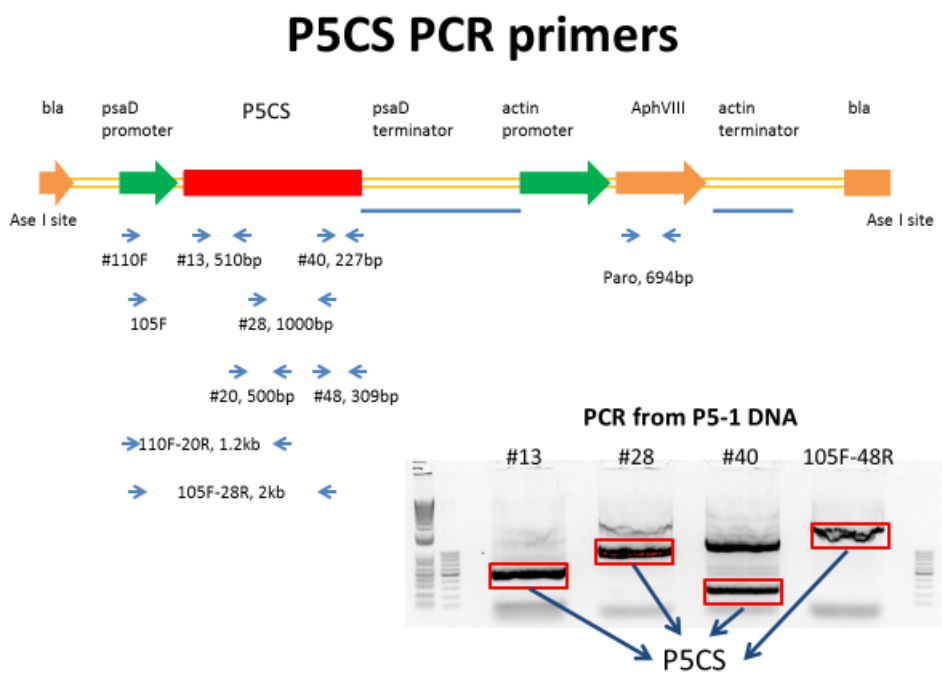

Figure 5.3.6.2: Gene construct used to introduce the mothbean P5CS gene into *C. sorokiniana* and PCR primer verification of P5CS gene in transgenics.

Results: The PCR positive bands were subsequently sequences and encode the mothbean P5CS gene. The Cs-1230 was transformed with the P5CS gene and transgenics were confirmed by PCR and DNA sequence analysis. The mutant demonstrated a 5-fold increase in cytoplasmic proline concentrations compared to wild type. Thermotolerance experiments were completed which indicate that the P5CS transformant can survive constant temperatures (40 C) for 24 hours, which is lethal for wild type when grown in 12 hr light-dark cycles in ePBRs.

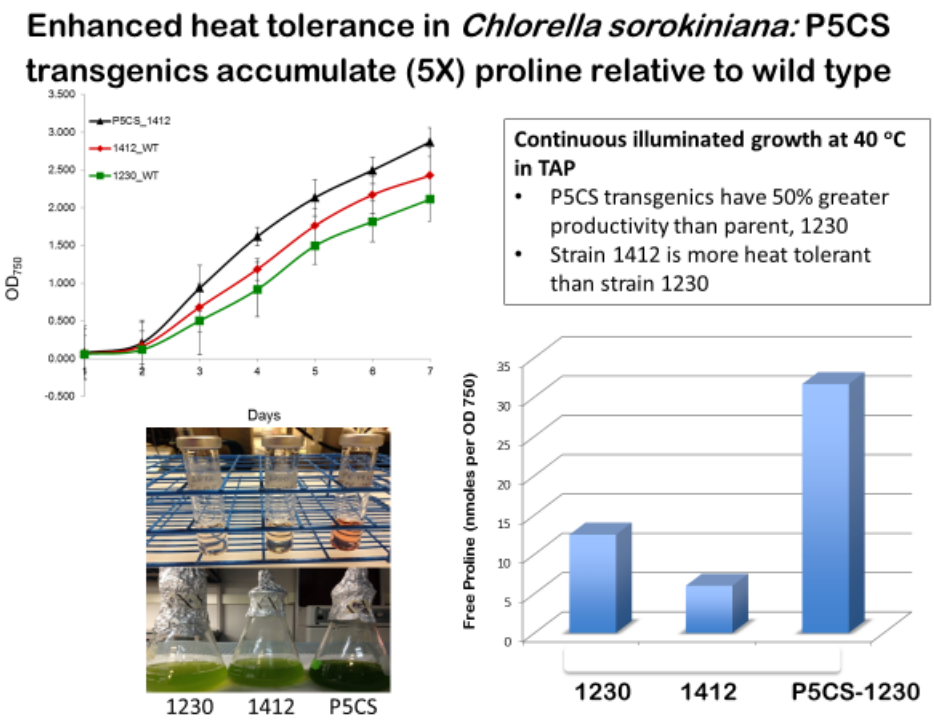

Figure 5.3.6.3: Growth rates of P5CS transgenic under continuous heat stress and relative cytoplasmic proline content.

Algae were then grown in ePBRs with a 12 hr light/dark cycle to mimic a more natural heat stress condition. Solar noon light intensities were equivalent to full sunlight intensities. Night temperatures were 25 C and the peak day temperature (45 C) was reached and held for 2 hours before and after solar noon.

As shown below, the elevated chlorophyll fluorescence values are indicative of impairment in charge separation by photosystem II in WT strains at 45 C peak temperature. The Chl fluorescence rise kinetics of algae grown in ePBRs with a peak temperature of 45 C were identical to WT algae grown at a peak day temperature of 37 C. Since PSII activity is one of the most sensitive biochemical activities susceptible to heat inactivation, the lack of any apparent damage to PSII at 45 C peak temperature is indicative of proline protection against its inactivation.

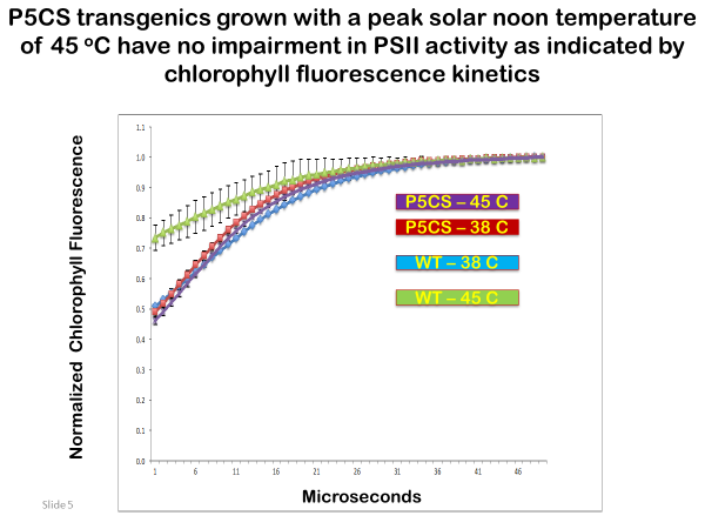

Figure 5.3.6.4: Normalized (Fmax) chlorophyll fluorescence rise kinetics of dark adapted P5CS transgenic and wild-type cells grown at different temperatures.

Chl fluorescence analyses were followed by measurements of growth rates at various temperatures in wild-type and transgenic algae. As shown in figure 5.3.6.5, wild-type Cs-1230 died when grown at a peak solar noon temperature of 45 C. In contrast the P5CS transgenic grew at growth rates at 45 C equivalent to wild type at 38 C, the optimal growth temperature for wild-type Cs-1230. Thus, we achieved an increase in thermal tolerance by 7 C in P5CS transgenics without any impairment in growth. This is a notable achievement since elevated heat tolerance will allow this high biomass yielding algal species (up to 32 gdw/m^2/day in outdoor cultivation) to be cultivated in closed reactor systems where maximum daily temperatures (55 C peak temperatures in Tempe) far exceed Chlorella's normal thermotolerance.

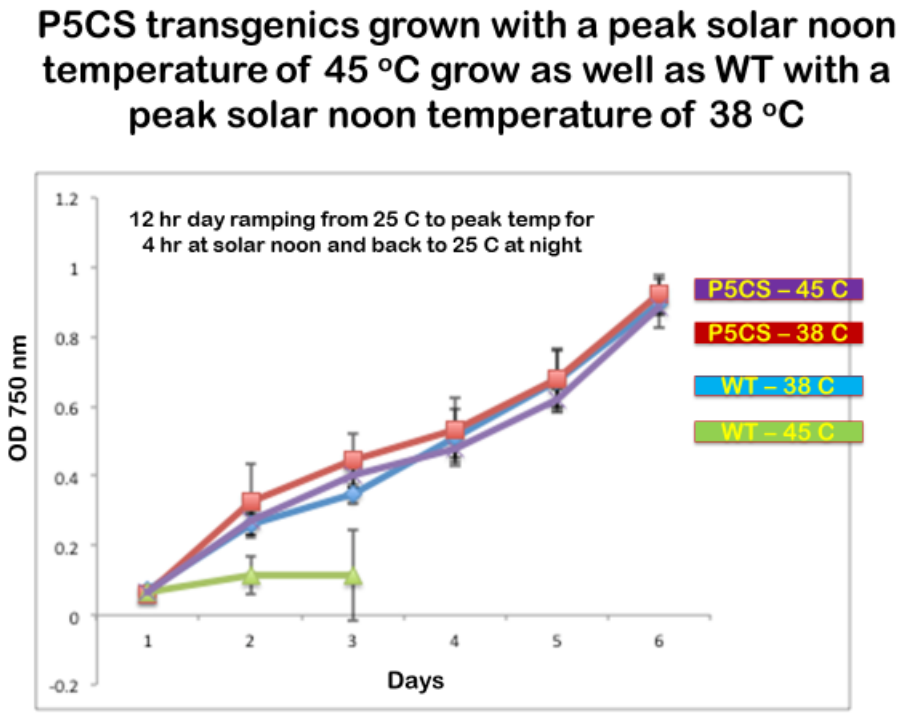

Figure 5.3.6.5: Growth rate of P5CS transgenic and wild-type algae in ePBRs with 12 hr light and 12 hr dark cycle. Temperatures ramped up for 4 hours from 25 C to peak temperature indicated, were held there for 4 hours across solar noon (2,000 uE/m2/sec) and then ramped down over 4 hours back to 25 C, the night temperature.

Conclusions: The P5CS transgenics met our objective for heat tolerance (Fig. 5.3.6.5). We are currently generating additional P5CS transgenics to confirm the generalized case. In one outdoor trial at AzCATI the P5CS transgenics survived daytime temperatures up to 55 C. That experiment has not been repeated.

References:

Siripornadulsil S, Traina S, Verma DP and Sayre RT (2002) Molecular mechanisms of proline-mediated tolerance to toxic heavy metals in transgenic microalgae. *Plant Cell* 14: 2837-2847.

5.3 Strain Development Summary: Overall, the transgenic strain development program achieved the following results:

1) Successful demonstration of enhanced thermotolerance in Cs-1230 transgenics expressing the P5CS gene to enhance cytoplasmic proline levels. This work further demonstrates that quenching ROS generated during a variety of stress conditions by elevated cytoplasmic proline levels can be an effective means to enhance abiotic stress tolerance and achieve high algal biomass growth rates in closed bioreactors having elevated temperatures, substantially reducing water loss from ponds. In one

outdoor field trial at AxCATI P5CS transgenics grew well at peak temperatures up to 55 C when wild-type algae all died. Following generation of additional P5CS transgenics and reconfirmation of the enhanced thermotolerance in P5CS transgenics, we anticipate publishing these results. Given that proline is a natural metabolite, we do not anticipate any human or animal health issues regards the use of these transgenics.

2) Successful demonstration of enhanced growth and oil accumulation in β-glucosidase expressing transgenic Cs-1230 algae fed cellobiose (non-food sugar). We demonstrate that a ten-hour, post-harvest cellobiose boost using concentrated algae can increase oil yields up to 3.3-fold without concern for biocontaminant metabolism of cellobiose due to the high algal concentrations (20X) achieved after initial post-harvest algal concentration.
3) Successful demonstration of a knock-out gene, photoropin (PHOT), conferring elevated global regulation of genes involved in enhanced growth (2X) in *Chlamydomonas*. We determined that Cs-1230 has two identical Phot genes and we are currently attempting to knock out the PHOT genes as well as overexpress growth regulatory control genes early in the PHOT-mediated signal transduction pathway to enhance growth in Cs-1230. This transgenic work has been delayed, as well as the following transgenic experiment, due to a barrier in transformation efficiency that was only recently overcome. This work has led to a patent application.
4) Successful identification of multi-functional AMPs that can deter growth of rotifers and *Vampirovibrio* but not impede growth of Cs-1230. Transformation of Cs-1230 to express these AMP genes is underway.
5) Successful demonstration of a caffeine regulated suicide gene switch technology in the model organism *Chlamydomonas* that is currently being further optimized in Cs-1228. The cost of caffeine use in ponds is estimated to account for 1.5% of the total algal biomass production costs.

5.4 Harvesting and dewatering

***Task summary**:*

The objective of this section was to demonstrate innovative harvesting and dewatering systems. The expected outcome was to achieve harvesting algae resulting in 5% solids, dewatering resulting in at least 20% solids, and the total energy of harvesting and dewatering less than 10% of calorific value of algae. The major research activities performed under this task include: harvesting 3 strains with different flocculants, then dewatering the flocculated biomass with centrifugation. The major results obtained under this task include: (1) harvesting *Chlorella sorokiniana* UTEX 1602 (1g/L) by applying cationic Polyacrylamide (CPAM) in a dose of 15mg/L with output of ~90% in flocculation efficiency and ~5% solids; (2) harvesting *Galdieria sulphuraria* 5587.1 at high pH with the optimum dose of NaOH at 0.44g/L and an output of ~80% in flocculation efficiency and 8 % solids ; (3) harvesting *Kirchneriella cornutum* by adding HNO_3 with output of ~90% in flocculation efficiency and ~2% solids; (4) proving that the dose of HNO_3 used was feasible by recycling in the subsequent culture; (5) algae paste concentration achieved after centrifugation was ~32% solids. The centrifugation performance of flocculated biomass of *Galdieria sulphuraria* 5587.1 was deemed acceptable because it only consumed between 0.125 ~0.25 kWh/kg biomass, less than 10% of algae combustion value (generally ~10 kWh/kg biomass); (6) The total energy demand of harvesting and dewatering was less than 10% of algae calorific value. Therefore, the anticipated targets were achieved. Sections 5.4.1 – 5.4.4 provide more detailed information.

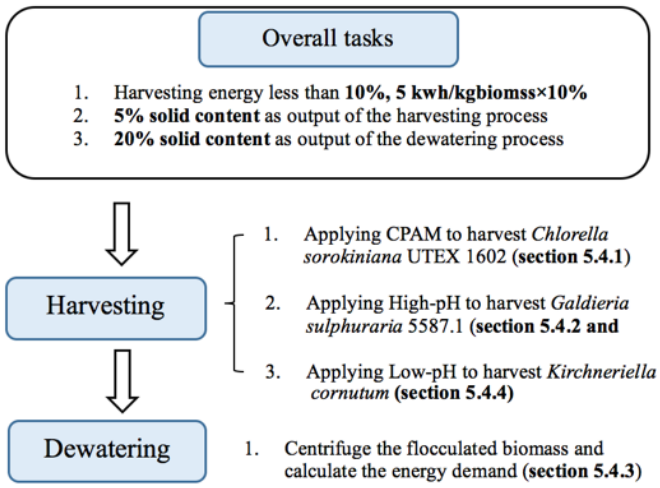

In order to accomplish the goals of the proposal, flocculation was chosen as a promising dewatering process to reduce the great energy demand of centrifugation, for its high compressibility of the treated volume, short operation time. In addition, the characteristic of algae also was the main reason, that is, low biomass density with great amount of volume in industrial scale, negative charged cell wall leading to stable suspension. However, traditional cationic flocculants, like $FeCl_3$ and $Al_2(SO_4)_3$, were not feasible for its huge dose (>0.5g/L), exorbitant cost and residual harmful ions in biomass as well as treated medium. Thus, an

innovative flocculation should be developed to fulfill these goals. CPAM and pH-inducing flocculation were investigated in these research activities.
We harvested *Chlorella sorokiniana* UTEX 1602 (1g/L) by applying cationic polyacrylamide (CPAM) in a dose of 15mg/L with output of ~95% in flocculation efficiency and ~5% solids. *Galdieria sulphuraria* 5587.1 can be flocculated at high pH, which mainly was due to the forming of $Mg(OH)_2$ positively charged colloids. With the optimum dose of NaOH at 0.44g/L, a flocculation efficiency of ~80% and 8 % of solid content in the flocculated biomass was achieved. Furthermore, a ~32% of solid content was achieved after centrifugation of the pre-flocculated culture. The centrifugation performance of flocculated biomass of *Galdieria sulphuraria* 5587.1 was acceptable because it only consumed between 0.125 ~0.25 kWh/kg biomass, less than 10% of algae combustion value (generally ~10 kWh/kg biomass). *Kirchneriella cornutum* can be flocculated at low pH of ~2.5, mainly because $[H^+]$ in acid condition bonded the cell wall thus decreasing Zeta potential then flocculating algae biomass. The dose of HNO_3 used to flocculate *Kirchneriella cornutum* was equivalent to that of BM11's; thus, it is feasible that this process may be accomplished by coupling the culture and subsequent flocculation using the medium. Therefore, the anticipated target was achieved. Sections 5.4.1 to 5.4.4 provide more detailed information.

5.4.1 Flocculation performance in harvesting *Chlorella sorokiniana* UTEX 1602

In order to tackle the disadvantages of traditional flocculants, two organic polymer flocculants were studied for their advantage of high charge density, CPAM (cationic Polyacrylamide) and CQAC (cationic quaternary ammonium salt of chitosan). *Chlorella sorokiniana* UTEX1602 was cultured in a 10 L flat acrylic panel (L x H x W= 52 x 45 x 8 cm) using BBM medium with constant illumination of ~75μmol/m^2 for 14 days. When the biomass density achieved a value of ~1g/L (plateau) the pH was adjusted to 7.0, and then several different doses of CPAM (cationic Polyacrylamide) and CQAC (cationic quaternary ammonium salt of chitosan) were added. A standard stirred flocculation test was conducted using the methods described as standard jar tests, and the flocculation efficiency was determined after 2 hours settling.

Both flocculants were found to be suitable for harvesting *C. sorokiniana* UTEX1602, because the flocculation efficiency of both flocculants arrived at its ultimate value (90~95%) in the dose range of 10 ~15 mg/L. Less or more than this dose both produced a smaller flocculation efficiency. However, owing to its lower cost, CPAM (~2 US dollar/kg) is considered more viable than CQAC (~26 US dollar/kg). Moreover, CPAM is not a single type but a whole family of variable flocculants that may be custom fit for specific algae suspensions or different strains. Additionally, CPAM also produced a high concentration factor of ~50 (data not shown in the figure), thus produced ~5% solids in the flocculated biomass (concentration factor × biomass density× flocculation efficiency). Therefore, CPAM was considered for further optimizing.

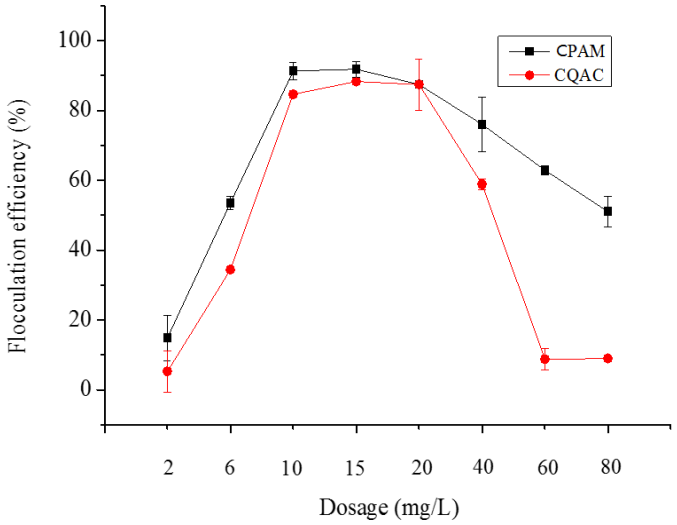

Figure 5.4.1 Flocculation Efficiency of CQAC and CPAM for harvesting *Chlorella sorokiniana* UTEX1602 (~1g/L biomass density and pH = 7.0)

5.4.1a Optimizing pH for harvesting Chlorella sorokiniana with CPAM

Since most of the flocculants perform exceptionally under certain pH condition, and cell wall components of algae also have their isoelectric point, so an optimum pH should improve CPAM's performance in flocculation efficiency. *Chlorella sorokiniana* UTEX1602 was cultured in a 10 L flat acrylic panel (L x H x W= 52 x 45 x 8 cm) using BBM medium with constant illumination of ~75µmol/m^2 for 14 days. When the biomass density achieved a value of ~1g/L (plateau) the pH was adjusted to 4.0, 4.5, 5.0, 5.5, 6.0, 6.5, 7.5 and 8.0, respectively. Following, 15mg/L CPAM (cationic Polyacrylamide) were added to the corresponding algae suspensions. A standard stirred flocculation test was conducted and the flocculation efficiency was determined after 2 hours.

The pH value of 4.0 was determined to be the most suitable among pH range for achieving the highest flocculation efficiency. This result can be explained by the Zeta potential hypothesis [1, 2], that indicates that Zeta potential of most algae strains decreases to 0 mV when lowering the pH of the culture. This is further elucidated by the isoelectric point of protein and polysaccharide components in the cell wall. Since the work [1] [2] showed that the uronic acid content of the extracellular acid and surface area possessed a positive relationship with DAF's efficiency. It also made sense that quite a great amount of protein with isoelectric points close to 4.0 possess lowest charge density at pH 4.

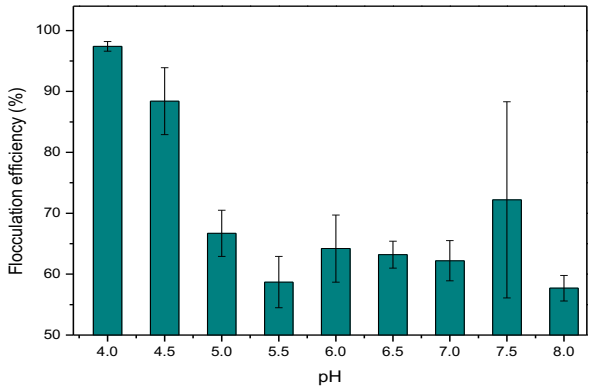

Figure 5.4.2 Flocculation Efficiency of CPAM (15mg/L) for harvesting *Chlorella sorokiniana* UTEX1602 (1g/L) under different pH conditions

Table 5.4.1 Different Algae Cell Characteristics [2]

Particle	Size (mm)	Colonial	Shape	Zeta potential, ζ (mV)
Cyanobacteria				
Microcystis aeruginosa	3~7	Globular	Sphere	−25~−30
Microcystis	N/A[1)]	Globular	Sphere	−7.5~−26
Synechocystis minuscula	6	Single cell or micro-colonies	Sphere	−22.3, −25.8, −32.2
Synechocystis minuscula	5	Single cell or micro-colonies	Sphere	−14.9~−24.8
Green algae				
Chlorella vulgaris	5.3	Single cell	Sphere	−10.0, −19.8 (log growth), −17.4 (stationary growth)
Chlorella sp.	3.5	Single cell	Sphere	−10, −14.9~−19.8
Scenedesmus quadricauda	13.1	Row(s) of 4~16 cells with spinal appendages	Ellipsoidal	−25~−35
Scenedesmus obliquus	3~9(*d*)[2)], 6~17(*l*)[3)]	Row(s) of 4~16 cells with spinal appendages	Ellipsoidal	−23~−25
Selenastrum	2~3(*d*), 6~8(*l*)	Single cell	Crescent	−35
Diatoms				
Cyclotella sp.	6.1	Chain	Sphere	−19.8~−22.3
Stephanodiscus hantzscii	8~20(*d*), 40(spines)	Chain	Disc with spines	−12.4
Fragillaria crotonensis	2~3(*d*), 40~150(*l*)	Cells joined along length	Elongated	−18.6
Nitzschia linearis	35(*l*)	–	Elongated	−30 (initial)~−35 (log growth) −28 (stationary growth)
Syendra acus	4.5~6(*d*), 100~300(*l*)	–	Needle	−34~−40

Note: 1) N/A denotes not available, which means that the data were not given by the references; 2) Diameter; 3) Length.

Further pH optimization trials were developed for harvesting algae with CPAM. The *Chlorella sorokiniana* culture was prepared (~0.5g/L) as previously detailed, then the pH was adjusted to 4.0, 4.5 and 5.0 with HCl (~2M), respectively. Next, several different doses of CPAM (4, 6, 8, 10, 12, 14, 16 mg/L) were added in order to induce flocculation. A standard stirred flocculation test was conducted and the flocculation efficiency was determined after 2 hours.

The flocculation efficiencies of CPAM under pH conditions of 4.0 and 4.5 were very similar with doses ranging from 4.0 to 16 mg/L. However, the flocculation efficiencies at pH of 5 were significantly lower. The pH of 4.0 and 4.5 were better, potentially owing to the fact that the isoelectric point of *Chlorella* is equal to 4.0 [3]. In view of the cost of the acid used, pH 4.5 would be the optimum condition and HNO_3 and/or H_3PO_4 were preferentially used for they can be reused as nutrients in the subsequent culture [3]. And by coupling a nutrient reusing subsequent culture, CPAM showed greater feasibility in industrial scale. So in this case, only 4mg/L dose of CPAM were demanded to harvest *Chlorella sorokiniana* UTEX 1602 (~0.5g/L).

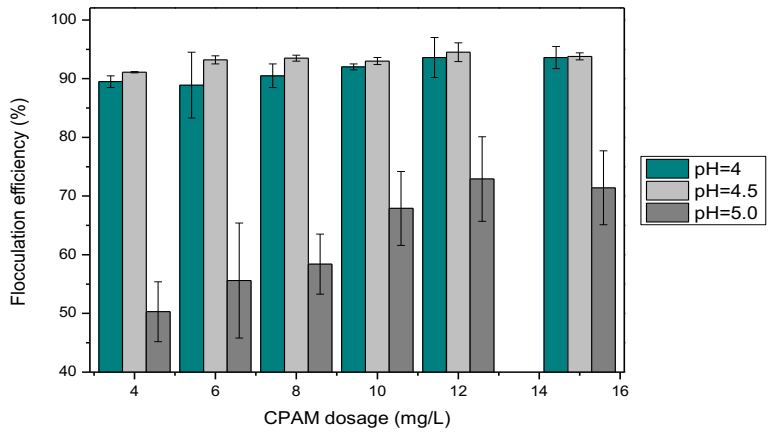

Figure 5.4.3 pH Optimizing (4.0~5.0) for Flocculation Efficiency with varying dosages of CPAM (4 ~16 mg/L) for harvesting *Chlorella sorokiniana* UTEX1602 (0.5g/L)

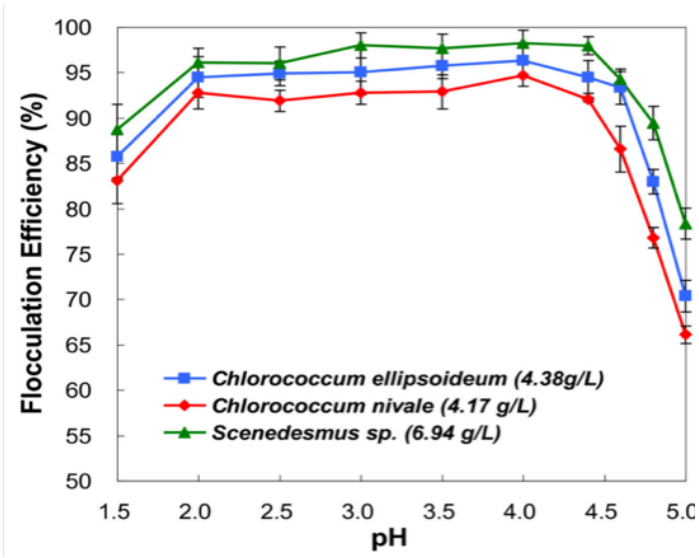

Figure 5.4.4 Flocculation Efficiencies as a function of pH for different microalgae [3]

5.4.1b The Effect of pre-oxidation on Flocculation Efficiency of CPAM when harvesting Chlorella sorokiniana

A previous study [2] reported that a pre-oxidation treatment of the culture could improve the flocculants' efficiency during the harvesting stage. The *Chlorella sorokiniana* UTEX 1602 cultures (~0.5g/L) were prepared as detailed before. After adjusting the pH to 7.0, using various dosages of H_2O_2 (~30%) and NaClO (~12%), the cultures were subjected to pre-oxidation

treatments for 30 min. Then, the CPAM (10 mg/L) was added into the treated cultures, and a standard stirred flocculation test was conducted. The flocculation efficiency was measured after 2 hours.

The NaClO (~12%) solution was deemed more suitable to improve CPAM's flocculation efficiency. This may be due to its stronger reactivity, and also owing to the lower dose required that ultimately represents lower costs.

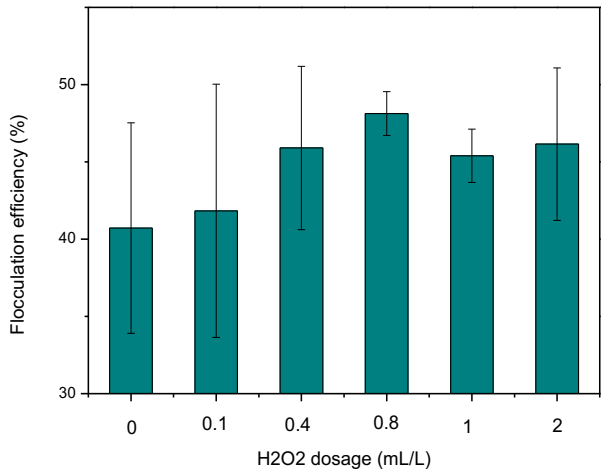

Figure 5.4.5 Effect of H_2O_2 on CPAM's (10 mg/L) flocculation efficiency when harvesting *Chlorella sorokiniana*(0.5g/L)

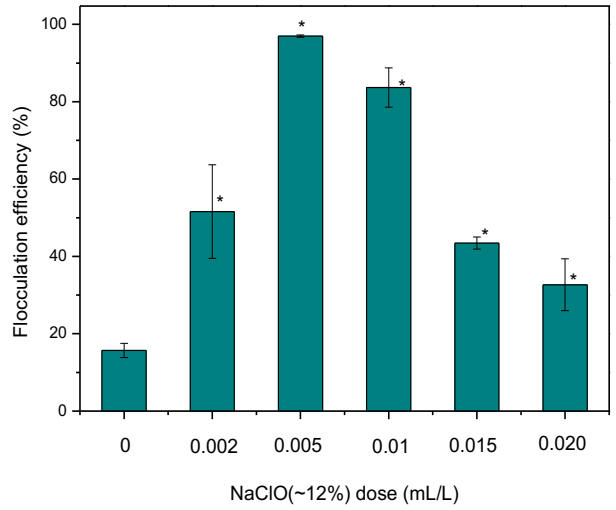

Figure 5.4.6 Effect of NaClO on CPAM's (10 mg/L) flocculation efficiency when harvesting *Chlorella sorokiniana* UTEX 1602

Table 5.4.2 Evaluation of H_2O_2 and NaClO solutions for pre-oxidation Treatment to improve the CPAM's flocculation efficiency

	CPAM dose*	CPAM cost	Flocculation efficiency	Oxidant dose	Oxidant dose	Total cost
H_2O2	20g	0.7 RMB	48%	20 L	40RMB	40.70RMB
NaClO	20g	0.7 RMB	95%	0.125 L	0.05RMB	0.75RMB

*For 1 kg of *Chlorella sorokiniana* UTEX 1602 at 0.5 g/L in biomass density.

5.4.2 High pH *Galdieria sulphuraria* induced flocculation

Galdieria sulphuraria 5587.1 was cultured in a 1000 L flat plastic panel (L x H x W= 12 x 1.3 x 4 m) using CM medium for 3 months. When the biomass density achieved a value of ~4g/L, the pH of the culture samples was adjusted from 2 to 9 by adding NaOH solution (2 M). Following, the samples were transferred into individual receptacles were the recovery efficiency trials were developed. After settling for 1, 2, 4 and 24 hours, the cultures were sampled at 1/3 height from the bottom of jars. Then, the flocculation efficiency (FE) was determined using the equation listed below:

$$FE = 1 - \frac{OD_{750\ sample}}{OD_{750\ original}} * 100\%$$

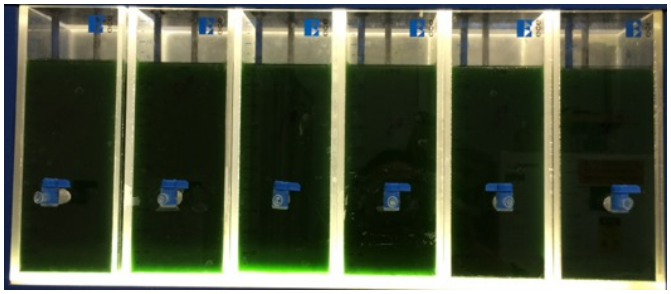

Figure 5.4.7 Experimental set-up for Standard Jar Test

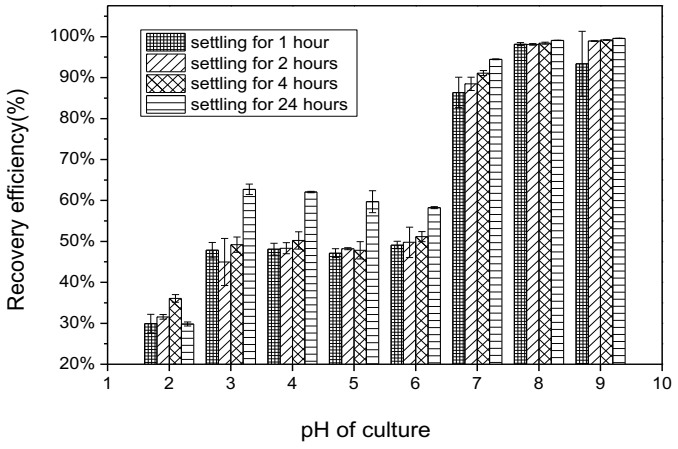

Figure 5.4.8 Recovery Efficiency of *Galdieria sulphuraria* 5587.1 at various pH

As shown in the figure 5.4.9, flocculation started at pH 7 and gradually increased at higher values. The flocculation efficiency at pH 7 was ~90% with 1 hour settling, and then increased to ~92% after 4 hours. However, a 4-hour settling period is too extensive and is not acceptable for industrial applications. In addition, for achieving higher pH values (8 – 9), larger quantities of NaOH would be required. Nonetheless, it was demonstrated that high pH does induce the flocculation of *Galdieria sulphuraria* 5587.1, and the pH 7 would be the most suitable condition.

5.4.2a Optimizing the NaOH dose used for inducing flocculation of Galdieria sulphuraria 5587.1

Galdieria sulphuraria 5587.1 was cultured as previously detailed. Gradual addition of the NaOH solution (2 M) was developed and culture pH was closely monitored. The recovery efficiencies were determined at various settling times of 0.5, 1, 2 and 3 hours.

The optimum dose of NaOH was found to be 11 mM, equivalent to 0.44g/L. Based on the average price of NaOH (~300 US dollar/kg), the High-pH flocculation process expense is around 0.041 US dollar/kg biomass equaled to 0.25 kWh/kg biomass (assumed electricity price 16 cent/kWh).

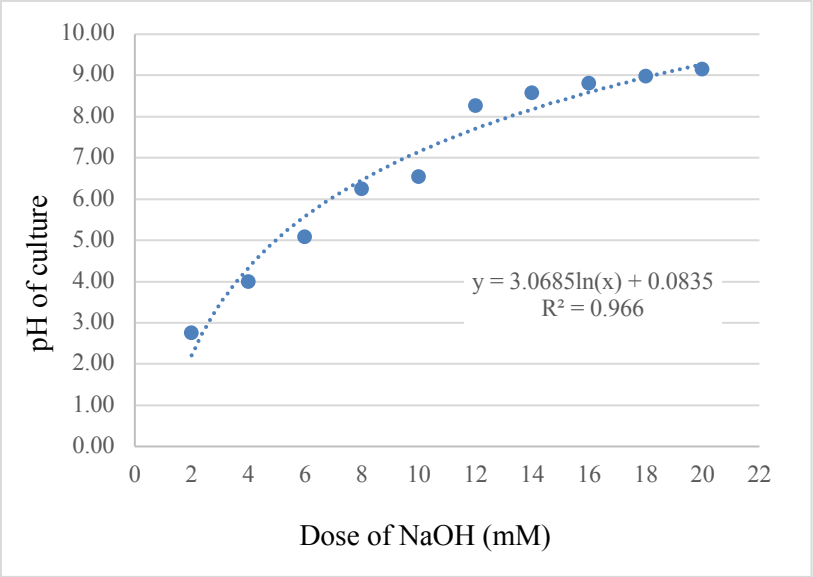

Figure 5.4.9 Optimizing the NaOH dose for High pH flocculation of *Galdieria sulphuraria* 5587.1

As disclosed in several published papers, the High-pH flocculation mechanism is characterized by the formation of positively charged colloids of $Mg(OH)_2$ during the increase in pH, followed by the adsorption of these unto the algae cells. Thus, the presence of EDTA molecules should restrict this process. Another culture set was prepared; the pH of the culture samples was adjusted to 9. Following, several doses of EDTA-$2H_2O$ were supplied into the culture. With a settling period of 2 hours, the flocculation efficiency was determined.

The main role of EDTA-$2H_2O$ is functioning as a sequestering agent, that bonds the insoluble sediment. By assessing the CM growth medium components, it was determined that only the $[Mg^{2+}]$ accounted for the insoluble colloids that could be chelated by EDTA-$2H_2O$. Moreover, the research [4] related to high-pH flocculation in algae harvesting processes, have established that the either a precipitate of $Mg(OH)_2$ or $Ca_3(PO_4)_2$ induced the flocculation process. Although the $[Fe^{3+}]$ could potentially play a role in the flocculation, this can be neglected because of the very low concentration. According to most Ferric-flocculation reported, the process was induced when the concentration was at least 0.5g/L of $FeCl_3$. Thus, based on the Ksp of $Mg(OH)_2$ we inferred that at a certain pH, the $[Mg^{2+}]$ will transition into $Mg(OH)_2$. The calculation was listed as bellow:

$$Ksp = 1.2 \times 10^{-11} = 1.01 \times 10^{-3} \times [OH^-]^2$$

$$\Downarrow$$

$$[OH^-] = 1.18 \times 10^{-4}$$

$$\Downarrow$$

$$pH = 8.072$$

In addition, as shown in figure 5.4.10, flocculation efficiency was inhibited by adding EDTA-$2H_2O$, and reached its minimum at dose of 4.5 g/L. However, an EDTA-$2H_2O$ dose of 3.5 g/L may have chelated all the $Mg(OH)_2$ sediment, since the flocculation efficiencies between doses of 3.5, 4.0 and 4.5 g/L are very similar. With an EDTA-$2H_2O$ dose of 3.5 g/L, the amount of $Mg(OH)_2$ formed at pH 9 should be equivalent to 10.6mM (3.5g/L/MW $_{EDTA\text{-}2H2O}$). This means that at least 21.2mM NaOH was needed to induce the sedimentation of $Mg(OH)_2$; this value is approximately equal to the NaOH dose used (20 mM at pH 9). Thus, the high-pH inducing flocculation of *Galdieria sulphuraria* 5587.1 should be induced by $Mg(OH)_2$ sediment during pH increasing.

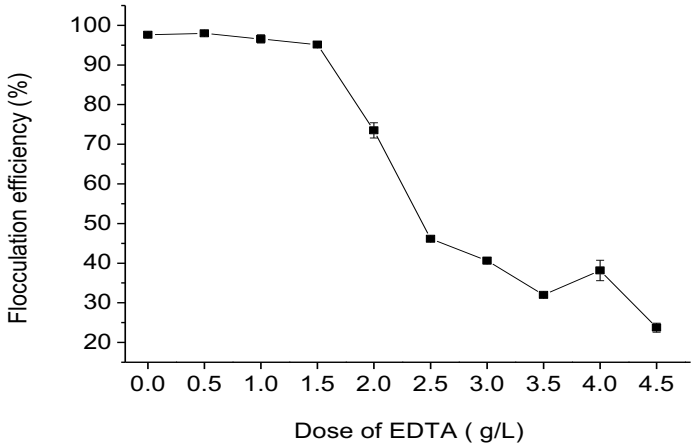

Figure 5.4.10 Flocculation Efficiency of *Galdieria sulphuraria* 5587.1 during the High-pH induced with various adding EDTA•$2H_2O$

Table 5.4.3 Cyanidium Medium used to cultivate *Galdieria sulphuraria* 5587.1

Chem. Compound in 1 Liter Cyanidium Medium (CM)			MW	mM	ppm	Elem.
Ammonium sulfate	$(NH_4)_2SO_4$	1.32 g	132.14	9.99	279.84	N
Potassium phosphate monobasic	KH_2PO_4	0.10 g	136.09	0.73	22.76	P
Sodium Chloride	NaCl	0.12 g	58.44	2.05	47.21	Na
Magnesium sulfate	$MgSO_4 \cdot 7H_2O$	0.25 g	246.48	1.01	24.65	Mg
Calcium Chloride	$CaCl_2 \cdot 2H_2O$	0.07 g	147.02	0.48	19.08	Ca
Ferric chloride solution (1.45 g/L)	$FeCl_3$	1.0 mL	270.30	0.0054	0.3	Fe
Nitsch's trace elements (1000X)		1.0 mL				
Adjust pH to 2.5 with ca. 200-500 µL H_2SO_4 (Conc.) before autoclave. **Add 0.25 mL F/2 vitamins solution (filtered sterilized) before use.**						

5.4.2b Optimizing the pH for ideal Solid contents in the Flocculated Cultures

The target of the project was a harvesting process that would yield a solids content of no less than 5%. Thus, optimizing the process to determine the most suitable pH was required.
Galdieria sulphuraria 5587.1 was cultured as previously described, and the pH of the culture samples was adjusted to high values from 7 to 9.5. Following, flocculation efficiency was and the solids concentration factor were measured at various settling times. The concentration factor was determined with the equation listed:

$$Concentration\ \ Factor = \frac{Height_{total}}{Height_{flocculated\ layer}}$$

And the solid content was estimated using the equation:

$$Solid\ content = Biomass\ density * Flocculation\ efficiency * Concentration\ factor$$

As shown in the figure 5.4.12, the flocculation efficiency increased from pH 7 (~80%) and reached a maximum at pH 9 – 9.5 (~97%). However, these high pH values were not considered the optimal conditions because the concentration factor that directly impacts the solid content and the subsequent dewatering process, exhibits an opposite trend to the flocculation efficiency. As illustrated by figure 5.4.13, the concentration factor decreased as the pH increased, reaching a minimum at pH 9.5 (~6). Consequently, the optimum conditions were determined to be a pH 7 with a 3 hour settling period. These parameters were then used to estimate the solid content; approximately 8% (=80%*4g/L*25).

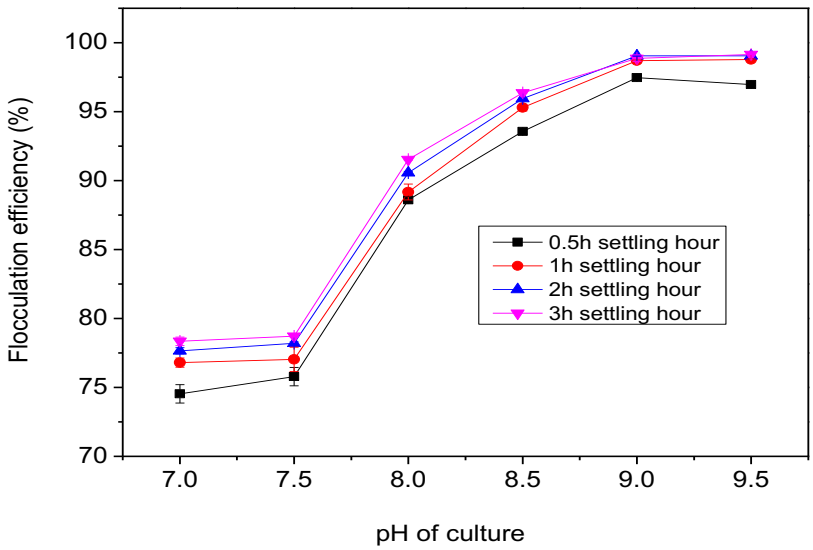

Figure 5.4.11 Flocculation Efficiency of *G. sulphuraria* 5587.1 at various pH

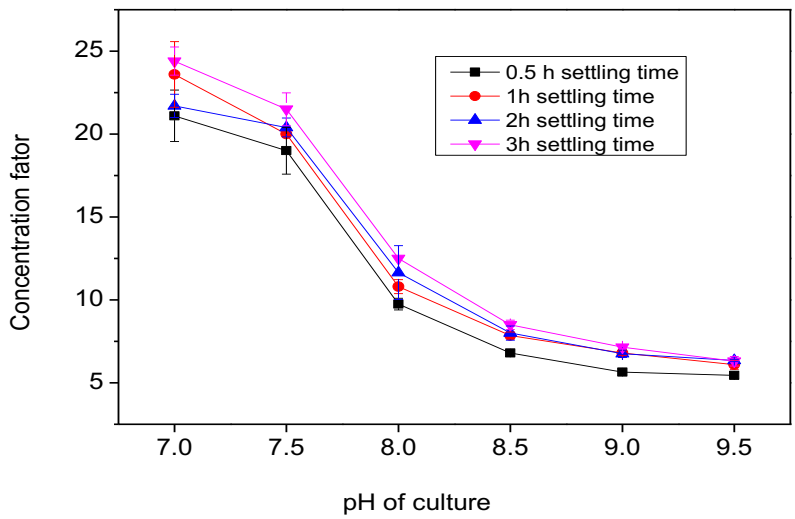

Figure 5.4.12 Concentration Factor of *G. sulphuraria* 5587.1 at various pH conditions

5.4.2c Optimizing the Settling Time for increased Concentration Factors

Owing to the significance that the concentration factor has in decreasing the treated volume for dewatering process (such as filtration and centrifugation), an optimization for the settling time was developed.
Galdieria sulphuraria 5587.1 was cultured as previously described, and the pH of the culture samples was adjusted to 8.5. Following, the culture was poured into the acrylic settling device. The settling column was fitted with seven mini taps installed at specific heights from the bottom (1.5, 3, 5, 10, 20 and 25 cm). Following, using the taps, the culture was sampled at various settling times.

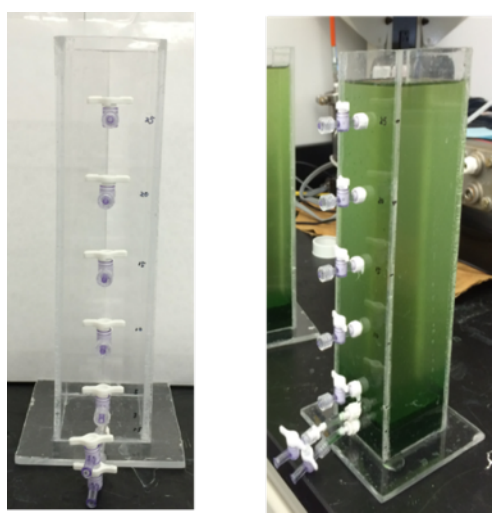

Figure 5.4.13 Settling Time measuring device (7.1 x 7.1 x 30 cm)

As shown in Figure 5.4.14, most of the biomass was concentrated in the 0 –3cm layer after 2 hours. This proved that high-pH flocculation effectively decreases the treated volume, thus would inevitably sharply cut down the harvesting energy required in centrifugation. In addition, at higher settling times, the concentration factor fluctuated from 10~20. However, the concentration factor does not increase by the extending settling time. This concurs with previous reports and other research. This is because the flocculated cells possessed electron double layers that repel each other and inhibit unlimited compression.

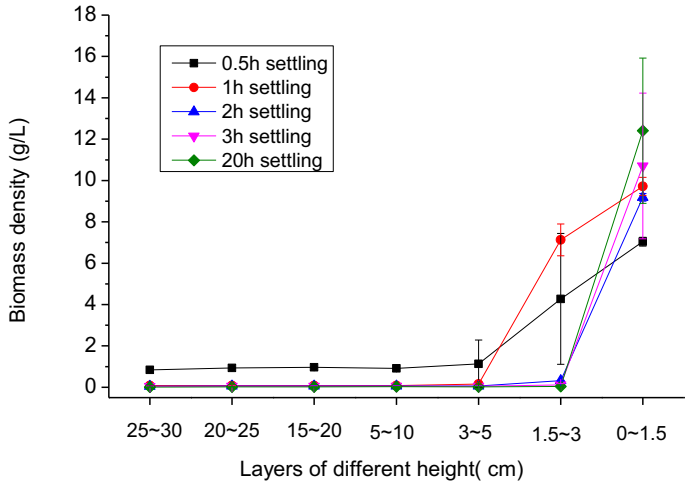

Figure 5.4.14 Biomass Distribution during the settling process of High-pH (~8.5) flocculation

5.4.3 Scale up the High-pH flocculation process

5.4.3a Scale up the High-pH flocculation process

Approximately 500 L of *Galdieria* culture at ~ 1.2 g/L were collected and poured into a cone-bottom tank (shown in Figure 5.4.27). Then, 524g NaOH and 124.76g $MgSO_4 \cdot H_2O$ were added accompanied by strong stirring for 10 min. Settling as allowed for 4 hours. Next, 30 L of the flocculated layer was slowly drained and collected through the bottom. The biomass density of the flocculated culture was determined.

Figure 5.4.15 Cone-bottom tank used to scale up high-pH flocculation

The biomass density of concentrated culture was ~17.6 g/L, thus 528 g biomass was concentrated in 30 L. A harvesting efficiency of ~88% was obtained. The calculation process is detailed as:

- Original biomass in 500L, 1.2 g/L*500 L=600 g;

- Biomass concentrated in 30L, 17.6 g/L*30 L=528 g;

- Harvesting efficiency=528/600=88%.

5.4.3b Dewatering the flocculated culture

The centrifugation performance of the attained concentrated culture was also explored. The dewatering process was conducted in a Laboratory centrifuge (Allegra X-15R centrifuge). The untreated culture was used as control, and the experimental settings were:
- For concentrated culture; 500, 625 and 750 rpm were respectively applied, with variable operation times of 2, 4, 6, 8, 10 and 12 min.
- The control groups were centrifuged at 1000, 1250 and 1500 rpm, respectively, with variable operation times of 2, 4, 6, 8, 10 and 12 min.

Based on the results, the parameter of minimum speed and operation time were used into comparing the energy demands. As shown in the Figure 5.4.16, the drum is needed to start and

keeps running. So the power demand of the drum should contain 2 sections, N_{start} and N_{runing}. They could be calculated in the following equations:

$$Ns=N1+N3+N4; \qquad Nr=N2+N3+N4;$$

$$N1=\frac{Jr\omega^2}{2t}; \qquad N2=Q\,\rho\,\omega^2 r^2;$$

$$N3=\frac{1}{2}\omega f(P1d1+P2d2); \qquad N4=11.3*10^{-3}\,\rho g L\omega^3(R'4+R_0^4)$$

Where:
Ns is the start-up power; Nr is the running power; N1 is the start-up power of the drum; N2 is the acceleration power of the materials and N3 is the power of bearings' friction
N4 is the power of friction between air and drum
Jr is the moment of inertia of the drum; Ω is angular velocity; *t* is the time of start time
Q, the flow of the input; p, the density of the input; f, friction factor
P1 and P2, are the loading of the 2 bearings

The starting power can be neglected in long runs at large scale. For instance, industrial centrifuges only need 2~5 min to arrive at its working speed, and usually keep working 2~8 hours. Thus, a simplified calculating process would be:

$$N' \approx Nr = Q\,\rho\,\omega^2 r^2 + \frac{1}{2}\omega f(P1d1+P2d2) + 11.3*10^{-3}\,\rho g L\omega^3(R'4+R_0^4)$$

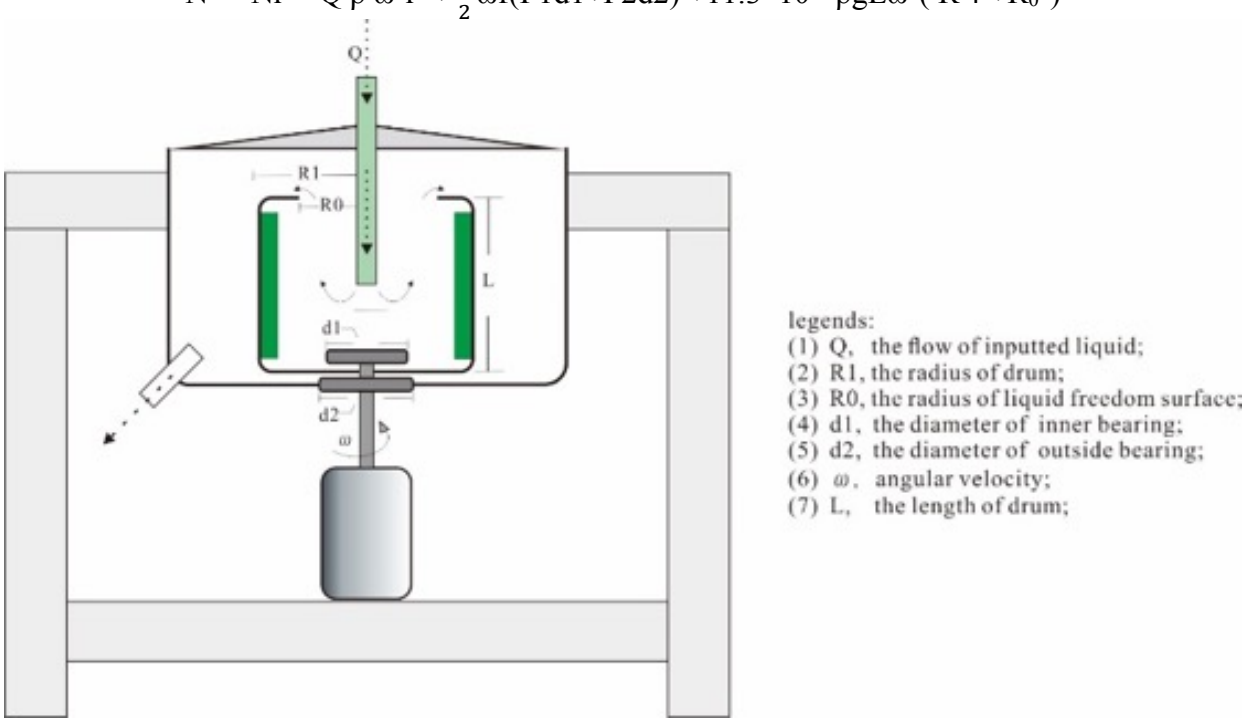

Figure 5.4.16 the diagram of batch-type sedimentation centrifuge

A recovery efficiency of ~90% can be obtained at 750 rpm for 4 min for flocculated culture but at 1500 rpm for 4min for un-treated culture. So the energy demand of the flocculated culture in a certain flow and running time should be calculated as:

$$E_{flocculated} = Q\,\rho\,750^2 r^2 *4 + \frac{1}{2}750\,f(P1d1+P2d2)*4 + 11.3*10^{-3}\,\rho g L750^3(R'4 + R_0^4)*4$$

Similarly, the energy demand of the un-flocculated culture in a certain flow and running time should be calculated as:

$$E_{un\text{-}flocculated} = Q\,\rho\,1500^2 r^2 *4 + \frac{1}{2}1500\,f(P1d1+P2d2)*4 + 11.3*10^{-3}\,\rho g L1500^3(R'4 + R_0^4)*4$$

Obviously, $E_{flocculated} < 1/2\ E_{un\text{-}flocculated}$. Additionally, the biomass density of the flocculated culture is 16 times more than the un-flocculated culture. Consequently, the comparison in energy demand per unit quality among two groups should be calculated as:

$$E_{flocculated\ per\ unit\ quality} < 1/2 * 1/16\ E_{un\text{-}flocculated\ per\ unit\ quality},$$

$$E_{flocculated\ per\ unit\ quality} < 1/32\ E_{un\text{-}flocculated\ per\ unit\ quality}$$

According the literature related to algae centrifugation energy demand, most scientist believe that 4~8 kWh/kg biomass was needed. Thus, we can infer that the total energy demand of high-pH flocculation as well as sequent centrifugation is 0.125~0.25 kWh/kg biomass. The algae paste from concentration after centrifugation was ~ 32.2%.

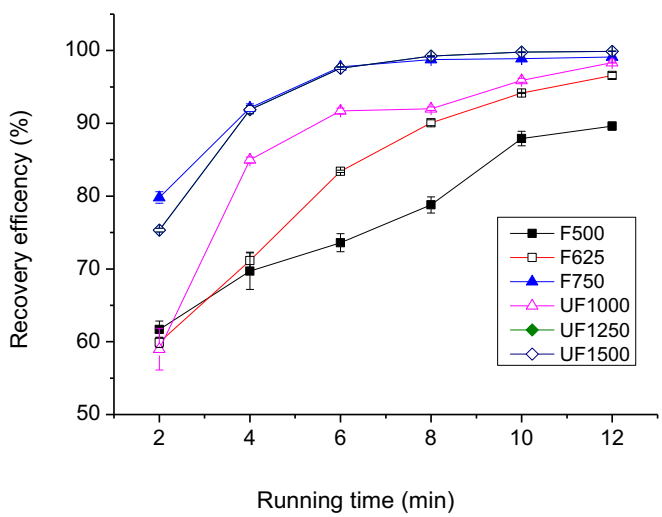

Figure 5.4.17 Centrifugation Performance of *G. sulphuraria* 5587.1 culture
(F500 refers to 500 rpm flocculated culture; UF 1000 refers to 1000 rpm un-flocculated culture)

5.4.4 Harvesting *Kirchneriella* sp. by low-pH and recycling the used HNO_3

Dr. Chenwu Zhang revealed an interesting phenomenon [5], in which certain strains of microalgae can be flocculated by simply adding acid. Correspondingly, it was found that *Kirchneriella* sp. also possesses this similar behavior. Thus, a low-pH-induced flocculation and a following sequent N-resource recycling from the used medium was developed.

Kirchneriella sp. culture (~ 1.8 g/L) was prepared, and then the pH was adjusted between 2.5 – 9, by adding 1.5 M HNO_3. Next, the samples were poured into standard jars, were the recovery efficiency was determined at various settling times. Additionally, another batch of prepared culture with a biomass density of ~4.2, was treated with 1.5 M HNO_3, while pH was monitored at different doses of acid.

As shown in figure 5.4.18, the highest flocculation efficiency was obtained at a pH of 2.5. This result concurs with the work developed by Dr. Chengwu Zhang (Jinan University, Guangzhou China), in which three fresh algae strains (*Chlorococcum nivale, Chlorococcum ellipsoideum*, *Scenedesmus* sp.) were harvested at a flocculation efficiency of ~90% with a low pH of ~2.0. In this study, the author believed that $[H^+]$ bonded to the cell wall and decreased cells' Zeta potential.

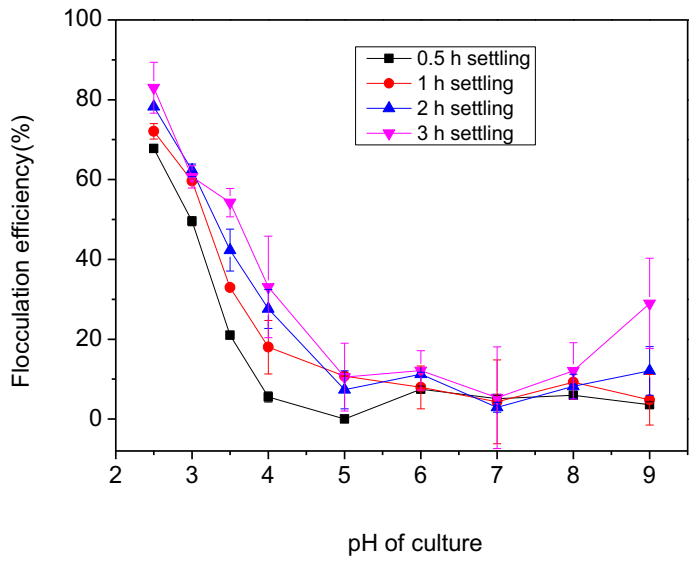

Figure 5.4.18 Flocculation Efficiency of *Kirchneriella* sp. at various pH

According to Figure 5.4.19, the practical dose of HNO_3 is higher than the theoretical dose. That means that there are certain ions groups that adsorbed $[H^+]$ existing in this culture. The primary purpose of this trial was to use less HNO_3 to flocculate biomass, then recycling the N-resource easily. But the experimental dose is ~9 times more than theoretical demand (2mM). Nevertheless, this result is acceptable, because this value (16.5mM) approximately corresponds to the N concentration of BM11 (17.6mM). Thus, the amount of HNO_3 used for inducing flocculation should be consumed completely in subsequent culture. At last, the work[3] in Dr.

Chengwu Zhang showed that most of algae cells were viable and the N-resource of HNO_3 used to induce flocculation can be uptake in the subsequent culture. And the performance of subsequent culture shew no significant differences with the culture with fresh medium. Therefore, *Kirchneriella cornutum* was more suitable for low-pH harvesting and medium-recycling.

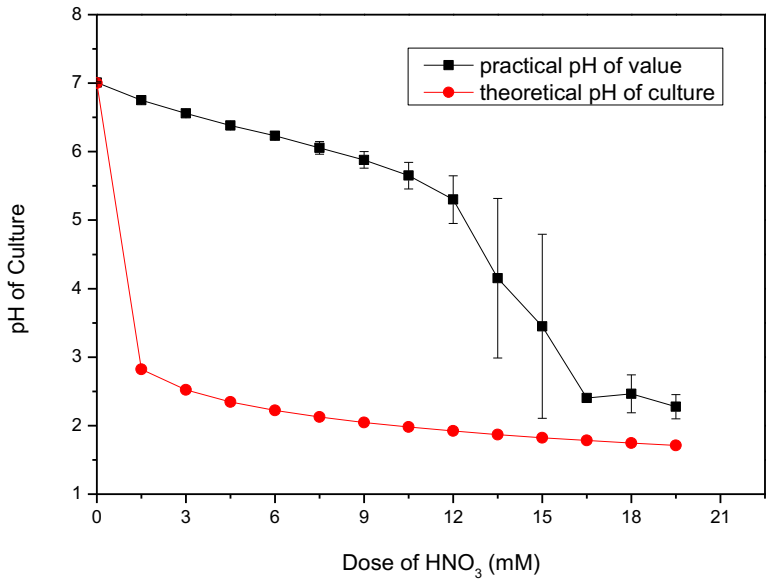

Figure 5.4.19 Dose of HNO_3 used in flocculating *Kirchneriella* sp.

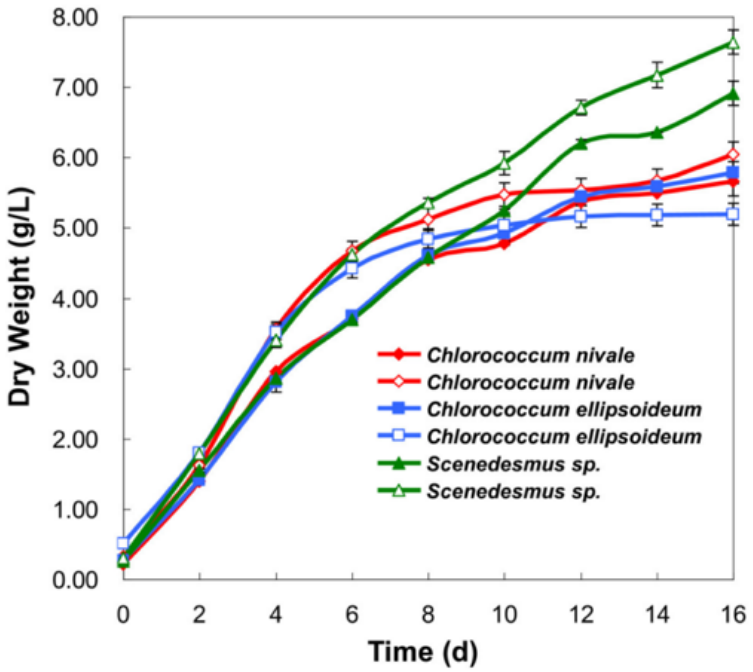

Figure 5.4.20 Growth curve of microalgae: fresh medium (filled points) and flocculated medium (empty points)[3]

5.4.5 References

1. Henderson, R.K., S.A. Parsons, and B. Jefferson, *Successful Removal of Algae through the Control of Zeta Potential.* Separation Science and Technology, 2008. **43**(7): p. 1653-1666.

2. Henderson, R., S.A. Parsons, and B. Jefferson, *The impact of algal properties and pre-oxidation on solid–liquid separation of algae.* Water Research, 2008. **42**(8–9): p. 1827-1845.

3. Liu, J., et al., *Freshwater microalgae harvested via flocculation induced by pH decrease.* Biotechnology for Biofuels, 2013. **6**(1): p. 98.

4. Chen, F., et al., *Using ammonia for algae harvesting and as nutrient in subsequent cultures.* Bioresource Technology, 2012. **121**: p. 298-303.

5. Vandamme, D., et al., *Flocculation of Chlorella vulgaris induced by high pH: Role of magnesium and calcium and practical implications.* Bioresource Technology, 2012. **105**: p. 114-119.

6. Vandamme, D., et al., *Flocculation of Chlorella vulgaris induced by high pH: role of magnesium and calcium and practical implications.* Bioresource Technol, 2012. **105**.

5.5 Analytics

5.5.1 Proximate analysis of biomass

Proximate analysis for all biomass samples was performed using the laboratory analytical procedures promulgated by NREL. Algal tissue samples were lyophilized per "Method C" in the NREL biomass sample preparation guide (http://www.nrel.gov/docs/gen/fy08/42620.pdf). Ash, protein, carbohydrate, and lipid content (as FAME) were performed as specified (http://www.nrel.gov/bioenergy/biomass-compositional-analysis.html). Values determined for feedstock and HTL samples are incorporated into other sections throughout this report.

5.5.2 Elemental analysis of biomass

5.5.3 Compositional Analysis of *C. sorokiniana* Hydrothermal Liquefaction Bio-oils Produced at Variable Temperature

We utilize FT-ICR mass spectrometry at ultrahigh mass resolving power to provide a detailed compositional characterization of hydrothermal liquefaction (HTL) bio-oils of ABY-relevant *Chlorella sorokiniana* 1412 across a variable temperature profile. Quantitation of fatty acids is accomplished by GC/MS and heteroatom containing compounds are identified by direct-infusion electrospray ionization FT-ICR MS in both positive and negative ionization modes. Ultra high mass resolving power ($m/\Delta m50\% > 400{,}000$) of FT-ICR-MS enables observation of several thousand peaks in each mass spectrum and sub-part-per-million mass accuracy combined with Kendrick mass sorting facilitates the assignment of unique elemental compositions to each peak in the spectrum. Detailed characterization provided by FT-ICR MS in terms of heteroatom content, type (number of rings plus double bonds to carbon, Double Bond Equivalents = DBE) and carbon number provides insight to illuminate strategies for enhanced processing and upgrading.

Sample Production

Chlorella sorokiniana cultures (DOE 1412) and were grown in a temperature-controlled outdoor photobioreactor at NMSU and enriched with 0.8% CO_2 and the temperature was maintained at ~25 ^{0}C. Biomass was harvested at densities of 0.7-1.0 g/L and enriched with 0.8% CO_2 and the temperature was maintained at ~25 ^{0}C. Cells were separated from the media by centrifugation and the resultant supernatants and biomass were kept frozen until oil production by hydrothermal liquefaction.

Hydrothermal Liquefaction of Microalgae

Hydrothermal liquefaction was performed in a PARR 4593 stainless steel bench top reactor (Parr Instrument Company, Moline, IL) equipped with a 4843 controller unit. HTL oils were produced from both algal strains at 180, 200, 225, 250, 275 and 300 ^{0}C reaction temperature. A 5.0 g portion of dry biomass was loaded to the reactor and supernatant water collected from biomass centrifugation (i.e. culture media) was added to the reactor to achieve 10% biomass loading. Residual air was removed from the reactor by three pressurizing/purging cycles with nitrogen (~ 300 psi). An initial pressure of 200 psi was applied (by filling with

nitrogen) to the reactor to achieve a rapid boiling of water. The temperature of the reactor was then increased at a rate of 10 ^{o}C/min until the desired reaction temperature is reached and maintained at that temperature thereafter. Three replicate runs were performed at each reaction temperature. After the reaction time of 30 min had elapsed, the reactor was cooled to room temperature and 30 mL of dichloromethane was added to the reactor and the contents were mixed. Solid residue was separated via filtration and the remaining reactor contents were transferred to a glass funnel and allowed for phase separation (~15 min). After the aqueous and organic phases had separated, dichloromethane phase was withdrawn and evaporated in a rotary evaporator at 65 ^{o}C to recover the HTL oil.

Sample Preparation and Mass Spectrometry

The HTL oils were prepared for mass spectral analysis by dissolution in chloroform:methanol (50:50) as previously described.[18] The concentration of the final dilute oil samples in the electrospray ionization solution was 0.5 mg/mL in both positive- and negative-ionization modes. ESI FT-ICR mass spectrometry was performed with a hybrid linear ion trap 7 T FT-ICR mass spectrometer (LTQ FT, Thermo Fisher, San Jose, CA) equipped with an Advion Triversa Nanomate (Advion Biosystems, Inc.) as recently described.[19] A total of 500 and 400 time-domain transients were co-added for each sample in positive- and negative-ion modes, respectively prior to fast Fourier transformation and frequency to mass-to-charge ratio conversion.

Internal mass calibration of FT-ICR mass spectra was based on homologous alkylation series of known compounds, whose elemental composition differ by integer multiples of CH_2. High-resolution FT-ICR mass spectra confirm that all observed ions are singly charged as evidenced by the 1 Da spacing between $^{12}C_c$ and $^{13}C_1{}^{12}C_{c-1}$ peaks for the species with the same molecular formula. Peak lists were generated from m/z values in the range of 100-900 Da with peak magnitudes greater than 10 times the standard deviation of the baseline noise. IUPAC measured masses (CH_2 = 14.01565 Da) were converted to the Kendrick mass scale (CH_2 = 14.0000 Kendrick mass units) as previously described[20] and sorted by Kendrick mass defect to facilitate identification of homologous series [i.e. compounds with the same heteroatom composition and the same double-bond equivalents (DBE, number of rings plus double bonds to carbon) but differing in the degree of alkylation]. Elemental compositions could be assigned to >96% and >80% of the total mass spectral signal for *C. sorokiniana* and *N. gaditana* HTL oils, respectively in both ionization modes.

A variety of non-lipid reaction products from HTL processing at different reaction temperatures were identified by their heteroatom class. Residual lipids in the oils were identified as a given lipid class by matching the assigned elemental compositions to an in-house assembled lipid database derived from Lipid Maps (Nature, Lipidomics Gateway) as previously described.[21] Tandem mass measurement was performed for selected species in each abundant compound class for structural identification where possible. For this process, ions of interest were first isolated in the FT-ICR and signals from isobars within 1 Da of the selected ion mass were determined. If no significant/high-abundance interfering peaks were observed, MS^n fragmentation was performed in the linear ion trap by collision induced dissociation (CID) with high-resolution/accurate mass measurement FT-ICR MS detection of the fragment ions. The MS^n spectra were evaluated by manual inspection and elemental composition of fragment ions was

determined directly from sub-part-per-million mass measurement accuracy. These data represent a detailed qualitative analysis where comparison of individual compound signals is possible between samples, but compound-to-compound signal magnitudes is impossible due to a lack of available analytical standards for each of the 1,000+ compounds observed.

Results

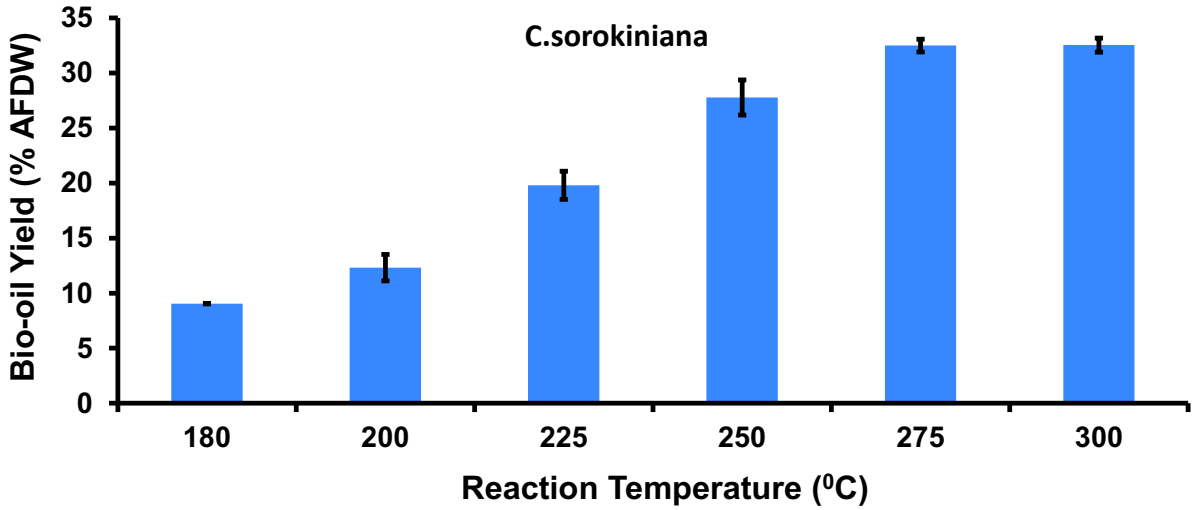

Figure 5.5.3.1. HTL bio-oil yields.

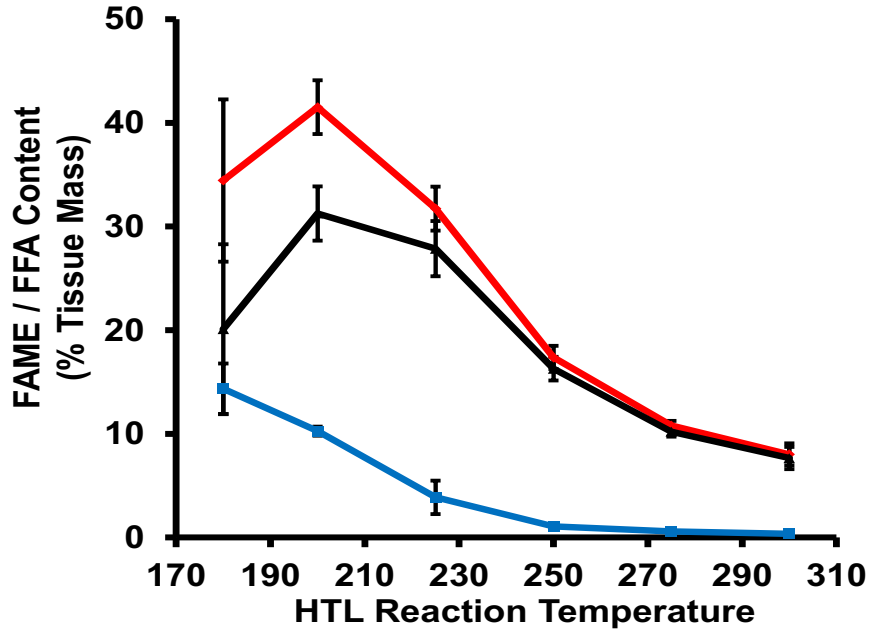

Figure 5.5.3.2. FAME and FFA quantitation by GC/MS for *C. sorokiniana* bio-oils produced at variable temperatures with total FAME shown in red, lipid-bound FAME in black and free fatty acid content shown in blue. The observed decrease in the FFA content above 200 ^{0}C for *C. sorokiniana* bio-oil can be due to the transformation of free fatty acids into other molecular species with the same heteroatom content (see Figure 5).

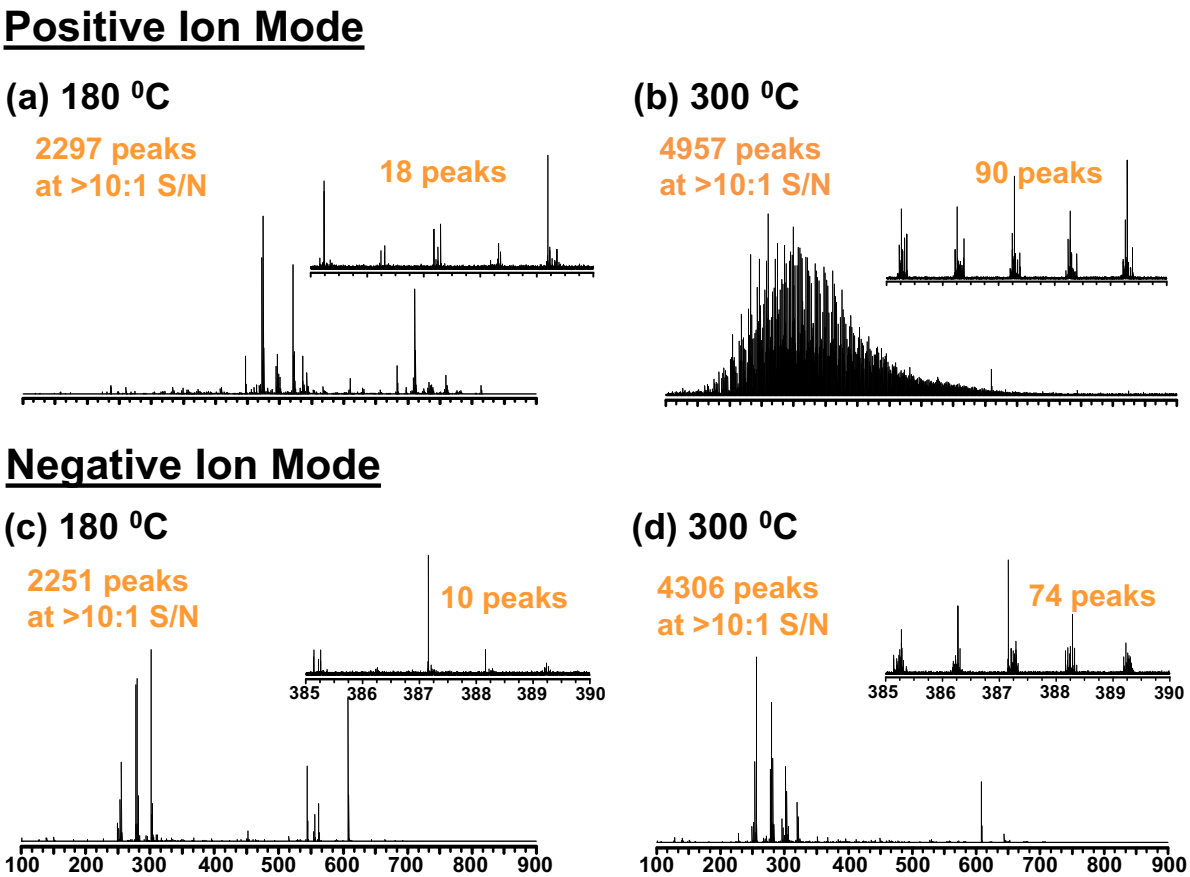

Figure 5.5.3.3. (±) ESI FT-ICR mass spectra of *C. sorokiniana* bio-oils produced at 180 C and 300 C. Bio-oil produced at high temperature shows elevated spectral complexity.

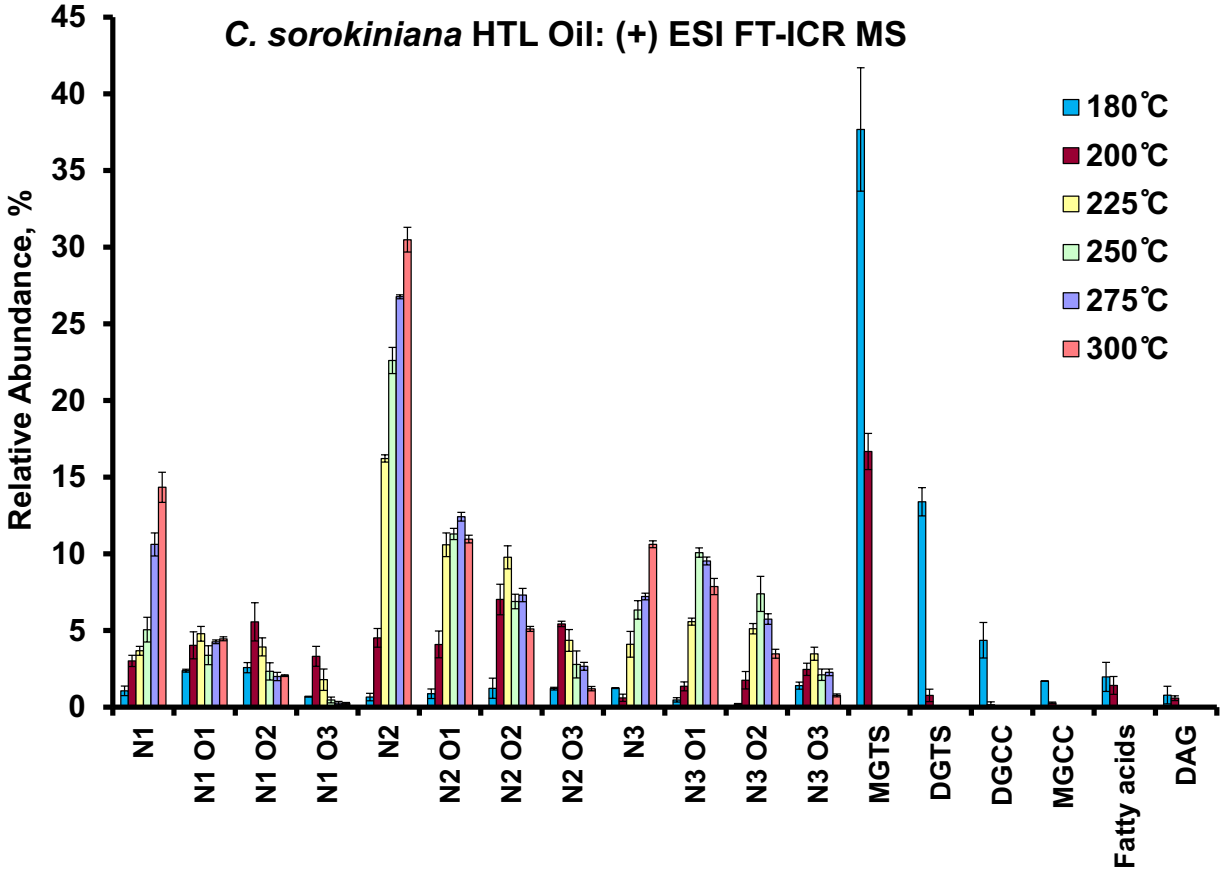

Figure 5.5.3.4. Class distribution for *C. sorokiniana* bio-oils produced at different reaction temperatures derived from (+) ESI FT-ICR MS. We observe a variety of NxOy heteroatom classes with low oxygen number (y≤3) and several lipid classes O3-O6 and N_1O_6-N_1O_9. $N_{1-4}O_{0-3}$ heteroatom classes show a continuous increase in the abundance with increasing reaction temperature, where lipid classes show the opposite trend. Observed betaine lipids are very unstable at higher temperatures and most classes are absent above 200 C reaction temperature.

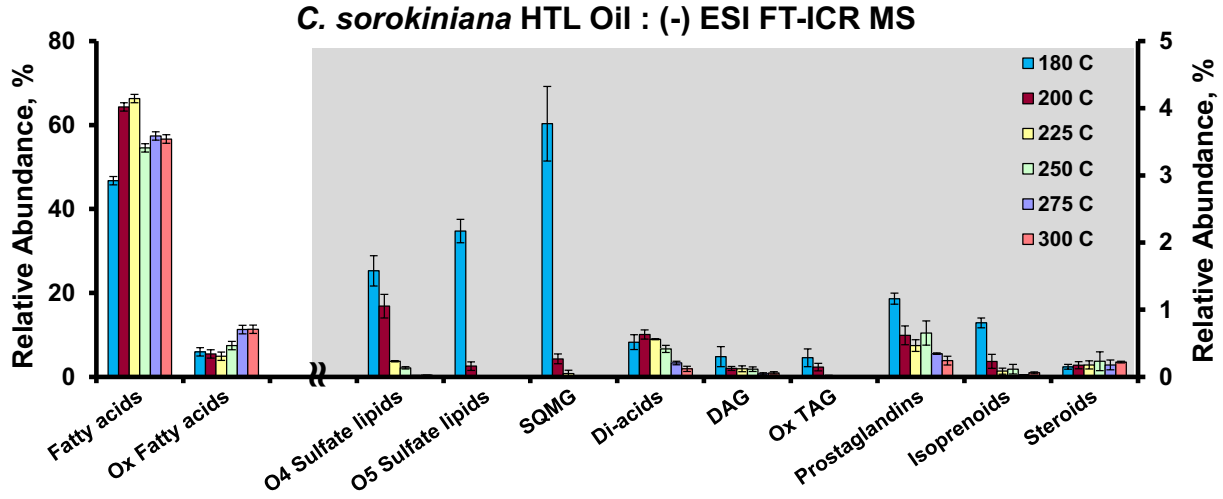

Figure 5.5.3.5. Class distribution for *C. sorokiniana* bio-oils produced at different reaction temperatures derived from (-) ESI FT-ICR MS. Primary compounds include highly-oxygenated species (O_2-O_{10}), nitrogenous compounds and sulfate lipids. The highest abundance is observed for O_2 compounds which correspond to free fatty acids as well as various other compounds containing two oxygen atoms per molecule. Sulfate lipids show low abundance at elevated temperatures and predominant compounds the indicated lipid classes are confirmed by tandem mass spectrometry.

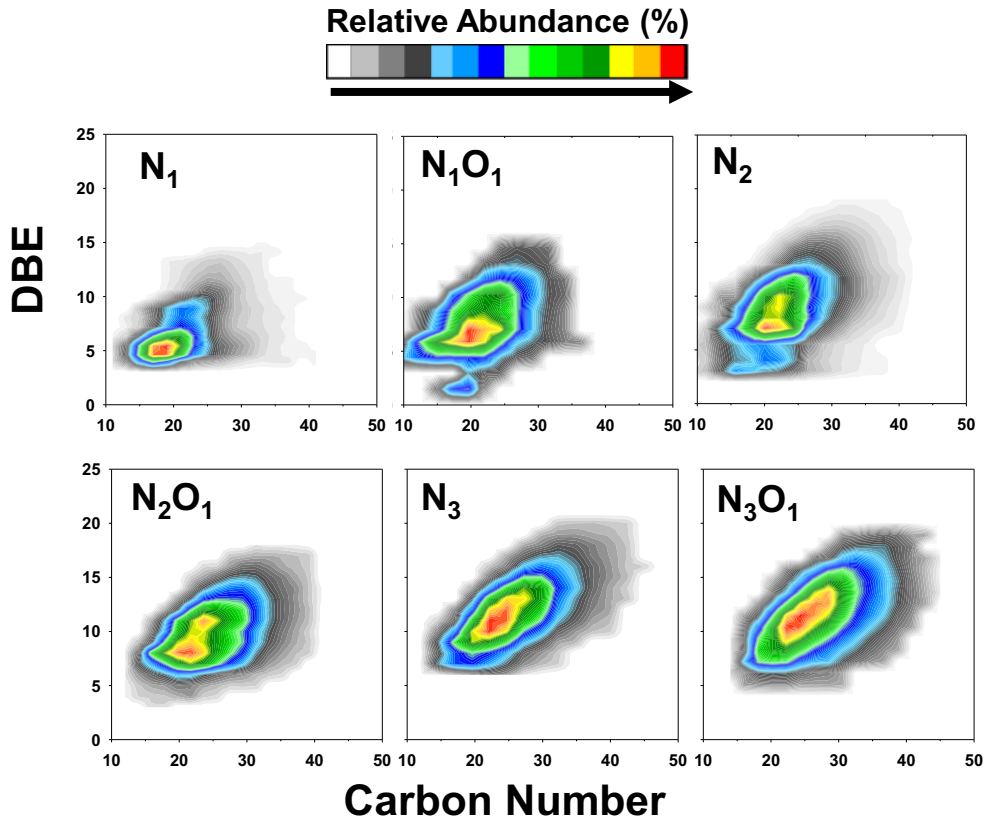

Figure 5.5.3.6. Abundance contour plots of DBE versus the carbon number for *C. sorokiniana* and N. bio-oil produced at 300 C from (+) FT-ICR MS. The prevalent compounds shown in the above mass spectral images correspond primarily aromatic amines, various nitrogen heterocycles (such as piperidines, pyridines, pyrrolidinones, pyrroles, indoles, imidazoles, etc.), fatty-amides and aromatic amides.

Discussion

Oil yields (dry weight basis) from hydrothermal liquefaction of *C. sorokiniana* show a continuous increase with HTL reaction temperature (**Figure 5.5.3.1**). There was 9% oil yield at 180 ^{0}C and that increased to 33% at 300 ^{0}C. A dramatic increase in oil yield was observed above 275 ^{0}C with the highest oil yield of 48% observed at 300 ^{0}C. HTL oil yields reported for higher temperatures (>200 ^{0}C) exceed the lipid content of the biomass, which indicates the conversion of other cellular constituents (e.g. protein, carbohydrate and algaenan) to HTL oils in the HTL reaction processes. The FAME profiles for total, lipid-bound and free fatty acids are shown in **Figure 5.5.3.2** and **Figure 5.5.3.3** illustrates the variation in spectral complexity with HTL reaction temperature.

Figures 5.5.3.4 and 5.5.3.5 show broadband positive- and negative-ion ESI FT-ICR mass spectra of *C. sorokiniana* HTL oils produced at 180 ^{0}C and 300 ^{0}C. Not surprisingly, high temperature (300 ^{0}C) HTL oil is more compositionally complex than the low-temperature (180 ^{0}C) oil for both ionization modes. Broadband FT-ICR mass spectra provide molecular-weight distribution information and illustrate the compositional complexity of these materials. These data are sorted in several ways to provide visual and accessible interpretation of composition with regard to HTL reaction temperature. Molecular elemental composition assignment combined with Kendrick mass sorting provide three layers of information; class (heteroatom content), type (molecular rings/and or double bonds, double bond equivalents (DBE)) and carbon number distribution (extent of alkylation). Three-dimensional mass spectral images of DBE versus carbon number with relative abundance in the third dimension (color) provide compact visualization of the molecular features for inter-class compositional analysis (**Figure 5.5.3.6)**. Heteroatom class analysis for the observed non-lipid constituents of the HTL oils is achieved by grouping the assigned elemental compositions to compound classes with the same heteroatom content. Similarly, lipids (identified by matching elemental composition to those found in the Nature Lipidomics Gateway library followed by confirmation by tandem mass spectrometry) are grouped by lipid class and plotted with the observed heteroatom classes. Relative abundance for each class is calculated by summing the peak magnitudes of all observed ions for each class and dividing by the summed peak magnitude for all assigned monoisotopic masses.

The positive-ion ESI FT-ICR MS class distribution for *C. sorokiniana* HTL oils produced at 180 - 300 C is shown in Figure 4. Predominant species observed at high temperatures include a variety of nitrogen-containing compounds with up to 2 oxygen atoms per molecule. A range of lipid classes including monoacylglyceryl-*N,N,N*-trimethyl-homoserine (MGTS), diacylglyceryl-*N,N,N*-trimethyl-homoserine (DGTS), diacylglyceryl-carboxyhydroxymethylcholine (DGCC), monoacylglyceryl-carboxyhydroxymethylcholine (MGCC), diacylglycerol (DAG) and free fatty acids are identified for the low-temperature HTL oils. The contribution from non-lipid HTL reaction products to the low-temperature oil is minimal, resulting a lipid-dominated bio-oil at low reaction temperatures, whereas HTL processing at higher temperatures produce oil that mainly comprised of non-lipid molecules that include contribution from protein and carbohydrate degradation.

Low-temperature *C. sorokiniana* HTL oil is rich in betaine lipids. Molecular identifications for the reported lipid classes in Figure 3 were confirmed by tandem mass measurements of the abundant members from each lipid class. Positive ion ESI/MS^n experiments performed for the abundant MGTS and DGTS compounds showed characteristic structural fragmentation of betaine lipids, i.e. a loss of 87 Da representing $-CH_2-CH_2-N^+(CH_3)_3$, a loss of 73 Da denoting $-CH_2-N^+(CH_3)_3$ and a loss of 59 Da indicating trimethylamine [$-N^+(CH_3)_3$]. Depending on the loss of fatty acyl moieties from the parent ion, three most abundant MGTS species with DBE = 2, 3 and 7 are identified as 16:0 MGTS, 16:1 MGTS and 20:5 MGTS, respectively.

Protein and carbohydrate degradation and secondary reactions at elevated temperature produce basic-nitrogen compounds that are selectively ionized by positive-ion ESI.[1] Mono-, di- and tri-nitrogen species observed for *C. sorokiniana* HTL oils show a continuous increase with HTL reaction temperature. Di-nitrogen (N_2) compounds show a ~46-fold increase in abundance when HTL reaction temperature increased from 180 to 300 C. The heteroatom classes N_1O_1, N_2O_1, N_2O_2, N_3O_1 and N_3O_2 also show a 10-fold average increase between the lowest and the highest HTL reaction temperature. The increase in nitrogenous compounds with HTL reaction temperature corresponds directly to the observed increase in the HTL oil yield with temperature,

as well as high nitrogen and oxygen content in the higher reaction temperature oils (a characteristic of microalgae-derived bio-oils).
Positive-ion ESI abundance-contoured plots of DBE versus carbon number for the abundant nitrogen-containing heteroatom classes observed for *C. sorokiniana* HTL oil produced at 300 ^{0}C are shown in **Figure 5.5.3.5**. Tandem mass measurements for these observed nitrogen-containing species were not possible because they could not be isolated from nearby mass isobars for fragmentation. High carbon content/low DBE observed for the predominant N_1 compounds suggest low aromaticity. The N_1O_1 species with 1-4 DBE and ~15-22 carbons observed are presumably fatty acid amides formed by the condensation of fatty acids and ammonia from protein decomposition. The N_1O_1 compounds in both strains that span 4-15 DBE show similar carbon number and DBE distribution as N_1 compounds of the corresponding strain.

The N_2 compounds in *C. sorokiniana* HTL oils show DBE = 2-20 and carbon content of 10-40 atoms.. Compounds with DBE = 3 and DBE = 4 contain 20-23 carbon atoms per molecule, and indicate highly alkylated species with low aromaticity. ESI MS^n measurements for structure elucidation were not available for these ions due to the high complexity of the sample. The observed compounds likely correspond to long-chain diamines, alkyl-substituted imidazoles (DBE = 3) or alkylated pyrazines (DBE = 4) as reported for *N. salina* HTL oil in previous work.[2]

Figure 5.5.3.5 shows the negative-ion ESI FT-ICR MS class distributions for *C. sorokiniana* HTL oils produced at each reaction temperature. Acidic compounds are dominated by free fatty acids (FFA) that originate from the lipid portion of the microalgae. To verify the observed trends in the relative abundance of free fatty acids with temperature between the two algal strains, FAME and FFA quantitation was performed by gas chromatography/mass spectrometry (**Figure 5.5.3.2**). Free fatty acids observed for *C. sorokiniana* HTL oils decrease significantly above 225 ^{0}C which can be explained by their fatty acid distribution. FAME profiles generated by GC/MS show *C. sorokiniana* biomass is rich in polyunsaturated fatty acids (PUFA) which are highly sensitive to temperature and susceptible to oxidation due to their high degree of unsaturation.[3] Therefore, increasing reaction temperature can generate non-volatile degradation products of PUFAs as well as facilitate the oxidation, transforming the PUFAs to their corresponding oxidation products, thus decreasing the detectable FFA content by GC/MS and FFA ion abundance in (-) ESI FT-ICR MS (an important consideration when considering lipid quantitation by GC/MS for any feedstock/oil).
The O_4 and O_5 sulfate lipids observed for *C. sorokiniana* low-temperature HTL oils correspond to alkyl sulfate lipids and hydroxyl alkyl sulfate lipids, respectively. Predominant compounds in each of these lipid classes contain a 30-32 carbon aliphatic chain and a sulfate head group as identified/confirmed by tandem mass spectrometry. Long-chain saturated and mono-unsaturated alcohols and alkyl diols with similar carbon number distributions (C_{30}–C_{32}) as the sulfate lipids observed here, have been previously identified in marine environments [4,5, lacustrine sediments [6] as well as in marine and freshwater microalgae.[7,8 Holguin *et al*. have recently reported similar sulfate lipids from the lipid extracts of *Nannochloropsis salina* and *Scenedesmus obliquus*.[9] The O_4 sulfate lipid (i.e. $C_{32}H_{63}O_4S_1$) shown in Figure S6 likely originates from the dehydration of the corresponding hydroxyl alkyl sulfate lipid (i.e. $C_{32}H_{65}O_5S_1$). The location of the double bond in $C_{32}H_{63}O_4S_1$ can be at C-14 or C-15. A similar mechanism for the

transformation of diols to n-alkenols through dehydration by living organisms in a freshwater environment has been proposed by Xu et al.[6]
The selection of reaction temperature for hydrothermal liquefaction depends on the desired specifications of the final product. For example, if a lipid-rich biocrude is preferred as the end product, low reaction temperatures should be used, whereas high temperatures are more suitable if a crude-like oil is preferred.[8] FT-ICR MS results indicate relatively low HTL processing temperatures (< 225 ^{0}C) allow extraction of lipids and the chemical composition of the oil is determined by the microalgal species used in the process as well as the harvesting period as the cellular lipid and fatty acid composition vary during the growth cycle.[30] The lipid compositional analysis shown here for the low-temperature HTL oil will aid microalgal HTL process optimization when the desired end product is a lipid-rich bio-oil.

For microalgae with a low lipid content, HTL processing temperature can be optimized to maximize oil yield. Reaction temperatures as high as 375 ^{0}C have been used to obtain the maximum oil yield from *Desmodesmus sp.*, a relatively low-lipid microalgae [8]. At temperatures above 200 ^{0}C, protein and carbohydrate degradation increases the oil yield. Protein decomposition and cross reactions of protein-carbohydrate derived materials produce a variety of nitrogen- and oxygen-containing species that increase both nitrogen and oxygen content of the bio-oil. Therefore, even if a high oil yield is obtained from low-lipid microalgae at higher processing temperatures, high nitrogen and oxygen content will affect the direct utilization of the oil and will require upgrading for the removal of these polar species from the oil. Among many upgrading methods, hydrotreatment is a promising technique for the treatment of these polar species and the efficiency of the process highly depends on the chemical nature of the oil.[18, 31] Therefore, the detailed compositional description of the high-temperature HTL oil shown here will benefit to devise efficient upgrading strategies to produce a high-quality liquid fuel from HTL of microalgae.

5.5.4 References

[1] Torri C, Garcia Alba L, Samorì C, Fabbri D, Brilman DWF. Hydrothermal Treatment (HTT) of Microalgae: Detailed Molecular Characterization of HTT Oil in View of HTT Mechanism Elucidation. Energy & Fuels 2012;26:658.
[16] Anderson R. Algal Culturing Techniques. California : Elsevier Academic Press 2005.

[2] Sudasinghe N, Dungan B, Lammers P, Albrecht K, Elliott D, Hallen R, et al. High resolution FT-ICR mass spectral analysis of bio-oil and residual water soluble organics produced by hydrothermal liquefaction of the marine microalga Nannochloropsis salina. Fuel 2014;119:47.

[3] Fournier V, Deataillats F, Juaneda P, Dionisi F, Lambelet P, Sebedio JL, et al. Thermal degradation of long-chain polyunsaturated fatty acids during deodorization of fish oil. European Journal of Lipid Science and Technology 2006;108:33.

[4] Rampen SW, Willmott V, Kim JH, Uliana E, Mollenhauer G, Schefub E, et al. Long chain 1,13- and 1,15-diols as a potential proxy for palaeotemperature reconstruction. Geochimica et Cosmochimica Acta 2012;84:204.

[5] Damste JSS, Rampen SW, Irene W, Rijpstra C, Abbas B, Muyzer G, et al. A diatomaceous origin for long-chain diols and mid-chain hydroxy methyl alkanoates widely occurring in Quaternary marine sediments: Indicators for high-nutrient conditions. Geochimica et Cosmochimica Acta 2003;67:1339.

[6] Yunping X, Simoneit BRT, Jaffe R. Occurrence of long-chain n-alkenols, diols, keto-ols and sec-alkanols in a sediment core from a hypereutrophic, freshwater lake. Organic Geochemistry 2007;38:870.

[7] Allard B, Templier J. Comparison of neutral lipid profile of various trilaminar outer cell wall (TLS)-containing microalgae with emphasis on algaenan occurrence. Phytochemistry 2000;54:369.

[8] Volkman JK, Barrett SM, Dunstan GA, Jeffrey SW. C30-C32 alkyl diois and unsaturated alcohols in microalgae of the class Eustigmatophyceae. Organic Geochemistry 1992;18:131.

[9] Holguin OF, Schaub TM. Characterization of microalgal lipid feedstock by direct-infusion FT-ICR mass spectrometry. Algal Research 2013;2:43.

The following sections are a wild guess. Whoever actually writes this- Change it however you wish. The HTL and SEQHTL sections will describe how they analyze their products separately in Sections 5.6 and 5.7

5.6 Sequential hydrothermal liquefaction

Task summary:

The objective of this task was to design and demonstrate sequential hydrothermal liquefaction technology to produce bio-fuel intermediate with C, N, and P recycle to cultivation. The Expected outcome is SEQHTL process design balancing high efficiency bio-oil extraction and bio-char production for heating energy requirement. The major research activities performed under this task include: (1) batch SEQHTL studies with 10 wt% solids at 160°C and 240°C for the first stage and second reaction respectively, with *Chlorella sorokiniana* 1412.1, *Galdieria sulphuraria* 5587.1 and *Chlorella vulgaris* biomass samples (Sections 5.6.1a – b); (2) batch studies with 20 wt% solids at variable operating conditions of 160°C and 240°C, and 180°C and 300°C for the first stage and second reaction respectively, with *Chlorella sorokiniana* 1412.1, *Galdieria sulphuraria* 87.1, *Kirchneriella cornutum* and *Galdieria sulphuraria (2016)* biomass samples (Section 5.6.1c); (3) conducted char combustion trials to assess viability as a low value fuel (Section 5.6.2); (4) determined nutrient availability in SEQHTL water effluents and verified microalgae growth trials on this product stream (Sections 5.6.1b & 5.6.3); (5) worked on developing a continuous-flow SEQHTL design (Section 5.6.4). The major results obtained under this task include: (1) batch studies to generate the core comprehensive biomass and product streams property database for modeling efforts and techno-economic analyses; (2) Design of continuous sequential hydrothermal liquefaction system including considering of heat integration and biochar utilization, supported by an ASPEN model; (3) SEQHTL system evaluation and fine-tuning at the testbed to meet the performance expectation target. (4) Complete bio-crude oil characterization of different culture and conversion conditions.

Preliminary batch SEQHTL studies with 10 wt% were developed to generate a detailed feedstock and product stream characterization in order to determine trade-offs between species based on product yields, and to assist in developing comprehensive material and elemental balances. The results provided the necessary core data required for process simulation and for coherent integrated end-to-end techno-economic analyses. The algae grown in enclosed mixotrophic systems, *Chlorella* sp. displayed the highest biocrude yield (~30 wt%).and the *Galdieria sulphuraria* achieved moderate crude production (20.46 wt%), despite its low lipid content. In terms of char production, the *Galdieria* algae exhibited the lowest value (11.69 wt%), and *Chlorella* sp. showed comparable results (from 13.68 – 15.31 wt%). Sections 5.6.1a – b provide more detailed information.

Studies have shown that large quantities of inorganic nutrients that partition to the HTL aqueous effluents could potentially be used to increase algae productivity. Given that the versatility of SEQHTL and distinctive mild operating conditions, specifically in the first stage, could facilitate the harvesting of significant quantities of water-soluble nutrients and sugars; nutrient recovery was evaluated for different algae, as well as the potential to culture microalgae using the recycled effluents was tested. The mild temperatures of SEQHTL allowed the recovery of greater quantities of phosphorous than direct HTL, whereas nitrogen salvaging in all its forms was lower in comparison. For *C. sorokiniana*, phosphorous recovery was quite high with 3650 mg/L, followed by *C. vulgaris* and *G. sulphuraria,* with 2640 and 946 mg/L, respectively. Results highlighted the high potential of SEQHTL to recover water-soluble nutrients. Moreover, it was

found that the SEQHTL stage 1 water product is very suitable for microalgae culture due to the high nutrient recovery. However, the pure Stage 1 effluent was toxic to microalgae and thus some preconditioning dilution was inevitable. Sections 5.6.1b – c and 5.6.3 provide more detailed information.

One of the major products of HTL or SEQHTL is the solid residue "biochar". Biochar yields vary depending on the algae, its chemical composition and the operating conditions employed in the process. Developing a cost-effective application for this product fraction will play a significant role in the development of microalgae bio-refineries. To assess the viability of employing the solid charcoal residue as low-value fuel for heat energy, dried biochar samples were combusted. For the *Chlorella* algae, experimental heating values were only moderately lower than calculated results. For *Galdieria sulphuraria*, the char did not combust completely. More research is needed to elucidate the reason for this behavior. Nonetheless, results confirmed the potential of using the biochar fraction as a low-value fuel to supply a portion of the required heat energy; thus, mitigating a portion of the operational costs and making the process more feasible. Section 5.6.2 provides more information.

Relevant transport and thermophysical properties must be determined to provide more accurate data for material and energy balances, and modeling efforts. Estimations were carried out for slurries with solid concentrations from 10 – 20 wt%. As expected, increasing the solid content in the slurry produced an effective viscosity escalation for the slurries. This amounted to an average of 0.055, 0.438 and 0.701 Pa-s per wt% increase for *C. sorokiniana*, *C. vulgaris* and *G. sulphuraria*, respectively. The slurry mixtures displayed non-Newtonian, shear thinning behavior, so the effective viscosity decreased when shear rate increased. Also, the thermogram results confirmed that the amount of heat required to increase the temperature by one degree decreased as solid concentration increased. Thus, it would be advantageous to increase the solid loading to minimize the energy required to preheat the slurry feeds.
Consequently, batch SEQHTL studies with 20 wt% were developed at variable operating conditions to generate supplementary feedstock and product stream data and to assess optimal reaction conditions for strains that exhibited low product yields under conventional SEQHTL parameters. Overall, the algae exhibited better results in terms of biocrude production, at the higher temperature set. However, although the higher temperatures favored an increased crude yield; for these algae oil the quality decreased mainly owing to the concentration and structure of oxygen-rich compounds. *Galdieria* 87.1 showed the highest crude yield (36.5 wt%) and lowest char (0.54 wt%) at 300°C. Conversely, mainly owing to the lower lipid content in the new *Chlorella* 1412 algae, the crude yield compared unfavorably with previous SEQHTL results attained at 10 wt% solids feed. SEQHTL is considered more suitable for processing algae with moderate to high lipid contents, while traditional single stage HTL is more flexible in terms of biomass. These results also provided the necessary core data required for material and elemental balances for process simulation and for subsequent techno-economic analyses. Sections 5.6.1b – c provide more detailed information.

The research groups that have investigated HTL with high temperatures have successfully worked with different species; yet most of these studies have been limited to batch reactor testing. Furthermore, complexities in product recovery have resulted in the use of toxic organic solvents, contributed to significant material loss and have produced inconclusive mass balances.

Therefore, there is pressing need to advance this conversion route by developing a continuous-flow operating system that can be easily modeled, scale-up, allows nutrient recovery and does not include the use of organic solvents. A continuous-flow SEQHTL prototype reactor system was developed in our lab based on previously determined process metrics, operating conditions and relevant engineering data. The configuration includes two slurry pumps, two product separation stages, pre-heating sections and two tubular plug-flow reactors for each reaction stage. The C-SEQHTL prototype was designed with SS 316L material, standard fittings for adaptability, and custom separation units; with capacities are 2 – 2.5 L/hr and 1 – 1.5 L/hr for 1st and 2nd stage respectively. Trials for first reaction stage with 20 wt% solids feed *Kirchneriella cornutum* and *Galdieria sulphuraria* 87.1 were developed at temperatures of 160 and 180°C. Higher reaction temperatures led to more biomass breakdown and corresponding less solids; yet the difference was relatively small. Technical and maintenance issues have not allowed the development of the second reaction stage. Also, further testing and optimization is required. Reactor systems for established commercial processes are usually complex designs developed and evolved over several years to suit the requirements of the industry. Nonetheless, with the C-SEQHTL system, an initial exploratory continuous-flow performance assessment of biocrude production and potential co-product recovery from different microalgae species will be developed. Section 5.6.4 provides more information.

Hydrothermal liquefaction (HTL), is considered a viable option for converting wet biomass such as algae to biocrude, because it circumvents the need for drying [7, 8]. In HTL, biomass slurries go through chemical and physical transformations at elevated temperatures and pressures from 200 to 400°C and 5 to 40 MPa respectively [9, 10]. Under such operating conditions, ionic reaction and the high activity of water enhance biomass fragmentation and reconstitution into molecules of higher energy density [11, 12]. Recent microalgae related HTL studies have focused on biocrude production in a single step process with variable residence times and high reaction temperatures, usually from 300 to 370°C [13-15]. These studies mainly focused on improving conditions for increasing fuel yield, but have not considered the potential for extracting other high-value components from algae biomass that may contribute to improving the process economics [16, 17]. The harsh HTL reaction conditions decrease the ability to recover or develop value-added co-products. Besides, when protein and carbohydrate are not removed, the quality of the biocrude is compromised, because these compounds introduce large amounts of oxygen and nitrogen [18]. The bio-oils obtained possess high heteroatom contents, causing unwanted qualities such as oil acidity, polymerization, high viscosity, and high-boiling distribution [19]. Thus, given these product characteristics, complex and expensive upgrading processes are unavoidable in order to make the biocrude into fuels [20, 21]. Furthermore, in hydrothermal media, carbohydrate and protein components may degrade and generate toxic chemicals such as furfural, hydroxymethyl furfural, and other complex aromatic compounds, ultimately representing a waste of valuable components from the culture system [22, 23].

To meet such a need, a two-stage Sequential Hydrothermal Liquefaction (SEQHTL) process was developed as an alternative for simultaneous extraction of co-products and production of biocrude [23]. In SEQHTL, the first step uses low temperature hydrothermal pretreatment (between 140–180°C), in which solvolysis and hydrolysis are the dominant reactions [11, 24], to remove nonfuel components such as polysaccharides, protein derivatives and inorganic compounds [25]. Next, the residual biomass is treated at moderate temperatures (between 240–

300°C) to produce the biocrude. By fine-tuning process conditions the reactions may be adapted to favor desired pathways and discerningly recover different types of compounds [26]. Nutrients such as inorganic nitrogen and phosphate may be retrieved in the aqueous product, and then may be recycled to the algae growth system [22, 27]. Additionally, recovered algal sugars may be hydrolyzed into simple sugars and used for mixotrophic cultivation or fermentation, or as substitute for starch-derived thermoplastics [28].

5.6.1 Batch SEQHTL trials

5.6.1a Experimental Methods & Product Characterization

Based on previous work performed at WSU [23], the first set of batch reactions were conducted under the following conditions: Stage 1 at 160°C for 20 min with 10 wt% solids loadings, and Stage 2 at 240°C for 20 min with 10 wt% solids loadings.
Trials with slurry samples were tested at 160 and 240°C, respectively, in a bomb type reactor (1 L, Parr4522, Parr Instrument Co.). In the first stage, 100 g of the 1:9 slurry feed ratio was prepared by mixing with complementary deionized water. After loading the sample and purging the oxygen with 5 minutes of nitrogen bubbling, the temperature of the reactor was ramped to 160˚C and held for 20 min. Next, the reactor was cooled to room temperature using chilled water. The reaction mixture was collected and filtered with Whatman quantitative ashless grade-42 filter paper (2.5 µm). The filtrate, consisting of the aqueous product, was collected and stored for subsequent nutrient analyses. In other trials, the filtrate was collected and treated with ethanol at 4°C, 1:4 V/V to precipitate the algal polysaccharides. The ethanol-water mixture was subsequently centrifuged and the recovered sugar pellet was air-dried for 36 h and then weighed.
Next, the filtered treated algae residue was returned to the reactor for the next reaction step. To maintain the water to biomass ratio, the moisture content (oven-dried at 105˚C for 6 hours) and weight of the filtered biomass were measured and complementary water was added. In the second stage, after loading the sample and purging the oxygen with 5 minutes of nitrogen bubbling, the temperature of the reactor was ramped to 240˚C and held for 20 min. Following the reactor was cooled to room temperature using chilled water. Initially, the gaseous product was collected and stored using gas sampling Tedlar bags (SASSCO, 500 mL, polypropylene2n1-valve). The rest of reaction mixture was washed and thoroughly mixed with three successive 50 mL portions of methylene chloride. The solvent soluble phase in the mixture was removed gravimetrically in a separatory funnel, and the insoluble solid residue was filtered out with Whatman quantitative ashless grade-42 filter paper (2.5 µm). After this, the solid residue defined as biochar was collected and oven-dried at 105˚C for 6 hours. The organic solvent soluble fraction was processed in a rotary evaporator for 15 min under vacuum to remove the methylene chloride. The remaining viscous liquid product was deemed as bio-crude. Figure 5.6.1 summarizes the experimental procedure for these trials.

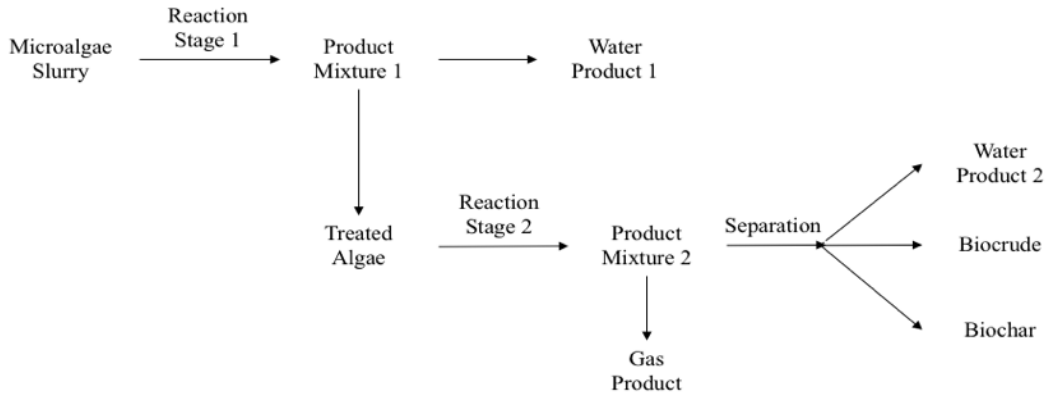

Figure 5.6.1 SEQHTL Experimental Set-up

The major process streams of SEQHTL were treated algae, bio-oil, polysaccharides and bio-char. The yields were calculated on a dry algae mass basis with equations 1–4:

$$Treated\ Algae\ (wt\%) = \frac{M_{treated\ algae}}{M_{dry-algae}} \times 100\% \quad (1)$$

$$Polysaccharides\ (wt\%) = \frac{M_{polysaccharides}}{M_{dry-algae}} \times 100\% \quad (2)$$

$$Biocrude\ (wt\%) = \frac{M_{biocrude}}{M_{dry-algae}} \times 100\% \quad (3)$$

$$Char\ (wt\%) = \frac{M_{char}}{M_{dry-algae}} \times 100\% \quad (4)$$

Where $M_{treated\ algae}$ is the mass of treated algae (g), $M_{polysaccharides}$ is the mass of polysaccharides (g), M_{char} is the mass of the solid residue (g), and $M_{biocrude}$ is the mass of biocrude (g), and $M_{dry-algae}$ is the initial mass of dry algae feed (g).

Proximate & Elemental Analyses

Proximate analyses (PA) were used to determine the distribution of fractions attained when each sample was heated under specified conditions. Experiments were conducted on a TGA/SDTA 851 thermogravimetric analyzer (Mettler Toledo) equipped with STARe data analysis software. The carbon, hydrogen, nitrogen and sulfur content were determined with a TruSpec Micro elemental analyzer (LECO Corporation) following the corresponding ASTM procedures (D-5291, E-777, E-778) for indirect quantification and characterization of the gases produced after combustion with pure O_2. Approximately 0.15 g of each sample were analyzed in triplicate. As described by the ASTM D3176 and the Handbook of Coal Analysis, Ultimate Analyses values were attained by adjusting the experimental results to a dry ash-free basis (daf) [29]. The oxygen content for each sample was determined by difference. Finally, the higher heating value (HHV)

in MJ/kg was estimated from the elemental composition with the empirical Dulong Formula (eq. 5) [7, 30].

$$HHV\left(\frac{MJ}{kg}\right) = 0.3383 \cdot C + 1.443 \cdot \left(H - \frac{O}{8}\right) + 0.0942 \cdot S \qquad (5)$$

Biocrude Characterization

Fatty acid methyl ester analyses were performed on the microalgae and biocrude samples following the method described by O'Fallon [31]. Briefly, 0.10 g of dried algae sample were placed into a 16 x 125 mm screw-cap Pyrex culture tube. Then 0.7 mL 10 N KOH in water and 5.3 mL MetOH were added. The sample was then dissolved and hydrolyzed by incubation in an 85°C water bath for 15 min. After cooling to room temperature, 0.58 mL of 24 N H_2SO_4 in water were added. Subsequently, the tube was mixed vigorously and incubated again in an 85°C water bath for 15 min. Following fatty acid methyl ester synthesis, 2 mL water and 2 mL hexane were added to the mixture. Then the tube was vortexed again for 5 min. Finally, the tube was centrifuged for 7 min in a tabletop centrifuge. Consecutively, the hexane layer containing the fatty acid methyl esters was recovered and placed into the corresponding GC vial. For biocrude samples, the alkaline cell hydrolysis step was omitted, while every other step was equivalent. FAME analysis was performed on an Agilent 7890A GC equipped with an auto-sampler (Agilent 7683B), a flame ionization detector (FID) and a FAMEWAX column (30 m x 320 µm x 0.25 µm) (Restek). Helium was used as the carrier gas. The injection volume was 1 µL, with split ratio at 20. The parameters of the oven temperature program started at 120˚C, with 20˚C/min intervals up to 240°C and held for 15 min. The temperatures of the injector and detector were set at 300˚C and 250°C, respectively [32]. Fatty acids were identified and quantified with external fatty acid methyl standards, and all samples were analyzed in triplicate.

The chemical nature of the crudes was assessed via GC–MS. Approximately 100 mg of biocrude sample were placed in a 16 x 125 mm screw cap Pyrex culture tube. Next, 6.5 mL of octanol solution (1.297 mg/mL) in acetonitrile were added as internal standard. Prior to analysis, the mixtures were filtered with glass fiber syringe filters (37 mm, 0.2 µm pores) and placed in GC vials. The GC–MS analysis was performed on an Agilent 5975C inert GC–MS instrument on electron impact mode equipped with a HP-5MS capillary column (30m x 250µm x 0.25µm) (Restek) and He carrier gas. The temperature program started from 45 to 250°C at a rate of 3°C/min. The injector and MS-transfer line was kept at 250°C, and the data were processed with Xcalibur v2 software package. Compound identification was based on retention times and the NIST MS compound library (2008).

Gas Product Analyses

Gas samples collected in Tedlar bags (SASSCO, 500 mL, polypropylene 2n1-valve), were analyzed in a Varian CP-3800 Gas Chromatograph equipped with a thermal conductivity detector to determine H_2, O_2, CO_2 and CO, and a Flame Ionization Detector for CH_4 as established in a similar study [33].

Water Product Analyses & Nutrient Assay

Water samples were diluted 100x with deionized water. Next, samples from the first reaction stage were analyzed for nutrients with analyses kits and a DR/2400 spectrophotometer (HACH Company). The phosphate content was determined using the digestion molybdovanadate method.

The chromotopic acid method was used to determined nitrate nitrogen, while ammonia nitrogen was quantified with the salicylate method. Finally, the total nitrogen content was estimated with the persulfate digestion method. The carbon distribution within the water product fractions was then measured with a Shimadzu TOC-5000 Carbon Analyzer operating with the combustion/non-dispersive inferred (NDIR) gas analysis method. Products of combustion at 680°C were analyzed to determine the total carbon content. The CO_2 generated from the acid digested product allowed inorganic carbon determination, while total organic carbon was determined by difference.

Transport & Thermophysical Properties

Relevant transport and thermophysical properties were determined to provide more accurate data for material and energy balances, modeling efforts and continuous-flow large-scale system development. In prior studies, completely or partial aqueous properties were usually assumed [7, 23, 34]. In this study, since reactions with increased solid loadings would improve the energy balance because less water would require preheating, estimations were carried out for slurries with solid concentrations from 10 – 20 wt%.

Thermal degradation and specific heat of the process feed streams of raw algae and treated algae were determined with Differential Scanning Calorimetry (DSC). Trials were conducted with a DSC Q2000 (TA Instruments) in a N_2 atmosphere (50 mL/min). Samples were prepared by weighing 12–14 mg in Tzero capsules. Then the samples were heated from 25°C to 300°C, with a constant heating rate of 10 K/min [35, 36]. Additionally, rheology measurements were carried out through strain-controlled steady-rate sweep tests using a Discovery HR-2 Hybrid Rheometer (TA Instruments) with 25 mm ETC Steel parallel plates maintained at 25°C. Experiments were conducted with a 1000 µm gap for shear rates from 5 to 280 s^{-1}, while data were collected and processed with complementary TRIOS v3.3 software [37]. All experiments were conducted in triplicates.

5.6.1b Results & Discussion

In order to distinguish between the *C. sorokiniana*'s and the *G. sulphuraria*'s coming from different culture conditions, in this study the algae developed in outdoor open systems are deemed as strains "1" while the species grown in enclosed photobioreactor (PBR) systems are denoted as strains "2".

Some separation issues of organic and aqueous products from Stage 2 affected the capacity of establishing accurate water extractive yields. The average results on a dry algae basis are 7.68 wt %, 5.05 wt % and 5.01 wt % for *C. sorokiniana*, *G. sulphuraria* and *C. vulgaris* respectively.

Table 5.6.1 SEQHTL Product Yields

Sample	Treated Algae	Biochar	Biocrude	Poly
C. sorokiniana 1	50.85%	16.53%	27.09%	4.31%
C. sorokiniana 2	62.36%	13.68%	30.69%	
G. sulphuraria 1	62.00%	37.41%	13.83%	9.69%
G. sulphuraria 2	72.06%	11.69%	20.46%	
C. vulgaris	59.29%	15.31%	30.95%	8.97%

In terms of char production, the *Chlorella* species exhibited comparable results, ranging from 15.31 to 17.11%; unlike *Galdieria* 1 that had the highest char yield (37.4 wt%). It is most likely that this particular strain had some issues during the culture process.
When assessing the differences between the *C. sorokiniana's*, it was noteworthy that species 1 had less treated algae than species 2 that had roughly 12% more. This possibly indicates that less solvolysis occurred for strain 2 during the first reaction stage. Potential differences in carbohydrate configuration may help explain these variable results. It is known that thermal decomposition is easier in hemicelluloses due to their amorphous structure, while cellulose degradation is intermediate due to crystalline structure and glucosidic linkages [38]. Hypothetically, if species 1 had less cellulosic and slightly more hemicellulosic-nature carbohydrates, more solubilization was possible and less treated algae were produced. Strain 2 produced approximately 5% more crude, but of inferior quality composition-wise.
Complementary polysaccharide product fractions were determined to examine influence of strain specific qualities on the SEQHTL performance and resultant yields. It was observed that under conventional SEQHTL operating conditions (Stage 1 at 160°C, 20 min & Feed 1:9), recovery was roughly twice as much for *G. sulphuraria* and *C. vulgaris* than from *C. sorokiniana*, but these values were significantly lower than expected. Therefore, fine-tuning the first stage operating conditions must be explored if the target is algal sugar recovery in the form of native intact polysaccharides.

Proximate & Elemental Analyses
Tables 5.6.2 and Tables 5.6.2 detail the PA and Elemental Analyses data.

Table 5.6.2 Proximate Analyses Results

Sample	Moisture	Dry Mass	Volatiles	Fixed Carbon	Ash
C. sorokiniana 1	1.801	98.199	67.547	21.231	9.420
Treated Algae	1.500	98.500	65.681	26.003	6.816
Biocrude	3.280	96.720	78.507	17.703	0.510
Biochar	0.624	99.376	42.421	49.518	7.437
C. sorokiniana 2	2.815	97.185	64.620	22.482	10.084
Treated Algae	2.987	97.013	62.357	31.638	3.018
Biocrude	3.291	96.709	85.382	10.876	0.452
Biochar	1.218	98.782	47.536	45.479	5.766
G. sulphuraria 1	3.768	96.232	42.673	18.306	35.253
Treated Algae	6.463	93.537	27.991	15.687	49.859
Biocrude	9.040	90.960	71.094	18.695	1.172
Biochar	4.140	95.860	13.851	12.818	69.191
G. sulphuraria 2	2.411	97.589	63.413	20.903	13.272
Treated Algae	2.240	97.760	63.391	27.351	7.018
Biocrude	3.674	96.326	79.310	16.625	0.391

Biochar	1.735	98.265	43.947	49.124	5.194
C. vulgaris	1.555	98.445	63.070	27.015	8.360
Treated Algae	0.447	99.553	63.137	33.235	3.181
Biocrude	4.387	95.613	72.253	21.676	1.684
Biochar	1.613	98.387	36.281	46.523	15.583

Table 5.6.3 Elemental Analyses Data

Sample	C	H	N	S	O**	HHV (MJ/kg) [a]
C. sorokiniana 1	56.612	7.960	12.234	0.780	22.414	26.67
Treated Algae	61.692	8.017	11.278	0.740	18.272	29.21
Biocrude	73.133	9.284	6.172	0.836	10.575	36.31
Biochar	67.732	8.292	8.277	0.550	15.149	32.20
C. sorokiniana 2	58.021	7.659	10.519	0.728	23.074	26.59
Treated Algae	57.622	7.313	7.507	0.639	26.920	25.25
Biocrude	71.473	9.746	5.658	0.439	12.685	36.00
Biochar	69.033	7.513	7.943	0.525	14.987	31.54
G. sulphuraria 1	48.049	7.460	10.680	3.075	30.736	21.77
Treated Algae	47.040	7.399	8.618	1.664	35.279	20.38
Biocrude	71.020	9.119	6.819	1.374	11.668	35.21
Biochar	50.061	9.085	9.272	1.125	30.457	24.66
G. sulphuraria 2	57.316	7.843	12.145	1.447	21.249	27.01
Treated Algae	55.597	7.399	11.022	1.188	24.793	25.13
Biocrude	69.686	8.688	7.166	1.292	13.167	33.86
Biochar	66.381	6.650	10.716	0.936	15.317	29.38
C. vulgaris	55.928	7.670	10.431	0.898	25.072	25.55
Treated Algae	57.611	7.577	9.955	0.768	24.089	26.15
Biocrude	74.021	9.568	7.742	0.867	7.802	37.52
Biochar	70.675	7.872	8.737	0.502	12.214	33.11

**By Difference

[a] Dulong Formula

Only minor differences were verified between the *Chlorella* species; specifically, the treated algae, the biocrude and the char exhibited slight variations (from 4 to 6%) among the volatiles and fixed carbon contents. However, the differences between *Galdieria* 1 and 2, were quite substantial in terms of the volatiles, the fixed carbon and critically in the ash portion. The largest difference pertained to the ash content of the biochars that amounted to a 63% variation. These large amounts of inorganics were distinctly reflected in the increased char production of strain 1.
All of the biocrudes attained had relatively low oxygen content (less than 14%) and reduced nitrogen content (less than 8%). Nonetheless, both the O and N were still higher than that of petroleum crude (Oxygen < 2.0%, Nitrogen < 0.5%, Sulfur < 6.0%) [39], thus upgrading processes are still necessary to attain transportation fuels. Nevertheless, all crudes produced were

very low sulfur (S <1.4%), which improves the quality of said fraction. For the *Chlorella* sp., the O content in the crude was moderately lower than the content (12 to 13.5%) reported in an analogous DHTL study that operated with 10% solids loading between 300 to 350°C [40]. Congruently, the C partitioning into the crude fraction was comparably higher (71.5 – 74.0% vs. 69.1 – 70.7%). For *C. vulgaris*, the O content in the crude was significantly lower than the value (14.8 wt%) reported in an analogous DHTL study that operated with 10% solids loading at 350°C for 1 hour [7]. Additionally, the C recovery in the biocrude was approximately 4% higher for SEQHTL.

Biocrude Characterization

Fatty Acid Methyl ester analyses were performed on the biocrude and the dry algae samples. The major fatty acids identified in the crude oil were palmitic acid, stearic acid and oleic acid, while to a reduced degree tridecanoic acid, linoleic acid, linolenic acid and arachidic acid. *C. sorokiniana* 1 crude had a saturated fatty acid content of 45.03%, a monounsaturated fatty acid (MUFA) of 7.60% and a polyunsaturated fatty acid (PUFA) of 14.44%, whereas *C. sorokiniana* 2 crude had 45.75%, 24.95% and 7.12% respectively. Similarly, *G. sulphuraria* 1 crude had a saturated fatty acid content of 87.83%, a MUFA of 12.17% and a PUFA below the limit of detection, whereas *G. sulphuraria* 2 crude had 67.77%, 20.23% and 8.54% respectively. *C. vulgaris* crude had a saturated fatty acid content of 37.15%, a MUFA of 7.35% and a polyunsaturated fatty acid of 19.29%. In most scenarios, the reduction in longer-chain and PUFA content from the original biomass, accompanied by the corresponding increase in saturated fatty acid content in the crude was observed. This concurs to the thermal degradation (cracking) of long-chain fatty acids and the associated hydrolysis reactions described for the HTL mechanism [9, 41] although, the extent of the aforementioned phenomena varied from one strain to another and between differently grown algae. For instance, for *C. sorokiniana* 1 there was a greater shift towards the production of saturated and short-chained FFA, while for *C. sorokiniana* 2 there was more MUFA content in the crude and the reduction in long-chain FFA from the original biomass was less pronounced. Figure 5.62 illustrates comparative results between the Chlorella sorokiniana's and their corresponding biocrudes.

(a)

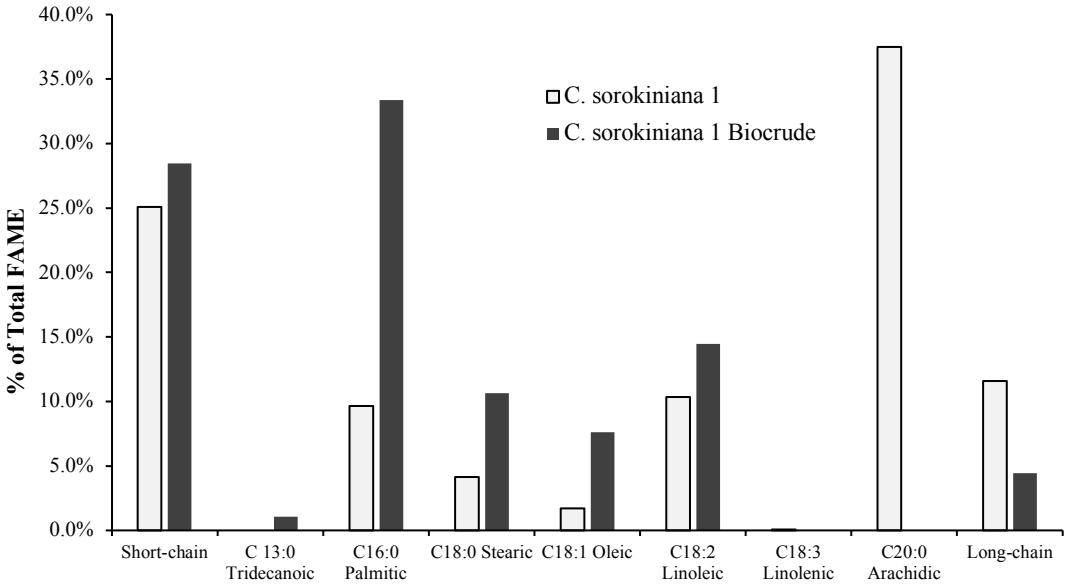

(b)

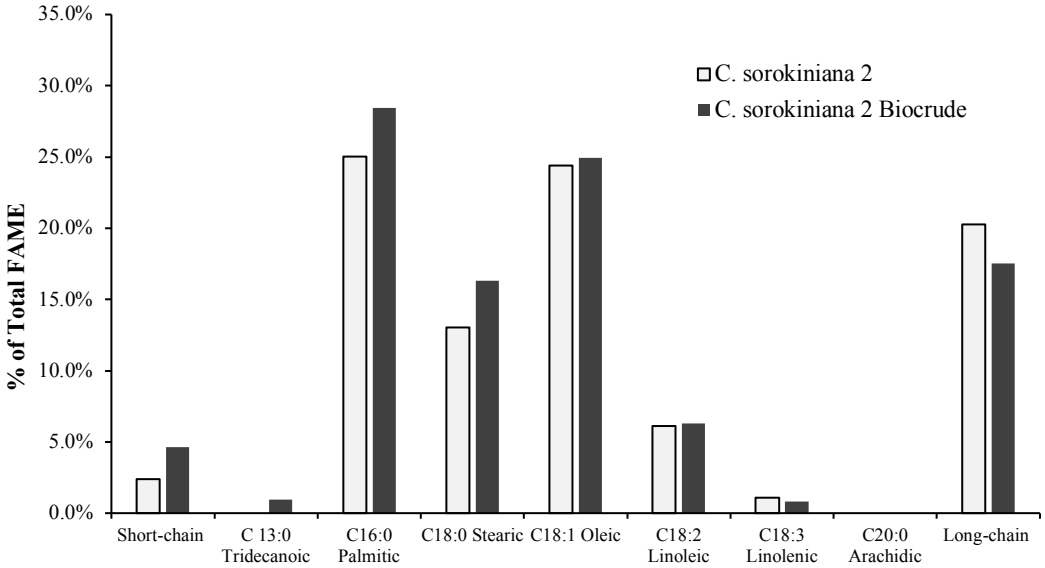

Figure 5.6.2 *C. sorokiniana* FAME Analyses, (a) Strain 1, (b) Strain 2

Consistent with other reports, the GC/MS analyses revealed a variable compilation of components that indicated the contribution to the oily fraction from lipids, as well as carbohydrates, proteins and carotenoid fragments [34]. Only a fraction of the products formed were identifiable by GC–MS, possibly owing to high molecular weights and boiling point distributions of the biocrude [19]; and because some low boiling point compounds may have been masked by the solvent peak or lost when evaporating the solvent. The attained plots correlate to a previous study that estimated that the crudes contain many compounds; and suggested that oxygenated compounds were likely derived from lipid and carbohydrate

degradation, while protein degradation formed nitrogenous compounds [42]. Interestingly, the *Galdieria* crudes had more heteroatoms and complex aromatics, reflected in a higher viscosity lower-quality product.

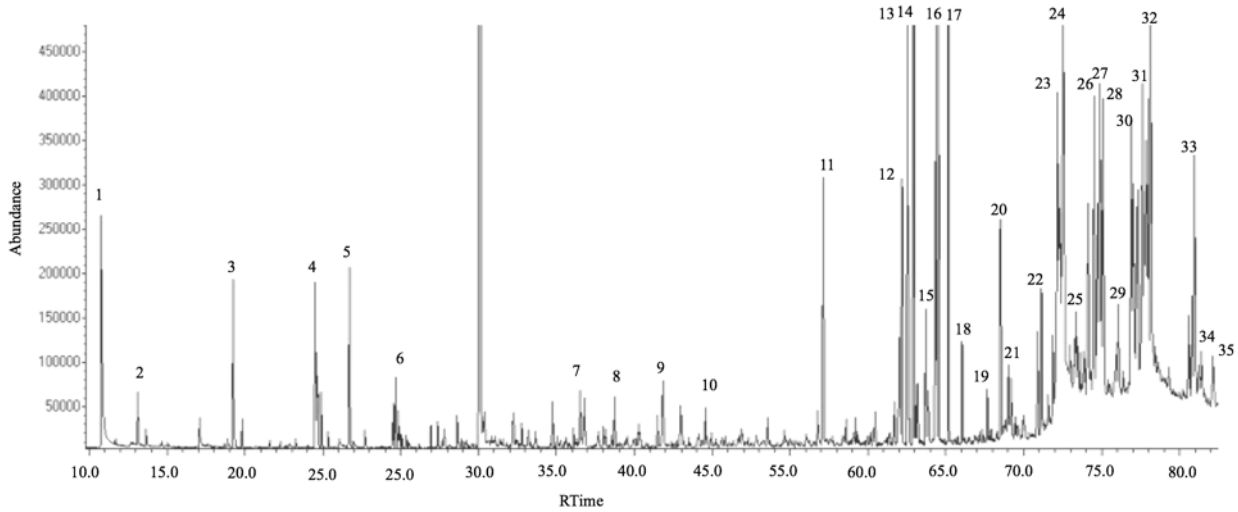

Figure 5.6.3 *C. sorokiniana* 2 Biocrude GC/MS Chromatogram

Gas Product Analyses

The gas samples collected in Tedlar bags were analyzed in a Varian CP-3800 Gas Chromatograph. The gases identified were carbon dioxide, carbon monoxide, hydrogen and methane. The major

component detected was CO_2, and in some runs the levels of carbon monoxide and hydrogen were below the limit of detection. In all runs the thermal conductivity detector (TCD) plot displayed a downwards peak for oxygen. Even though N2 was used to purge oxygen out of the reaction system, the TCD had issues in establishing the baseline for this gas. This was attributed to possible issues in the sampling procedure or when injecting the sample into the analytical instrument. Nonetheless, in all the reports the values for oxygen content were zero. Correspondingly, since the samples were largely diluted with N2, the quantification efforts were at best moderately accurate. Table 5.6.4 details the attained results, which were comparable to a similar HTL study [33].

Table 5.6.4 Gas Product Data

	Composition (mol%)			
SAMPLE	H_2	CO	CO_2	CH_4
C. sorokiniana 1	2.463	0.125	96.968	0.444
G. sulphuraria 1	2.876	0.143	96.671	0.310
C. vulgaris	2.270	0.408	96.876	0.446

Water Product Analyses & Nutrient Assay

Table 5.6.5 describes the attained results and contrasts with a similar study. Due to the variations introduced by the performed dilutions and by the suspended solids in the samples, the minimum, maximum and average values were conveyed. Complementary, the carbon distribution of the water
effluents is reported in Table 5.6.6.

Table 5.6.5 SEQHTL Stage 1 Water Product Nutrient Analyses

	C. sorokiniana 1412.1			*G. sulphuraria* 5587.1			*C. vulgaris* (ASU)			Jena et al., 2011
Parameter	**Max**	**Min**	**Average**	**Max**	**Min**	**Average**	**Max**	**Min**	**Average**	**Average**
pH	5.6	5.3	5.4	2.9	2.6	2.8	5	4.9	4.9	-
Phosphate (mg/L)	3940	3460	3648.9	1160	770	946.3	3050	1990	2640	795.0
Nitrate - N (mg/L)	90	10	56.7	120	40	78.8	60	20	41.3	26.8
Ammonia - N (mg/L)	570	400	488.9	290	190	230	230	130	185.7	12700.0
Total Nitrogen (mg/L)	7300	2200	3711.1	3300	1300	2250	3000	1300	2187.5	16200.0
Organic - N (mg/L)	6650	1790	3165.6	3020	990	1942.5	2810	1260	1983.8	-

Table 5.6.6 Carbon Distribution in SEQHTL Aqueous Effluents

Sample	TC (ppm)	IC (ppm)	TOC* (ppm)
C. sorokiniana Stage 1	11830.0	0.0	11830.0
C. sorokiniana Stage 2	17175.0	131.7	17043.3
G. sulphuraria Stage 1	10345.0	0.0	10345.0
G. sulphuraria Stage 2	11815.0	0.0	11815.0
C vulgaris Stage 1	13805.0	0.0	13805.0
C vulgaris Stage 2	26660.0	108.0	26552.0

For *C. sorokiniana*, phosphorous recovery was quite high with 3650 mg/L, followed by *C. vulgaris* and *G. sulphuraria,* with 2640 and 1580 mg/L, respectively. Phosphorus consumption in

agricultural applications recently has been focused because the already depleting supplies will not be able to fulfill the continuously growing demands [43]. In this study, the highest total nitrogen partitioning into the water effluent, followed a similar trend, *C. sorokiniana* > *C. vulgaris* > *G. sulphuraria*. However, these values compare unfavorably to the DHTL trials, amounting to only 10 – 22% of the values described in the DHTL study. The mild temperatures of SEQHTL used in this study allow for the recovery of greater quantities of phosphorous than direct HTL, whereas nitrogen salvaging in all its forms was lower in comparison. Another HTL study informed that using milder liquefaction conditions favored phosphorus recovery in the aqueous phase [41]. These results highlight the high potential of SEQHTL to recover and recycle water-soluble nutrients either to increase algae productivity or produce value-added products through fermentation or anaerobic digestion. Nonetheless, it is still essential to evaluate the actual contribution of recycling the water soluble nutrients with comprehensive techno-economic analysis.

Transport & Thermophysical Properties

Increasing the solid content in the slurry produced an accompanying effective viscosity escalation for the unprocessed microalgae in this study. This amounted to an average of 0.055, 0.438 and 0.701 Pa-s per wt% increase for *C. sorokiniana*, *C. vulgaris* and *G. sulphuraria*, respectively. Figure 5.6.4 illustrates the rheology data for the microalgae slurries and corresponding treated algae mixtures. It is notable that shear stress increased with the rising shear rate for all strains and concentrations. The mixtures displayed non-Newtonian, shear thinning behavior, so the effective viscosity decreased when shear rate increased. This accords with a similar study in which the observed increased effective viscosity rate was approximately $2x10^{-5}$ Pa-s per % increase [37]. In that report, results indicated that the effective viscosity of the *Chlorella* sp. was more dependent on the shear rate at increased solid loadings, possibly owing to larger cell sizes that were more susceptible to greater elastic deformations under shear.

In this study, for the treated algae slurries, control over particle settling was significantly more challenging during experimental trials. In addition, the effective viscosity escalation rate was less pronounced at 0.032, 0.225 and 0.180 Pa-s per wt% increase on average for *C. sorokiniana*, *C. vulgaris* and *G. sulphuraria*, respectively. This highlights the importance of incorporating adequate homogenization mechanisms prior to feeding the second stage reactor.

Figure 5.6.5 displays specific heat measurements for the microalgae tested at variable solid concentrations. The results confirm that the amount of heat required for a unit mass to elevate the temperature by one degree increased as the temperature of the medium increased. However, this was more pronounced at temperatures below 50°C, and progressively declined at higher temperature levels. In contrast, all the calorimetric thermographs of the treated algae exhibited some exothermic peaks between 150 and 200°C. As seen in previous studies, this was attributed to thermal degradation reactions, in which C-C and C-O bonds break down, discharging moderate quantities of energy [36]. As the solid concentration increased the slurry specific heat diminished, on average by 4.76, 2.90 and 4.96 % for *C. sorokiniana*, *C. vulgaris* and *G. sulphuraria*, respectively. Thus, from this perspective, it would be advantageous to increase the solid concentration to minimize the energy required to preheat the slurry feeds and increase the quantity of biomass processed per volume unit. However, this operation must be balanced with the additional energy that would be expended in harvesting and dewatering the algae [40]. Therefore, a comprehensive energy balance that includes upstream and downstream operations is necessary for determining the ideal scenario for each strain.

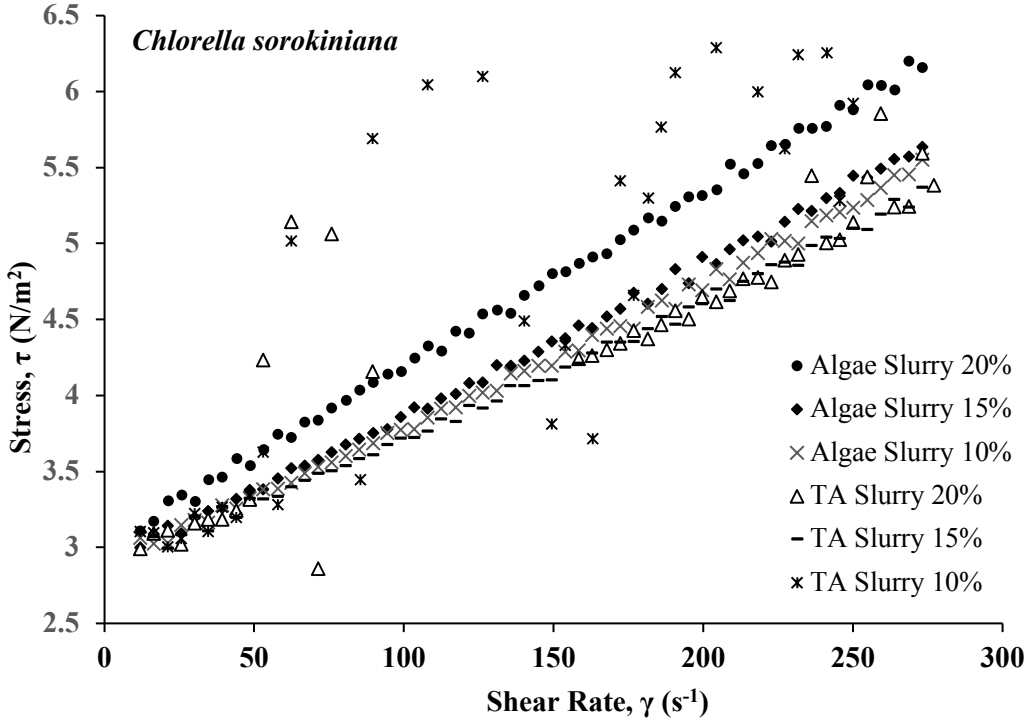
Chlorella sorokiniana
Stress, τ (N/m²)
Shear Rate, γ (s⁻¹)
6.5
6
5.5
5
4.5
4
3.5
3
2.5
0
50
100
150
200
250
300
Algae Slurry 20%
Algae Slurry 15%
Algae Slurry 10%
TA Slurry 20%
TA Slurry 15%
TA Slurry 10%

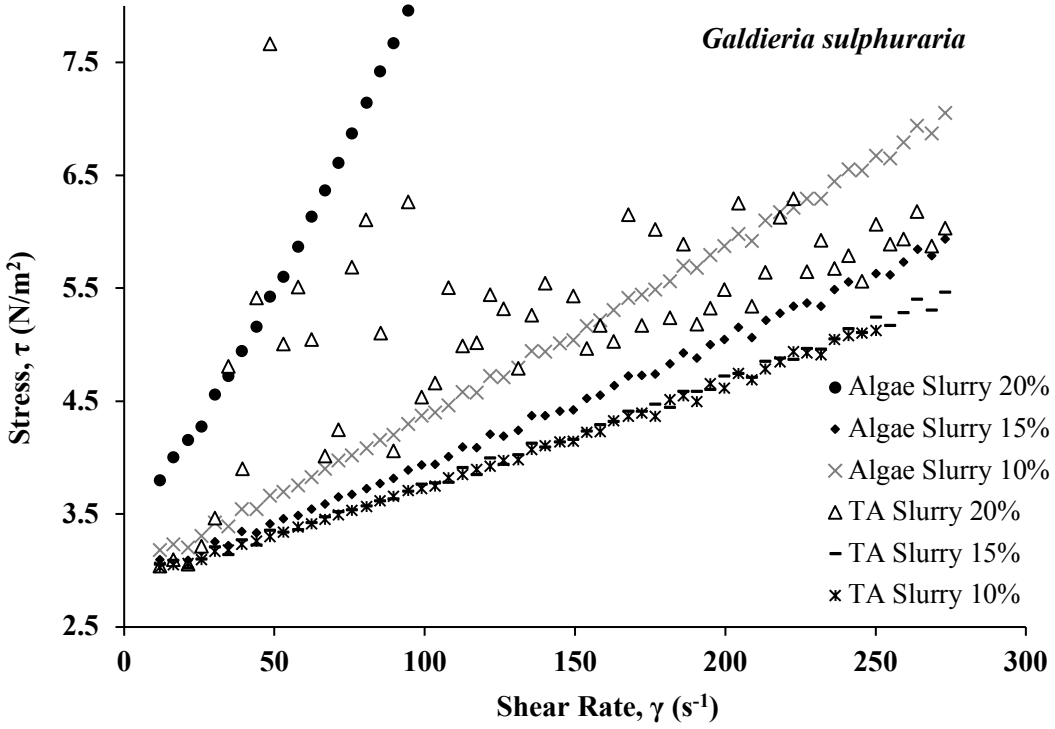
Galdieria sulphuraria
Stress, τ (N/m²)
Shear Rate, γ (s⁻¹)
7.5
6.5
5.5
4.5
3.5
2.5
0
50
100
150
200
250
300
Algae Slurry 20%
Algae Slurry 15%
Algae Slurry 10%
TA Slurry 20%
TA Slurry 15%
TA Slurry 10%

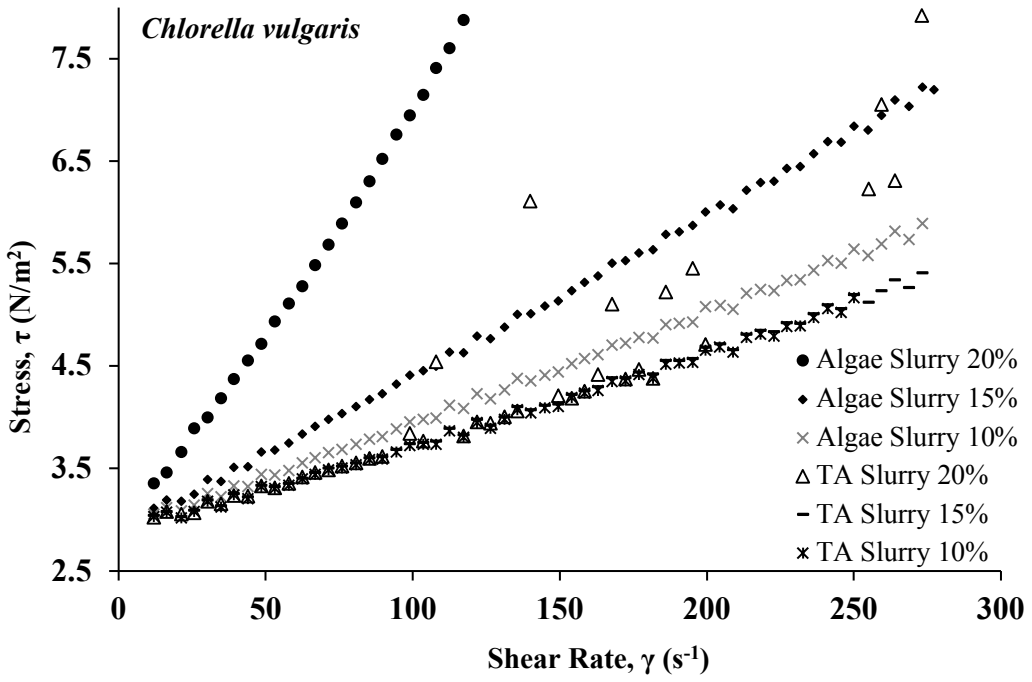

Figure 5.6.4 Shear stress as a function of shear rate, for (a) *C. sorokiniana* (b) *G. sulphuraria*, and (c) *C. vulgaris* for all concentrations at 25°C

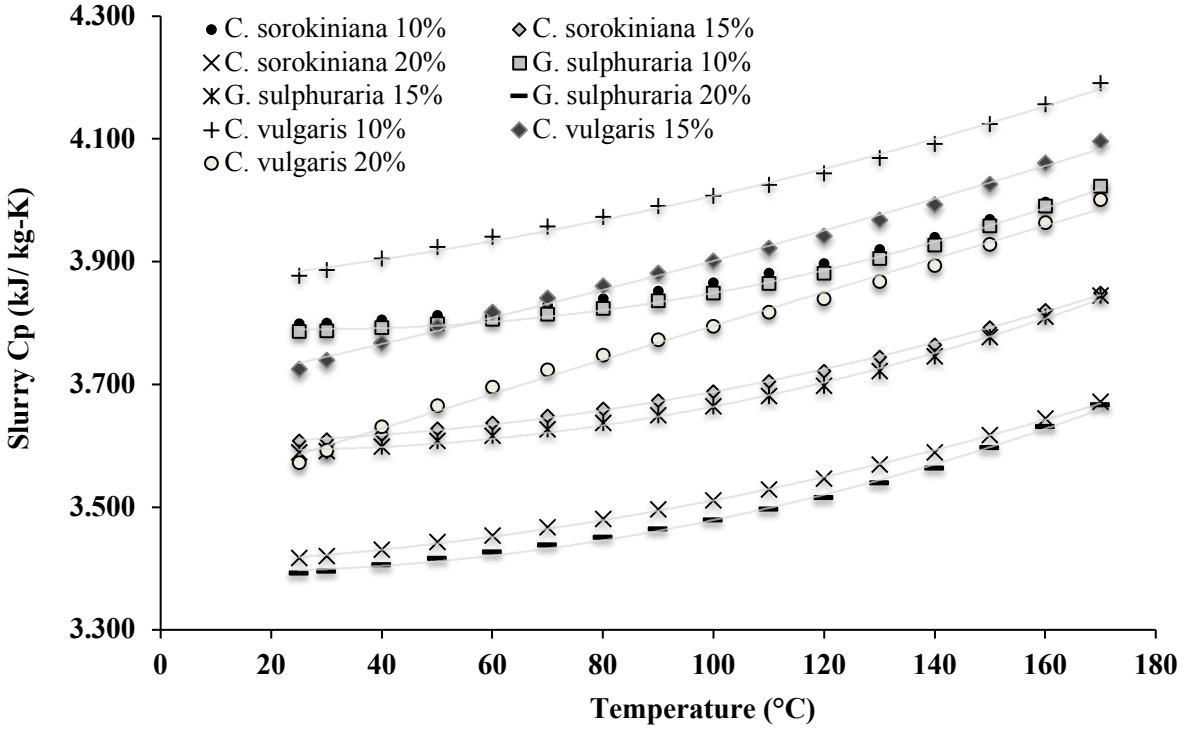

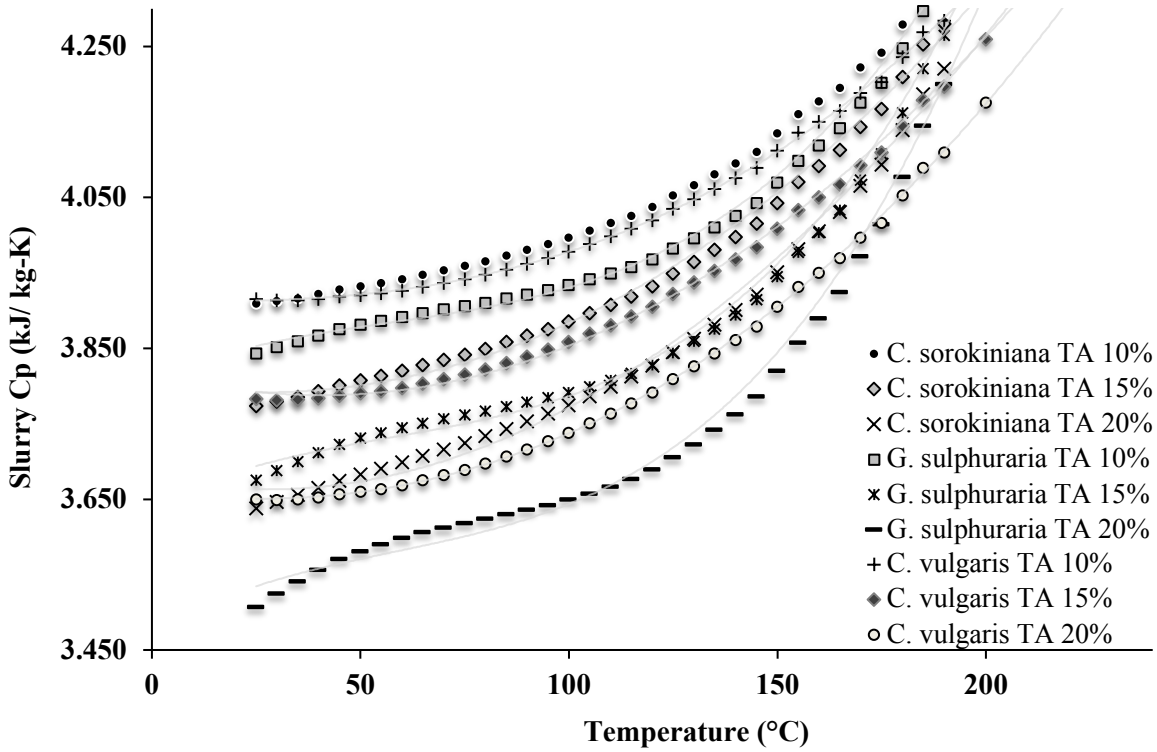

Figure 5.6.5 Specific heat as a function of temperature, for (a) microalgae slurries, and (b) treated algae slurries at different solid loadings

5.6.1c Complementary SEQHTL Trials with 20 wt% solids loading

Based on the preliminary simulation and modeling results from PA3, a slurry feed of 20 wt% was deemed most suitable to reduce energy consumption and related operating costs. Additional batch process trials with *Kirchneriella cornutum*, *Chlorella sorokiniana* 1412 (2016), *Galdieria sulphuraria* 87.1 and *Galdieria sulphuraria* (2016) at 20 wt% were developed to supply the necessary back-up and reference data. All the biomass samples were tested at two different sets of operating conditions: (1) Feed 20 wt%, Stage 1 at 160℃, Stage 2 at 240℃ and (2) Feed 20 wt%, Stage 1 at 180℃, Stage 2 at 300℃. Yields are detailed in Table 5.6.7. Overall, all the algae exhibited better results in terms of biocrude production, at the higher temperature set. Char reduction was also improved. However, results for the lower temperature set may be slightly underestimated because product separation was found to be extremely complicated even with the use of organic solvent. The *Galdieria* 87.1 showed the highest crude yield and lowest char production at 300°C. Conversely, mainly owing to the lower lipid content in the new *Chlorella* algae, the crude yield drastically decreased compared with previous SEQHTL results attained at 10 wt% solids feed.

Thus, SEQHTL is considered more suitable for processing algae with moderate to high lipid contents, while traditional single stage HTL is more flexible in terms of biomass. However, several strategies may be employed in order to increase SEQHTL crude yields, such as developing strain-specific tailored operation conditions or recycling organic carbon and nutrients to increase biomass and lipid productivity through mixotrophic cultures.

Table 5.6.7 Additional Batch SEQHTL Data

Sample	Op Conditions	Treated Algae	Biochar	Biocrude
K. cornutum	1	66.53%	38.11%	17.18%
	2	57.30%	11.89%	26.29%
Galdieria 87.1	1	70.11%	12.61%	20.03%
	2	66.31%	0.54%	36.52%
Chlorella 1412(2016)	1	58.05%	28.09%	7.68%
	2	64.73%	22.86%	14.52%
Galdieria (2016)	1	63.44%	18.75%	5.12%
	2	51.09%	3.70%	23.54%

Product stream characterization was subsequently developed as previously detailed. Results are summarized in Tables 5.6.8 – 5.6.10. Regarding composition, no major differences were assessed between the Treated algae samples at different operating conditions. However, the biocrude and biochar fractions exhibited significantly different characteristics in all scenarios. In the crudes, the high temperature set generally displayed much higher C and H contents, and considerably less O. Interestingly, in some instances the biochars attained for the high temperature reaction set had a higher C recovery and O removal values than the biocrudes, fact that would inevitably would lead to a greater HHV and quality as a fuel product. Yet, it may be possible that some crude may be adsorbed to the char surface, thus causing said increment.

Nutrient recovery varied greatly among species and between different operating conditions. For *Kirchneriella* the nutrient recovery increased slightly, particularly for inorganic Nitrogen, at higher operating conditions. *Chlorella* 1412 exhibited a similar behavior. Contrastingly, the *Galdieria sp.* displayed completely opposite results. For Galdieria 87.1, an increase in reaction temperatures led to a significant increase in nutrient recovery, whereas for Galdieria (2016) the temperature increased led to significant nutrient loss in the water effluent. This highlights the importance of characterizing different biomass alternatives and their corresponding process performance to determine the tradeoffs between species based on desired product and industrial applications.

Similarly, the C partitioning to the water effluents, was only slightly increased for *Kirchneriella* and *Chlorella* at higher temperatures. Yet, for *Galdieria* 87.1 the C loss to the water effluents was substantially higher, and for *Galdieria* (2016) the Water products at higher temperatures showed less C.

Table 5.6.8 Product Fractions Elemental Analyses

Sample	Op Conditions	C	H	N	S	O
K. cornutum		59.832	8.179	6.299	0.557	25.133
Treated Algae	1	63.104	8.623	5.612	0.533	22.129
	2	66.041	8.711	5.496	0.528	19.224
Biocrude	1	56.882	7.404	2.113	0.342	33.259
	2	76.6602	9.8768	4.0790	0.2591	9.1249
Biochar	1	56.357	8.190	6.419	0.538	28.497
	2	84.479	9.698	4.591	0.306	0.926
Galdieria 87.1		52.012	7.098	11.038	1.243	28.609
Treated Algae	1	54.337	7.159	11.067	1.195	26.242
	2	56.595	7.129	11.241	1.128	23.907
Biocrude	1	64.552	8.292	8.570	1.221	17.365
	2	73.9168	8.0409	7.0473	0.9885	10.0066
Biochar	1	67.820	7.044	10.271	0.844	14.021
	2	55.486	5.860	6.807	0.851	30.996
Chlorella 1412		49.003	6.942	5.336	0.447	38.272
Treated Algae	1	55.042	7.005	6.203	0.489	31.261
	2	57.568	6.967	6.615	0.519	28.331
Biocrude	1	72.566	8.968	5.629	0.495	12.342
	2	77.647	8.867	5.794	0.365	7.327
Biochar	1	68.510	6.602	7.979	0.468	16.441
	2	80.678	6.567	7.225	0.218	5.311
Galdieria (2016)		49.201	6.769	9.827	1.392	32.810
Treated Algae	1	52.931	6.782	10.070	1.337	28.879
	2	55.656	6.937	10.532	1.290	25.584
Biocrude	1	69.561	8.780	5.907	1.003	14.749
	2	78.8028	7.5066	6.8127	0.6898	6.1881
Biochar	1	70.572	6.959	9.588	0.864	12.017
	2	79.146	6.912	7.468	0.563	5.912

Table 5.6.9 Water Product Nutrient Analyses

Sample	Op Conditions	pH	PO_4^{3-} (mg/L)	NH_3 (mg/L)	Total N (mg/L)
Kirch Stage 1	1	4.50	3670.0	450.0	3900.0
			3780.0	460.0	3400.0
Kirch Stage 2	1	6.00	3840.0	1890.0	6600.0
			3870.0	1990.0	6600.0
Kirch Stage 1	2	4.30	5950.0	900.0	6400.0
			5930.0	950.0	5900.0
Kirch Stage 2	2	8.50	2740.0	4100.0	7500.0
			2700.0	4230.0	6100.0

Gs 87.1 Stage 1	1	5.00	8020.0	1150.0	9300.0
			8910.0	1220.0	8800.0
Gs 87.1 Stage 2	1	8.10	7550.0	5000.0	18700.0
			6650.0	4870.0	18600.0
Gs87.1 Stage 1	2	5.20	18040.0	2820.0	17700.0
			18970	2790	18400
Gs 87.1 Stage 2	2	8.9	2490.0	10900.0	17500.0
			2530	8140	18300
Cs 1412 Stage 1	1	4.70	4180.0	600.0	4100.0
			4210.0	570.0	4200.0
Cs 1412 Stage 2	1	6.40	4810.0	2800.0	8000.0
			4890.0	2800.0	8600.0
Cs 1412 Stage 1	2	4.30	5370.0	940.0	6400.0
			5380.0	900.0	6000.0
Cs 1412 Stage 2	2	8.00	5300.0	5720.0	9800.0
			5270.0	5560.0	9800.0
Gs 2016 Stage 1	1	4.10	6050.0	830.0	8600.0
			5730.0	920.0	8700.0
Gs 2016 Stage 2	1	7.90	10250.0	5140.0	21100.0
			9920.0	5220.0	21300.0
Gs 2016 Stage 1	2	4.20	8860.0	1940.0	12000.0
			9170.0	1900.0	12900.0
Gs 2016 Stage 2	2	9.10	2410.0	9980.0	16000.0
			2460.0	10100.0	16500.0

Table 5.6.10 Water Product Carbon Distribution

Sample	Op Conditions	TC (mg/L)	IC (mg/L)	TOC (mg/L)
K. cornutum Stage 1	1	29940	0	29940
K. cornutum Stage 2		27680	0	27680
K. cornutum Stage 1	2	40940	0	40940
K. cornutum Stage 2		20490	0	20490
Gs 87.1 Stage 1	1	39670.0	0.0	39670.0
Gs 87.1 Stage 2		56560.0	0.0	56560.0
Gs 87.1 Stage 1	2	80150.0	0.0	80150.0
Gs 87.1 Stage 2		29280.0	4616.0	24664.0
Cs 1412 Stage 1	1	35340	0	35340
Cs 1412 Stage 2		26500	0	26500
Cs 1412 Stage 1	2	41890	0	41890
Cs 1412 Stage 2		23060	0	23060

Gs 2016 Stage 1	1	36490	0	36490
Gs 2016 Stage 2		63000	0	63000
Gs 2016 Stage 1	2	56300	0	56300
Gs 2016 Stage 2		31200	3802	27398

The Fatty acid profile of the crude also varied significantly at the two operating conditions. Overall all strains except *Galdieria* (2016) exhibited a pronounced decrease in the saturated fatty acid content (particularly in stearic and palmitic acid) as the temperature increased. Yet, this alga displayed a substantial content of long chain fatty acids at 300°C.

(a)

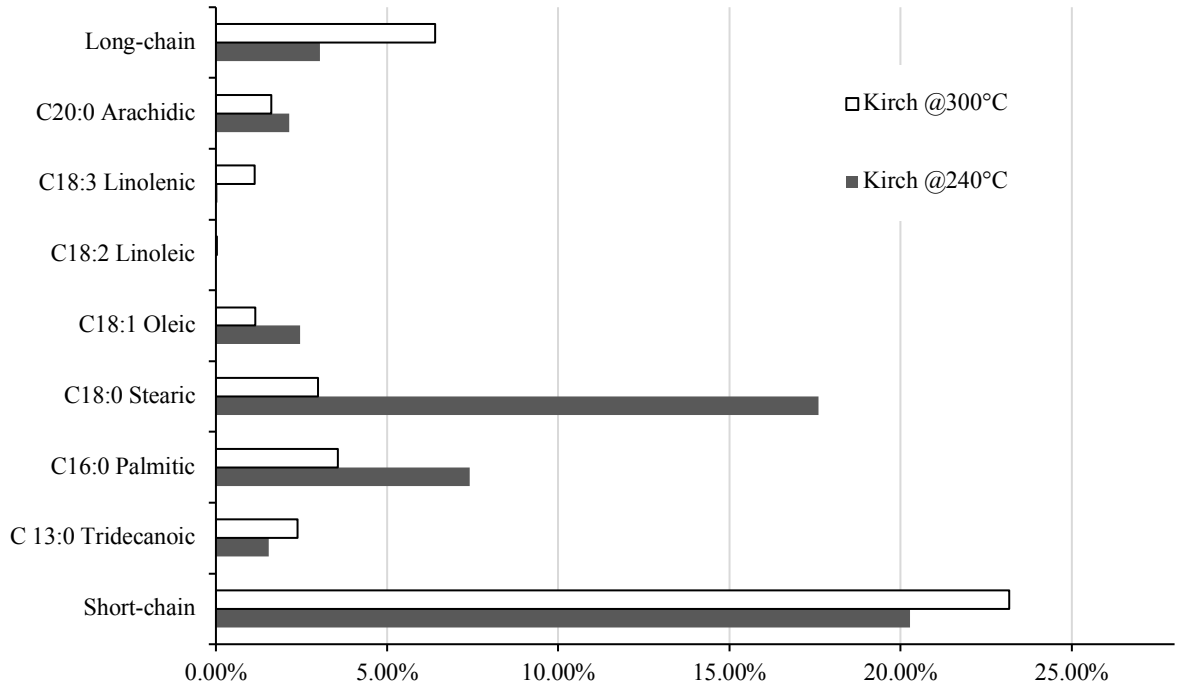
Long-chain
C20:0 Arachidic
C18:3 Linolenic
C18:2 Linoleic
C18:1 Oleic
C18:0 Stearic
C16:0 Palmitic
C 13:0 Tridecanoic
Short-chain
Kirch @300°C
Kirch @240°C
0.00%
5.00%
10.00%
15.00%
20.00%
25.00%

(b)

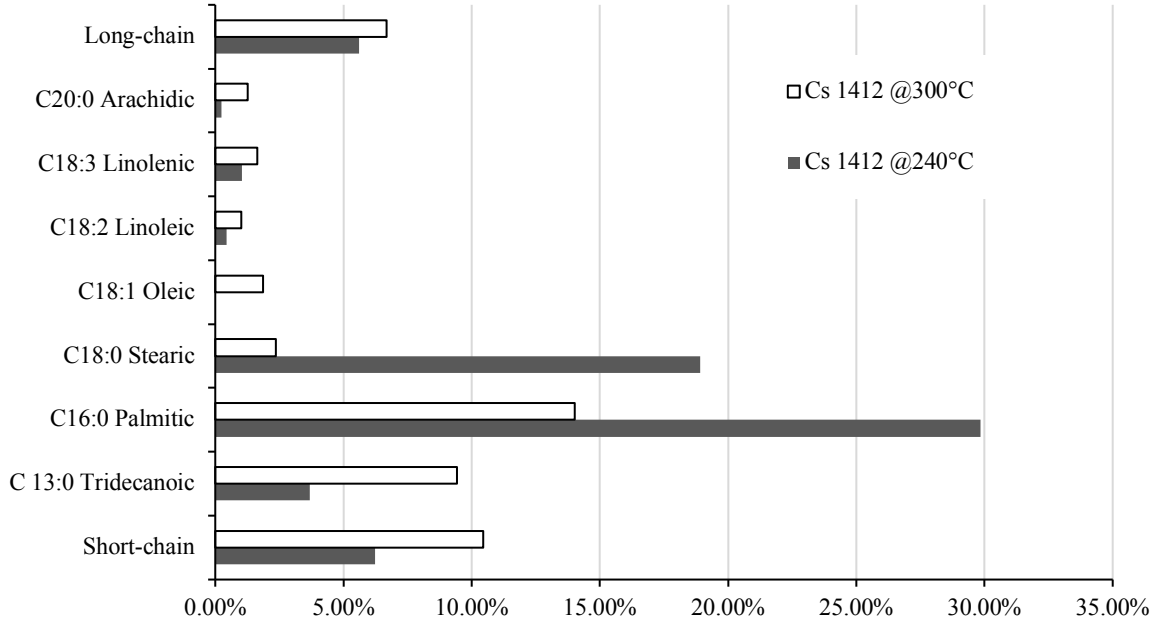
Long-chain
C20:0 Arachidic
C18:3 Linolenic
C18:2 Linoleic
C18:1 Oleic
C18:0 Stearic
C16:0 Palmitic
C 13:0 Tridecanoic
Short-chain
Cs 1412 @300°C
Cs 1412 @240°C
0.00%
5.00%
10.00%
15.00%
20.00%
25.00%
30.00%
35.00%

(c)

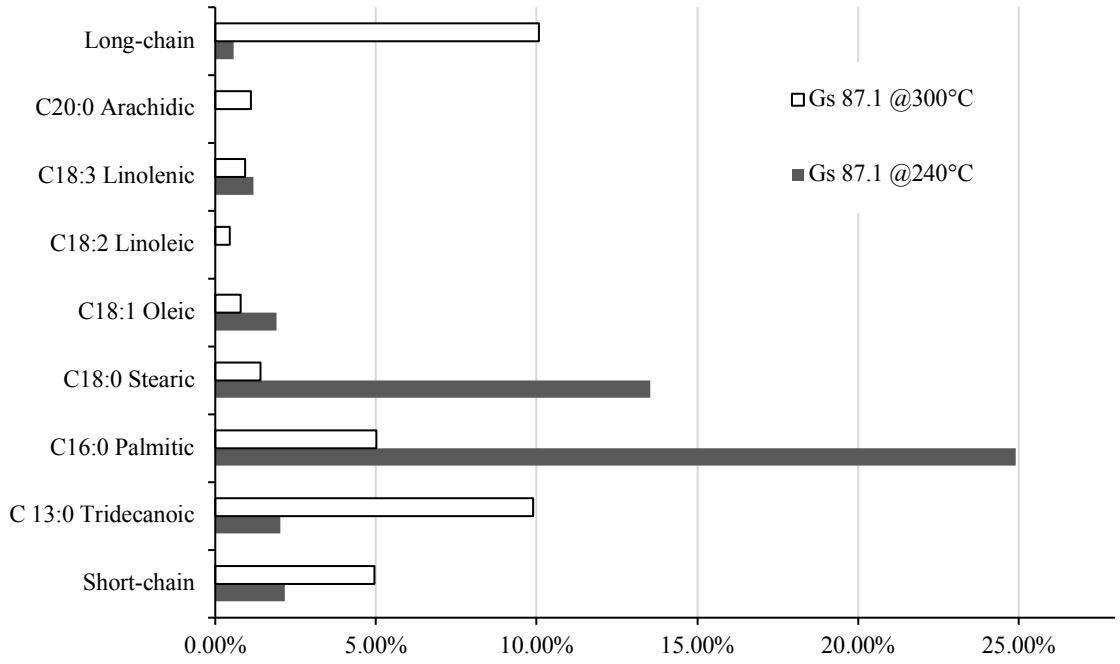

(d)

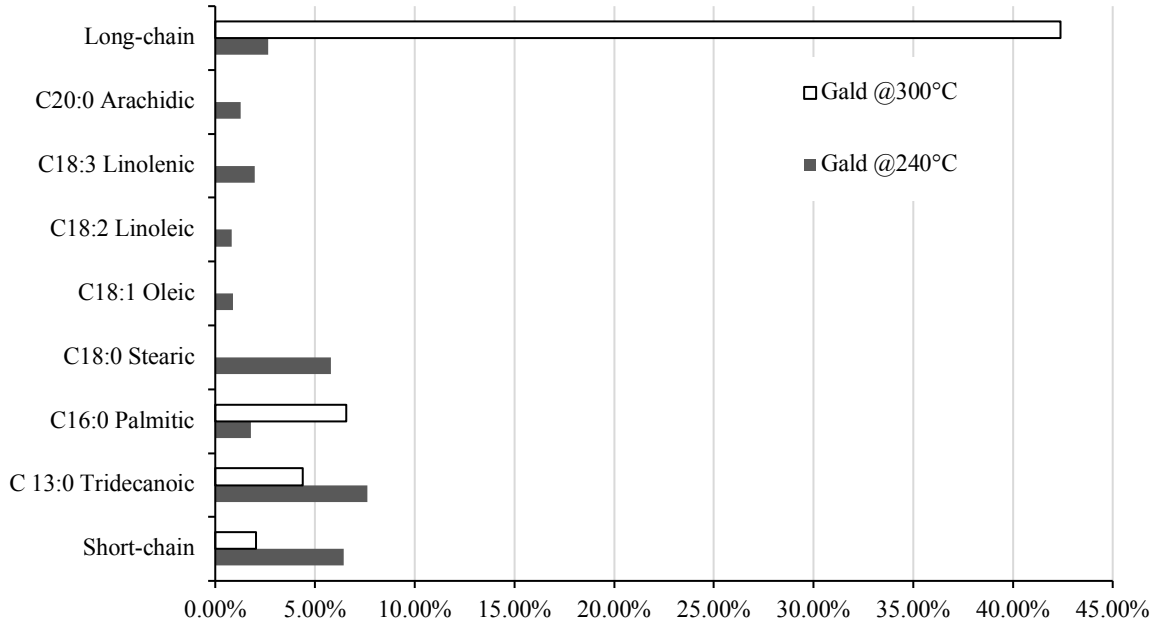

Figure 5.6.6 Fatty Acid Profile variation with Temperature, (a) *Kirchneriella*, (b) *Chlorella* 1412, (c) *Galdieria* 87.1, (d) *Galdieria* 2016

In terms of the GC/MS results, both the *Galdieria* 2016 and the *Chlorella* 1412 exhibited a sharp decrease in the detectable volatiles. Potentially the higher reaction temperatures favored polymerization and condensation reactions that led to the formation of complex high molecular weight compounds that are not detectable by the GC/MS. This correlated with the increased content of oxygen rich heteroatoms and the observed amplified crude viscosity. Thus, although the higher temperatures favored an increased crude yield; for these algae oil the quality decreased mainly owing to the concentration and structure of oxygen-rich compounds. These compounds are of particular concern since they can polymerize, leading to storage instability, and high hydrogen consumption and operation severity in upgrading processes. Contrastingly, the *Galdieria* 87.1 crudes displayed a completely opposite behavior. The higher temperature favored the formation of more detectable volatiles.

(a)

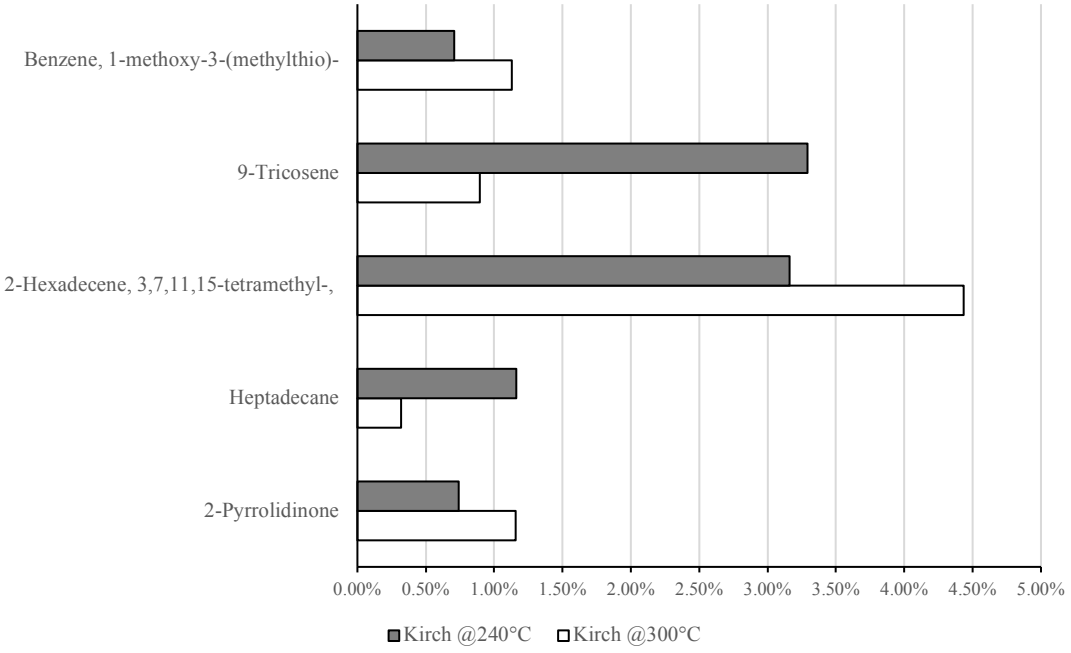

(b)

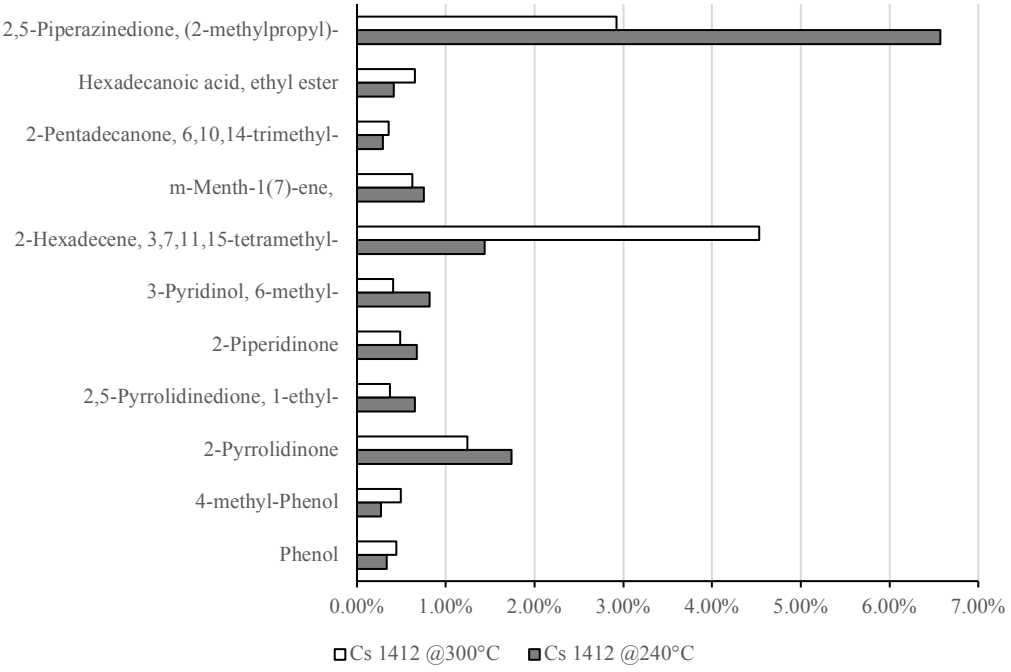
2,5-Piperazinedione, (2-methylpropyl)-
Hexadecanoic acid, ethyl ester
2-Pentadecanone, 6,10,14-trimethyl-
m-Menth-1(7)-ene,
2-Hexadecene, 3,7,11,15-tetramethyl-
3-Pyridinol, 6-methyl-
2-Piperidinone
2,5-Pyrrolidinedione, 1-ethyl-
2-Pyrrolidinone
4-methyl-Phenol
Phenol
0.00%
1.00%
2.00%
3.00%
4.00%
5.00%
6.00%
7.00%
Cs 1412 @300°C
Cs 1412 @240°C

(c)

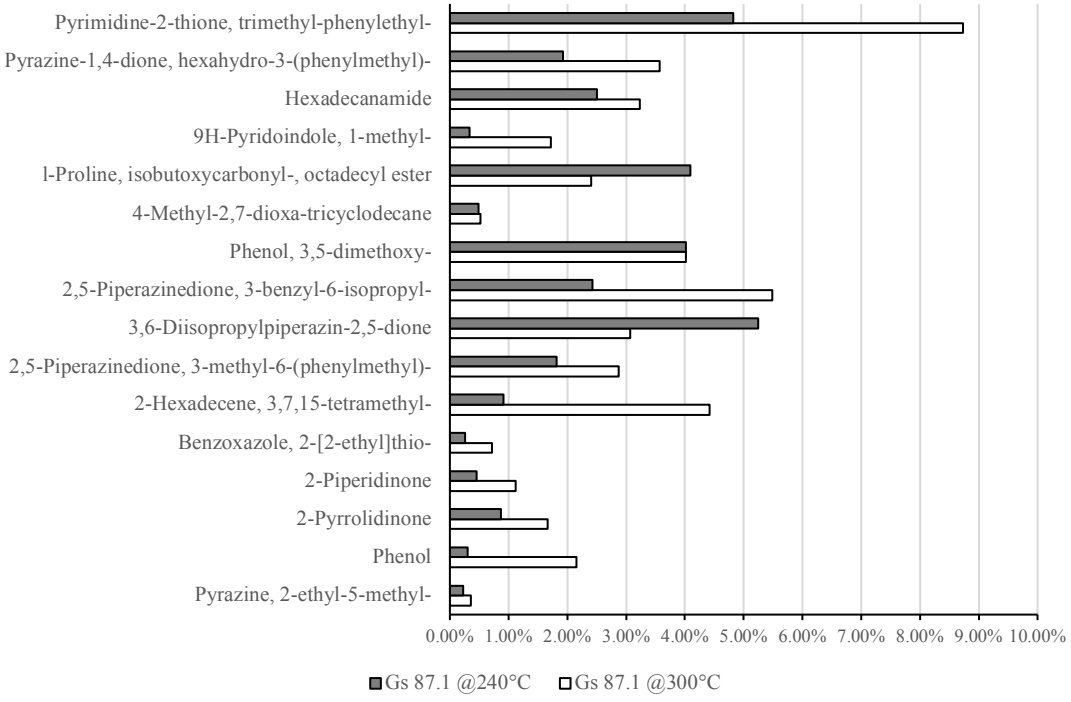
Pyrimidine-2-thione, trimethyl-phenylethyl-
Pyrazine-1,4-dione, hexahydro-3-(phenylmethyl)-
Hexadecanamide
9H-Pyridoindole, 1-methyl-
l-Proline, isobutoxycarbonyl-, octadecyl ester
4-Methyl-2,7-dioxa-tricyclodecane
Phenol, 3,5-dimethoxy-
2,5-Piperazinedione, 3-benzyl-6-isopropyl-
3,6-Diisopropylpiperazin-2,5-dione
2,5-Piperazinedione, 3-methyl-6-(phenylmethyl)-
2-Hexadecene, 3,7,15-tetramethyl-
Benzoxazole, 2-[2-ethyl]thio-
2-Piperidinone
2-Pyrrolidinone
Phenol
Pyrazine, 2-ethyl-5-methyl-
0.00%
1.00%
2.00%
3.00%
4.00%
5.00%
6.00%
7.00%
8.00%
9.00%
10.00%
Gs 87.1 @240°C
Gs 87.1 @300°C

(d)

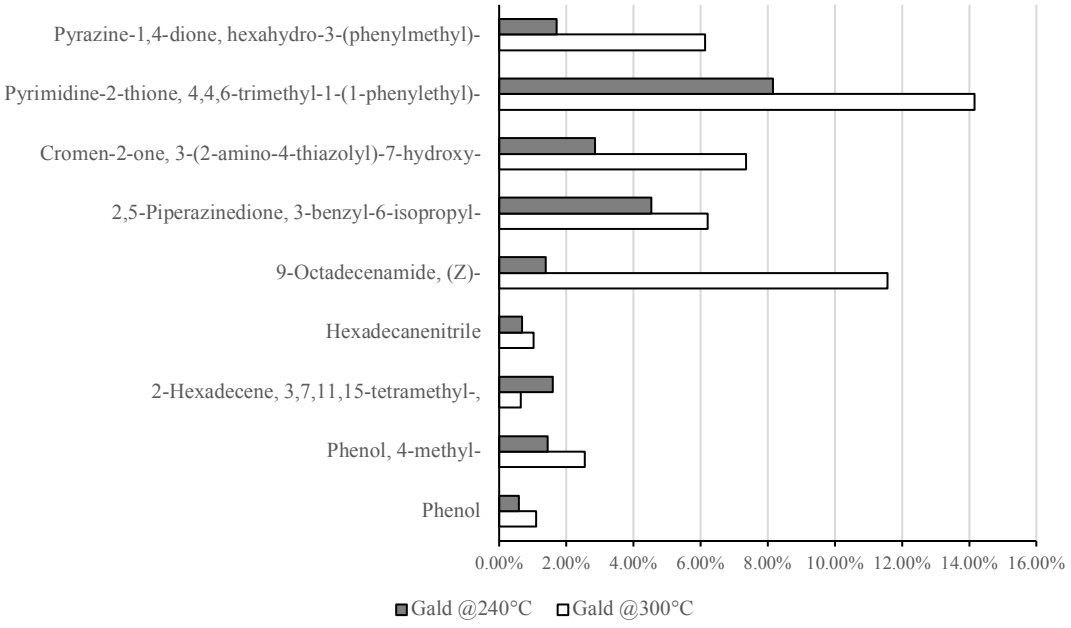

Figure 5.6.7 GC/MS variation with Temperature of some compounds, (a) *Kirchneriella*, (b) *Chlorella* 1412, (c) *Galdieria* 87.1, (d) *Galdieria* 2016

5.6.2 Char characterization and utilization

One of the major products of HTL or SEQHTL is the solid residue formed by biomass carbonization unofficially deemed as "biochar" [15, 44]. The solid biochar product consists of primarily reduced aromatic carbon compounds and most of the feedstock's mineral components. Biochar yields vary depending on the algae, its chemical composition and the operating conditions employed in the process. In one study the variation among solids yields was very large, ranging from 41.6 wt% for *S. obliquus* which is characterized by possessing a very resistant cell wall; to 17.8 wt% for *P. tricornutum* and 11.9 wt% for *D. tertiolecta*, these two lacking a resistant cell wall [45]. In other studies char yields were negligible [6, 46], yet these results were dependent on a particular algal species. Yet, for HTL and SEQHTL to develop a successful industrial platform, an "algae crop" rotation system, that ensures the high year-round productivity essential to an optimized LCA, will be required [8]. Moreover, it has estimated that at the scale of replacing petroleum with microalgae derived biofuels for the US gasoline supply, approximately 75 – 232 million tons of char (with yields ranging from 10 – 30wt%) would be produced annually [47]. Therefore, developing a cost-effective application for this product fraction will play a significant role in the development of microalgae bio-refineries.

To assess the viability of employing the solid charcoal residue as low-value fuel for heat energy, the collected and dried biochar samples were combusted on an isoperbol Bomb calorimeter

(Parr6200, Parr Instrument Co.) following guidelines detailed in ASTM procedures D-4809 and D-5865.

The biochar combustion trials results are detailed in Table 5.6.11. For the *Chlorella* algae, experimental values were only moderately lower than calculated results. For *Galdieria sulphuraria*, we observed a prominent decrease, and the experimental value was not comparable to that of the other strains. Although the experiments employed excess amounts of oxygen and ideal combustion conditions, the *Galdieria* char did not undergo complete reaction. More research is needed to elucidate the reason for this behavior. Nonetheless, this results confirm the potential of using the biochar fraction as a low-value fuel to supply a portion of the required heat energy; thus mitigating a portion of the operational costs and making the process more feasible.

However, a comprehensive energy balance that considers heat integration mechanisms from reactor effluent streams, the energy expended in drying the biochar, as well as inevitable heat losses during conversion and due to combustion inefficiencies, is still required. Also, due to the significant nitrogen content in the char, excess NOx emissions would be produced during combustion. Thus, in order to comply with established environmental regulations and to reduce the process' environmental footprint, given the nitrogen content in the char, this application may not be suitable. Consequently, the exploration of alternative uses for the biochar product fraction is an area of research that warrants further development.

Table 5.6.11 Char Combustion Trials

	C. sorokiniana	*G. sulphuraria*	*C. vulgaris*
Heating Value (MJ/kg)			
Estimated [a]	31.54	29.38	33.11
Experimental	30.43	6.47	29.11

[a] Estimated with Dulong Formula.

5.6.3 Microalgae Growth Trials and Nutrient Recycling

Task summary:

The objective of this task was to determine the ability to utilize N and P from SEQHTL. Nutrition recovery is important for a sustainable future algal biomass technology. The major research activities performed under this task include evaluating the utilization of nutrition from SEQHTL by microalgae and oleaginous yeast. The major results obtained under this task include: (1) determine the N/P/C recovery from SEQHTL by three microalgae species, (2) determine the capability of growing oleaginous yeast.

SEQHTL Stage 1 water product was used to grow microalgae and oleaginous yeast biomass. Since phosphate is the most abundant element from SEQHTL (10 time higher compared to normal algae medium), a dilution was conducted for the growth of algae. SEQHTL liquid product can be effectively reutilized by

some algae species, e.g. *Chlorella sorokiniana* and *Chlorella vulgaris*. It was determined that approximately 60 –70% of the total sugar content was consumed during the cultivation period. Around 70 –80% of the total nitrogen was used up; most of the ammonia –N was expended in the second day. Additionally, 80-90% of the phosphate can be recovered by microalgae. There were no significant differences in the fatty acid contents of algae produced under the different treatments. It was determined that SEQHTL Stage 1 effluent cannot adequately support fast growth of oleaginous yeast.

In summary, most of the nutrients from SEQHTL Stage 1 can be utilized by microalgae, e.g. *Chlorella sorokiniana* and *Chlorella vulgaris*, particularly phosphate. However, the imbalance of available nutrient ratio (C: N: P) in SEQHTL Stage 1 does not allow fast biomass growth. Moreover, because most of the sugar is in polysaccharide form and most of the Nitrogen is organic nitrogen (not NH_4^+), the algae take longer periods of time to either metabolize or partially process these compound. Due to low contents of mono sugars can be assimilated by yeast, SEQHTL Stage 1 cannot support rapid growth of oleaginous yeast. Therefore, for growth of biomass applications, further optimization and conditioning of the SEQHTL Stage 1 aqueous effluent is recommended.

5.6.3a Experimental Methods

The phenol-sulfuric acid method was used to determine the total carbohydrates in the medium. Total nitrogen, NO_3^--N, Ammonia-N and $PO4^{3-}$ were determined by a HACH DR/2400 according to pre-established procedures. The mono sugar content was determined by ion chromatography. The Fatty Acid profile and composition was determined via GC-FID.

In preliminary Chlorella growth trials, the medium was first incubated at 26°C, then centrifuged at 150 rpm for less than 48 h as a pre-conditioning step. Seed inoculums (5%, v/v) were then added to each culture medium, containing up to 100 mL of Stage 1 effluent and supplemented with 1.5g/L NaNO3. Cultures were maintained at 26°C and 150 rpm in 250 mL flasks. *Chlorella* growth with BG-11 medium served as a control. Subsequently, 1 mL broth samples were collected accordingly for OD analysis and lipids assessment. Finally, cells were harvested by centrifugation to determine dry weight measurement, and the supernatant was used for sugar measurement.

Yeast strains were grown in a pre-culture medium consisting of 3 g/L yeast extract, 3 g/L malt extract, 5 g/L peptone, and 10 g/L xylose. The medium was first incubated at 30°C and 150 rpm for less than 24 h as a pre-culturing step. Seed inoculums (10%, v/v) were then added to the culture medium containing 50 mL of non-detoxified liquid hydrolysate (NDLH) and 50 mL of Main Culture Medium (0.4 g/L $MgSO_4$-$7H_2O$, 2 g/L KH_2PO_4, 0.003 g/L $MnSO_4$-H_2O, 0.0001 g/L $CuSO_4$-$5H_2O$, and 1.5 g/L yeast extract). Cultures were maintained at 28 –30°C and 200 rpm in 250 mL flasks. Several samples were collected for assessing cell dry weight and fatty acid analyses.

5.6.3b Results & Discussion

Preliminary Growth Trials

Water product samples from SEQHTL process, stage 1 were used for growth of *Chlorella*. The optimal concentration of SEQHTL effluent samples for culture were determined. It was found

that the SEQHTL stage 1 aqueous product mainly contains mono- and poly-sugars, phosphorous-derived compounds and organic nitrogen. The best dilution rate for *Chlorella sorokiniana* was around 25 – 30. Foaming posed a serious issue during culture aeration, which was directly linked to the lower dilution values and led to material loss. Thus, 100µl of anti-foaming agent was added after 2 h of culture. It was deemed that the SEQHTL stage 1 water product is very suitable for microalgae culture due to the high nutrient recovery. However, the pure Stage 1 effluent was toxic to microalgae and thus some preconditioning dilution was inevitable. The *Chlorella* grew better with inorganic N supplementation than without it. However, in some treatments, the algae did grow significantly in absence of an inorganic N source; thus further studies are required to elucidate if *Chlorella* used some forms of organic N present. Interestingly, the P concentration in the effluent with a dilution of 120 was equal to that in BG11 medium; thus, all other lower dilution rates had significantly more P content than the commercial growth medium. This highlighted the potential of SEQHTL technology to recover said nutrient.

5.6.3.1 Sugar utilization (mono sugars and polysaccharides)

Table 5.6.12 Sugar Content in the medium (mg/L)

Total Sugar	Mono-sugar
307.48 ± 10.83	1.35 ± 0.19

The total sugar in the aqueous product included mono-sugars (arabinose, galactose, glucose, xylose) and polysaccharides. Table 1 indicates the total sugar content in the initial culture medium. Most of the sugar content was in the form of polysaccharides, while the mono-sugar content was very low.

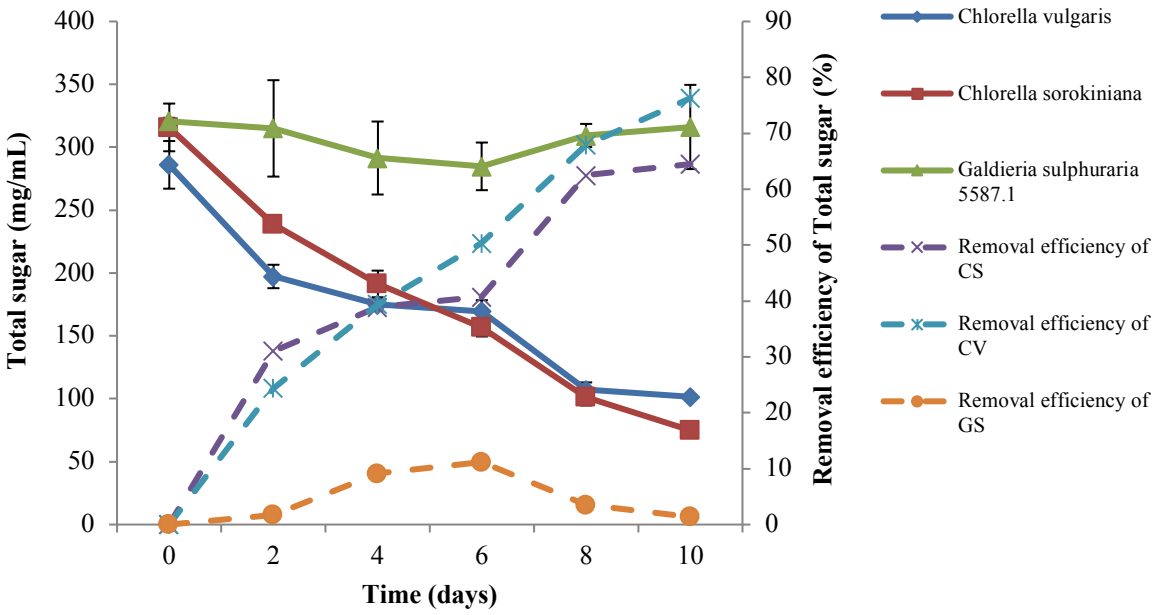

Figure 5.6.8 Total Sugar Utilization and Removal Efficiency by three different Microalgae

Figure 5.6.8 illustrates the total sugar consumption by the microalgae studied. Total sugar utilization decreased as the culture period was prolonged. For *Chlorella vulgaris* (CV), the initial and final (after cultivation) total sugar content were 286.0±18.9 mg/L and 101.6±2.1 mg/L, respectively. Contrastingly, for *Chlorella sorokiniana* (CS), the initial and final total sugar were 315.8±19.0 mg/L and 74.9±5.4 mg/L, respectively. Thus, the total sugar utilization was 64.5% and 76.3% for CV and CS, respectively. *Chlorella sorokiniana* had a higher sugar consumption than CV. Conversely, total sugar consumption by *Galdieria sulphuraria* 5587.1 (GS) was minimal.

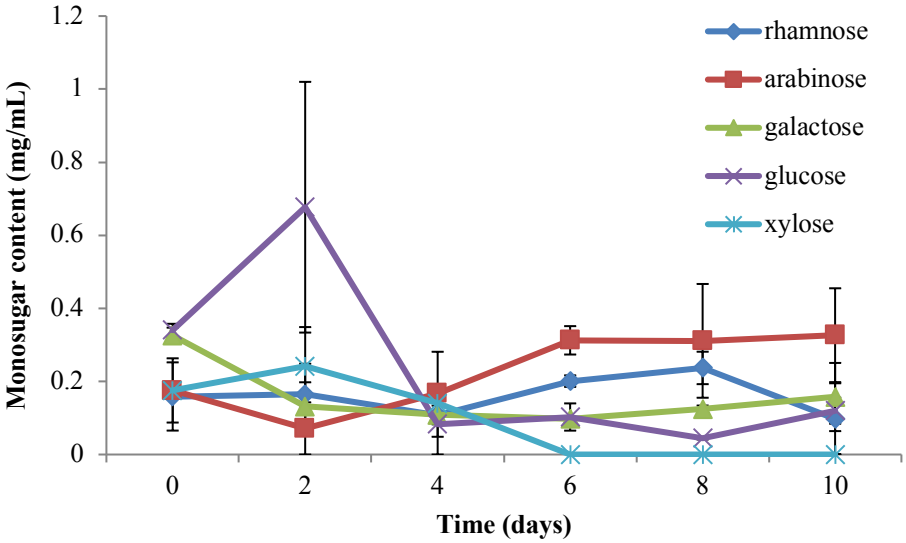

Figure 5.6.9 Mono-sugar Content during culture of CS

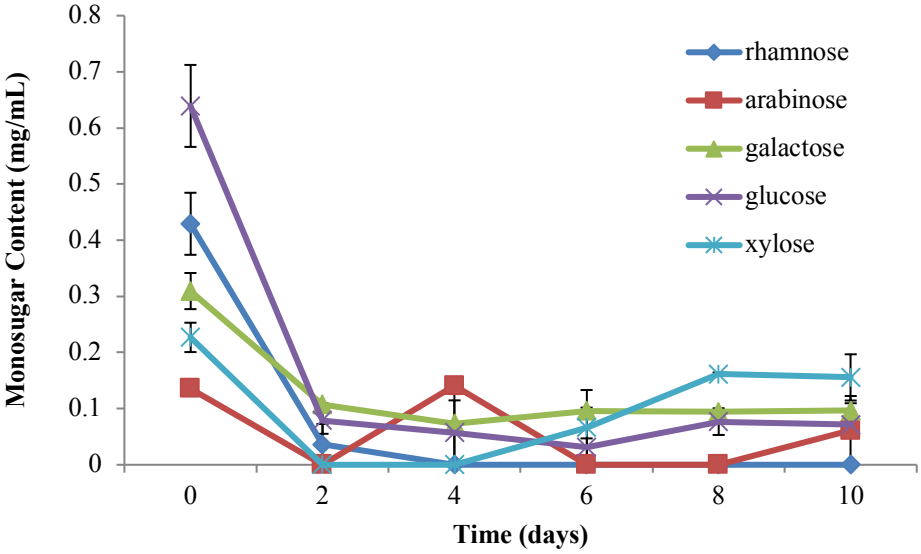

Figure 5.6.10 Mono-sugar Content during culture of CV

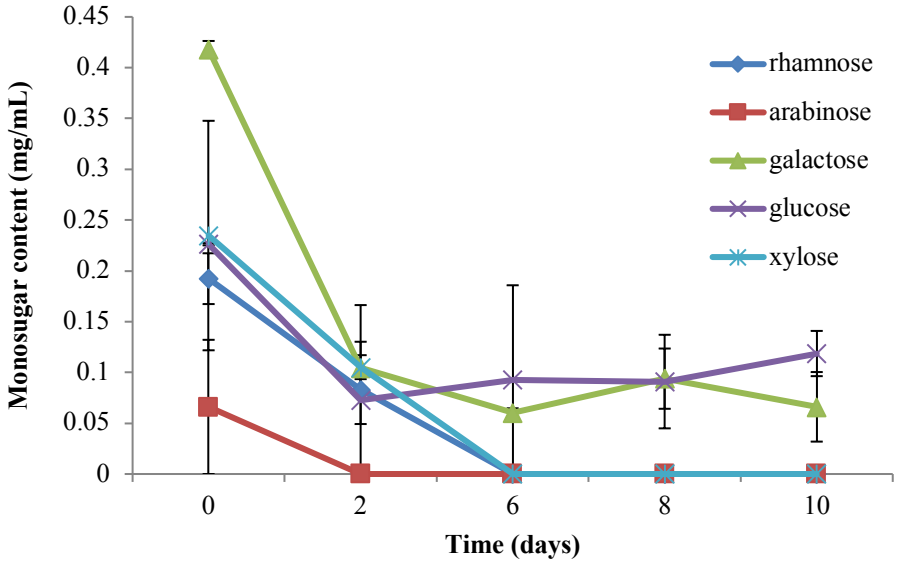

Figure 5.6.11 Mono-sugar Content during culture of GS

Figure 5.6.9 – 5.6.11 illustrate how the mono-sugar content varied during the culture periods for the different algae. By assessing the total sugar and the mono-sugar content variations, it becomes evident that part of the polysaccharides were hydrolyzed into simple sugars by CS and CV microalgae. However, there was no arabinose, rhamnose, xylose after 2 – 6 days' culture period of GS. These data coupled with the mono-sugar and total sugar contents, indicate that no polysaccharides were hydrolyzed and used during by GS. Consequently, the sugar removal efficiency of GS is very low.

5.6.3.2 Nitrogen utilization (NH_3 and Organic Nitrogen)

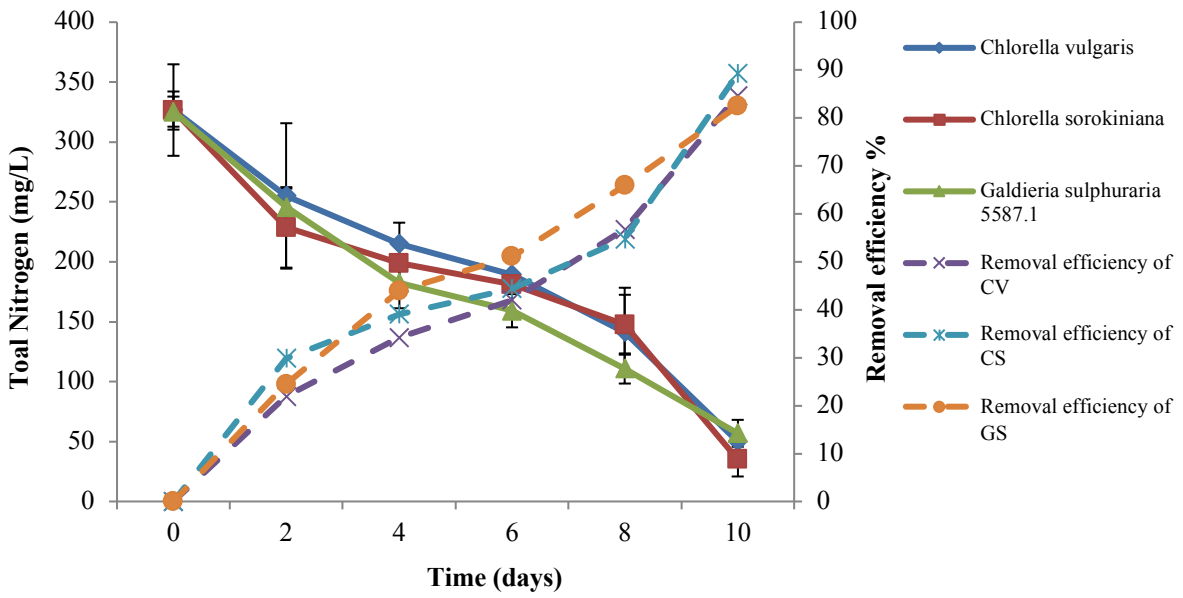

Figure 5.6.12 Total Nitrogen Utilization and Removal Efficiency by three different Microalgae

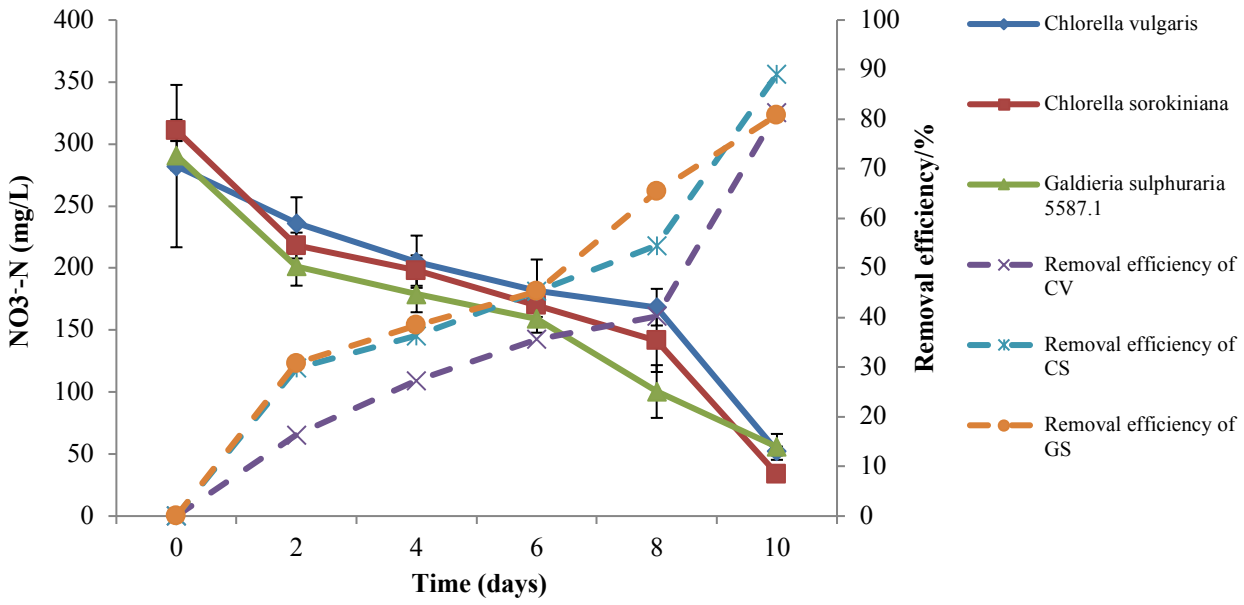

Figure 5.6.13 Nitrate Utilization and Removal Efficiency by three different Microalgae

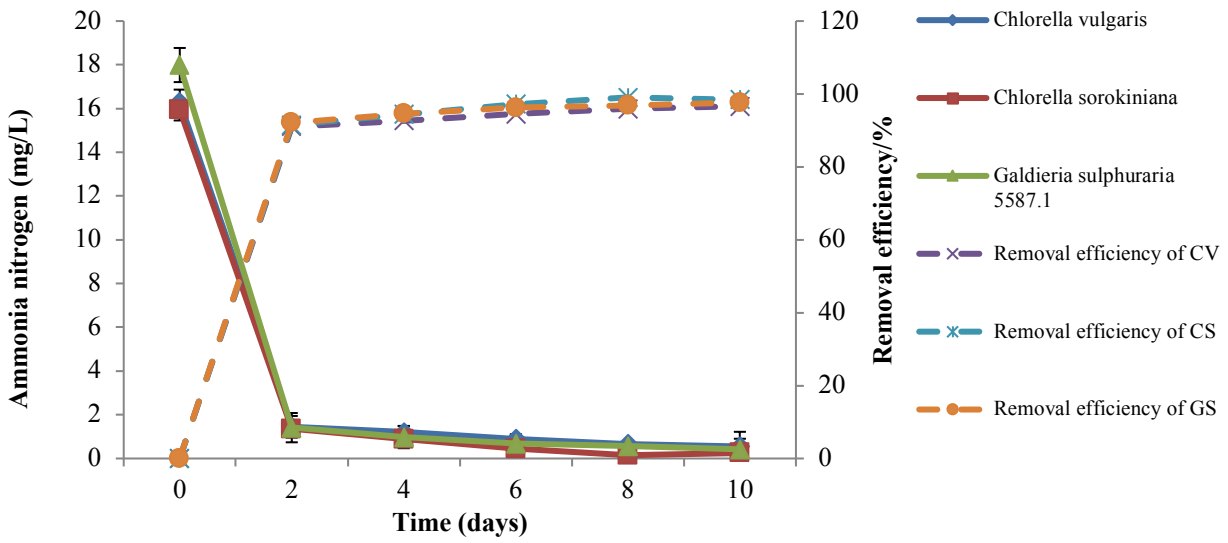

Figure 5.6.14 Ammonia Utilization and Removal Efficiency by three different Microalgae

The culture medium mixed with SEQHTL water product enhanced the nitrogen utilization, as indicated by the higher N utilization compared to the control. Approximately between 30 – 60mg/L nitrogen remained in the medium at the end of the cultivation, most of which was in the form of NO_3^--N. Most of the Ammonia-N was consumed by the 2nd day of the culture, which led to a removal efficiency of 100%.

5.6.3.3 Phosphate recovery (PO_4^{3-})

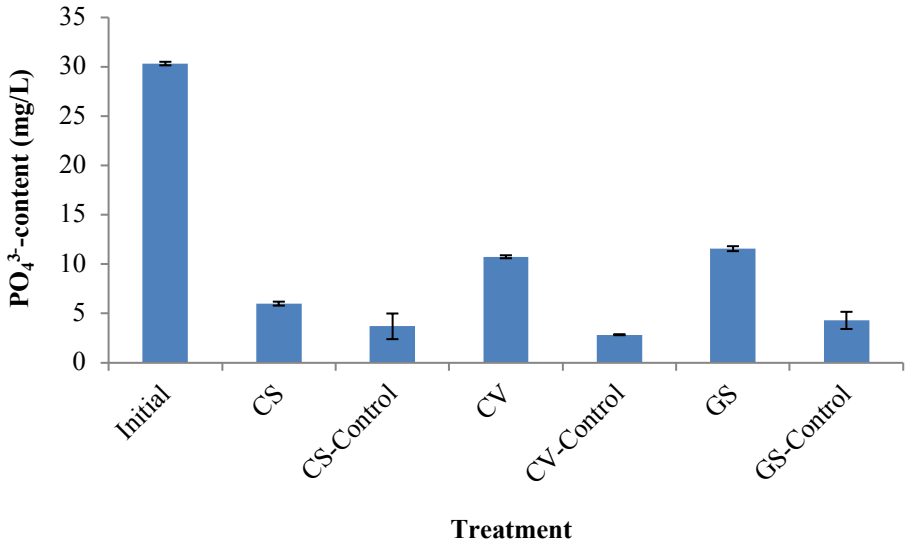

Figure 5.6.15 PO_4^{3-} concentration, Initial (before cultivation) vs final (after cultivation)

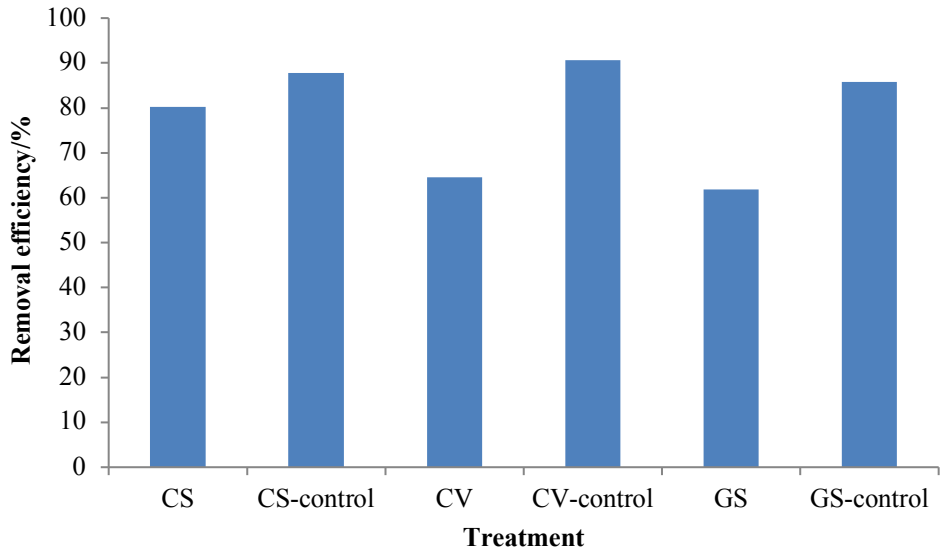

Fig 5.6.16 PO_4^{3-} removal efficiency

The results indicated that between 60 –80% of the phosphate in the aqueous effluent was removed by the algae. However, the removal efficiency was lower than the control under autotrophic cultivation.

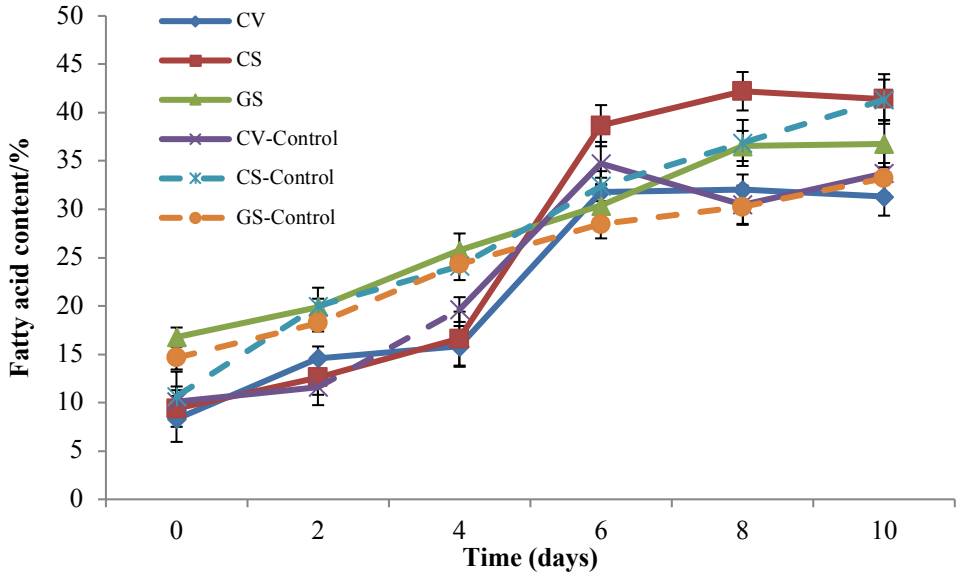

Figure 5.6.17 Fatty acid content of the microalgae

Table 5.6.13 Fatty acid profile of the microalgae

	CV	CV-Control	CS	CS-Control	GS	GS-Control
Palmitic acid	19.89±1.11	16.34±1.99	24.34±2.57	36.89±1.55	26.78±1.49	35.11±1.45
Stearic acid	5.47±2.02	5.2±1.08	1.8±0.12	4.45±1.23	13.39±2.34	21.25±0.74
Oleic acid	18.67±1.88	2.6±1.23	10.21±1.77	15.35±0.89	37.45±0.99	26.45±0.38
Linoleic acid	35.82±1.32	17.22±1.82	30.46±1.53	27.99±0.83	15.31±0.27	9.89±1.21
a-Linolenic acid	16.71±1.01	33.78±1.22	15.38±2.11	7.92±1.36	0	0
others	3.44±0.67	24.86±1.33	17.81±1.89	7.4±0.99	7.07±1.62	7.3±1.86

The overall fatty acid content in the microalgae ranged between 30 – 40%. However, as illustrated by Table 5.6.13, the fatty acid composition was influenced by the different treatments, autotrophic or mixotrophic.

5.6.3.4 Nutrition recovery by growing yeast

Water product samples from SEQHTL stage 1 were used for the growth of yeast, *Cryptococcus curvatus*. WSU group has illustrated that the Soaking Aqueous Ammonia pretreatment (SAA) is the best process for growing yeast; thus, the liquid hydrolysate from SAA of wheat straw was used as a control. The biomass was measured and the sugar contents were determined by IC.

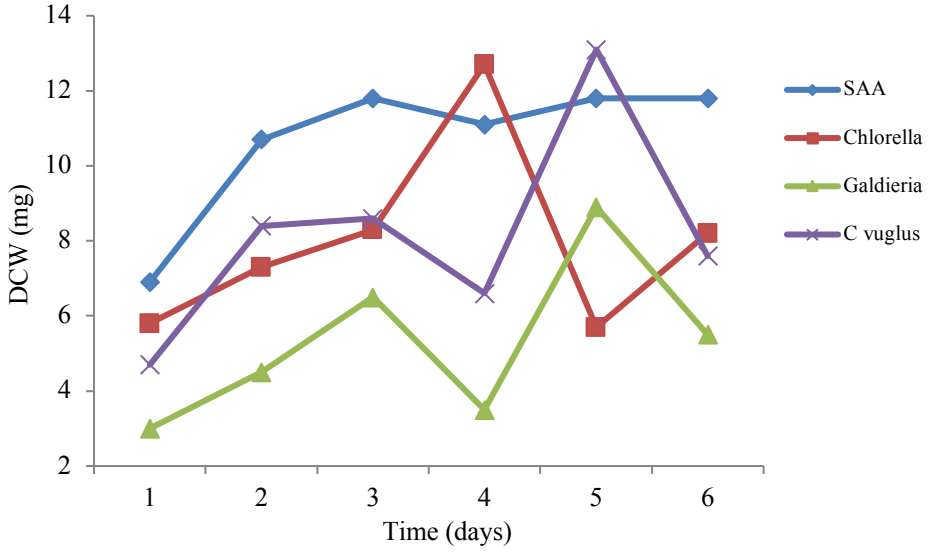

Figure 5.6.18 Growth curve of *C. curvatus* with SEQHTL stage 1 effluent from different algae

5.6.4 Continuous Sequential Hydrothermal Liquefaction

The research groups that have investigated HTL with high temperatures have successfully worked with different species such as *Chlorella vulgaris* and *C. pyrenoidosa*, *Nannochloropsis occulata*, *Porphyridium cruentum*, *Desmodesmus sp.* as well as *Chlorogloeopsis fritschii* and *Spirulina cyanobacteria* [21, 48]. However, most of these studies have been limited to batch reactor testing [49]. Furthermore, the un-recovered carbohydrate portion emulsifies the aqueous and organic phases, significantly affecting the final product separation and leading to the formation of more of biochar. This product fraction hinders product recovery because the desired biocrude adheres to this highly porous material. These complexities have contributed to a significant loss of material from both the aqueous and organic phases, and produce inconclusive mass balances [50]. Investigators have thus resorted to using environmentally toxic and costly organic solvents to recover the biocrude. Yet, it has been shown that such solvents can significantly and negatively alter the product yield and chemical composition [51].

Therefore, there is pressing need to advance this conversion route by developing a continuous-flow operating system that can be easily modeled, scale-up, allows nutrient recovery and does not include the use of organic solvents. The successful elaboration of a continuous-flow process is critical for the sustainable commercialization of microalgal-derived biofuels.

Currently, two groups have worked with assembling continuous reactor systems for one stage HTL. The first team described processing at 350°C and 20 MPa and product recovery without the use of organic solvents [46]. High conversions were achieved even with high slurry concentrations; yet nutrient salvage was limited, particularly with regards to phosphorous. Whereas the second team similarly explored single stage continuous-flow HTL operations with two strains *Chlorella* and *Spirulina* under variable operating conditions and use of organic solvent on some instances of product recovery [40]. Crude yields were found to increase with increasing biomass loading, higher temperatures and longer residence times, yet harmoniously the nitrogen content in the crude increased.

A continuous-flow SEQHTL prototype reactor system was developed at WSU, based on process metrics, operating conditions and relevant engineering data. The configuration includes two slurry pumps, two product separation stages, pre-heating sections and two tubular plug-flow reactors for each reaction stage. Plug flow reactors (PFR) were selected because their design equations are relatively simple and identical in mathematical form to those of batch reactors [52, 53], and because for most kinetic schemes, these are substantially better than the CSTR for attaining high conversions and greater selectivity [54]. The C-SEQHTL prototype was designed with SS 316L material, standard fittings for adaptability, and custom separation units; with capacities are 2 – 2.5 L/hr and 1 – 1.5 L/hr for 1st and 2nd stage respectively

The overall scheme includes the low-temperature subcritical water extraction of nutrients/co-products and biofuel production via liquefaction. The prototype is illustrated in Figure 5.6.19 The system also includes two custom separation sections, located after each reaction stage. The first separation unit was built with a commercially available SS 316L metal cartridge and an auger screw

feeder (for transporting solid particles) with power-consumption requirements that can be fine-tuned by dimensions, rotational speed, and clearance [55, 56]. Similarly, the char removal unit was developed as a flange sealed SS 316L pressure bin, also integrated with a SS 316L metal filter cartridge to achieve the phase separation. Previous studies have shown that removal of the char fraction favors liquid product separation [46, 50]. The process operation summary is illustrated in Figure 5.6.20.

The reactor systems for established commercial processes are usually complex designs developed and evolved over several years to suit the requirements of the industry. However, with the C-SEQHTL system, an initial exploratory continuous-flow performance assessment of biocrude production and potential co-product recovery from different microalgae species can be developed.

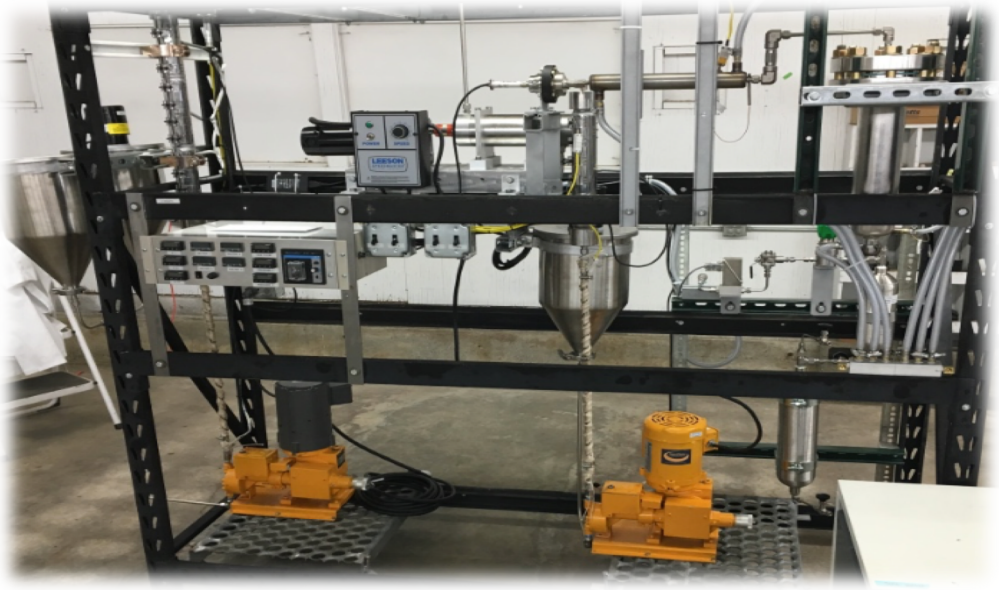

Figure 5.6.19 C-SEQHTL Prototype

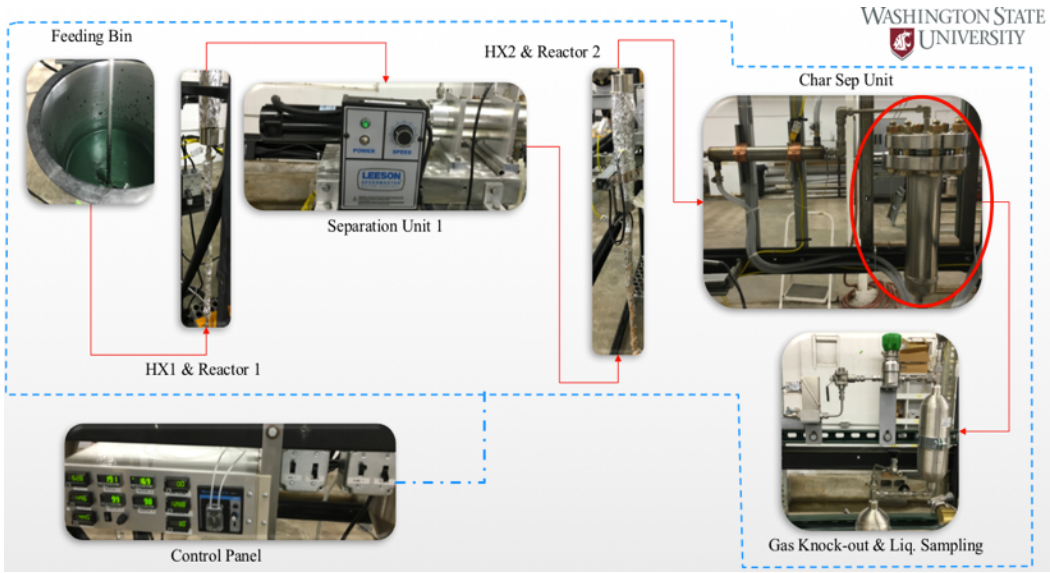

Figure 5.6.20 C-SEQHTL Operation Schematic

A detailed process evaluation would contribute to system modeling efforts by providing information for techno-economic analyses and ensuring that end-to-end analyses are reasonable and comprehensive. Therefore, additional research is needed to conduct performance valuations of C-SEQHTL for biocrude production Fundamental data may be collected, that may be further utilized to survey optimization possibilities. For instance, it is critical to understand the properties of process streams, which are determined by the feedstock [46]. Information on comprehensive biomass characterization and selection for targeted conversion is needed, as well as assessing the tradeoffs between species according to lipid content, product yield and quality along with the availability of co-products [21].

Additionally, environmental factors that serve as sustainability indicators, such as greenhouse gas (GHG) emissions, fossil energy consumption, carbon-to-fuel efficiency, water consumption, and wastewater generation can be assessed in order to determine the real impact of such an emerging technology [8, 57]. Moreover, separation unit ideal operating conditions, capacities and efficiencies are critical aspects that may be explored in such a system.

5.6.4a Experimental Methods & Product Characterization

Experiments with slurries of the different types of biomass will be tested at two at two different sets of operating conditions: (1) Stage 1 at 160℃, Stage 2 at 240℃ and (2) Stage 1 at 180℃, Stage 2 at 300℃; in the custom continuous-flow Sequential Hydrothermal Liquefaction prototype. In the first stage, 500 – 1000 g of slurry at either 10 wt% or 20 wt% are loaded in the SS304 feeding hopper (TMS Company). The slurry is then fed via slurry pump #1 (TMG Services) into the preheater section #1 where the temperature is elevated to within ±5℃ of the reaction temperature by an electric heater (Omega Engineering). Following the slurry moves into plug flow reactor #1, (TW Metals) heated by band heaters (WATTCO) and where the subcritical

water extraction of algal nutrients occurs. Pressure is maintained via a backpressure regulator (KCB Series, Swagelok); and the temperature controller keeps isothermal operation (Omega Engineering).
Following the reaction and cool-down in heat exchanger #1, the solid-liquid separation of the product mixture of stage 1 is performed in the auger screw feeder equipped with SS316 filter cartridge (Filtersource, Inc.). The aqueous product #1 is collected separately, and stored for subsequent nutrient analyses. Prior to the second reaction stage, a sub-sample of the treated algae product, gathered in the secondary SS304 hopper, is tested for moisture content. Consequently, approximately 500 g of treated algae slurry are prepared with additional DI Water; and is eventually fed via slurry pump #2 (TMG Services). The treated algae slurry flows through the preheating section #2 where the temperature was elevated to within ±5℃ of the reaction temperature by a second an electric heater (Omega Engineering) the ultra-high temperature heating tape; and subsequently moves into plug flow reactor #2, heated by band heaters and where the liquefaction reaction occurs. Pressure is maintained via a backpressure regulator (KPB Series, Swagelok); and the corresponding temperature controller keeps isothermal operation.
Following the reaction and partial cool-down in heat exchanger #2, the solid-liquid separation of the product mixture of stage 2 is performed in the SS316 pressure bin equipped with SS316 filter cartridge. The char product is deposited within the filter cartridge and is collected after completing process runs. Then, after cool-down in heat exchanger #3, the gas product is vented from the knockout drum and monitored by an on-line gas flow meter (Omega Engineering). Finally, the liquid product mixture is collected in the sampling cylinder where it is separated into the corresponding organic biocrude and aqueous product #2 fractions.Product yields and characterization are estimated and determined as previously detailed.

5.6.4b Results & Discussion

Trials with *Galdieria sulphuraria* 5587.1 at 10wt% solids were developed at 160 and 240°C for stage 1 and 2 respectively. Slurry feed in stage 1 was approximately at 2.08 L/hr, and the first separation stage was performed at 90°C. Contrastingly, stage 2 feed was 1.067 L/hr and the Char removal unit operated at 155°C. Samples from stage 1 were collected and characterized accordingly, but results for stage 2 were not available due to issues with material leaks and heating elements. In C-SEQHTL the treated algae yield was 42.8 wt% but in batch trials the corresponding yield was 72.1%. Differences were attributed to material loss and potentially owing to higher heating rates achieved in the C-SEQHTL system. Studies have shown that "fast HTL" promotes rapid cell decomposition [6].

Table 5.6.14 *G. sulphuraria* 5587.1 Stage 1 Continuous vs. Batch CHN

Sample	C	H	N	S	O*	HHV (MJ/kg) [a]
G. sulphuraria 2	57.316	7.843	12.145	1.447	21.249	27.01
Batch TA	55.597	7.399	11.022	1.188	24.793	25.13
Batch WE 1	61.749	8.987	15.042	2.116	12.107	-
Cont TA	57.096	7.835	11.096	1.047	22.926	26.58
Cont WE 1	57.481	7.848	12.930	1.747	19.994	-

*By difference

[a] Dulong Formula

Table 5.6.15 *G. sulphuraria* 5587.1 Stage 1 Continuous vs. Batch Nutrient Assay

	Batch (mg/L)			Continuous (mg/L)		
NUTRIENT	**Max**	**Min**	**Average**	**Max**	**Min**	**Average**
Phosphate	1160	770	946.3	1620.0	1550.0	1580.0
Nitrate - N	120	40	78.8	N/A	N/A	NA
Ammonia - N	290	190	230	250.0	50.0	192.5
Total Nitrogen	3300	1300	2250	2400.0	1200.0	1675.0

Results showed the C partitioning and O removal after reaction stage 1 improved by 3.0 wt %; which will inevitably be reflected on the final product's quality. Additionally, it was noted that the average nutrient phosphorous recovery in the water product was increased by 67%.
Following, several mechanical optimizations and adjustments within the system were successfully developed. Material leaks at metal-on-metal contact sites after reactor 1 were successfully sealed off with permatex and appropriate high-temperature resistant gaskets. Additionally, for trials with 20 wt % solid content slurry feeds, some small port ¼" check-valves were replaced with appropriate ½" Swagelok check-valves and 3/8" adapters. Afterwards, the whole system plumbing was cleaned and purged.
The first reaction stage of the Continuous SEQHTL process with 20 wt% solids feed *Kirchneriella cornutum* was developed at temperatures of 160 and 180°C. Preliminary sample collection and characterization was performed. As expected higher reaction temperatures led to more biomass breakdown and corresponding less solids; yet the difference was relatively small. However, these values were comparably lower than those of the analogous Batch trials, 66.53 wt% and 57.30 wt% for Stage 1 at 160°C and 180°C respectively. Given that system leaks were fixed prior to these tests; it is likely to consider that the continuous system's rapid heating rates favors rapid cell decomposition.

Table 5.6.16 C-SEQHTL *K. cornutum* Stage 1 Treated Algae Yields

	Treated Algae (wt %)
SEQHTL Stage 1 @160 °C	52.73%
SEQHTL Stage 1 @180 °C	50.76%

The first reaction stage of the Continuous SEQHTL process with 20 wt% solids feed *Galdieria sulphuraria* 87.1 was developed at a reaction temperature of 160°C. Preliminary sample collection and characterization was performed. The treated algae yield was 49.5 wt%; yet, this value was significantly lower than the yield attained in the analogous batch trials 70.11 wt%.

This behavior was also observed for *K. cornutum*, that exhibited 52.73 wt% and 50.76 wt% compared to 66.53 wt% and 57.30 wt% for continuous and batch experiments at 160°C and 180°C respectively. Potentially the rapid heating rates promoted and enhanced rapid cell decomposition. Further studies are required to elaborate on this nuance.
Also, nutrients availability in the water product from stage 1 was determined with HACH DR/2400 spectrometer and corresponding test kits, according to established procedures.

Table 5.6.17 C-SEQHTL *Galdieria* 87.1 Nutrient Assay

T (degC)	pH	PO_4^{3-} (mg/L)	NH3 (mg/L)	Total N (mg/L)	Organic N
160	5.60	4530.0	1260.0	8100.0	
		4560.0	1050.0	6900.0	
		4545.0	1155.0	7500.0	6345.00

Sample	Op Conditions	TC (mg/L)	IC (mg/L)	TOC (mg/L)
Stage 1	160 degC	37260.0	0.0	37260.0

Solid-liquid separation operation has yet to be optimized. Current trials have yielded mixed and inconsistent results. Further testing is required to improve operation and efficiency, particularly pertaining to material residence time within the first stage S/L separator.
Technical and maintenance issues have not allowed the development of the second reaction stage. Trials with *Galdieria sulphuraria* 87.1 for the second reaction stage at 240°C, and experiments with *Chlorella vulgaris* are pending.

5.6.5 References

[1] R.K. Henderson, S.A. Parsons, B. Jefferson, Successful Removal of Algae through the Control of Zeta Potential, Separation Science and Technology, 43 (2008) 1653-1666.

[2] R. Henderson, S.A. Parsons, B. Jefferson, The impact of algal properties and pre-oxidation on solid–liquid separation of algae, Water Research, 42 (2008) 1827-1845.

[3] F. Chen, Z. Liu, D. Li, C. Liu, P. Zheng, S. Chen, Using ammonia for algae harvesting and as nutrient in subsequent cultures, Bioresource Technology, 121 (2012) 298-303.

[4] D. Vandamme, I. Foubert, I. Fraeye, B. Meesschaert, K. Muylaert, Flocculation of Chlorella vulgaris induced by high pH: role of magnesium and calcium and practical implications, Bioresource Technol, 105 (2012).

[5] J. Liu, Y. Zhu, Y. Tao, Y. Zhang, A. Li, T. Li, M. Sang, C. Zhang, Freshwater microalgae harvested via flocculation induced by pH decrease, Biotechnology for Biofuels, 6 (2013) 98.

[6] J.L. Faeth, P.J. Valdez, P.E. Savage, Fast hydrothermal liquefaction of Nannochloropsis sp. to produce biocrude, Energy & Fuels, 27 (2013) 1391-1398.

[7] P. Biller, A.B. Ross, Potential yields and properties of oil from the hydrothermal liquefaction of microalgae with different biochemical content, Bioresource technology, 102 (2011) 215-225.

[8] S.B. Jones, Y. Zhu, L.J. Snowden-Swan, D. Anderson, R.T. Hallen, A.J. Schmidt, K.A. Albrecht, D.C. Elliott, Whole Algae Hydrothermal Liquefaction: 2014 State of Technology, Pacific Northwest National Laboratory (PNNL), Richland, WA (US), 2014.

[9] A.A. Peterson, F. Vogel, R.P. Lachance, M. Fröling, J.M.J. Antal, J.W. Tester, Thermochemical biofuel production in hydrothermal media: A review of sub- and supercritical water technologies, Energy & Environmental Science, 1 (2008) 32.

[10] G. Brunner, Near critical and supercritical water. Part I. Hydrolytic and hydrothermal processes, The Journal of Supercritical Fluids, 47 (2009) 373-381.

[11] N. Akiya, P.E. Savage, Roles of Water for Chemical Reactions in High-Temperature Water, Chemical Reviews, 102 (2002) 2725-2750.

[12] D.C. Elliott, Hydrothermal processing, John Wiley & Sons, Ltd Chichester, UK2011.

[13] K. Anastasakis, A.B. Ross, Hydrothermal liquefaction of the brown macro-alga Laminaria saccharina: effect of reaction conditions on product distribution and composition, Bioresource technology, 102 (2011) 4876-4883.

[14] U. Jena, K.C. Das, J.R. Kastner, Effect of operating conditions of thermochemical liquefaction on biocrude production from Spirulina platensis, Bioresource technology, 102 (2011) 6221-6229.

[15] C. Tian, B. Li, Z. Liu, Y. Zhang, H. Lu, Hydrothermal liquefaction for algal biorefinery: A critical review, Renewable and Sustainable Energy Reviews, 38 (2014) 933-950.

[16] C. Safi, A.V. Ursu, C. Laroche, B. Zebib, O. Merah, P.-Y. Pontalier, C. Vaca-Garcia, Aqueous extraction of proteins from microalgae: effect of different cell disruption methods, Algal Research, 3 (2014) 61-65.

[17] A.C. Guedes, H.M. Amaro, F.X. Malcata, Microalgae as sources of high added-value compounds--a brief review of recent work, Biotechnology progress, 27 (2011) 597-613.

[18] A.B. Ross, P. Biller, M.L. Kubacki, H. Li, A. Lea-Langton, J.M. Jones, Hydrothermal processing of microalgae using alkali and organic acids, Fuel, 89 (2010) 2234-2243.

[19] D.R. Vardon, B.K. Sharma, J. Scott, G. Yu, Z. Wang, L. Schideman, Y. Zhang, T.J. Strathmann, Chemical properties of biocrude oil from the hydrothermal liquefaction of Spirulina algae, swine manure, and digested anaerobic sludge, Bioresource technology, 102 (2011) 8295-8303.

[20] C. Torri, L. Garcia Alba, C. Samorì, D. Fabbri, D.W.F. Brilman, Hydrothermal treatment (HTT) of microalgae: detailed molecular characterization of HTT oil in view of HTT mechanism elucidation, Energy & fuels, 26 (2012) 658-671.

[21] Y. Zhu, K.O. Albrecht, D.C. Elliott, R.T. Hallen, S.B. Jones, Development of hydrothermal liquefaction and upgrading technologies for lipid-extracted algae conversion to liquid fuels, Algal Research, 2 (2013) 455-464.

[22] U. Jena, N. Vaidyanathan, S. Chinnasamy, K.C. Das, Evaluation of microalgae cultivation using recovered aqueous co-product from thermochemical liquefaction of algal biomass, Bioresource technology, 102 (2011) 3380-3387.

[23] C. Miao, M. Chakraborty, S. Chen, Impact of reaction conditions on the simultaneous production of polysaccharides and bio-oil from heterotrophically grown Chlorella sorokiniana by a unique sequential hydrothermal liquefaction process, Bioresource Technology, 110 (2012) 617-627.

[24] P.E. Savage, Organic Chemical Reactions in Supercritical Water, Chemical Reviews, 99 (1999) 603-622.

[25] M. Chakraborty, C. Miao, A. McDonald, S. Chen, Concomitant extraction of bio-oil and value added polysaccharides from Chlorella sorokiniana using a unique sequential hydrothermal extraction technology, Fuel, 95 (2012) 63-70.

[26] S. Chen, M. Chakraborty, Sequential hydrothermal liquifaction (seqhtl) for extraction of superior bio-oil and other organic compounds from oleaginous biomass, Google Patents, 2013.

[27] A. Bhatnagar, S. Chinnasamy, M. Singh, K.C. Das, Renewable biomass production by mixotrophic algae in the presence of various carbon sources and wastewaters, Applied Energy, 88 (2011) 3425-3431.

[28] M. Chakraborty, A.G. McDonald, C. Nindo, S. Chen, An α-glucan isolated as a co-product of biofuel by hydrothermal liquefaction of Chlorella sorokiniana biomass, Algal Research, 2 (2013) 230-236.

[29] J.G. Speight, Handbook of coal analysis, John Wiley & Sons2015.

[30] S.A. Channiwala, P.P. Parikh, A unified correlation for estimating HHV of solid, liquid and gaseous fuels, Fuel, 81 (2002) 1051-1063.

[31] J.V. O'fallon, J.R. Busboom, M.L. Nelson, C.T. Gaskins, A direct method for fatty acid methyl ester synthesis: application to wet meat tissues, oils, and feedstuffs, Journal of Animal Science, 85 (2007) 1511-1521.

[32] T. Dong, J. Wang, C. Miao, Y. Zheng, S. Chen, Two-step in situ biodiesel production from microalgae with high free fatty acid content, Bioresource technology, 136 (2013) 8-15.

[33] T.M. Brown, P. Duan, P.E. Savage, Hydrothermal Liquefaction and Gasification of Nannochloropsis sp, Energy & Fuels, 24 (2010) 3639-3646.

[34] Z. Du, M. Mohr, X. Ma, Y. Cheng, X. Lin, Y. Liu, W. Zhou, P. Chen, R. Ruan, Hydrothermal pretreatment of microalgae for production of pyrolytic bio-oil with a low nitrogen content, Bioresource technology, 120 (2012) 13-18.

[35] S. Grierson, V. Strezov, G. Ellem, R. McGregor, J. Herbertson, Thermal characterisation of microalgae under slow pyrolysis conditions, Journal of Analytical and Applied Pyrolysis, 85 (2009) 118-123.

[36] M. Sostaric, D. Klinar, M. Bricelj, J. Golob, M. Berovic, B. Likozar, Growth, lipid extraction and thermal degradation of the microalga Chlorella vulgaris, New biotechnology, 29 (2012) 325-331.

[37] A. Wileman, A. Ozkan, H. Berberoglu, Rheological properties of algae slurries for minimizing harvesting energy requirements in biofuel production, Bioresource technology, 104 (2012) 432-439.

[38] J. Akhtar, N.A.S. Amin, A review on process conditions for optimum bio-oil yield in hydrothermal liquefaction of biomass, Renewable and Sustainable Energy Reviews, 15 (2011) 1615-1624.

[39] J.G. Speight, Handbook of industrial hydrocarbon processes, Gulf Professional Publishing2010.

[40] C. Jazrawi, P. Biller, A.B. Ross, A. Montoya, T. Maschmeyer, B.S. Haynes, Pilot plant testing of continuous hydrothermal liquefaction of microalgae, Algal Research, 2 (2013) 268-277.

[41] P.J. Valdez, M.C. Nelson, H.Y. Wang, X.N. Lin, P.E. Savage, Hydrothermal liquefaction of Nannochloropsis sp.: Systematic study of process variables and analysis of the product fractions, Biomass and Bioenergy, 46 (2012) 317-331.

[42] N. Sudasinghe, B. Dungan, P. Lammers, K. Albrecht, D. Elliott, R. Hallen, T. Schaub, High resolution FT-ICR mass spectral analysis of bio-oil and residual water soluble organics produced by hydrothermal liquefaction of the marine microalga Nannochloropsis salina, Fuel, 119 (2014) 47-56.

[43] D. Cordell, J.-O. Drangert, S. White, The story of phosphorus: global food security and food for thought, Global environmental change, 19 (2009) 292-305.

[44] J.A. Libra, K.S. Ro, C. Kammann, A. Funke, N.D. Berge, Y. Neubauer, M.-M. Titirici, C. Fühner, O. Bens, J. Kern, Hydrothermal carbonization of biomass residuals: a comparative review of the chemistry, processes and applications of wet and dry pyrolysis, Biofuels, 2 (2011) 71-106.

[45] D. Lopez Barreiro, C. Zamalloa, N. Boon, W. Vyverman, F. Ronsse, W. Brilman, W. Prins, Influence of strain-specific parameters on hydrothermal liquefaction of microalgae, Bioresource technology, 146 (2013) 463-471.

[46] D.C. Elliott, T.R. Hart, A.J. Schmidt, G.G. Neuenschwander, L.J. Rotness, M.V. Olarte, A.H. Zacher, K.O. Albrecht, R.T. Hallen, J.E. Holladay, Process development for hydrothermal liquefaction of algae feedstocks in a continuous-flow reactor, Algal Research, 2 (2013) 445-454.

[47] K. Wang, R.C. Brown, S. Homsy, L. Martinez, S.S. Sidhu, Fast pyrolysis of microalgae remnants in a fluidized bed reactor for bio-oil and biochar production, Bioresource technology, 127 (2013) 494-499.

[48] S.S. Toor, L. Rosendahl, A. Rudolf, Hydrothermal liquefaction of biomass: A review of subcritical water technologies, Energy, 36 (2011) 2328-2342.

[49] D. López Barreiro, W. Prins, F. Ronsse, W. Brilman, Hydrothermal liquefaction (HTL) of microalgae for biofuel production: State of the art review and future prospects, Biomass and Bioenergy, 53 (2013) 113-127.

[50] L. Garcia Alba, C. Torri, C. Samorì, J. van der Spek, D. Fabbri, S.R.A. Kersten, D.W.F. Brilman, Hydrothermal treatment (HTT) of microalgae: evaluation of the process as conversion method in an algae biorefinery concept, Energy & fuels, 26 (2011) 642-657.

[51] D. Xu, P.E. Savage, Characterization of biocrudes recovered with and without solvent after hydrothermal liquefaction of algae, Algal Research, 6 (2014) 1-7.

[52] H.S. Fogler, Elements of chemical reaction engineering, (1999).

[53] J.M. Smith, Chemical engineering kinetics, McGraw-Hill1981.

[54] E.B. Nauman, Chemical reactor design, (1987).

[55] C.R. Branan, Rules of thumb for chemical engineers, Butterworth-Heinemann2012.

[56] H. Zareiforoush, M.H. Komarizadeh, M.R. Alizadeh, M. Masoomi, Screw conveyors power and throughput analysis during horizontal handling of paddy grains, Journal of Agricultural science, 2 (2010) p147.

[57] A. Singh, S.I. Olsen, A critical review of biochemical conversion, sustainability and life cycle assessment of algal biofuels, Applied Energy, 88 (2011) 3548-3555.

5.7 Hydrothermal liquefaction

5.7.1 HTL background

Hydrothermal treatment is one of the conversion processes for the production of biofuels. There are three different processes in hydrothermal treatment. The process that involves processing of biomass below 200°C is called hydrothermal carbonization. The main product in this process is char. The process well above 375°C is called hydrothermal gasification which mainly produces syngas. The process at intermediate temperatures between 200°C and 375°C is called hydrothermal liquefaction (HTL) which predominantly produces biocrude oil that can be upgraded into transportation fuel. This HTL converts algal biomass into biocrude oil that is similar to petroleum derived product but with higher viscosity and oxygen content (10-20 wt %). During HTL, the macromolecules (lipids, carbohydrates and proteins) present in microalgae will be first hydrolyzed into smaller fragments (fatty acids, glucose and amino acids). Then these small fragments will be converted into smaller compounds (e.g. amino acids undergo deamination and decarboxylation to produce hydrocarbons, amines, aldehydes and acids). These compounds are unstable and will be rearranged into larger compounds by condensation, polymerization and cyclization reactions. This HTL yields four different products. The important and predominant to be biocrude oil which is a black and viscous crude oil like materials that need to be upgraded to be used as fuel. This can be done by mixing it with regular petroleum crude or directly by hydrocracking and hydro isomerization to break the long chain hydrocarbons (usually C14-C22) into light hydrocarbons. The other products obtained during HTL are water phase, solid phase and gases. The water phase will be rich in nutrients and other valuable by products. The valuable by products such as amino acids, sugars, sugar alcohols and glycerol can be separated or can be fermented to produce bioethanol. The nutrient rich water can be recycled to the algal growth facility to cultivate algae. The solid residue can be used as char or for cattle feed.

5.7.2 Overview of HTL work

HTL of Galdieria sulphuraria, chlorella and coelastrella.

HTL of C. merolae and the influence of catalysts on product fractions.

Sequential HTL of Galdieria sulphuraria.

Continuous HTL of chlorella.

Co-liquefaction of two algal species.

HTL water process recycle to enhance biocrude oil yield.

HTL of Galdieria, Chlorella and Kirchneriella grown at ASU.

Analysis of algae and HTL products.

5.7.3 Experimental methods

Hydrothermal liquefaction experiments were performed in a 100 mL bench top PARR 4593 and 4598 Micro reactors with a 4843 and 4848-controllers (Parr Instrument Company, Illinois, USA) which can be operated up to 500°C and 340 bars pressure. 50 grams of microalgae slurry with desired concentration was prepared using harvested algae and by adding sufficient amount of DI water or supernatant water obtained during harvesting. This slurry was then fed to the reactor and nitrogen was purged to sweep away the undesirable air in the reactor. The reactor was then heated after pressurizing with nitrogen to control rapid boiling of water and the residence time is taken from the point the reactor reaches desired temperature. All the experiments were conducted with 10-20 % biomass loading, 0-60 min of reaction time and in triplicates by varying reaction temperatures from 120°C to 375°C. After liquefaction, the reactor was cooled down to room temperature and the gases produced during the reaction were vented off. 30 mL of DCM was added to the reactor and stirred for 10 min to extract the biocrude oil present in the reaction mixture and from the reactor walls. The product mixture was then transferred to the separation unit to separate the biochar using a filter paper and to separate the DCM using a separation funnel. The biochar was washed with 5 mL of DCM to collect the residual biocrude and then dried before storing. The DCM was evaporated using rotary evaporator and thus separated biocrude oil along with the remaining aqueous phase were stored separately at -5°C for further analysis. Catalytic HTL experiments were performed by adding different types of catalysts (KOH, NaOH, CH3COOH and H2SO4) to make the reaction mixture approximately 0.5M concentration. SHTL was performed at 180°C and 300°C as 1st and 2nd steps respectively. Co-liquefaction was done by varying the fractions of two algal species in the algal feed. In HTL process recycle experiments, the HTL water obtained in the first HTL reaction was used as water solvent to liquefy a new biomass in the next HTL reaction.

All the analysis was done using Hach spectrophotometer, GC-MS, ICP-OES, semi micro calorimeter and CHNS/O elemental analyzer. The residue left after heating the algae sample at 600°C for 24 hours was considered as ash. FAME analysis was performed to determine the lipid content present in the microalgae and NREL protocol was followed to determine the total lipids present in the microalgae. The protein content was calculated as 6.25 times the amount of nitrogen evolved during the combustion of microalgae/TOFMS analysis of biocrude samples was performed for 90 minutes per sample using a modified Petroleum refinery reformate standard procedure. Agilent 7890 A GC equipped with a ZB-5ms column (30m x .25mm I.D. x .25um film thickness) with 1uL injections were made split less. The oven program started at 40°C and held for .4 minutes then ramped at 5c/min to 110°C, then ramped to 320°C at 3c/min. A 6725 Semi micro calorie meter manufactured by the Parr Instrument Company (Moline, Illinois, USA) was used to determine the high heating value of the microalgae, biochar and bio-crude oil samples. Ultimate Analysis of the dry biochar and biocrude samples was performed using an Elemental Analyzer (PE 2400 Series II CHNS/O Analyzer). NH3-N, TN, and phosphate in HTL AP samples were measured using HACH DR6000 Spectrophotometer (HACH, Colorado, USA) (Salicylate TNT Method 10031, TNTplus 828 Method 10208 and Phosver 3 Method 8048). Carbohydrate levels in the AP samples were measured using phenol sulphuric acid assay method.

5.7.4 Results & Discussion

5.7.4a HTL of Galdieria sulphuraria, chlorella and coelastrella

The proximate, biochemical and ultimate analysis of the three algal biomass were presented in Table 5.7-1. The *Chlorella* sp. and *Coelastrella* sp. used in this work were green alga known for their fastest growth. The *Galdieria* sp. is red alga which was a low lipid acidophilic strain that can be grown at extreme environmental conditions like 56°C temperature and pH 0.5-4 where many other competitors, pathogens, predators and viruses cannot survive. The ash content in all the algal species were between 8-10%. *Coelastrella* sp. has 4.93 % lipids, Chlorella and Galdieria sp. has less than 3% of lipids present in the algal biomass. The protein content of *Chlorella* and *Galdieria* are quite high compared to that of *Coelastrella* sp. (29.81%). The carbon content of *Chlorella* and *Coelastrella* sp. were higher than 50% but the *Galdieria* sp. has 39.8% carbon content. The higher heating values are calculated using Dulong's formula and are 23.86, 22.33, 12.94 MJ kg^{-1} for *Chlorella*, *Coelastrella* and *Galdieria* sp. respectively. The lower carbon content and higher oxygen content present in the *Galdieria* sp. was the reason for lower HHV compared to the other algal species.

Table 5.7-1: Analysis of microalgae.

Microalgae	***Chlorella* sp.**	***Coelastrella* sp.**	***Galdieria* sp.**
Proximate (wt. %)			
Ash	8.3	8.8	9.4
Moisture	83.4	89.1	69.6
Biochemical (wt. %)			
Lipids	2.58	4.93	2.33
Proteins	45.13	29.81	54.81
Carbohydrates[a]	52.29	65.26	42.86
Ultimate (wt. %)			
C	54.15	52.25	39.80
H	7.54	7.49	5.06
N	7.22	4.77	8.77
S	1.0	0.92	1.96
O[a]	30.09	34.57	44.41
HHV(MJ kg^{-1})	23.86	22.33	12.94

[a] Determined by difference; HHV=higher heating value

Hydrothermal liquefaction experiments were conducted for 30 min of reaction time, 10% solid loading and the effect of reaction temperature on the biocrude oil yield was investigated for all the three algal species from 180°C to 300°C. The HTL product distribution for Chlorella, Coelastrella and Galdieria sp. were presented in Figure 5.7-1, Figure 5.7-2 and Figure 5.7-3 respectively. As shown in the figures, the biocrude oil yield for Chlorella sp. increased from 1.36% at 180oC to 12.01% at 250°C and reached a maximum of 28.83% at 300°C. The same trend was followed in the case of other two species where the biocrude oil increased with the increase in temperature and a maximum biocrude oil yield of 14.76% and 22.33% were obtained

for Coelastrella sp. and Galdieria sp. respectively at 300°C. Chlorella sp. produced higher biocrude oil yields and Coelastrella sp. produced lower oil yields.

The variation in the oil yields for different algae depends on the biochemical composition of individual species. In all the cases, the biocrude oil yield was higher than the lipid content indicating that the all the compounds present in the algae such as lipids, carbohydrates and proteins contribute to the biocrude oil. Temperature was the major influencing factor that can significantly affect the biocrude oil yields and properties.

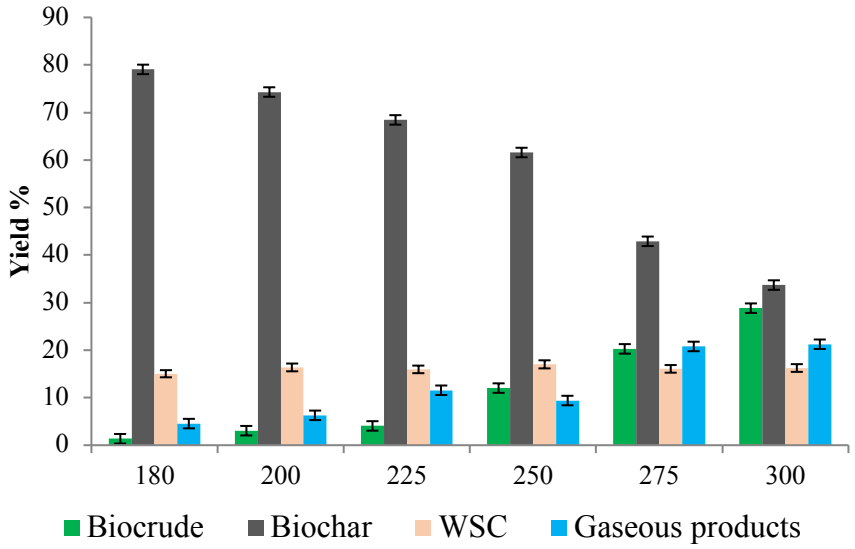

Figure 5.7-1: HTL product distribution of Chlorella sp.

The solid residue or biochar which is low in carbon mainly consists of unconverted algae cells and inorganic mineral components. The biochar produced for all the species was more than 70% at 180°C and decreased with the increase in the temperature. The biochar yields at optimum temperature (300°C) were 33.69%, 30.72%, 21.57% for Chlorella sp., Coelastrella sp. and Galdieria sp. respectively. Less biochar was produced with Galdieria sp. compared to that of other microalgae. The high amount of biochar production at lower temperatures was due to the incomplete conversion of algal biomass into HTL products other than biochar (residue). However the higher temperatures favored HTL and converted the biochar into liquid, gaseous and water soluble fractions. Higher temperatures (>300°C) might be needed to convert residual biochar into HTL products and to increase the biocrude oil yield.

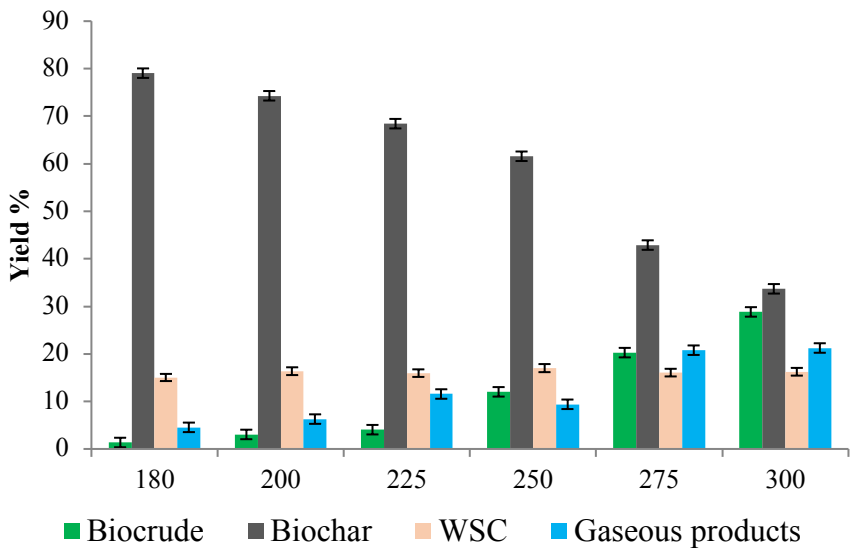

Figure 5.7-2: HTL product distribution of Coelastrella sp.

The HTL aqueous phase contains compounds obtained from carbohydrate breakdown, degradation of metabolites, nitrogen based compounds derived from proteins and various other water soluble compounds. The high amount of ash present in the microalgae also contributes to the water soluble compounds. Generally, the water soluble compounds fractions increase with the temperature up to certain point and further increase in temperature should decrease the water soluble compounds due to the repolymerization or gasification of carbohydrate and protein derived compounds into biocrude oil or gaseous product. In this work, for Chlorella sp. the water soluble compound recovery was not affected by the temperature a maximum recovery of 15-16% wat obtained at 180° C and 300°C. For Coelastrella and Galdieria sp. the water soluble compounds were decreased with increase in temperature and the amount of water soluble compounds obtained in this study are quite higher than literature. At 300°C, 15.47% and 25.34% of water soluble compounds were obtained for Coelastrella sp. and Galdieria sp. respectively. The gases produced during the HTL were increased with the increase in temperature and very high gaseous concentrations were observed above 250°C. Chlorella sp. produced less gases at high temperatures compared to other algal species. The gases primarily consist of carbon dioxide and lower amounts of hydrogen, CH4, C2H4 and C2H6.

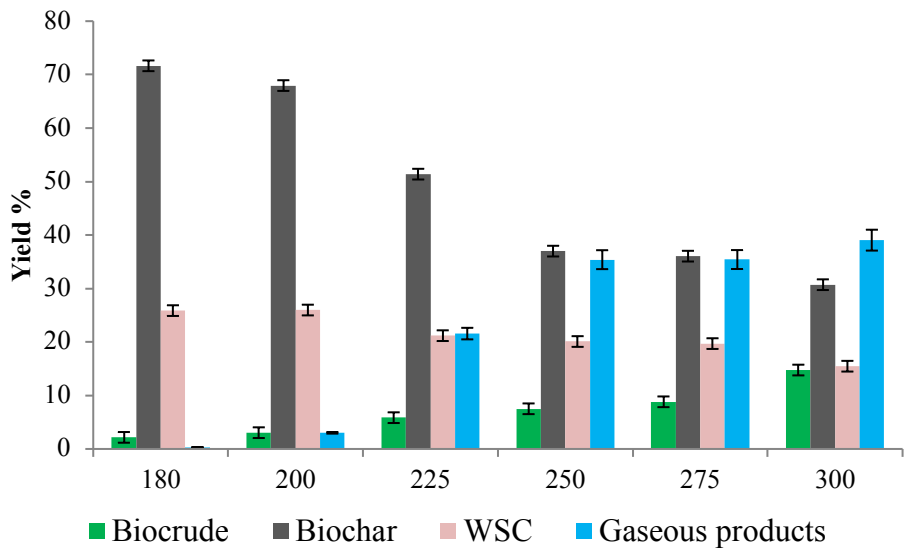

Figure 5.7-3: HTL product distribution of Galdieria sp.

5.7.4b HTL of C. merolae and the influence of catalysts on product fractions

The ash content in the merolae was 7.1% and moisture content was 67.13% after harvesting. This microalgae sample has a very low lipid content (1.99 %) and high proteins (56.5 %) in it. The ultimate analysis indicated that C. merolae has high oxygen content of 36.45 %. The high heating value of this microalgae was 18.11 and was determined using a bomb calorimeter. The yields were 0.65% at 180°C and 2% at 200°C. This might be mainly due to the extraction of lipids but there is no sign of biocrude oil formation up to 225°C. At 225°C the biocrude oil yield obtained was 4.95% which is well above the amount of lipids present in the microalgae. The biocrude oil yields increased to 11% at 250°C which shows rapid formation of biocrude oil from 200°C to 250°C. Further increase in the temperature increased the biocrude oil yield.

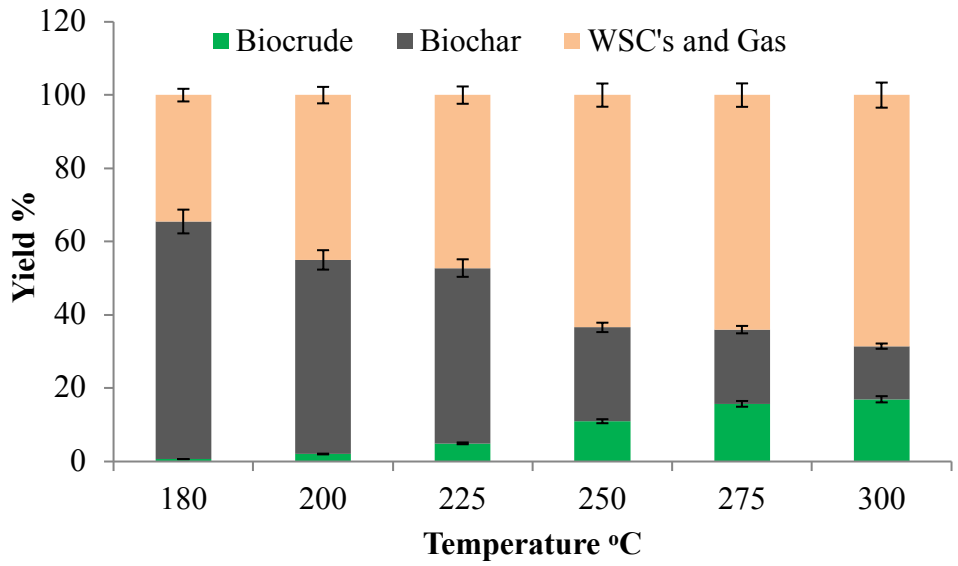

Figure 5.7-4: HTL product distribution of C.merolae

A biocrude oil yield of 15.74 % was obtained at 275°C and a yield of 16.98% was obtained at 300°C. It is evident that the increase in the temperature increases the biocrude oil yield due to the formation of biocrude oils not only from lipids but from other non-lipid components as well. The high temperatures encourage the cleavage of bonds to fragment the basic compounds and enhanced reactions like hydrolysis and repolymerization which improves the bio-oil yield at various process conditions. Further increase in temperatures might lower the yields due to intensified gasification at higher temperatures. Even though the biocrude oil comprises of components fragmented from lipids, carbohydrates and proteins, the higher lipid content in the algae can result in the higher biocrude oil yield. The biochar yields decreased with the increase in the temperature from 64.85% at 180 °C to 14.50% at 300 °C. The decrease in the biochar yield with increasing temperature might be due to the conversion of the residual components to biocrude oil at higher temperatures which are not converted at lower temperatures. The remaining water soluble compounds (WSC), gases and losses during product separation was calculated by difference. This WSC and gas yields ranged between 35 to 69% and was increased with temperature. The introduction of catalyst into the HTL system is to increase the yield of biocrude and to improve fuel properties. The biocrude oil yields increased from 16.98% without catalyst to 21.23% with CH_3COOH, 21.78% with NaOH and to 22.67% with KOH and no noticeable increase in the biocrude oil yield was observed with H_2SO_4. All the catalysts used in this study except H_2SO_4 tend to increase the biocrude oil yields but decreased the biochar yields. But the acid catalyst H_2SO_4 showed no effect of biocrude oil yield but increased the biochar yield.

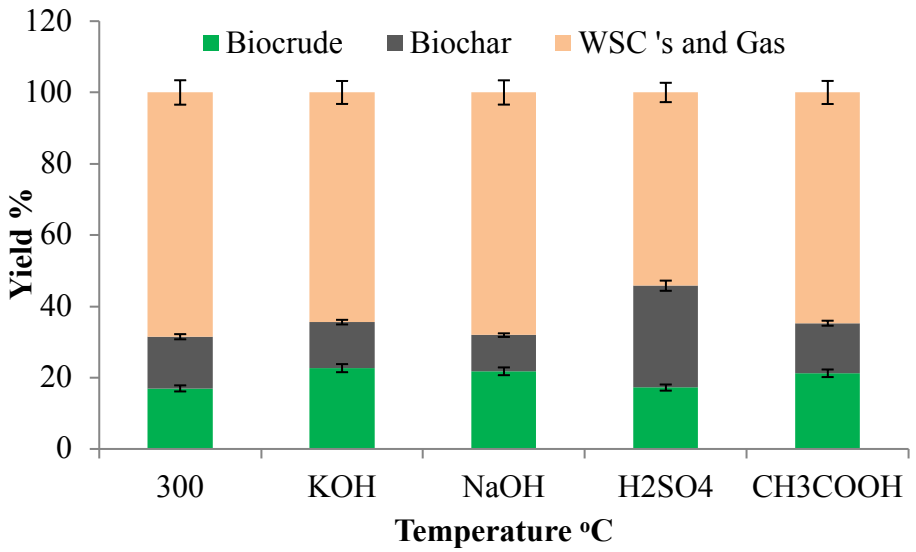

Figure 5.7-5: HTL product distribution for C.merolae with catalysts

The biocrude oil has been analyzed by a GC/TOFMS and the main compounds were identified by NIST library. The biocrude oil was a complex mixture and more than 1000 compounds were detected and more than 600 compounds were identified by the library. The principle segments (with area% >1) detected in biocrude oil obtained during direct HTL without catalysts at 300°C, 30 min of reaction time and 10% solids was presented in Table 5.7-2. The list with more identified compounds in the HTL biocrude oils obtained with and without using catalysts were presented in supplementary information S1-5. The biocrude oil may contain different compounds like amides, amines pyrollidine, hexadeconoic acid, indole, phenol piperidine, ketones, alkanes, alkenes and furans. The protein content present in the algae was rapidly hydrolyzed to amino acids which in turn converted into amines and amides by various decarboxylation and deamination reactions. The pyrazine derivatives might be due to the maillard reactions which are reactions between amines and sugars. The identified ketones and phenols were produced from carbohydrates via hydrolysis, dehydration, cyclization etc and alkenes (refer to supplementary information S1-5) might be generated from the conversion of unsaturated fatty acids present in the algae sample. The compounds detected in the biocrude oils produced from C.merolae were somewhat similar to the literatures but more compounds with less relative abundance (in% of total area of GC peaks) were identified in this work. This might be due to the GC/TOFMS procedure implemented for analysis of the biocrude oils and the chemical composition of the algal species.

Table 5.7-2: Main compounds detected in the biocrude oil obtained without catalyst at 300°C, 30 min and 10% solids by GC/TOFMS

Name	R.T (min)	(Area %)
TrimethylPyrazine	11.49	1.19
4-methylPhenol	14.53	1.09
1-(2-Isopropenyl-5-methylcyclopentyl)ethanone	43.56	1.15
11-Hexadecyn-1-ol	43.57	1.26
5,10-Diethoxy-2,3,7,8-tetrahydro-1H,6H-dipyrrolo[1,2-a;1',2'-d]pyrazine	46.37	2.97
2-(tert-Butylamino)ethyl methacrylate	46.93	1.37
Dodecanamide	54.30	3.35
N-Methyldodecanamide	55.20	2.47
N,N-Dimethyldodecanamide	56.45	1.74
N-(n-Propyl)acetamide	59.16	1.30
Tetradecanamide	60.30	2.01
3-Benzylhexahydropyrrolo[1,2-a]pyrazine-1,4-dione	60.33	1.04
N,N-Diethyldodecanamide	60.56	1.43
N-Acetylethylenediamine	60.58	1.25
N-Methyldodecanamide	61.18	1.19
1-Hexadecanamine	61.19	1.19
N-Decanoylmorpholine	63.43	2.03

5.7.4c Sequential HTL of Galdieria sulphuraria

The ash content in the merolae was 9.1% and moisture content was 66% after harvesting. This microalgae sample has a very low lipid content (2.51 %) and high proteins (56.5 %) in it. The ultimate analysis indicated that Galdieria has high oxygen content of 35.76 %. The carbon content is 48.37% which is comparable to other species of algae grown under similar conditions at NMSU. The high heating value of this microalgae was 18.15. Figure 5.7-6 shows the HTL product distribution of G. sulphuraria at different process temperatures with 30 min of reaction time, 10% biomass loading and 300 psi initial pressure. The HTL experiments were conducted at temperatures 180, 200, 225, 250, 275 and 300°C. The biocrude oil yields increased with the increase in temperature from 1.27% at 180 to 18.93% at 300°C. The biochar yields decreased from 65.86% at 180 to 125.61% at 300°C. The bio-char might have high amounts of crude protein if processed at lower temperatures. This high protein content makes it a good animal feed source. The bio-char can also be fired along with coal in power generation because of its higher calorific values. The gasification of the bio-char could be done to make syngas, which can be further converted into valuable industrial chemical products. Other possible applications for bio-char are water purification and soil remediation. There was a significant amount of water soluble compounds extracted into the HTL water phase at all temperatures. The water soluble compounds present in the water phase were analyzed calorimetrically. A two-step sequential hydrothermal liquefaction was conducted at two different temperatures. The first reaction was

conducted at 180ºC for 30 minutes and second reaction at 300ºC for 30 min. For comparison a direct HTL experiment for 60 min has been carried out. The liquefaction yields were presented in figure 5.7-7 below. The biocrude oil yield increased from 18.93 % to 29.34% with the increase of reaction time form 30 min to 60 min. For the sequential HTL the biocrude oil yield was almost doubled when compared with the direct HTL experimental yield. The biochar yield and water soluble compound yields decreased during SHTL as some of the products being removed in the earlier stage.

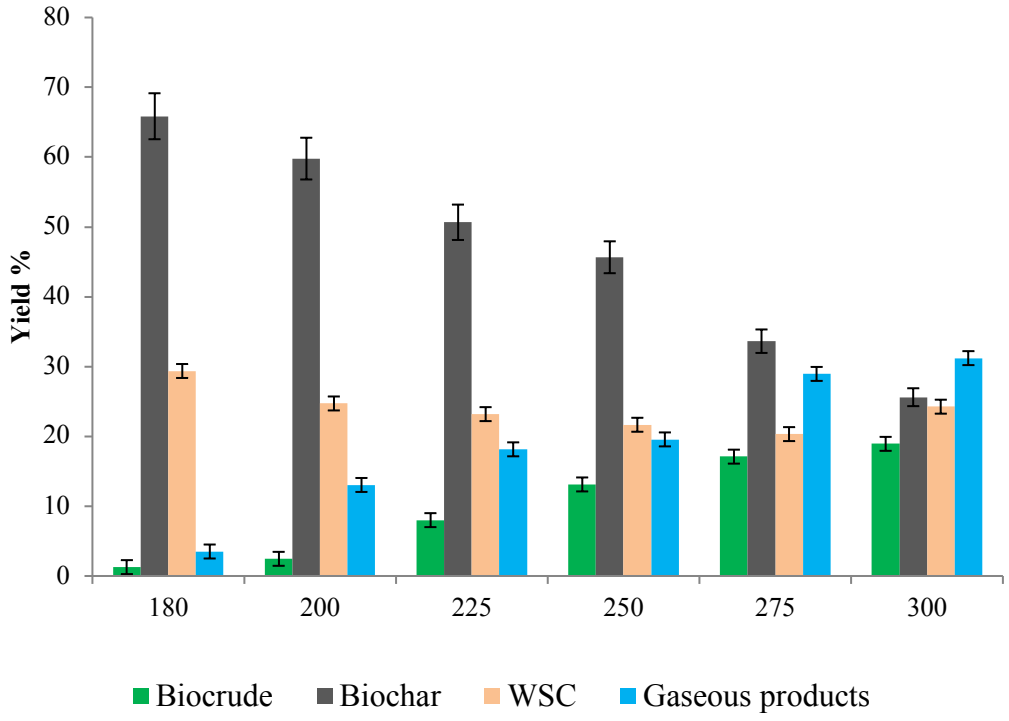

Figure 5.7-6: DHTL product distribution of G. sulphuraria

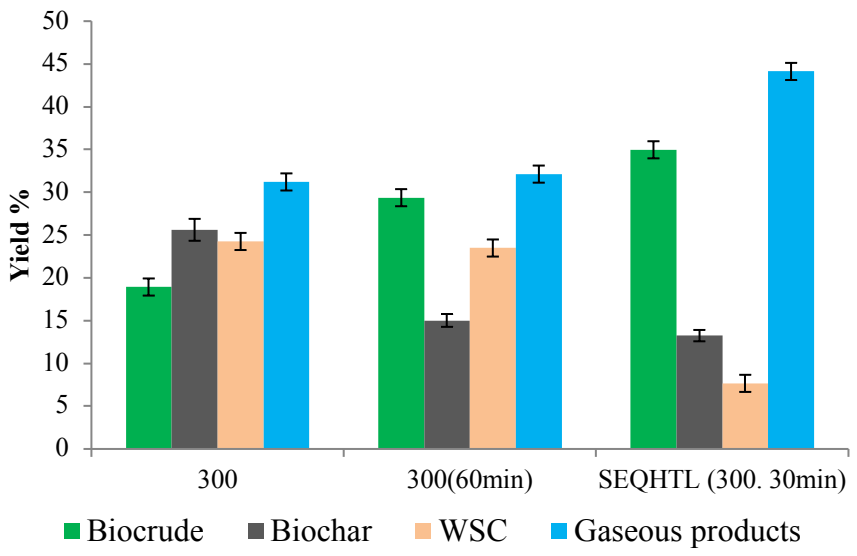

Figure 5.7-7: Sequential HTL of G. sulphuraria

To check the maximum extraction of water soluble compounds, HTL experiments were conducted from 120ºC to 300ºC. The aqueous phase at each experimental run was taken and analyzed for nutrients and co products. The ammonical nitrogen extracted from the algal biomass to the water phase increased with the reaction temperature. It was observed to be 100 mg/L at 120ºC and increased to ~4000 mg/L at 300ºC. The total nitrogen showed similar effect increasing from 2000 mg/L at 120ºC to 9000 mg/L at 300ºC. The extraction of phosphate levels increased from 120ºC to 200ºC where a maximum concentration of around 2800 was obtained and then decreased with further increase in reaction temperature.

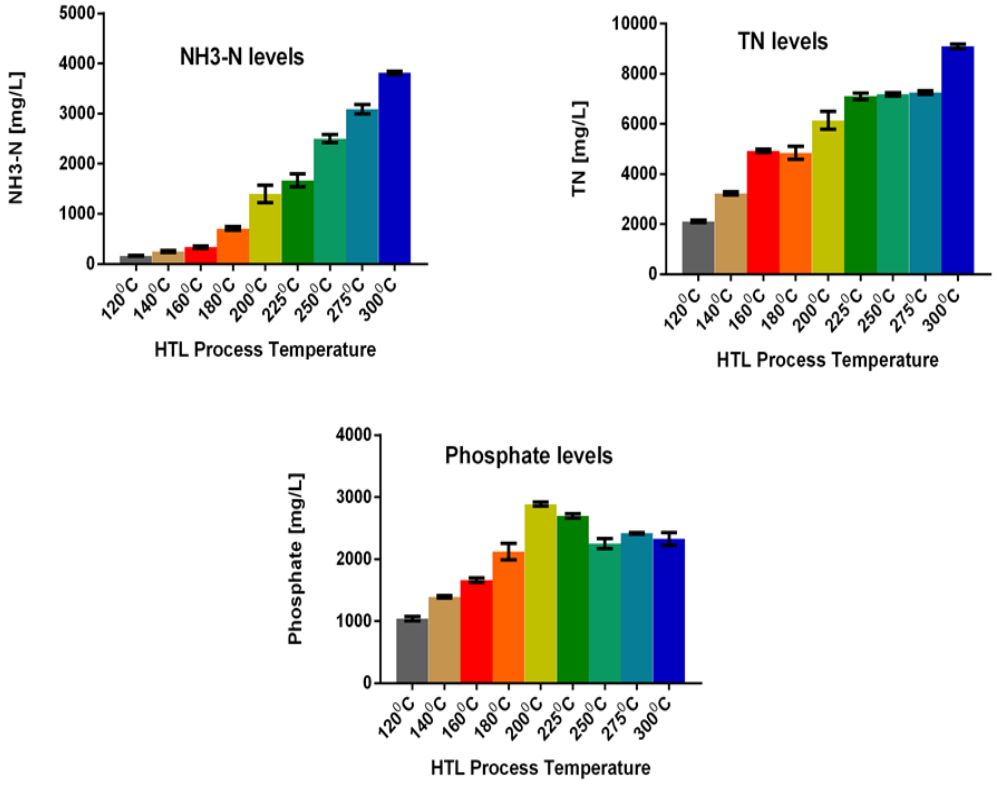

Figure 5.7-8: HTL AP analysis of G. sulphuraria

The carbohydrates extracted are around 2000 ppm at 120°C and increased to 12000 ppm at180°C and then showed a decrease there after. Similar effect was shown for soluble protein. The maximum proteins of 1700 mg/L were extracted at 160°C and then decreased thereafter. So we decided to do a direct HTL at 180°C and to experiment a sequential run with the solid residue obtained at 180°C run to be liquefied at 300°C. The HTL aqueous analysis of the water obtained after sequential HTL revealed higher concentrations of ammoniacal, total nitrogen, and phosphate levels. However, these concentrations were only half of the concentrations observed in the water obtained with direct HTL. This is because the nutrients are separated in the first step of sequential HTL. The soluble proteins tend to decrease further and the carbohydrate levels were increased with the sequential HTL compared to the direct liquefaction.

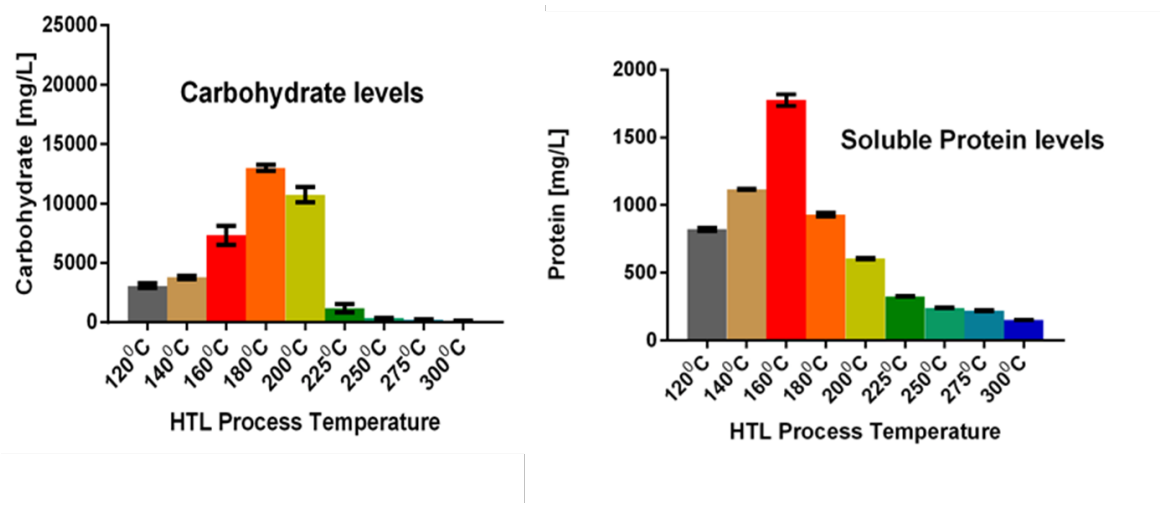

Figure 5.7-9: HTL AP analysis - coproducts Galdieria

Table 5.7-3: Sequential HTL AP analysis of Galdieria

	Concentration [mg/L]				
	NH3-N	**Total N**	**Phosphate**	**Soluble Protein**	**Carbohydrate**
DHTL	3813	9103	2327	156	141
Seq HTL	2280	4790	870	127	296

5.7.4d Continuous HTL of chlorella

The ash content in the chlorella was 5.03% and moisture content was 65.4% after harvesting. This microalgae sample has a high lipid content (21.2 %) than any other algal species used in this work. The ultimate analysis indicated that Chlorella has an oxygen content of 30.09 %, carbon content of 54.15% and the HHV was 23.86 based on Dulong's formula. The batch process produced a higher yield of 38.25% which was higher than the continuous process. But the reaction conditions were different for both the processes. The temperatures are same but the pressures in the batch process are two times higher than the continuous process. The batch process has a reaction time of 30 min and the heating time of ~60 min whereas for the continuous process, the slurry was pumped after the desired temperature was reached in the reactor and the residence time was 10 min for the continuous process. The solid loading was 5% for the continuous HTL and 10% for the batch HTL. The below results are based on ash free dry weight.

Table 5.7-4: HTL of Chlorella

Process	Algae	Temp °C	Pressure Psi	Time min	Solids %	Biocrude oil yield %
Batch	Chlorella	300	1400	30	10	38.25*
Continuous	Chlorella	300	700	10	5	21.51*

5.7.4e Co-liquefaction of two algal species:

In this study, Coe- Chl 80-20 refers to the mixture of 80% Coelastrella and 20% chlorella was used as feedstock. Similarly, 50-50 represents equal amounts of two algal biomasses in the feed stock and 100-0 represents the HTL was done without Chlorella but only with Coelastrella in the reaction mixture. The Coliquefaction results were presented in Figure 5.7-10. As presented below, the biocrude oil obtained when pure Coelastrella was used is 15.63% and biocrude oil obtained when pure chlorella was used is 24.6%. The 80-20 mixture tend to decrease the biocrude oil yield but the increase in the percentage of chlorella algae in the mixture increased the yield and at 40-60 the biocrude oil increased to 25.89% which is greater than the biocrude oil when pure species was used. This synergic effect might be due to effect of the fatty acids derived from one species on the conversion of other algal biomass. Irrespective to the increase or decrease in the biocrude oil, the biochar yield did not change very much and was between 25-30%. This suggests that the coliquefaction did not showed much effect on the conversion of solid residue to biocrude oil but influenced the reaction to form water soluble compounds and gaseous products.

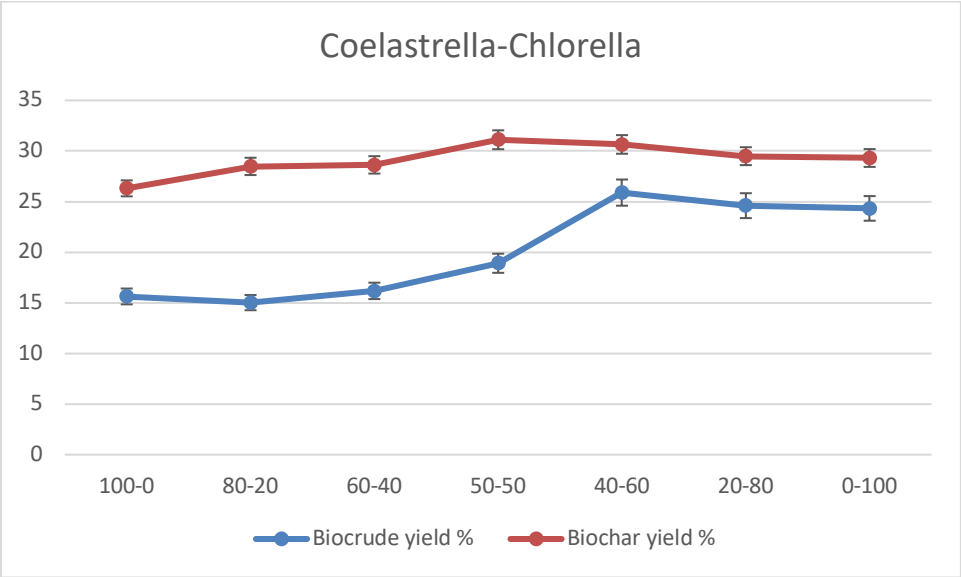

Figure 5.7-10: Coliquefaction of Coelastrella and Chlorella.

5.7.4f HTL water process recycle to enhance biocrude oil yield

In the process water recycle experiments, the water obtained in the initial HTL experiment was used as the water in the recycle run. The results of the process water recycle experiments were presented in figure 5.7-11. RR1 represents recycle run 1 and RR2 represents recycle run 2 where the HTL water obtained in RR1 was used as water in RR2.The biocrude oil obtained at 300°C with Nannochloropsis (lipids<5%) and chlorella (Lipids=21.2%) are 30.44 and 30.17%

respectively. Even though the lipid content of the two algal species are different, the biocrude oil is similar. For Nannochloropsis, the biocrude oil increased when the HTL was recycled from 30.44% to 38.87% after three recycles. For chlorella, the biocrude oil yield increased from 30.17 to 40.43& with two recycles and the third recycle reduced the biocrude oil yield to 35.21%. This increase was due to the catalytic effect of the water soluble compounds such as acetic acid on the conversion process. The biochar yields did not wary much throughout the recycle experiments which is consistent with literature.

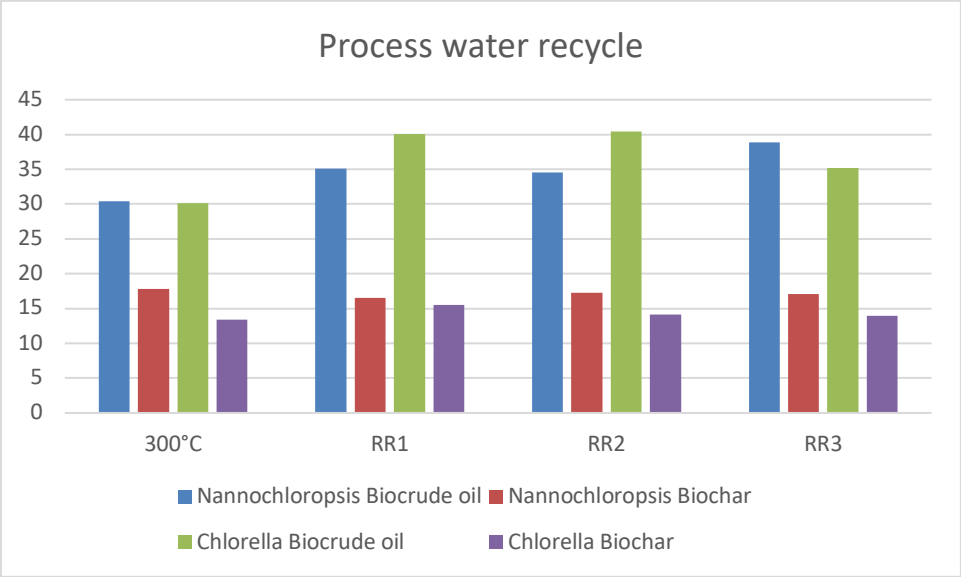

Figure 5.7-11: HTL product distribution with water recycle

5.7.4g HTL of Galdieria, Chlorella and Kirchneriella grown at ASU:

Table 5.7-5: Characterization of algae

ALGAE	KIRCHNERIELLA	GALDIERIA	CHLORELLA	Galdieria
Harvest Date	2/10/2016	7/6/2016	3/23/2016	10/15/2015
Ash	6.22	2.41	4.16	3.14
FAME	12.62	8.85	8.17	5.88
Carbohydrates	26.47	18.125	44.02	8.94
Proteins	28.11	43.4	26	49.52

The Galdieria species have high protein and low carbohydrate and ash content. Chlorella has highest carbohydrate content compare to other two species. Kirchneriella biomass has higher lipid content than Chlorella and Galdieria.

Table 5.7-6: HTL results

Algae	Kirchneriella (2/10/16)	Galdieria (7/6/16)	Chlorella (3/23/16)	Galdieria (10/15/15)
Biocrude oil	41	31.22	24.85	30.21
Biochar	14.23	4.85	17.88	2.48
Water solubles	14.73	8.2	10.40	5.04
Gas	30.05	55.74	46.87	62.26

All the algal biomass was hydrothermally liquefied at 300°C, 20% solid loading, 30 min of reaction time and around 100 bar pressure. The reported values in table 5.7-6 are yield percentages and the gas yield was calculated as difference. All the experiments were done in triplicates and their average was reported. The Kirchneriella biomass produced higher biocrude oil of 41% compared to other biomasses while chlorella produced less biocrude oil of 24.85%. The presence of high carbohydrate content might be the reason for lower biocrude oil since carbs are the least contributor for the HTL biocrude. Even though galdieria had more conversion (less biochar), the biocrude oil yield is not high and produced more gases.

The HTL water phase analysis results were tabulated below in table 5.7-7. The total organic carbon content is higher for Galdieria HTL water. Total phosphates present in HTL water for Kirchneriella biomass is 3-4 times higher than the other biomass.

Table 5.7-7: Analysis of HTL water

Algae	Kirchneriella (2/10/16)	Galdieria (7/6/16)	Chlorella (3/23/16)	Galdieria (10/15/15)
Total Organic Carbon (mg/L)	20666	29000	19500	29333
Ammoniacal N (mg/L) (NH3-N)	3033	5797	1933	7273
Total N (mg/L)	11130	11000	8867	8933
Total Phosphates (mg/L) (PO4)3-	8652	2196	2934	2133

.

5.7.5 ASU HTL Conclusions

Maximizing the biocrude oil yield is one of the important thing in biofuel production particularly algal biofuels. This can be done using several HTL techniques described above. Reaction temperature, pressure, time and solid loading are the important process parameters that effect the biocrude oil yield Direct HTL, catalytic HTL, sequential HTL, continuous HTL, HTL with co-liquefaction of two algal species, HTL with water recycle for enhanced biocrude oil were investigated in this study. The effect of all these HTL methods on biocrude oil yield was studied. The products of HTL such as biocrude oil, aqueous phase, and solid residue were analyzed using

various analytical instruments. Reaction temperature, pressure, time and solid loading are the important process parameters that effect the biocrude oil yield.

5.7.6 ASU HTL Recommendations

HTL should be conducted on model compounds to study the chemistry behind the HTL of microalgae.

Enough biomass should be grown in HTL process water to conduct another HTL run and study the effect of this biomass on biocrude oil.

Kinetic modelling should be done to predict the energy consumptions and to predict the decomposition of biomass.

Hydrothermal microwave processing of microalgae is a promising technology and should be implemented for biofuel production.

Pilot scale study on biocrude oil production will provide insight on sustainability and economic feasibility of HTL.

Upgrading biocrude oil into transportation fuels is the gateway to the sustainable production of renewable fuels from microalgae.

Solvents used in the HTL extraction might affect the properties of HTL products and this should be studied with different solvents.

Solvent free separation of HTL products should be investigated in a continuous scale.

5.7.7 ASU HTL Publications

Muppaneni, T., Reddy, HK., Selvaratnam, T., Dandamudi, K.P.R., Dungan, B., Khandan, N., Schaub, T., Holguin, O., Voorhies, W., Lammers, P., Deng, S.2016 Hydrothermal Liquefaction of Cyanidioschyzon Merolae and the Influence of Catalysts on Products. Bioresource Technology, 223,91-97.

Reddy, H.K., Muppaneni, T., Ponnusamy, S., Selvaratnam, T., Pegallapati, A., Sudhasinghe, N., Schaub, T., Holguin, F., Dungan, B., Seger, M., Cooke, P., Lammers, P., Voorhies, W., Nirmalakhandan, N., Deng, S. 2016. Temperature effect on hydrothermal liquefaction of Nannochloropsis gaditana and Chlorella sp. Applied Energy 165, 943-951.

Pan, J., Muppaneni, T., Sun, Y., Reddy, H.K., Fu, J., Lu, X., Deng, S. 2016. Microwave assisted extraction of lipids from microalgae using an ionic liquid solvent. Fuel 178, 49-55.

Sittithanaboon, W., Reddy, H.K., Muppaneni, T., Ponnusamy, S., Punsuvon, V., Holguin, F., Dungan, B., Deng, S. 2015. Single-step Conversion of Wet Nannochloropsis Gaditana to Biodiesel under Subcritical Methanol Conditions. Fuel, 147, 253-259

Muppaneni, T., Reddy, H.K., Deng, S. 2015 Supercritical Synthesis of Ethyl Esters via Transesterification from Waste Cooking Oil using a Co-solvent. Journal of Environmental Protection, 6, 986-994.

Sun, Y., Ponnusamy, S., Muppaneni, T., Reddy, H.K.., Wang, J., Zeng, Z., Deng, S. 2015.Transesterification of Camelina Sativa Oil with Supercritical Alcohol Mixtures. Energy Conversion and Management, 101, 402-409

5.7.8 ASU HTL Presentations

Muppaneni, T., Dandamudi, K.P.R., Mathew, M., Lammers, P., Deng, S. Sub and supercritical conversion of Kirchneriella algal biomass into biocrude oil, AIChE annual meeting, SanFrancisco, 13-18 November, 2016.

Muppaneni, T., Dandamudi, K.P.R., Mathew, M., Selvaratnam, T., Lammers, P., Deng, S. Biofuel production via thermochemical conversion of algae and optimizing coproduct utilization, AIChE annual meeting, SanFrancisco, 13-18 November, 2016.

Dandamudi, K.P.R., Muppaneni, T., Mathew, M., Lammers, P., Deng, S. Effect of process parameters and Extractive solvents on Hydrothermal Liquefaction of microalgae, AIChE annual meeting, SanFrancisco, 13-18 November, 2016.

Mathew, M., Selvaratnam, T., Muppaneni, T., Dandamudi, K.P.R., Lammers, P., Deng, S. Re-use of Hydrothermal Liquefaction bio-char to grow Galdieria sulphuraria, AIChE annual meeting, SanFrancisco, 13-18 November, 2016.

Muppaneni, T., Dandamudi, K.P.R., Mathew, M., Selvaratnam, T., Lammers, P., Deng, S. Hydrothermal treatment of microalgae: A potential pathway for biofuel production, Algal Biomass Summit, Phoenix, 23-26 October, 2016.

Mathew, M., Selvaratnam, T., Muppaneni, T., Dandamudi, K.P.R., Lammers, P., Deng, S. Optimization of Hydrothermal Liquefaction Co-products – Application of Biochar, Algal Biomass Summit, Phoenix, 23-26 October, 2016.

Muppaneni, T., Dandamudi, K.P.R., Mathew, M., Selvaratnam, T., Lammers, P., Deng, S. Microalgae: A potential feedstock for biofuel production and CO2 removal, The 7th Annual Closing the Carbon Cycle Conference, Phoenix, 28-30 September, 2016.Muppaneni, T., Dandamudi, K.P.R., Selvaratnam, T., Lammers, P., Deng, S. Conversion of Wet Algal Biomass to Biocrude Oil Using Hydrothermal Liquefaction, The 6th International Conference on Algal Biomass, Biofuels and Bioproducts, Sandiego, 26-29 June, 2016.

Muppaneni, T., Dandamudi, K.P.R., Reddy, H.K., Selvaratnam, T., Nirmalakhandan, N., Schaub, T., Dungan, B., Holguin, F., Lammers, P., Voorhies, W., Deng, S. Sequential Hydrothermal Liquefaction of Galdieria Sulphuraria Algal Biomass to Enhance Biocrude Oil Yield. AIChE annual meeting, Salt Lake City, 2015.

Dandamudi, K.P.R., Muppaneni, T., Norris, D.J., Nilusha, S., Schaub, T., Holguin, F., Deng, S. Co-Liquefaction of Mixed Culture Microalgal Strains Under Subcritical Water Conditions. AIChE annual meeting, Salt Lake City, 2015.

Muppaneni, T., Reddy, H.K., Ponnusamy, S., Nirmalakhandan, N., Schaub, T., Dungan, B., Holguin, F., Lammers, P., Voorhies, W., Deng, S. Hydrothermal Liquefaction of Wet Algal Biomass with/without Catalysts. AIChE annual meeting, Atlanta, 2014.

Reddy, H.K., Muppaneni, T., Ponnusamy, S., Selvaratnam, T., Dungan, B., Nirmalakhandan, N., Schaub, T., Holguin, F., Lammers, P., Voorhies, W., Deng, S. Kinetic Modeling of Hydrothermal Liquefaction of Algal Biomass. AIChE annual meeting, Atlanta, 2014.

Ponnusamy, S., Reddy, H.K., Muppaneni, T., Lammers, P., Downes, C.M., Deng, S. Life Cycle Assessment of Green Transportation Fuels Produced from Algal Biomass Via Hydrothermal Liquefaction. AIChE annual meeting, Atlanta, 2014

5.8 Life cycle analysis of energy use and GHG emissions

Ed Frank, Argonne National Laboratory

Life cycle analysis (LCA) of energy use and greenhouse gas (GHG) emissions associated with biofuel production seeks to compare anticipated emissions with the Renewable Fuels Standard (RFS2) target. In REAP, a conceptual scaled-up pathway utilizing REAP technologies is considered. This pathway produces renewable diesel (RD) by converting algal biomass to so-called "biocrude" via hydrothermal liquefaction. The RD is produced by hydrotreating the biocrude. The RFS2 target in this case is life-cycle emissions totaling less than or equal to 50% of the GHG emissions for conventional low-sulfur petroleum diesel. GHG emissions in this study are measured in units of grams equivalent of CO_2 (gCO_2e). Equivalence is computed by summing the 100-year global warming potential for CO_2, CH_4, and N_2O as set out by the Intergovernmental Panel on Climate Change (IPCC).

A life-cycle emissions basis means including not only emissions during combustion and manufacturing, but also emissions "up stream," associated with provisioning electricity, natural gas, and all other fuels and chemicals associated with the pathway. A system boundary defines the scope of activities to be considered. See Frank et al., 2011. The system boundary used in REAP analysis is consistent with the system boundary used for all other biofuels analyzed with GREET by Argonne National Laboratory. The life-cycle GHG emissions for low sulfur petroleum diesel total 93 gCO_2e per MJ of fuel (GREET 2015). Thus, the REAP target is 46 gCO_2e/MJ. The functional unit, 1 MJ of RD, is defined on a lower heat value (LHV) basis.

Prior LCA studies in REAP defined the major unit operations as shown in Figure 5.8-1. Cultivation comprised vertical flat panel PBRs mixed by aeration within which algae were grown to at least 2 g afdw/L prior to harvest. Settling, either by auto-flocculation or through the addition of coagulants, was envisioned followed by thickening in a filter-press. Biocrude would be produced via sequential hydrothermal liquefaction. Prior REAP LCA studies established several problems with this pathway definition:

- Energy consumption for aeration per gram of cultivated algae, as practiced at ASU, was 122-fold higher than the energy consumption per gram of cultivated algae in open pond models.
- REAP harvesting experiments have demonstrated good harvesting performance for some strains, but only after shifting pH. *Galdieria sulfuraria*, for example, required the pH to be increased. Adding 0.4 g NaOH per liter of harvested culture consumed 56% of the RFS2 emissions budget because of large upstream costs for manufacturing NaOH.

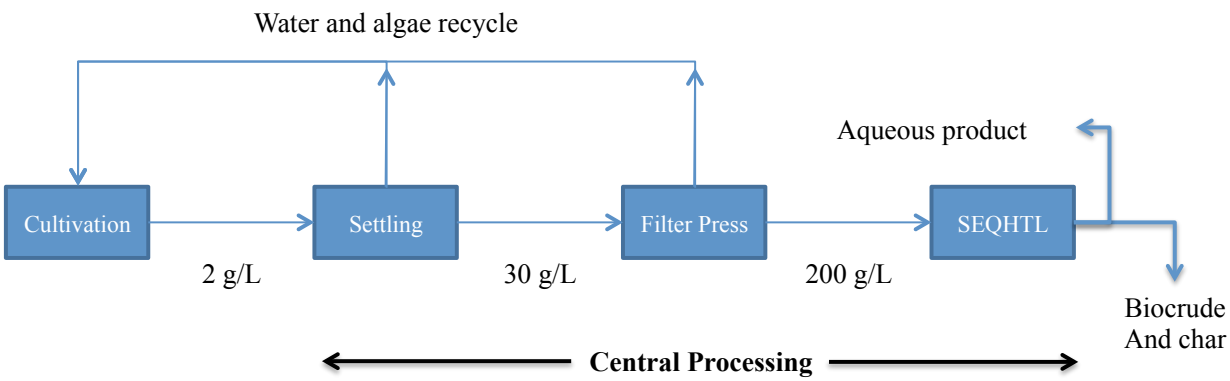

Figure 5.8-1: Process flow used in prior REAP LCA analyses

The present analysis modified the pathway definition by replacing the settling and filter press operations with the Global Algae Innovations (GAI) hollow fiber membrane Zobi Harvester followed by centrifugation. These operations do not require pH shifts. SEQHTL was replaced with direct hydrothermal liquefaction (DHTL) because DHTL showed higher yields with comparable oil quality in REAP data. Earlier REAP LCA analysis showed that high energy burdens are associated with recovering sugars from the low-temperature stream, which eliminates the benefit of using the sugar stream for co-products or recycling to the PBRs. Further work may establish a more workable low-temperature stream, but for the present analysis, we focus on the direct HTL process.

Since the energy budget is so challenging, the DHTL aqueous product is converted to biogas with catalytic hydrothermal gasification (CHG) in this model although no experiments have been performed with REAP streams. CHG produces biogas and a sterile aqueous stream containing ammonia, which is assumed to return to the cultivation process. See Figure 5.8-2.

The hollow GAI harvester is described in Davis et al. 2016 in a situation with a 10 g/L feed and 130 g/L product. GAI reported that the Zobi Harvester has been tested on small, *Chlorella*-like, algae successfully and that 2 g/L feeds can be handled (private email communication). Peter Lammers reports that the REAP productivities assumed here (described in the sequel) can be achieved with 5 g/L harvests.

In this analysis, we assume that the GAI Zobi Harvester can achieve a 13 wt% product with a 2 g/L feed. A centrifuge achieves the 20 wt% feed required for HTL. Energy consumption is taken from Davis et al. 2016, namely 0.04 kWh per m^3 of feed to the membrane system and 1.35 kWh/m^3 of feed to the bowl centrifuge. The membrane retention efficiency is 99.5% while the centrifuge retention efficiency is 97% (Davis et al. 2016). We assume that algae returned to the pond from centrifuge are viable. The Zobi Harvester energy demand is 10-fold less than other membrane systems, so a sensitivity case is considered with 0.4 kWh per m^3.

The present analysis will explore GHG and energy use for this pathway with the goal of establishing an energy budget for ongoing cultivation development.

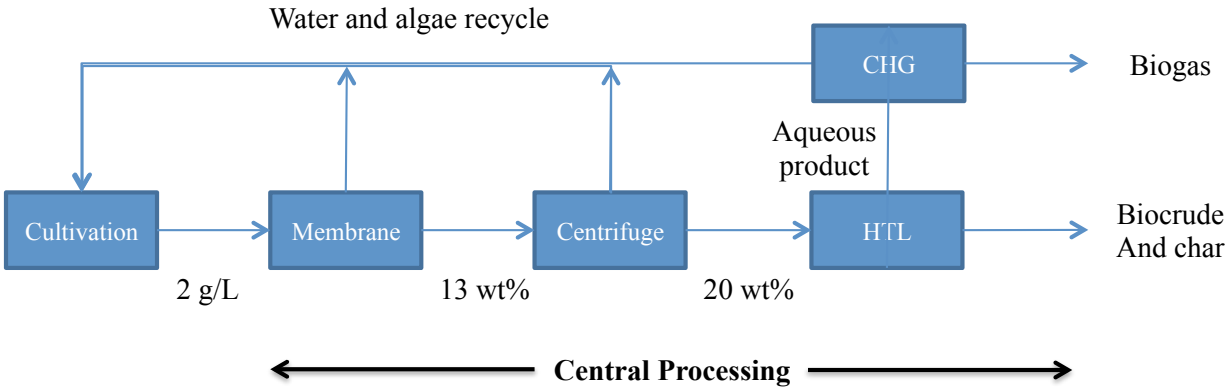

Figure 5.8-2: Process flow used in current REAP LCA analysis

5.8.1 Biomass and productivity

REAP has selected several strains for a crop rotation strategy as described in the REAP document, *REAP productivity and biocrude yield for final analysis,* E. Frank and P. Lammers, 10 Oct. 2016. See Table 5.8-1. Representative biomass samples were selected and analyzed. Table 5.8-2 summarizes the biomass properties.

To maximize the future utility of this study, results are often presented as a function of productivity rather than computing for specific values.

Table 5.8-1: Selected strains by month and assigned productivities. CS=*Chlorella sorokiniana* 1412 or 1230; GS= *Galdieria sulphuraria 5587.1;* KC= *Kirchneriella cornutum*

Month	Selected	Basis	g afdw/L/d	Std. Dev.
January	KC	Avg. Jan	0.16	0.044
February	CS	Avg. Feb-Apr	0.11	0.045
March	CS	Avg. Feb-Apr	0.11	0.045
April	CS	Avg. Feb-Apr	0.11	0.045
May	CS	May	0.28	0.048
June	GS	Avg. Jun	0.11	0.061
July	GS	Avg. Jul	0.13	0.061
August	GS	Avg. Aug-Sep	0.13	0.028
September	GS	Avg. Aug-Sep	0.13	0.028
October	GS	Oct	0.08	0.028
November	KC	Avg. Jan	0.16	0.044
December	KC	Avg. Jan	0.16	0.044

Table 5.8-2: Biomass properties

Strain	KC	CS	GS	GS	Avg. GS
Biomass properties					
Harvest Date	2/10/16	3/23/16	10/15/15	7/6/16	
Ash, wt%	6.2	4.2	3.1	2.4	2.8
FAME, %	13	8.2	5.9	8.9	7.4
Carbohydrates, wt%	26	44	8.9	18	14
Proteins, wt%	28	26	50	43	46

5.8.2 Cultivation and site model

In order to account for the realities of scaling up to a field of PBRs, we used the Algenol 2000-acre, "biomass-only" model, which considers a deployment of Algenol vertical PBRs each of which is 10 feet long, 36 inches high, and which has a 50L working volume. In the model, 4500 PBRs are arranged in a block and 24 blocks are arrayed around a field process pad where gas and liquid management equipment are located. The equipment serves the array of 24-blocks (called a module). Modules are repeated around a central main processing area, which contains inoculum, dewatering, and other processing services.

Figure 5.8-3 shows the process blocks in the Algenol biomass-only model. The following modifications to the Algenol model were made for REAP (See Figure 5.8-2):

- Gas management: Gas management describes the compressors and piping that are required to aerate the PBRs.

  Algenol has determined that aeration at 1.7 SLPM per 50L PBR (0.034 vvm) is the minimum, robust aeration rate for their relatively buoyant organism. This is the daily average (12-hr) aeration rate, which is adjusted according to light intensity throughout the day and is minimal during the night. The total energy use, integrated over a day, is equal to 9.6 Wh/PBR per day. A stretch case might consider at most a factor of two reduction in aeration power, but their pilot plant experience dictates a 0.034 vvm baseline. The power numbers include blower efficiency.

  For a given maximum aeration rate, Algenol designs the gas piping to achieve pressure drops across the piping, spargers, and the static head of the PBR water column of 3-5 psig with 1-2 psig from delivering gas to the PBR and 2-3 psig drop across the sparger and water column. Therefore, the gas management energy will scale linearly with the gas flow rate in sensitivity studies: $E_{aeration} = 2.47 \times 10^7 (v / 0.034)$ kWh/yr where v is the daily average aeration rate in vvm.
- Nutrient distribution: The nutrients block requires power to pump nutrients to the PBRs. REAP envisions supplying nutrients when returning water after dewatering or after HTL. Doing so avoids this pumping energy. Algenol reports 1.92×10^5 kWh/yr to deliver 4,840

Mg of urea and 1,071 Mg of phosphoric acid. REAP will require N and P in different ratios. In future studies, one could assume the energy for nutrient delivery scales with the urea mass: $E_{nutrient}$=39.7 kWh/(Mg urea yr).

- Inoculum field: The present analysis assumes that REAP and Algenol requires the same rate of seed culture production, which is 0.05 g dw/L four times per year. The inoculum field block includes all operations required for inoculum production as well as energy for pumping to the cultivation field. The energy demand for inoculum production is dominated by aeration. Algenol reports 1.06×10^6 kWh/yr for inoculum production.
- Cultivation field: The cultivation block reports energy for pumping cultures to dewatering assuming a pipeline velocity of 1.5 to 2 m/s and a total pumping head of 100 feet water equivalent. The total pump and motor efficiency is 70%. As a result, pumping requires 1.26×10^{-4} kWh/L. For sensitivity studies of pumping pressure, pumping energy is 1.26×10^{-4} (h/100) kWh/L where h is the total pumping head in feet water equivalent. The model assumes that the pumping energy will be equal to that from the flow rate corresponding to the average productivity and harvest concentration, e.g,. at 2.1 g afdw/L harvest concentration and 0.644 g/L/d productivity, each 50 L PBR produces 15.3 L of culture flow. In total, for the 7.04×10^6 PBRs, the energy for pumping culture to settling is 4.97×10^6 (p/0.644)(2.1/c)(h/100) kWh/yr where p is the volumetric productivity (g/L/d), c is the harvest concentration (g afdw/L), and h is the total pumping pressure (feet w.e.).
- Clean in place: Algenol CIP provides periodic chemical sterilization of the system. Associated costs are for piping, pumping, acids, and bases. REAP will not require sterilization for acidophilic cultures. No operational data exist for REAP strains to guide whether CIP will be needed for non-acidophilic strains. The baseline case will exclude CIP (1.61×10^6 kWh/yr).
- Plant electricity: Although co-generation of power and heat on site benefits the process, REAPs operations have different heat and electricity demands compared to Algenol. Thus, Algenol's CHP design cannot be carried over to REAP without a full evaluation. This portion of the Algenol model was excluded and the biogas co-generation model from Frank et al. 2011 was used instead.
- Biomass dewatering block: This block was excluded and will be covered by the REAP downstream model.
- Biomass processing: This block was excluded and will be covered by the REAP downstream model.
- Water treatment block: The Algenol model includes ultra-filtration of new make-up water, treatment of waste water, and pumping water recovered during harvest and dewatering back to the PBR and inoculum fields. The first two were dropped. Only pumping for return of water back to the fields was included. Water is returned assuming 1.5 to 2 m/s flows with 100 ft of total pumping head. Thus, this portion is identical to the cultivation harvest pumping and the specific energy demand will be equal to 1.26×10^{-4} (h/100) kWh/L where h is the assumed pumping pressure difference in feet w.e.

5.8.3 CO_2 supply

Work in other projects showed that energy use during post-combustion carbon capture at coal-fired power plants leads to a large GHG penalty. For example in the "State of Technology" and "Revised 2022 Target" scenarios in Pegallapati et al. 2016, carbon capture increased the GHG

emissions by 16 gCO_2e / MJ-fuel relative to the same scenarios using low-pressure flue gas. Carbon capture consumed 35% of the total GHG budget in these scenarios. Therefore, in this analysis, we assume that low-pressure flue gas from a coal power plant is used to supply carbon. Note that low-pressure flue gas transport is limited to short distances of approximately 5 miles (Benemann and Oswald 1996, Campbell et al. 2009, Frank et al. 2011, Davis et al. 2016).

The Algenol site design assumed that pure CO_2 would be delivered at 8 psi, which is adequate to deliver the gas at the bottom of the PBR columns; hence, no pumping energy was required for the CO_2. We will consider flue-gas from a coal-fired power plant that is 20 wt% CO_2 and that arrives at site with inadequate pressure for transfer into the water column. The Algenol model computes the energy for distributing gas at a specified rate specified in volumes of gas per volume of PBR per minute (vvm). Although Algenol did not add energy for transferring the CO_2 into the PBRs, they also did not take a credit for the pressure in the 8 psi gas. Therefore, as long as this analysis describes results as a function of the total aeration gas rate (CO_2 plus ambient air), no additional energy must be added to the computation. No corrections to blower efficiency were made, e.g., for altitude or temperature.

The flue-gas baseline assumes that the CO_2 demand can be computed stoichiometrically from the carbon content of the algae. The ASU PBRs use only a small fraction of the CO_2 that is introduced because of the high aeration rate, lack of counterflow, and lack of headspace recirculation; however, a realizable PBR implementation must have high CO_2 utilization efficiency because CO_2 supply appears to be a limiting factor in models to date (Langholtz et al., 2016). In order to model the behavior of a realizable system, we arbitrarily assume 18% loss of CO_2 to match our prior algae studies. See also Lundquist et al., 2010.

The three algae strains have 0.52, 0.49, and 0.49 g C per g of biomass for KC, CS, and GS, respectively. Given the arbitrary nature of the 18% CO_2 utilization efficiency, we assume the same CO_2 demand for all three strains based upon the average carbon content (0.5 gC/g dw). Thus, 1.83 g net CO_2 is required, which requires delivery of 2.2 g CO_2 / g dw of biomass. We do not consider recycling of CO_2 from the HTL off gas or from the co-generation flue gas.

Flue-gas delivery to site by low-pressure pipeline requires 1.16×10^{-5} kWh/g CO_2 (Frank et al., 2011).

5.8.4 Water supply to site

REAP cultivation experiments at ASU have observed water consumption between 50 to 150 L/kg biomass at 0.13 to 0.16 g/L/day in the mobile mini and long acrylic vertical PBRs. These PBRs are not sealed, so water vapor can be lost. Indeed, water vapor is driven off through the aeration. It should be possible to close the PBRs to manage water loss, but we lack data demonstrating growth performance under these conditions. We therefore choose to use the open-PBR water use numbers for now to be conservative and choose to use (60 L/kg)*(0.172 g/L/d)/p where p is the volumetric productivity in g afdw/L/d. The scaling method is described in Frank et al. 2016. For comparison, the average open pond water consumption in the FY13 Harmonization Study, evaporative plus blowdown, was 67.1 L H_2O/kg afdw of harvested algae. The energy to pump water to site is 4.37×10^{-4} kWh/L, which is the average over sites in the FY13

Harmonization study as determined by the PNNL Biomass Assessment Tool. This is the pumping energy to lift water from underground, if needed, and to deliver it to site.

REAP does not have data for blowdown. Blowdown was set to zero in this study, but blowdown has had a negligible effect on prior LCA work (Frank et al., 2016).

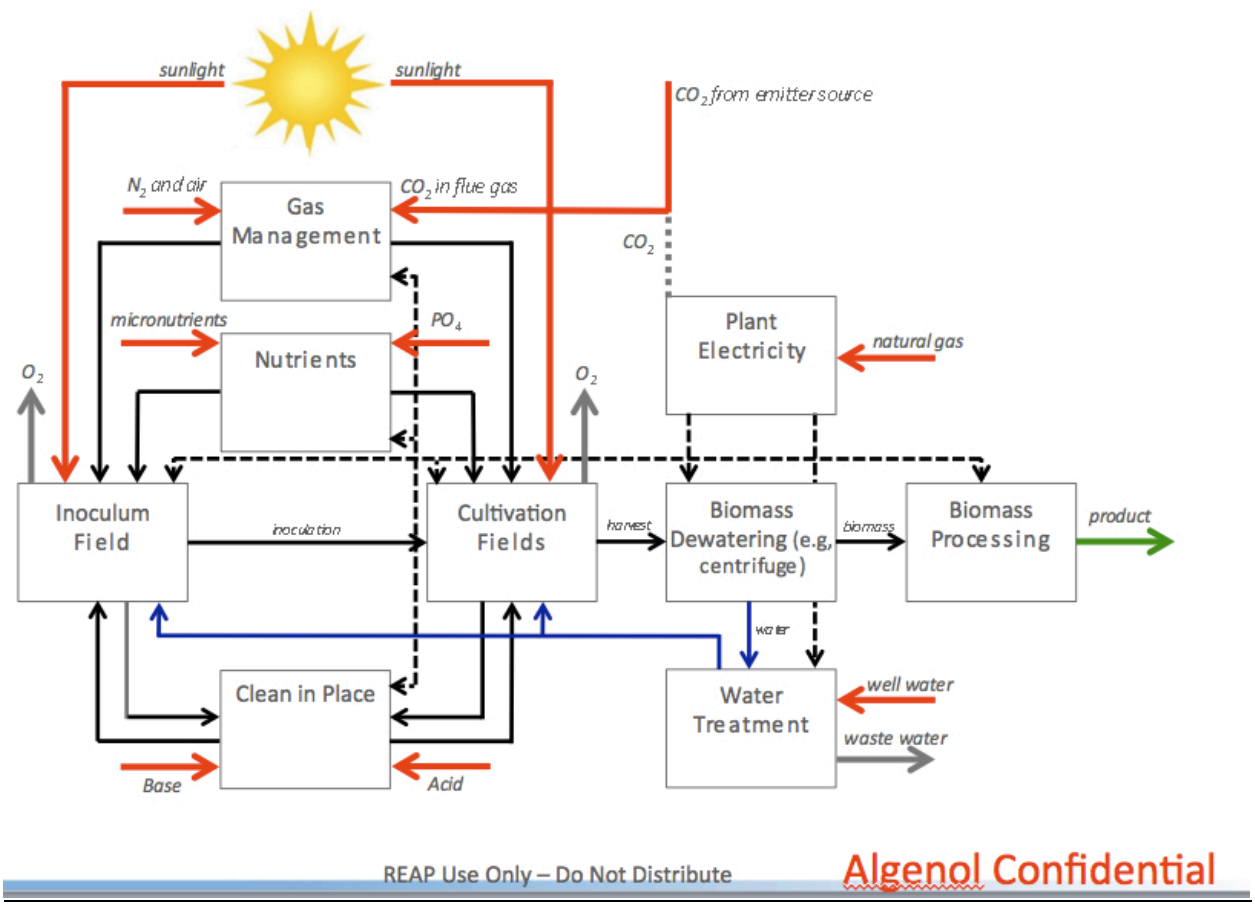

Figure 5.8-3: Algenol plant process flow diagram for a biomass-only scenario

Table 5.8-3: Summary of Algenol biomass-only model.

Parameter	Value	Units
Facility size	2000	Wet acres
PBR		
Length	10	ft
Height	36	inches
Working volume	50	L
Footprint	1.15	m^2 / PBR
Footprint	43.48	L / m^2
Spacing	0.377	m
Number	7.04×10^6	PBRs per 2000 acres
Productivity	0.644	g afdw / L / d
Harvest concentration	2.1	g afdw / L
Culture pumping		
Total pressure	100	ft water equivalent
Pump*motor effic.	70%	
Average aeration rate	0.034	vvm

Table 5.8-4: Summary of energy use model

Area #	Name	Reported Energy, kWh / yr	Modeled Energy	Notes
0100	Inoculum field	1,056,255	1,056,255 kWh/yr	
0200	Cultivation field, excluding aeration.	4,980,000	4.97×10^6 (p/0.644)(2.1/c)(h/100) kWh/yr	p=productivity (g afdw/L/d); c=harvest concentration, g afdw/L; h=pumping head, ft w.e.
0600	Nutrients	191,844	39.7 kWh/(Mg urea yr)	
0700	Clean in place	1,610,912	1,610,912 kWh/yr	
0800	Gas management for cultivation	24,388,000	2.47×10^7 (v / 0.034) kWh/yr	v=peak aeration rate, vvm
1000	Water treatment	4,921,300	1.26×10^{-4} (h/100) (V) kWh/yr	h=pumping head, ft w.e.; V= total volume pumped back to cultivation per year, L/yr.

5.8.5 Water and algae recycle loops

Harvesting and dewatering is modeled via hollow fiber membranes and centrifugation, as described in the introduction. Water is recycled from the membrane and centrifuge operations and some algae are returned to cultivation via those flows according to the separation efficiencies of each step. The analysis treats these algae as viable, meaning that they will continue to grow and that they and their progeny will eventually be captured in the separation processing. Under these assumptions, the fundamental observation with respect to conservation of mass is that the flow of algae into HTL (g/L/d) must be equal to the gross productivity in the PBRs (or else mass will accumulate at some point in the system). We are neglecting the small loss of algae via the blowdown stream.

A simple computation provides an algae mass balance for these flows. See Figure 5.8-3. Given the assumed concentrations at each step, water flows can be determined. As shown, the primary productivity, p, is supplemented in the cultivation block (left hand side) by the two return flows, thus increasing the flow from the cultivation field to membrane filtration. This increase in flow increases the pumping energy required to deliver material to the membrane filtration and to the centrifuge. This was handled in the model by increasing the Algenol pumping energy by scaling with the REAP retention efficiencies, e_m and e_c. For example, the pumping energy for pumping to settling shown in Table 5.8-4 becomes 4.97×10^6 (p/0.644)(2.1/c)(h/100) $(1/e_m e_c)$ kWh/yr.

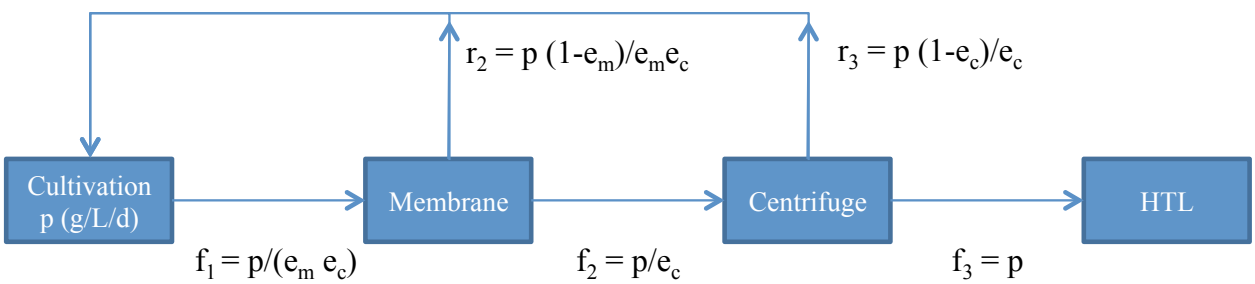

Figure 5.8-3: Algae recycle loops. Algae mass flows are shown (g/L/d). Notation: p = primary productivity (g/L/d); e_s = membrane retention efficiency; e_f = centrifug retention efficiency; $f_{1\text{-}3}$ = flows between unit operations; $r_{2\text{-}3}$ = return flows

5.8.6 Hydrothermal liquefaction

Representative biomass samples were selected for each of the crop-rotation strains and were treated via direct hydrothermal liquefaction in the Deng lab at ASU using a feed concentration of 20 dwt%. The feed comprised 10 g dw of algae in 40 mL of water and was processed for 30 minutes at 300 °C and 100 bar. Replicate samples were run. See the Deng lab section for details. The HTL yields are shown in Table 5.8-5. Yields are grams of product per gram dry weight of algae (including ash). The water solubles yield was measured by pipetting and weighing a volume of the aqueous product and subtracting the mass of an equal volume of water. The average of the two GS samples will be used in this analysis.

Another sample of GS from a different harvest and different PBR was processed in a continuous HTL reactor at PNNL. The run utilized 2 L/h of feed at 25.3 afdw% for 8 hours of running. The feed had 7.8 wt% ash, and yields of 33%, 0.9%, 9.2%, and 49% of biocrude, solids, gas, and aqueous product on a dw basis. The HTL biocrude had 79, 9.4, 3.7 and 7.3 wt% C, H, O, and N. The ASU and PNNL results are comparable for the oil yield, but the PNNL reactor produced 4 times less solids and 7.4 times less water solubles. The ASU experiments did not measure gas directly, but PNNL did.

The difference in aqueous product yield is of vital importance to the LCA because biogas will be produced from this product. In the ASU data, 10g of feed with 50 wt% carbon produced 39 mL of AP with 29 g/L total organic carbon, thus having a carbon yield of 0.23 gC/gC in the AP. The PNNL data reported 4.6 wt% total carbon in the wet AP, which implies a carbon yield of 0.27 g/g. We do not understand the difference in the AP yield, but since the same carbon yield is observed in both cases, we proceed onwards with the ASU data and note that a) An older survey of HTL data had AP yields similar to those reported by PNNL (Frank et al. 2013) and b) The organic carbon yield in the AP is what determines the biogas yield.

The mass balance amongst the DHTL products is shown in Table 5.8-6 while Table 5.8-7 shows the elemental composition of the DHTL products. The DHTL experiments only measured the biocrude, biochar, and aqueous phase products, not the gas phase. Table 5.8-6 shows the mass imbalance in the rows marked, "missing." The amount of N and P missing in the balance exceed what can reasonably be expected in the gas phase. PNNL reports that they have had difficulty measuring N in the gas phase because the levels are low, which is consistent with the pH of the AP. They find that the gas phase is approximately 93% CO_2, 0.19% CO, 0.85% H_2S, 0.41% H_2, and the balance is various simple hydrocarbons (methane, ethane/ethylene, propane, butane, and pentanes).

The DHTL energy demand was computed without Aspen. Two independent mechanical engineers and two chemical engineers checked the model approach. See Figure 5.8-4, which shows that the incoming cold algae stream at 20 wt% is heated against the hot oil and water stream from the HTL reactor through a heat exchanger. An effectiveness-NTU model was used to compute the heat exchanger performance. In an effectiveness-NTU model, the actual heat transferred divided by the maximum possible heat transfer (infinite area) is called the effectiveness. In a given application, heat exchanger cost is traded off against operating costs. The number of transfer units (NTU) is a measure of the heat exchanger area and, as a rule of thumb, does not often exceed 3 after economic tradeoffs are factored in. Figure 5.8-5 shows a plot of effectiveness vs. NTU for various values of C_r for counterflow shell and tube heat exchangers. In our system, C_r=0.8, which reflects the nearly equal heat capacity rate (c_p * dm/dt) in the hot and cold flows. Under these conditions, heat exchanger effectiveness is limited to between approximately 0.65 and 0.75. We assume a value of 0.7. The Shomate equation (NIST) was used to compute the temperature dependent water enthalpy. The heat capacity of the algae was assumed to be 2.09 kJ/kg.K (half that of water at room temperature), and the heat capacity of the HTL biocrude was assumed to be that of a light oil at 300C, 2.3 kJ/kg.K. The temperature dependence of the algae and oil heat capacities was neglected. With these values and assumptions, the algae influent exited the heat exchanger at 224 °C and required additional heat

to reach the 300 °C reaction temperature. The effectiveness-NTU method for this system shows that an economical system will not have a ΔT_{min} is much smaller than 76 °C.

The additional heat required after the heat exchanger defines the heating utility for the DHTL step. Cooling is assumed to be possible via water on site. Electrical power demand was calculated for a 9.9 MPa pressure difference across the pump and assuming a 50% total pump and motor efficiency because of the high solids content.

Cooling water requires careful analysis. We do not consider energy required to bring water to the DHTL equipment for cooling because we assume that water already at the central processing area, e.g., the return flow from sludge thickening, will be adequate; however, this may not be true depending upon the details of where various dewatering steps occur and how much cooling water is required. Future work must consider the tradeoffs between the location for dewatering, the location for thickening, and the costs of moving water-like cultures vs. thickened sludge. The results can then inform the cooling design and associated energy burden.

5.8.7 Catalytic hydrothermal gasification

CHG was modeled using information from Genifuel Corp. (James Oyler, private communication). In this model, 99% of the organic C in the CHG feed is reduced to biogas with 67% v/v methane and 33% v/v CO_2. Heat consumption is computed assuming a 30 °C temperature rise after heat exchange and a heat capacity of 5 kJ/kg/K. The model assumes that there is no net water production or consumption during the DHTL step. Thus, the flow of water into CHG equals the flow into DHTL minus the moisture entrained in the char. The suspended and dissolved AP products are less than 5% of the mass of the flow and will have heat capacities less than half of that of their water solvent. Therefore, they are ignored in the heating calculation. Electricity consumption is that of a feed pump with a pressure difference of 11 MPa and pump times motor efficiency of 68%. This pump is more efficient than that which is used in DHTL because the feed is water-like, but no real data are in hand.

As in previous Argonne analyses, 0.2% of the methane is assumed to be lost (fugitive emissions, Frank et al. 2011). There are additional methane emissions from uncombusted methane in the co-gen turbine. The co-gen electrical efficiency is 33% and is assumed to utilize a turbine rather than an internal combustion engine. Turbines require larger-scale installations, but internal combustion engines have substantially higher emissions, including higher fugitive methane emissions from uncombusted fuel. Future work must revisit this portion of the work and select a co-gen implementation that matches the plant scale.

Table 5.8-5: DHTL performance

Strain	KC	CS	GS	GS	Avg. GS
HTL yields					
Biocrude oil, g/g dw	0.41	0.25	0.30	0.31	0.31
Biochar, g/g dw	0.14	0.18	0.025	0.049	0.037
Water solubles, g/g dw	0.15	0.10	0.050	0.082	0.066
AP analysis					
Total Organic Carbon (mg/L)	20666	19500	29333	29000	29167
Ammoniacal N (mg/L) (NH3-N)	3033	1933	7273	5797	6535
Nitrate (mg/L) (NO3)-	68	87		84	84
Total N (mg/L)	11130	8867	8933	11000	9967
Phosphates (mg/L) (PO4)3-	4517	4330		1970	1970
Total Phosphates (mg/L) (PO4)3-	8652	2934	2133	2196	2164

Table 5.8-6: Mass based yields from DHTL. The entries for CHNSOP are the total grams of each element in the total amount of product. These are not the wt% compositions. See Table 5.8-4 for the product compositions. H and S were not measured for the AP.

		Total	C	H	N	S	O (difference)	P as P (ICP)
KC		g or mL						
	Algae feed	1.00	0.515	0.0596	0.0588	0.01100	0.355	0.014018
	Biocrude	0.41	0.314	0.0367	0.0214	0.00513	0.033	0.000044
	Biochar	0.14	0.094	0.0056	0.0059	0.00092	0.036	0.004484
	AP	3.95	0.082		0.0440			0.011145
	Missing, g		0.026		-0.0125			-0.001655
	Missing, %		5%		-21%			-12%
CS		g or mL						
	Algae feed	1.00	0.492	0.0648	0.0544	0.01140	0.378	0.030061
	Biocrude	0.25	0.186	0.0151	0.0156	0.00276	0.029	0.000126
	Biochar	0.18	0.116	0.0094	0.0103	0.00132	0.041	0.008977
	AP	3.90	0.076		0.0346			0.003731
	Missing, g		0.113		-0.0061			0.017226
	Missing, %		23%		-11%			57%
GS		g or mL						
	Algae feed	1.0	0.487	0.0635	0.1011	0.01700	0.333	0.014303
	Biocrude	0.31	0.226	0.0276	0.0231	0.00667	0.021	0.000036
	Biochar	0.037	0.020	0.0021	0.0025	0.00045	0.012	0.001664
	AP	3.93	0.114		0.0391			0.002770
	Missing, g		0.127		0.0364			0.009834
	Missing, %		26%		35%			69%

Table 5.8-7: Compositions of the DHTL feeds and products. Note that for the water-soluble component (WSC), phosphorus values are mg/L rather than mg/kg.

		C	H	N	S	O (by difference)	P (mg/kg) (ICP)
KC	Algae	0.5154	0.0596	0.0588	0.0110	0.3550	0.0140
	Biocrude	0.7663	0.0895	0.0522	0.0125	0.0794	0.0001
	Biochar	0.6601	0.0391	0.0418	0.0065	0.2524	0.0315
	WSC	0.3427	0.0560	0.1117	0.0163	0.4735	0.0862 [a]
CS	Algae	0.4917	0.0648	0.0544	0.0114	0.3777	0.0301
	Biocrude	0.7500	0.0608	0.0629	0.0111	0.1151	0.0005
	Biochar	0.6505	0.0528	0.0578	0.0074	0.2315	0.0502
	WSC	0.3792	0.0642	0.1034	0.0075	0.4459	0.1646 [a]
GS	Algae	0.4874	0.0635	0.1011	0.0170	0.3331	0.0143
	Biocrude	0.7374	0.0898	0.0751	0.0217	0.0692	0.0001
	Biochar	0.5076	0.0552	0.0651	0.0112	0.3502	0.0489
	WSC	0.3369	0.0688	0.1496	0.0124	0.4324	0.1105 [a]

[a] mg/L of AP

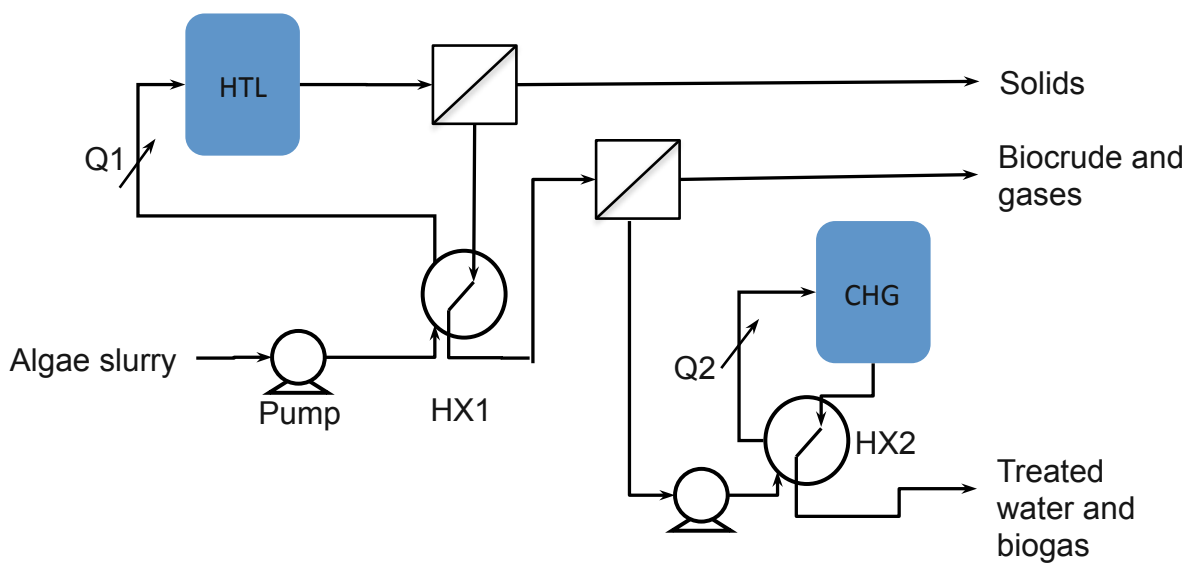

Figure 5.8-4: Process flow diagram for DHTL and CHG.

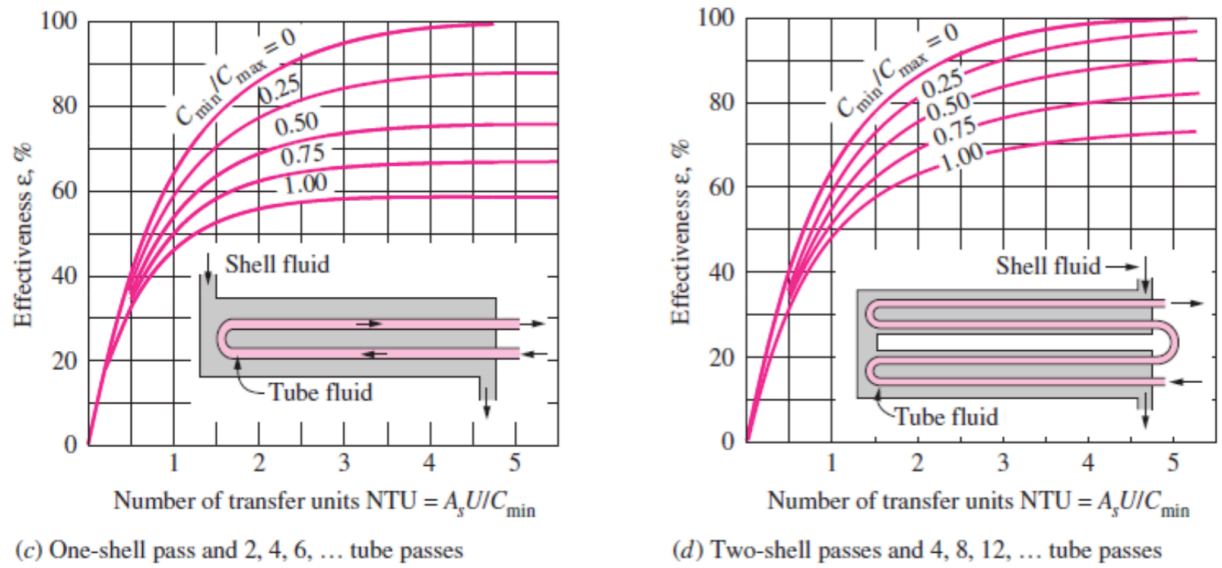

Figure 5.8-5: Heat exchanger effectiveness. Copied without permission from Talukdar

5.8.8 Mass balance and nutrient recycling

A mass balance is needed for the LCA to compute the net nutrient demand. The N and C balances have the most effect via the upstream costs for nitrogen fertilizer manufacturing and for carbon delivery to the site. Phosphorus affects sustainability through concerns over long-term supply limits, but has only a minor effect on the GHG and energy use results because it is a minor component in the biomass. We do not consider other elements at this time.

Table 5.8-6 showed the mass balances obtained for the representative biomass samples that underwent DHTL. The rows marked, "Missing," show the differences between the mass of each element in the biomass and the summed masses of each element amongst the biocrude, biochar, and AP.

Nitrogen accounting was not closed and has 11% and 21% excess for KC, CS, but is under-reported by 35% for GS. The mass balance does not include the gas product. PNNL reported very low levels of nitrogen in the gas phase in a reviewed paper (Davis et al., 2014, Figure SI-3). PNNL also found little nitrogen in the gas product when they processed GS biomass in their continuous HTL system. Therefore, we interpret the N imbalance in Table 5.8-6 as systematic experimental uncertainty rather than assigning it to the gas product. On the other hand, the nitrogen levels in the biocrude, between 5.2% and 7.5% (Table 5.8-7) are similar to those reported in the literature (Frank et al., 2013). Davis et al. 2014 reported that essentially all of the nitrogen that enters CHG ends up as nitrogen in ammonia in the CHG aqueous phase.

Taking all these facts together, the LCA analysis assumes that nitrogen in the HTL oil is lost (offsite upgrading to fuel) and that 95% of the remaining nitrogen is recovered as ammonia in the CHG aqueous product. The missing 5% is volatilization loss.

The phosphorus balance in Table 5.8-6 varies from 69% underreporting to 12% excess. The phosphorus data are too uncertain to be helpful. We simply assume 50% net recovery of bio-available phosphorus via sulfuric acid treatment of the CHG precipitate (Frank et al., 2011).

Carbon in the CHG off-gas and carbon from combustion of biogas are not returned to the cultures in this model. Most of the recovered carbon is CO_2 in the co-generation flue gas, which is hot and dilute. The CO_2 supply design must be defined to formulate a model for CO_2 return.

Table 5.8-8: Nutrient balances for the three algae strains

	KC	CS	GS
Biomass, gN/ g dw	0.059	0.054	0.10
Biocrude, gN/ g dw algae feed	0.021	0.016	0.023
Input to CHG, gN/ g dw algae feed	0.037	0.039	0.078
Net N demand per g dw algae	0.039	0.041	0.082
Biomass, gP/g dw	0.014	0.03	0.014
Net P demand per g dw algae	0.007	0.015	0.007
(NH2)2CO, g/g dw	0.071	0.058	0.16
(NH4)2HPO4, g/g dw	0.030	0.064	0.030

5.8.9 pH management

The cultivation team reported that the various strains were able to establish the culture target pH values metabolically. No inputs for pH swings were included in this analysis. Close review will be needed in future analyses including the need for pH swings for the downstream operations, e.g., for harvesting or to protect various reactor vessels.

5.8.10 Biochar utilization

REAP batch data are suggest char production rates between 2.5% and 18% while the PNNL continuous HTL operation is reporting rates of only a few percent. It may be inappropriate to use the batch char rates when extrapolating to a continuous process. The LCA analysis assumed 5% char yield and utilization of char as a soil amendment with 61 wt% C and 80% carbon sequestration (Wang et al., 2014). The carbon content is equal to the average elemental carbon content of the char from the three strains (KC- 0.66; CS- 0.65; GS- 0.51). The char is assumed to be recovered with 50% moisture content (Private communications with Shuguang Deng).

5.8.12 Miscellaneous factors

In order to carry the computations all the way through use in a vehicle, the default values in GREET1 2015 were used for upgrading bio-oils to renewable diesel (RD). In particular, the RD yield was 0.901 kg RD per kg of biocrude and 1582 BTU of hydrogen (LHV) was required per pound of RD product. The RD properties were 2.948 kg/gal, 122,887 BTU/gal (LHV). The boiler efficiency for raising steam was 80% on an LHV basis. Only fuel-cycle related emissions were considered. Infrastructure-cycle emissions were neglected. See Canter et al., 2014.

5.8.11 LCA Results

Previous REAP LCA studies showed poor GHG reduction performance because of high energy demand for mixing in the vertical PBRs and low oil yield. Figure 5.8-6 shows the GHG emissions for RD produced from KC biomass for the actual aeration rate at ASU (0.3 vvm) and for the aeration rate used by Algenol. Since KC demonstrated the highest DHTL yield and one of the highest productivities, the other strains will perform more poorly. The pathway achieves a 50% reduction in emissions for 0.034 vvm aeration when the autotrophic productivity is a little above 0.3 g/L/d and when a credit is taken for carbon sequestration in soil from the biochar; however, the 0.3 vvm case never achieves a 50% reduction. REAP photoautotrophic productivities are well below 0.3 g/L/d. The high mixotrophic productivities cannot be considered from this graph because emissions associated with substrate production would need to be added, e.g., corn stover farming, harvesting, transportation, and saccharification.

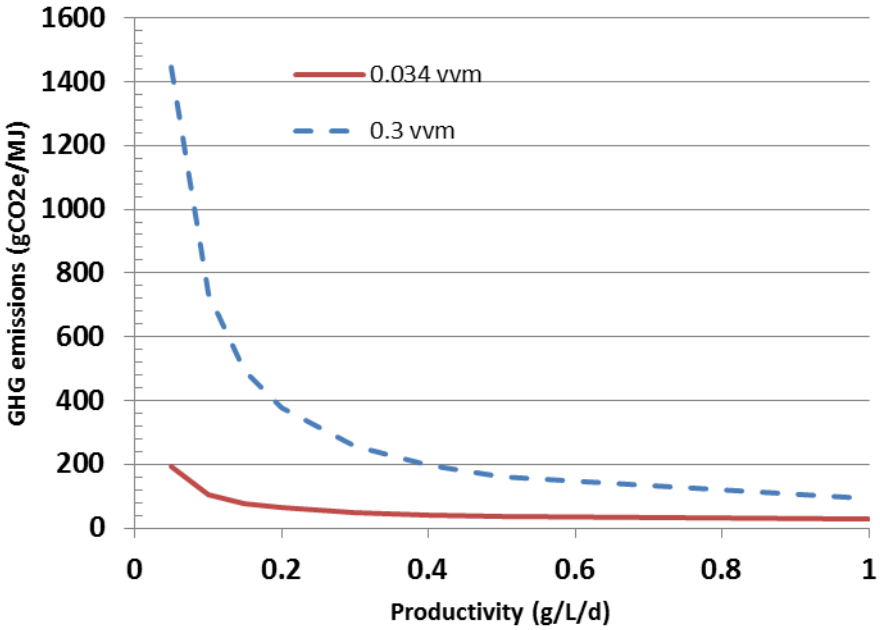

Figure 5.8-6: Life-cycle GHG emissions for KC

Given the poor GHG performance in Figure 5.8-6, this analysis must consider hypothetical scenarios with cultivation energy demand less than in vertical PBRs aerated below 0.034 vvm. The reader should understand that this analysis is using aeration rate as a proxy for various alternative cultivation methods that use less energy. Figure 5.8-7 is a plot of the total cultivation energy per gram of algae for various aeration rates and productivities. The cultivation energy includes inoculum production, cultivation, harvesting, dewatering, supply of water to site, pumping of cultures to harvesting, and pumping recycled water back to cultivation. These operations do not depend upon the algae strain, so the curves in Figuure 5.8-7 apply to all strains in this study.

The horizontal line in Figure 5.8-7 is the corresponding value from the recent NREL study of algae cultivation in open ponds at 25 g/m2/d (Davis et al., 2016) and was obtained by averaging over the eight scenarios in the NREL report (4.61×10^{-4} kWh/g). This figure shows that, to match the energy consumption in NRELs computational study, the REAP aeration would need to be reduced to 0.005 vvm for the system to match the open pond energy efficiency at the observed volumetric productivity of approximately 0.15 g/L/d. This is a sixty-fold reduction vs. the actual ASU aeration rate and 6-fold relative to the Algenol reported aeration rate.

This comparison should be made with caution because, if productivity improvements could be carried over to a paddle-wheel mixed pond, the horizontal line in Figure 5.8-7 would move down. Also, this plot does not consider the oil yield nor does it consider energy that might be recovered from the process residuals

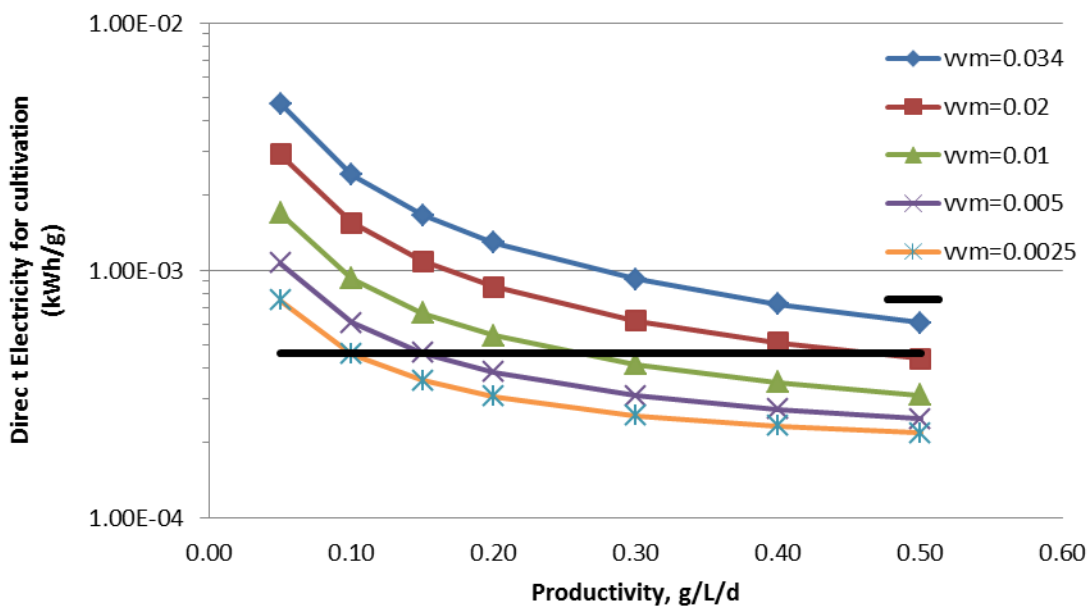

Figure 5.8-7: Direct cultivation energy. The horizontal line at 4.61×10^{-4} kWh/g is the value averaged over the 8 cases in Davis et al., 2016.

Figure 5.8-7 shows the need to investigate a broad range of aeration rates, which we choose to be 0.034, 0.015, and 0.005 vvm corresponding to the Algenol aeration rate, half of the Algenol rate, and a rate that entails direct energy use comparable to the NREL open pond scenarios. GHG emissions were computed for the three strains, the three aeration rates, and as a function of productivity. See Figure 5.8-8.

Considering the productivities reported in Table 5.8-1, KC almost achieves a 50% reduction in emissions when the aeration rate is 0.015; CS fails to achieve a 50% reduction even at 0.005 vvm but would pass if the productivity increased to 0.2 g/L/d; GS almost achieves the 50% target at 0.005 vvm.

The emissions performance is a competition between electricity demand and the availability of renewable electricity, generated from the AP. This is illustrated n Figure 5.8-9, which shows the total electricity demand as a function of productivity and which also shows the total on-site generated electricity. The latter is constant when expressed on the basis of total oil because the strain characteristics and the DHTL yields dictate the ratio of total organic carbon in the AP to the total mass of biocrude. The electricity for production is not constant because lower productivity implies longer residence time in the PBR and mixing-energy use accrues over that time.

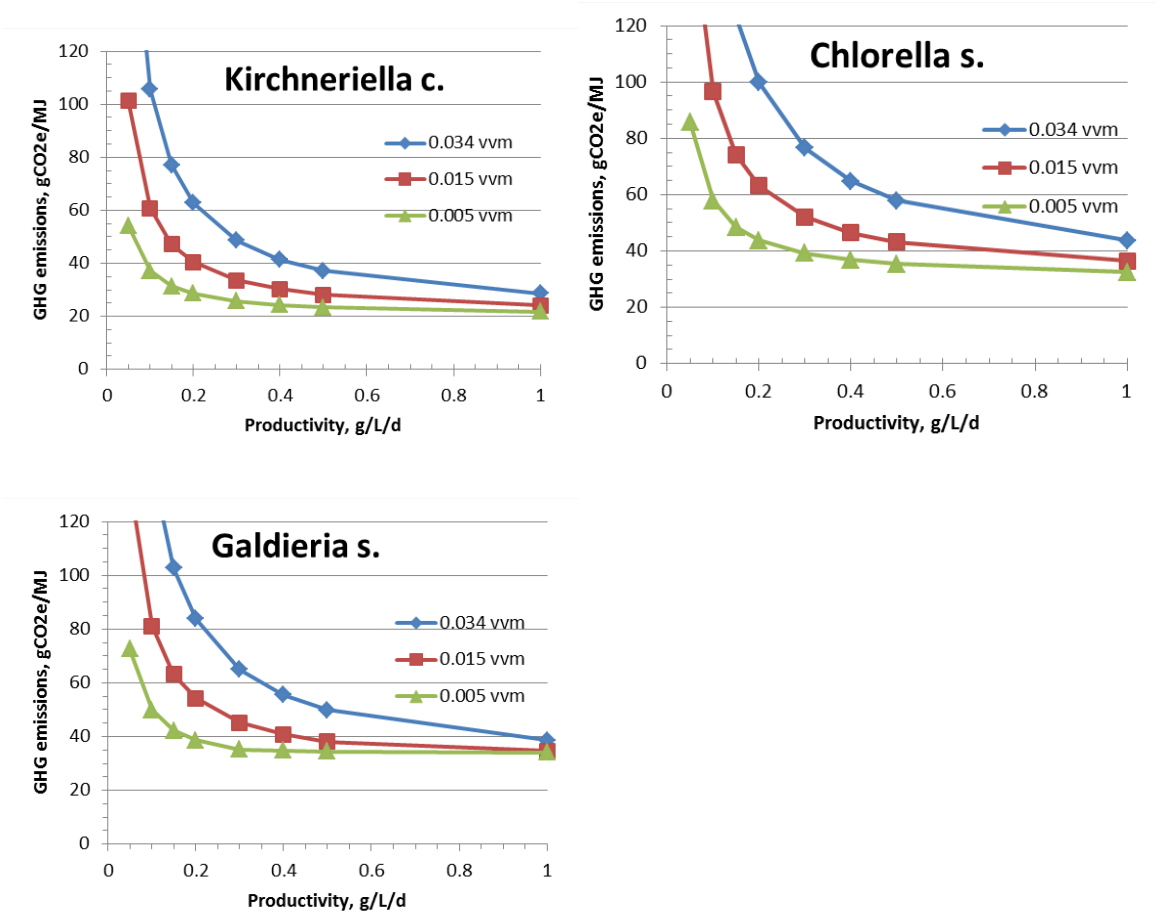

Figure 5.8-8: GHG emissions for the three REAP strains under various assumptions for productivity and aeration rate.

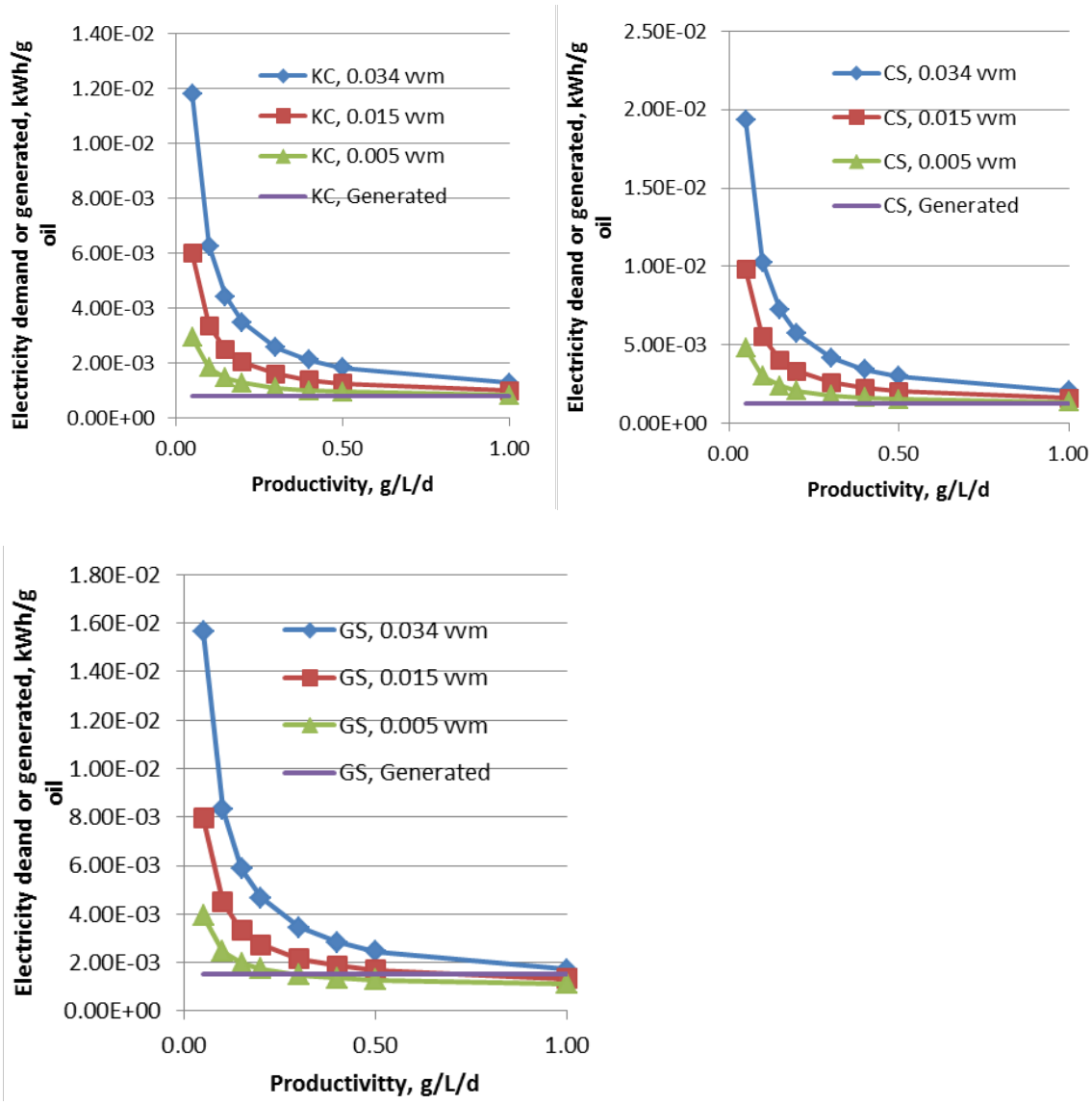

Figure 5.8-9: Total direct electricity demand for biocrude production and biogas-fired co-generation electricity.

The discussion above explored the sensitivity of the GHG emissions to the cultivation energy and productivity. Table 5.8-10 displays a computation of the fuel-weighted average GHG emissions and fossil energy use for the crop rotation schedule when the aeration rate is 0.005 vvm. Emissions on a fuel-weighted basis are 41 gCO2e/MJ, which meets the 50% reduction target. The life-cycle fossil energy is 0.68 MJ/MJ. Petroleum diesel fossil energy use is 1.2 MJ/MJ. Thus, the fossil energy savings are not as good as the GHG reduction, which likely reflects the fact that some of the GHG reduction was achieved via sequestration of carbon in the char. If the aeration rate is 0.015 rather than 0.005, then the GHG emissions increase to 63 gCO2e/MJ and the fossil energy use increases to 0.93 MJ/MJ. The fossil energy use is quite high in this case.

Sensitivity to several parameters was considered. The three strains contribute almost equally to the total annual biocrude production (KC- 36%; CS 31%; GS 33%). Therefore the sensitivity study used GS as the biomass since its biocrude yield (0.31 g/g dw) is closest to the fuel-weighted biocrude yield (0.34 g/g dw). The aeration rate was fixed at 0.005 vvm.:

- Increased membrane harvest energy: 0.5 kWh/m^3 was considered rather than 0.04 kWh/m^3
- Lower and higher char rates were considered: 0.025 g/g dw and 0.10 g/g dw rather than the baseline 0.05 g/g dw.

Results are in Figure 5.8-10. The scenarios with 0.025 and 0.1 g/g dw biochar yield satisfy a 50% GHG reduction at 0.16 g/L/d productivity, but the scenario with 0.5 kWh/L membrane filtration energy does not.

Table 5.8-10: Fuel-weighted average GHG emissions and fossil energy use

Month	**Strain**	**Productivity** g/L/d	**HTL Oil yield** g/g dw	**Gal oil /ha**	**GHG** gCO2e/MJ	**Fossil energy use** MJ/MJ
Jan	KC	0.16	0.41	681	31	0.51
Feb	CS	0.11	0.25	263	55	0.87
Mar	CS	0.11	0.25	291	55	0.87
Apr	CS	0.11	0.25	282	55	0.87
May	CS	0.28	0.31	916	40	0.69
Jun	GS	0.11	0.31	356	48	0.78
Jul	GS	0.13	0.31	411	45	0.74
Aug	GS	0.13	0.31	412	45	0.74
Sep	GS	0.13	0.31	399	45	0.74
Oct	GS	0.08	0.31	257	56	0.87
Nov	KC	0.16	0.41	659	31	0.51
Dec	KC	0.16	0.41	681	31	0.51
Fuel-weighted average		0.16	0.34		41	0.68

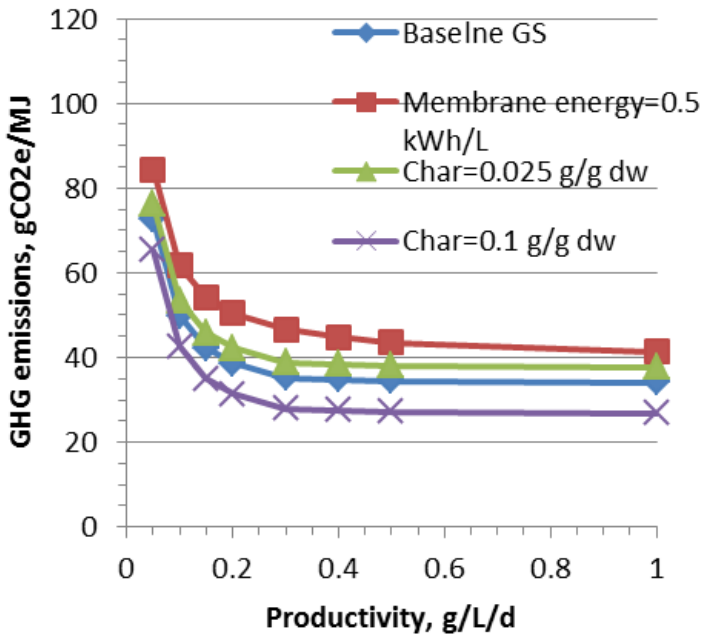

Figure 5.8-10: Sensitivity analysis. GS was used for computations with 0.005 vvm and with variations on membrane filtration energy and biochar rate. The baseline has 0.05 g/g dw biochar yield and 0.04 kWh/L energy demand for membrane filtration.

5.8.12 LCA Conclusions

A 50% reduction in GHG emissions was only possible when the cultivation energy was reduced 20 to 60-fold and when substantial amounts of organic carbon were available in the aqueous product for electricity generation. The TOC levels in the most recent REAP data were much higher than in earlier data, probably because of the change to DHTL from SEQHTL.

Previous DHTL models have achieved a 50% reduction in emissions without generating electricity from the AP (Davis et al., 2014). The conclusion to draw from Figure 5.8-9 is not the absolute necessity of on-site electricity but, rather, that there is an interdependence between productivity, carbon flow to AP, the use of co-generation, DHTL oil yield, and overall electricity demand. The DHTL study without go-generated power had high biocrude yield and used the AP-derived biogas for process heat (not electricity), including co-located upgrading.

The 50% GHG reduction target was satisfied even if the biochar rate fell to 0.025 g/ g dw, but it was not satisfied if the membrane filtration energy demand was increased from the GAI claimed value of 0.04 kWh/L to the more typical value of 0.5 kWh/L.

In general, the REAP DHTL oil yields are low compared to many published HTL studies; however, the REAP algae biomass has low oil content and has been grown to emphasize biomass productivity rather than oil productivity. This means a great deal of energy is being used to produce biomass that does not contribute to the biocrude product and this harms the LCA results. On the other hand, if the organic carbon is available in the AP and if it is used to produce power on site, some of the loss can be recovered. If the system is challenged by CO_2 supply, it may be better to emphasize higher fluxes to the oil product rather than to organic carbon that is converted to biopower.

As electrical power generation is limited in efficiency, future experiments should examine ways to increase the algae lipid yield. Achieving high areal fuel yields through high-productivity but low or moderate oil yield means that the energy used to grow and process the non-fuel fraction of the biomass is wasted. A strategy of high oil yield and low to moderate productivity makes the best use of the energy invested in the biomass production and processing although there is a tradeoff to be considered when increasing the oil yield decreases the productivity. This tradeoff should be studied experimentally, guided by LCA. It is possible that increasing the oil content will allow cultivation to consume more power.

One can consider supplementing the process with renewable power, but this approach must be assessed by economic analysis: Even if renewable power can be supplied at a price that matches fossil power, a high power budget will be associated with increased fuel costs. Renewable power may be free from an LCA perspective, but it is not free from a TEA perspective.

The uncertainties in this analysis are large. REAP data for mass balance are poor thus casting doubt on the values assumed for the total organic carbon in the aqueous phase and for the biochar yield. These parameters were critical to the analysis. Even if these data were in hand, CHG is unproven, especially with regard to catalyst lifetime and robustness against poisoning, e.g., with sulfur. The HTL/CHG energy demand is from computations rather than from data. One particular concern in this regard is establishing the heat exchanger performance in the face of high-solids feeds and fouling. A thorough analysis of the realizable effectiveness vs. cost tradeoff is required.

The PBR aeration rate (0.034 vvm) was associated with large energy use. R&D could be pursued to reduce this burden, but the value reflects Algenol pilot experience and includes consideration of adjusting the aeration rate to follow the illumination level. Reducing the PBR height (to reduce static head) would help, but would further challenge achieving adequate CO_2 mass transfer rates.

The analysis assumed that pH shifts will not be required. Prior REAP LCA studies demonstrated that pH shifts have large GHG implications. Harvesting and pre-processing without pH shifts must be demonstrated.

5.8.13 Other REAP LCA studies

Several LCA studies have resulted in separate reports which are listed below along with the key findings in each:

- *Preliminary LCA Model of REAP Energy Use and GHG emissions*, 9 Oct 2014
    - Hydrocyclone energy use was comparable to that for dissolved air flotation, yet the hydrocyclone performance was not established well.
    - REAPs plan to enhance performance by recycling residuals (rather than produce biopower) imply the need for high energy efficiency in the process. Thus, eliminating energy consumption comparable to the DAF unit assumed in the open-pond scenarios is important, thus ruling out the hydrocyclone. Downstream, heat burdens for the HTL process must be minimized, e.g., by using higher feed concentrations, and the solid-liquid separation between the two stages must be understood as it affects heat recovery. These issues, if understood, help set constraints on HTL experiments to avoid measuring yields with incorrect conditions.
    - It is unlikely that REAP can consume more than the equivalent of 48 kWh/ha/d at 13 $g/m^2/d$, which were used in the open pond scenarios we studied previously (Davis et al., 2012; Davis et al., 2014).
- *LCA Study of the REAP 2015 Roadmap Pathway using Sugars for Ethanol Production*, 22 Dec 2015
    - Using the carbohydrate stream to produce ethanol only increased the total fuel by 10%. Even when a more favorable carbohydrate yield of 22 g/L for a 10 wt% slurry) is assumed, the fuel yield only increases by 17%.
    - The carbohydrate stream had to be concentrated, which entailed adding a reverse osmosis stage.
    - The low feed concentrations to the two SEQHTL stages (10 wt% feed) makes downstream processing steps difficulty because of the water burden, e.g., the high water levels precluded GHG recovery of carbon as biogas and required the additions of a reverse osmosis unit.
    - Conclusions for GHG emissions and energy user were highly uncertain because of missing carbon balance data, e.g., TOC in the HTL2 aqueous product and carbon in the gas products as well as uncertainty in the char yield and char moisture content.
    - Given the poor performance as seen in the "on paper" LCA modeling, it was recommended that it was not worth carrying this idea further into an Aspen model or to look at TEA performance. Nevertheless, future work could revisit this idea for higher concentration feeds, which would reduce the water burden two-fold along with associated heating and separation energy burdens.
- *REAP 24-month LCA Report*, 27 Mar 2016, Edited 6 May 2016
    - Need to reduce aeration energy
    - Need to shift SEQHTL work to higher concentration feeds
    - Need to measure the TOC and TOC concentration in the aqueous products
    - Need to improve mass balances, especially for carbon
    - Need to establish the biochar production rate
    - Need to replace the cultivation model in the report with the Algenol scale-up model
    - Need to improve N and P recycling data (bioavailability and utilization)
- *REAP energy use and GHG emissions analysis based upon Algenol modeling data*, 29 Jul 2016
    - Urgent need to accurately assess the yield of TOC and TOC concentration in the aqueous products
    - Energy demand for cultivation must be reduced

- pH shifts with NaOH are not affordable because of high upstream burdens for manufacturing NaOH
- Low-oil/high-productivity strategies may not be compatible with cultivation methods that have low energy efficiency
- Carbon-capture must be avoided if MEA regeneration utilizes heat from a power plant.

5.8.14 References

Benemann, J. R. and W. J. Oswald (1996). Systems and Economic Analysis of Microalgae Ponds for Conversion of CO2 to Biomass. Final Report, Pittsburgh Energy Technology Center.

Campbell, Peter K., et al. (2009). Greenhouse gas sequestration by algae: energy and greenhouse gas life cycle studies. CSIRO Energy Transformed Flagship, 2009.

Canter, C. E., R. Davis, M. Urgun-Demirtas and E. D. Frank (2014). "Infrastructure associated emissions for renewable diesel production from microalgae." Algal Research 5(0): 195-203.

Davis, R., D. Fishman, E. D. Frank, M. S. Wigmosta, A. Aden, A. M. Coleman, P. T. Pienkos, R. J. Skaggs, E. R. Venteris and M. Q. Wang (2012). Renewable Diesel from Algal Lipids: An Integrated Baseline for Cost, Emissions, and Resource Potential from a Harmonized Model, National Renewable Energy Laboratory (NREL), Golden, CO.

Davis, Ryan E., Daniel B. Fishman, Edward D. Frank, Michael C. Johnson, Susanne B. Jones, Christopher M. Kinchin, Richard L. Skaggs, Erik R. Venteris, and Mark S. Wigmosta. 2014. "Integrated evaluation of cost, emissions, and resource potential for algal biofuels at the national scale." *Environmental Science & Technology*, 48, (10): 6035-6042.

Davis, Ryan, Jennifer Markham, Christopher Kinchin, Nicholas Grundl, Eric CD Tan, and David Humbird. "Process Design and Economics for the Production of Algal Biomass: Algal Biomass Production in Open Pond." (2016). No. NREL/TP-5100- 64772

Frank, E., Pegallapati, A., Davis, R., Markham, J., Coleman, A., Jones, S., Wigmosta, M. 2016. Life-cycle Analysis of energy Use, Greenhouse Gas Emissions, and Water Consumption in the 2016 MYPP Algal Biofuel Scenarios.

Frank, E. D., A. Elgowainy, J. Han and Z. Wang (2013). "Life cycle comparison of hydrothermal liquefaction and lipid extraction pathways to renewable diesel from algae." Mitigation and Adaptation Strategies for Global Change 18: 137-158.

Frank, E., Han, J., Palou-Rivera, I., Elgowainy, A., Wang, M. 2011. Life-cycle analysis of algal lipid fuels with the GREET model. Center for Transportation Research, Energy Systems Division, Argonne National Laboratory, Oak Ridge. ANL/ESD/11-5

GREET, (The Greenhouse Gases Regulated Emissions and Energy Use in Transportation) 2015. Available at https://greet.es.anl.gov/index.php?content=download1x

Langholtz, M., B. Stokes and L. Eaton (2016). "2016 Billion-Ton Report: Advancing Domestic Resources for a Thriving Bioeconomy (Executive Summary)." Industrial Biotechnology 12(5): 282-289.

Lundquist, T. J., I. C. Woertz, N. W. T. Quinn and J. R. Benemann (2010). Realistic Technology and Engineering Assessment of Algae Biofuel Production. Berkeley, CA, Energy Biosciences Institute.

NIST, http://webbook.nist.gov/cgi/cbook.cgi?Formula=h2o&NoIon=on&Units=SI&cTC=on , Accessed Noveber 2016

Talukdar, Prabal, http://web.iitd.ac.in/~prabal/MEL242/(30-31)-Heat-exchanger-part-2.pdf. Accessed November, 2016.

Wang, Z., J. B. Dunn, J. Han and M. Q. Wang (2014). "Effects of co-produced biochar on life cycle greenhouse gas emissions of pyrolysis-derived renewable fuels." Biofuels, Bioproducts and Biorefining 8(2): 189-204.

5.9 Technoeconomic analysis

Eric Dunlop, Yin Zhao
Pan Pacific Technologies

5.9.1 Executive Summary

Task Summary

The objective of this section is to present the Techno-Economic Analysis of the REAP process, a conceptual scale up process with the REAP technologies. The major research undertaken by Pan Pacific reported in this section includes:

1. End-to-end Aspen model (Milestone 1.3.1) for the REAP process to obtain the technical and engineering information for the REAP process. This work is presented in Section 5.9.3. The results of the end-to-end Aspen models with strain rotations (discussed in Section 2 of the full report) and the DHTL (discussed in Section 5.7 ASU report), are summarized below:

Algal strain	Operating period	Bio-crude productivities (Gal/acre/yr)
Kirschneriella	November to January	2,767
Chlorella	February to April	1,565
Galdieria	May to September	2,286

2. Models of integrated unit operations (Milestone 1.3.2): In this section, models for individual unit operations were set up to understand the parameters for scaling up the individual units while the experimental data are not available. These models become the basis of designing of the end-to-end Aspen model and the TEA model of the REAP process.

They are:

A. Aspen Plus models of DHTL to investigate the N and P recycling and the energy demand of the process. The results are shown in Section 5.9.4.1
B. Comsol Multiphysics models of the light integration and mass transfer of the PBR are demonstrated in Section 5.9.4.1
C. 3DS Max models of the spacing and light optimization of the layout of VPBRs are presented in Section 5.9.4.1
D. Energy integrated Aspen model of SEQHTL, using pinch analysis technology to optimize the SEQHTL process and set the thermodynamic target of the utility consumptions of the process. It is presented in Section 5.9.4.2
E. Shear-thinning viscosity behavior study of the algal suspension for SEQHTL is presented in Section 5.9.4.2

3. TEA of the REAP process (Milestone 1.3.3) for four cases are discussed in Section 5.9.5. This financial analysis is reported using the standard methods of NREL [1] and those based on industry standards developed by Pan Pacific as part of technical and financial modeling of algal biofuels. The minimum biocrude selling price of the four cases are summarized below:

Case description	Minimum Biocrude Selling Price ($/Gal)
Autotrophic cultivation with DHTL (Base Case)	15.19
Mixotrophic cultivation in summer with DHTL	13.66
Autotrophic cultivation with SEQHTL	19.10
Mixotrophic cultivation in summer with SEQHTL	16.20

Key results

The key results presented in this report include:

Milestone 1.3.1 – Integrated Systems Modeling

Strain Rotation: The strain rotation has been discussed in the Section 2. With the photosynthetic efficiency reconciled with the AzCATI data and the DHTL yield from ASU, the end-to-end Aspen models show the bio-crude productivity as:

Algal strain	Operating period	Bio-crude productivity (Gal/acre/yr)
Kirschneriella	November to January	2,767
Chlorella	February to April	1,565
Galdieria	May to September	2,286

Milestone 1.3.2 – Models of Integrated Unit Operations

DHTL: The nutrient recovery of the DHTL process is modeled byreconciliation of the experimental data of the three algal organisms. The annual average N recovery rate is 50% and the average P recovery rate is 77%. The individual N and P recovery rate of the three organisms are as:

Algal strain	Operating period	N recovery	P recovery
Kirschneriella	November to January	53%	68%
Chlorella	February to April	52%	70%
Galdieria	May to September	47%	87%

SEQHTL: A systematic method has been developed to calculate the required energetics for the SEQHTL process especially the heats of reaction based on the components. The Heat of Reaction of the two stage HTL reactions was calculated to be: 0.099MJ/kmol for the first stage and -0.865 MJ/kmol for the second stage. Pinch analysis was used to optimize the SEQHTL process. We then used this analysis, with the physical properties obtained above, to study the energy consumption of 10 wt% and 20 wt% algal slurry cases. The thermodynamic heating target of 10 wt% algal slurry was found to be 10.38kJ/g bio-crude, with that for 20 wt% algae slurry being 6.20 kJ/g bio-crude, making a clear case for using 20% slurry.

Milestone 1.3.3 – Techno-Economic Analysis

Techno-economic analysis of the REAP process baseline case (autotrophic cultivation condition with DHTL as the downstream conversion process) for a 10 MGY bio-crude facility shows the following results:

TEA parameter for REAP baseline case	Result
Capital cost	$522.2 MM
Annual operating cost	$54.2 MM/year
Minimum bio-crude selling price	$15.19/Gallon
Energy output	248 GJ/acre/year

Achievements

- End-to-end process Aspen models for the different seasons and different strains: winter (November to January) with *Kirschneriella*, spring (February to April) with *Chlorella,* and summer (May to September) with *Galdieria*. The biomass productivity and biocrude yields have been reconciled with the cultivation and DHTL experimental data to achieve mass and energy balances for the end-to-end process modeling.
- Techno-Economic Analysis (TEA) model of the integrated process, and estimated biocrude production costs for the different model scenarios
- SEQHTL Manual (Supplementary Material: Appendix 1): a manual to assist with the interpretation of experimental data and the setting up Aspen models for a SEQHTL process. The fundamental concepts in this manual, including (a) the estimation of the thermodynamic properties of biomass components and (b) pinch analysis of the process, are highly applicable to other similar biofuel processes in future work.

- Pinch analysis of SEQHTL process and resulting optimization of the process, which has proven to be a powerful tool in improving energy efficiency. The utility consumption of the optimized process has been used when estimating the operating cost for TEA and the GHG emissions for the LCA. The capital cost of the optimized process is then utilized in the Capex estimation of the REAP process.
- Comsol Mass Transfer Model of HPBR: this mass transfer model will also be highly applicable to other PBR/raceway pond designs in future work.
- Autodesk 3DS Max Shading models for VPBRs.

Future work

- The cost estimation for VPBRs is still rough - we require more commercial / pilot facility data to support the layout and piping costs.
- The flocculation of algal slurries is not well developed – the energy demand and cost estimation of sedimentation are still needed.
- The SEQHTL process data still needs to be clarified for *Kirschneriella* and *Galdieria.*
- Optimization of the direct HTL process by pinch analysis to understand the thermodynamic targets of DHTL process.

Milestone Report

5.9.2 Methods: An Overview

The TEA of the REAP process design was developed iteratively from a baseline model and optimized with multiple engineering studies to supply information, advise experimental work especially DHTL and SEQHTL and feed into the optimization of process models and reactor design. An overview of methods employed for different tasks are discussed in this section. Further details of methods are provided as required in the specific discussion of the results in later sections.

5.9.2.1 Software Programs used for all Tasks for Integrated System Modeling

Three main software programs were used in the process design and engineering studies for the TEA for REAP were the Aspen One Engineering Suite, Comsol Multiphysics and Autodesk 3DS Max. The particular features of these programs and their application in the REAP are as follows:

Aspen One Engineering Suite:

Aspen One – containing Aspen Plus, Aspen Energy Analyzer, and Aspen Economic Analyzer – is a process modeling platform for conceptual design, optimization and performance monitoring of chemical processes. It is the market leading chemical process simulation software and widely used in the bulk, fine, specialty, biochemical and polymers industries. Aspen Plus contains a database of pure component and phase equilibrium data for conventional chemicals, electrolytes, solids and polymers, which helps engineers to simulate the chemical process more easily. Aspen Energy Analyzer helps evaluate energy performance, and assists with optimizing the process to

maximize energy integration. Aspen Economic Analyzer is powerful tool for evaluating conceptual designs for capital and operating costs and resulting in economic optimization of designs.

Comsol Multiphysics:

Comsol Multiphysics is a software platform based on advanced numerical methods for modeling and simulating physics based problems. It has an integrated environment designed for cross-disciplinary product development, regardless of the application area, with numerous add-on modules for solving complicated and coupled physics phenomena such as mass transfer or biochemical kinetics. It permits the inclusion of user-defined equations for describing a material, property, boundary or source which allows the development of highly specialized models to focus on areas for optimization of designs. Built-in visualization capabilities enable the researcher to visualize just about any quantity of interest related to the simulation results. Comsol is used here for photobioreactors design to investigate issues relating to depth, photosynthetic efficiency, fluid flow and mass transfer to improve growth rates and lipid production.

Autodesk 3DS Max:

Predictive modeling using such programs as Comsol or Huesemann's extensive studies [2] [3] [4] have focused attention on light once it gets into the reactor. Further studies of sunlight were needed that focused on the light reaching PBR. Autodesk 3DS Max was selected to investigate the shading of the PBRs. This is a professional 3D animation, modeling and rendering software, widely used in the animation and architecture industries. We have been able to adapt its photometric lighting system used in architectural design to apply it to PBR design. In particular, we adapted it to quantitatively model sunlight at defined locations and times onto objects and casting realistic shadows for shading analysis.

5.9.2.2 Integrated Systems Modeling

Aspen Plus was used to create a baseline REAP process model and develop flowsheets for the critical mass and energy balance which were used to optimize the process model. An Excel spreadsheet collecting and reporting data took raw data from the converged Aspen flowsheet and Aspen Economic Analyzer and converted it into effective engineering and financial data. Aspen Energy Analyzer was used to calculate the required energetics for the DHTL and SEQHTL process, especially the heats of reaction based on the components.

There are, however, three challenges in using the Aspen program. The first challenge is the lack of detailed and reliable physical property biofuel production data. This lack of data was addressed by drawing on Pan Pacific's extensive knowledge and expertise gained from major companies and engineering groups in the area of bioprocess design. Importantly it is thermodynamics driven to find or bypass many missing parameters [5].

The second challenge is that the volume of data produced from a converged Aspen is comprehensive which can become an impediment to analyze effectively. It is certainly possible,

however, to collate data into tables of capital costs and these costs and their discussion are included in Section 5.9.2. The third challenge is that Aspen cannot deal well with light penetration and depth since it has no Computational Fluid Dynamics (CFD) facilities. We therefore turned to Comsol Multiphysics, a specialist CFD software program to address this issue.

5.9.2.3 Techno-economic Modeling Framework for REAP Process Model

The application of Aspen One Engineering Suite, Comsol Multiphysics and Autodesk 3DS Max creates an integrated framework for an end-to end techno-economic model (see Figure 5.9-1) that addresses critical steps in the research, development, and commercialization of sustainable advanced biofuels. It is this framework that was used for the development, optimization of the REAP process model and its TEA.

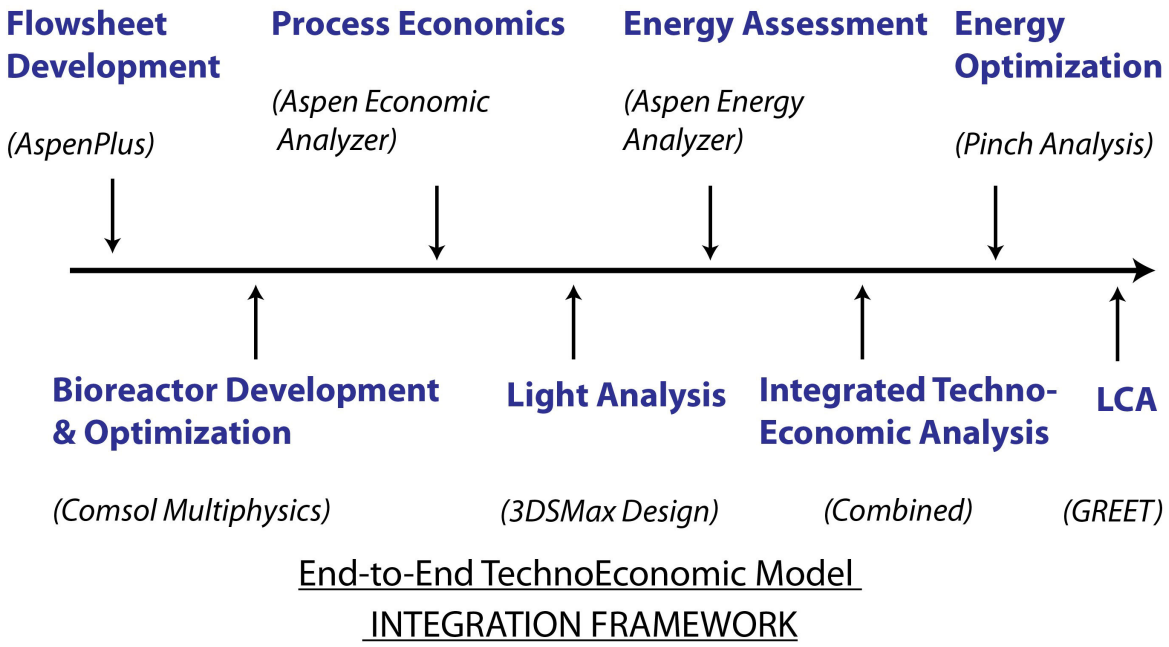

Figure 5.9-1: REAP Techno-economic Integrated Modeling Framework

As Figure 5.9-1 shows, the framework is built around the capabilities of the Aspen Plus program for flowsheet development, process economics, energy assessment, and importantly, energy optimization. It is complimented by the use of Comsol Multiphysics for bioreactor development and optimization and 3DS Max Design for light analysis. While these components stand alone, the potential of the sum of their parts was then realized to inform the TEA/LCA and guide the REAP experimental work. The techno-economic framework is applied to the analysis and interpretation of the TEA of REAP process model.

5.9.2.4 Scenario used for TEA modeling

At the concept design phase, the TEA can be based on either a given wetted area for the VPBR system or scaling to a given bio-crude capacity. Algenol Biofuel has developed the VIPER^{TM} system, which is a vertical PBR system using hanging bags as its reactor unit. The hanging bag unit is typically a 10 feet long plastic bag with 3 feet of the fluid level containing 50L of slurry. Algenol Biofuel recommends 0.38m as the spacing of the VIPER^{TM} system. A 2000 acre VIPER facility is designed by Algenol Biofuel, which is recommended for the design basis of LCA and TEA.The 10 MGY bio-crude capacity is the basis of the harmonized model reported in 2012. [6] For the baseline case of REAP, 4,530 acres of land is required for providing enough biomass for the 10 MGY bio-crude facility with DHTL as the downstream conversion process.

5.9.2.5 Sea water vs. fresh water

At the beginning of the REAP project, the locations of the cultivation experiments were intended to be at Fort Myers FL and Las Cruces NM. Sea water was used in Fort Myers FL site, and fresh water was used in Las Cruces NM. Finally, as the cultivation experiments were set in AzCATI, Mesa AZ, and fresh water cultivation conditions were used. Both options are retained in the Aspen model.

5.9.3 Milestone 1.3.1 – Integrated Systems Modeling

5.9.3.1 Unit Operations: An Overview

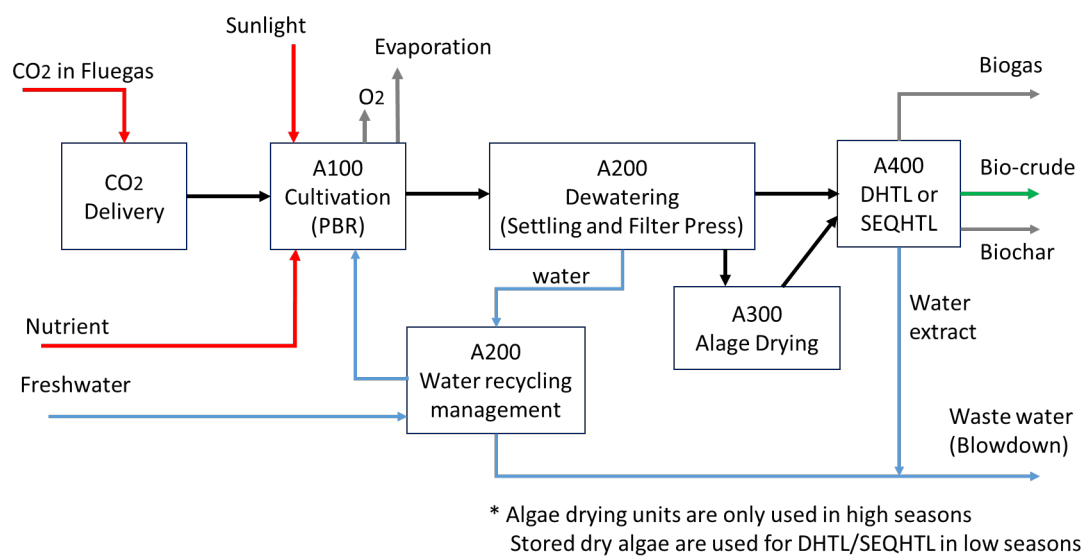

Figure 5.9-2 Simplified block process flow diagram of the unit operations of the REAP integrated process

Figure 5.9-2 presents a simplified block flow diagram of the REAP process It comprises five unit operations: 1. CO_2 delivery; 2. Cultivation; 3. Harvesting; 4. Biomass conversion system: DHTL or SEQHTL; and 5. Water recycling management. This section provides an overview of the unit

operations in the end-to end REAP process. Further discussion of individual unit operations are in later sections.

Area 100: Cultivation

Overview

This is the main section of the REAP process, accounting for the majority of the capital cost and facility footprint. PBRs are used in the REAP process, because they are more appropriate for sensitive strains of Algae bio-mass and make the control of contaminants easier, thus allowing for the investigation of growth in autotrophic as well as mixotrophic modes. Furthermore, with the higher algal mass concentration attained in the PBR system, the harvesting costs per unit mass are reduced. Two scenarios of the PBR system, horizontal and vertical, have been investigated in AzCATI in order to optimize cultivation conditions, as well as the productivity of the differing strains. However, many problems were encountered in the horizontal PBR experiments. The autotrophic cultivation in the vertical PBR system is selected as the baseline case of the TEA in this report.

Vertical PBR system

All nutrients (urea, DAP and $(NH_4)_2SO_4$) are mixed with the make-up water which is then fed into the PBRs for algal growth. The reactor setting used in the Aspen model is R-Stoic, meaning that the stoichiometric reactions are simulated in the model. The stoichiometric reaction settings in this reactor model are applied to both horizontal and vertical PBRs. The algal productivity obtained from experimental data, together with evaporation rate and solar radiation data, is then used to reconcile the model to calculate the PBR area needed. This is discussed later in this report.

Vertical PBR (VPBR) design

In AzCATI, three types of VPBRs are used to evaluate the cultivation conditions of the selected algae strains. The photographs are in Figure 5.9-3 and the dimensional measurements are in Table 5.9-1. Sparging lines along the bottom of the reactors are used for CO_2 injection. Scaling up of the experimental VPBR system is based on the Algenol's VIPER™ system, which is similar to the Hanging Bag (HB) system as used in AzCATI.

Figure 5.9-3 VPBRs used in AzCATI. Left above: Hanging bag (HB) system, right above: Mobile VPBR (MM), bottom: VL PBR

Table 5.9-1 Dimensional measurement of VPBRs

VPBR type	Length (m)	Width (cm)	Fluid level (m)	Spacing (m)
HB	1.2	N/A	1.0	0.5
MM	1.2	4.0	1.0	1 & 0.5
VL	14.6	10.0	0.8	2.4

CO_2 delivery

This section details the operation of flue gas delivery and injection to the PBRs. With the scope of the present design, no recycling of CO_2 is currently considered and all the requirements for flue gas are sourced from off site. The CO_2 source is assumed to be a separate production facility located within 5 miles.

Make up water delivery

The makeup water to the facility is provided by pipeline transfer from a nearby local water resource as per prior modeling work. The acidity of the makeup water is adjusted by NaOH for pH8 or H_2SO_4 for pH2.5, then pumped through the PBRs in the cultivation area.

Area 200: Dewatering and water recycle

Harvesting consists of the settling unit and filter press. The biomass is harvested from the PBRs at 2-5 g/L AFDW density. A coagulant reagent is mixed with the production stream sourced from the cultivation area in order to let the algae flocculate and settle in the settling unit. Then part of the water is separated, the slurry is filtered in the filter press obtaining 20 wt% AFDW algal slurry for the DHTL/SEQHTL process. Clarified water from each step is combined and recycled to the PBRs, minus a small fraction used as blowdown to mitigate buildup of salts and other inorganics.

Area 300: Algae drying and storage

These operations are designed for the drying and storage of excess biomass produced in high productivity seasons and then using the dry algae matter in low productivity seasons in order to keep a stable operation of the DHTL/SEQHTL process. The algae drying operation consists of an air dryer, an air compressor, a furnace, belt conveyor and silos for temporary storage of dried biomass. Dry algae is stored in covered dry storage facilities and is used during low productivity periods. This is the subject of a separate optimization study.

Area 400: Downstream biocrude conversion process

Hydrothermal treatment is one of the pathways for conversion of algal biomass to biofuels. The process at intermediate temperatures between 200°C and 375°C is called hydrothermal liquefaction (HTL) which predominantly produces biocrude oil that can be upgraded into transportation fuel. In REAP project, two scenarios of HTL process have been investigate. Direct HTL process (DHTL) is investigated in Deng's group in ASU (discussed in Section 5.7), and a 2-stage HTL process, the Sequential HTL process (SEQHTL) is investigated in Chen's group in WSU (discussed in Section 5.6). Both groups studied the experimental conditions to improve the conversion yield of the biocrude, the intermediate of the biofuel. In this report, process optimization of the SEQHTL has been undertaken by pinch analysis technologies, and it is presented in Section 5.9.4.

5.9.3.2 First order analysis of REAP process model using baseline data of Tech Fin Report

A first order analysis of the REAP model process flowsheet was undertaken. This was set up on an Excel spreadsheet using the Tech Fin baseline data and Process Flow Diagram to establish baseline data. One million simulations were run using Crystal Ball software. This first order analysis informed the setting up of the Baseline Aspen model reported as part of the 12 month deliverable which was an essential step in the development of the optimized Aspen model for the REAP process.

The Preliminary Flow Diagram (Figure 5.9-4) therefore represents the process design before optimization in Aspen. It includes the unit operations identified by Area numbers that continued to be used in process optimization during the REAP project. In this diagram, a single unit box is included for SEQ/HTL (Area 600) as the biocrude conversion process and separate boxes are identified for the downstream units that were the starting point of process design.

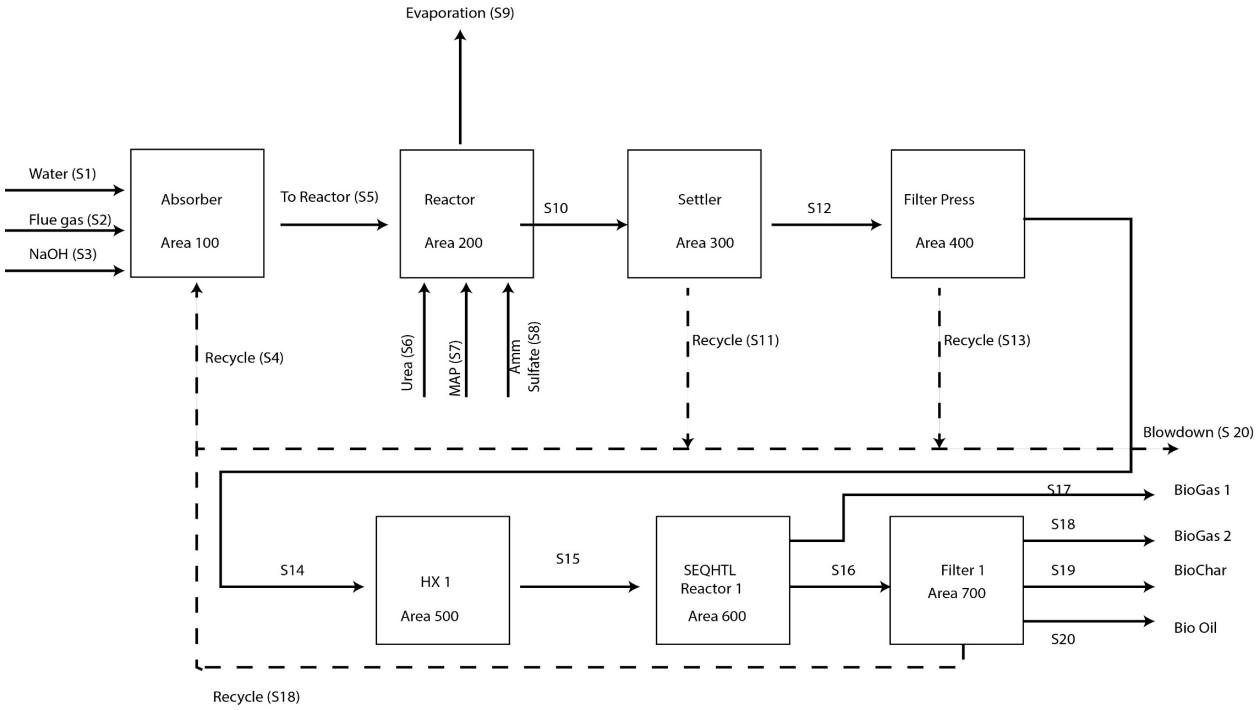

Figure 5.9-4 Preliminary Flow Diagram for REAP process before optimization in Aspen.

Figure 5.9-5 and Figure 5.9-6 presents the results of the one million simulations in Frequency and Cumulative Frequency views respectively. The actual numbers are smaller than one million (namely 935841 trials) because in the prcoess of simulation some combinations give negative numbers or are otherwise unrealistic. The results show that the projected cost per gallon is $23.70, but with a wide distribution of potential outcomes ($13 to $60/gallon).

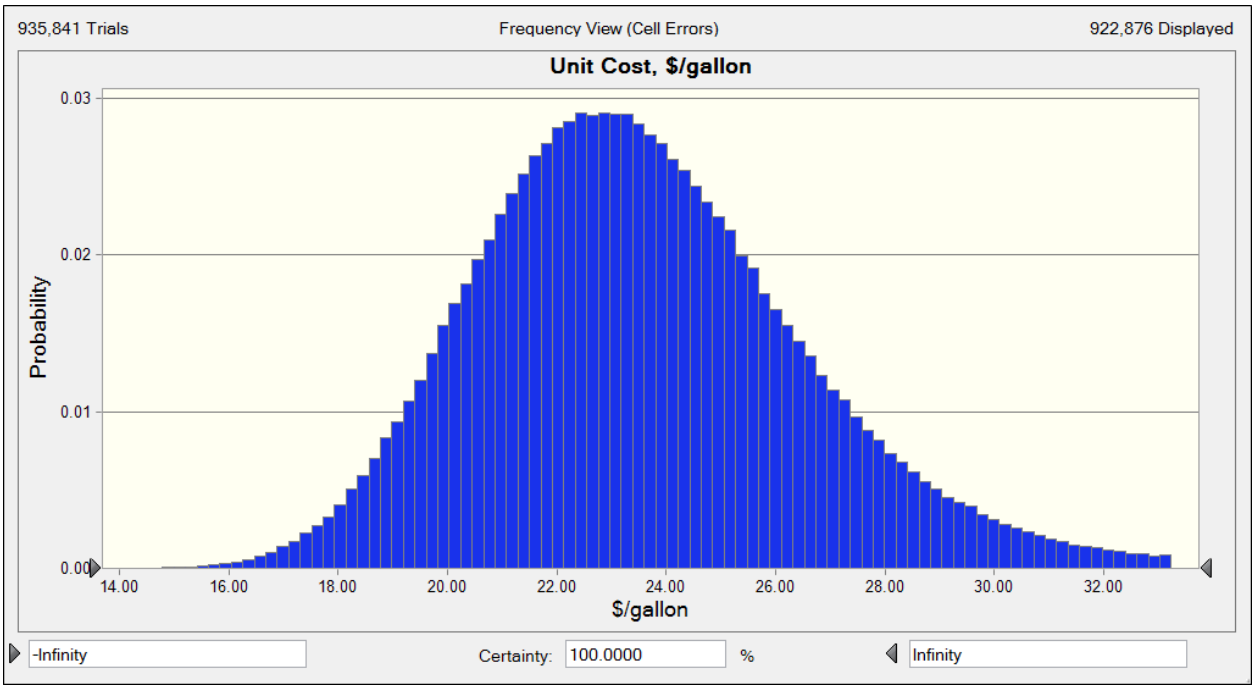

Figure 5.9-5 Monte Carlo Frequency Diagram for one million simulations of the REAP process. $/gallon

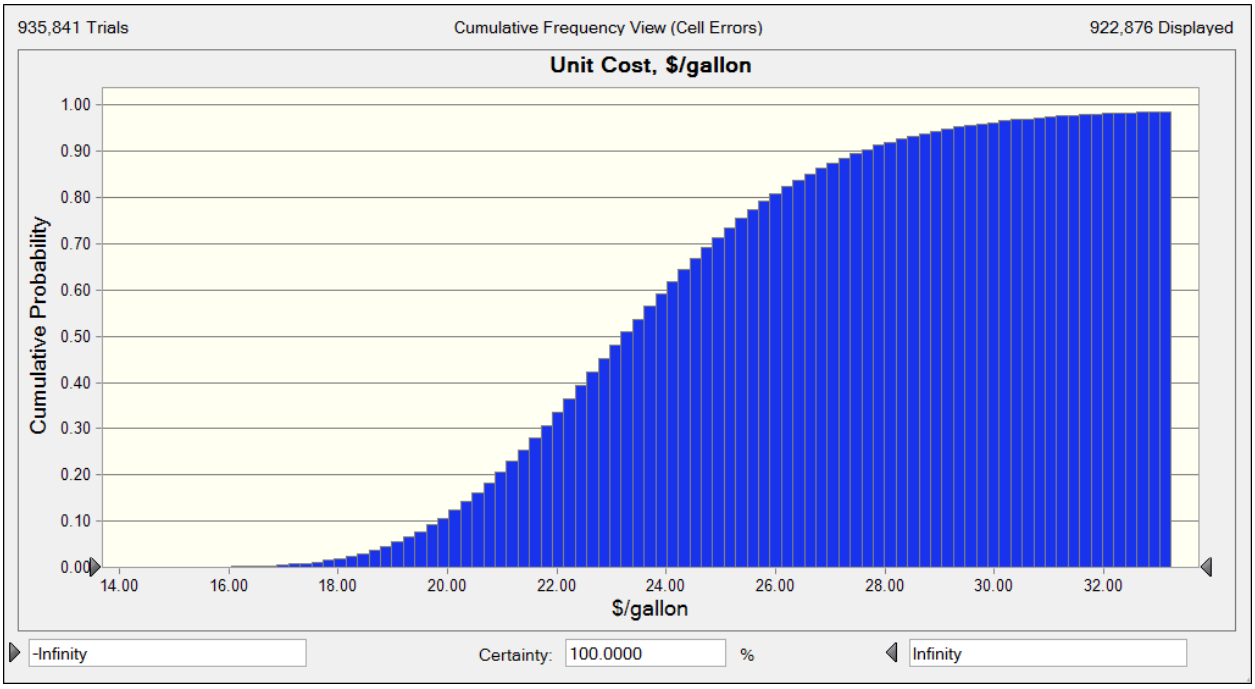

Figure 5.9-6 Monte Carlo Cumulative Frequency Diagram for one million simulations of the REAP process. $/gallon

Figure 5.9-7 presents the statistics of the Monte Carlo simulations for the forecast of the unit cost for the REAP process. These imply that the results are close to being a normal distribution. It highlights that the mean cost is $23.70 per gallon with a standard deviation of 3.41.

Forecast: Unit Cost $/gallon	
Statistic	**Forecast values**
Trials	935,841
Base Case	22.91
Mean	**23.7**
Median	23.32
Mode	'---
Standard Deviation	3.41
Variance	11.61
Skewness	1.48
Kurtosis	9.15
Coeff. of Variation	0.1437
Minimum	13.43
Maximum	60.27
Mean Std. Error	0
Cell Errors	64,159

Figure 5.9-7 Statistics of Monte Carlo simulations for forecast of unit cost for REAP process. $/Gallon

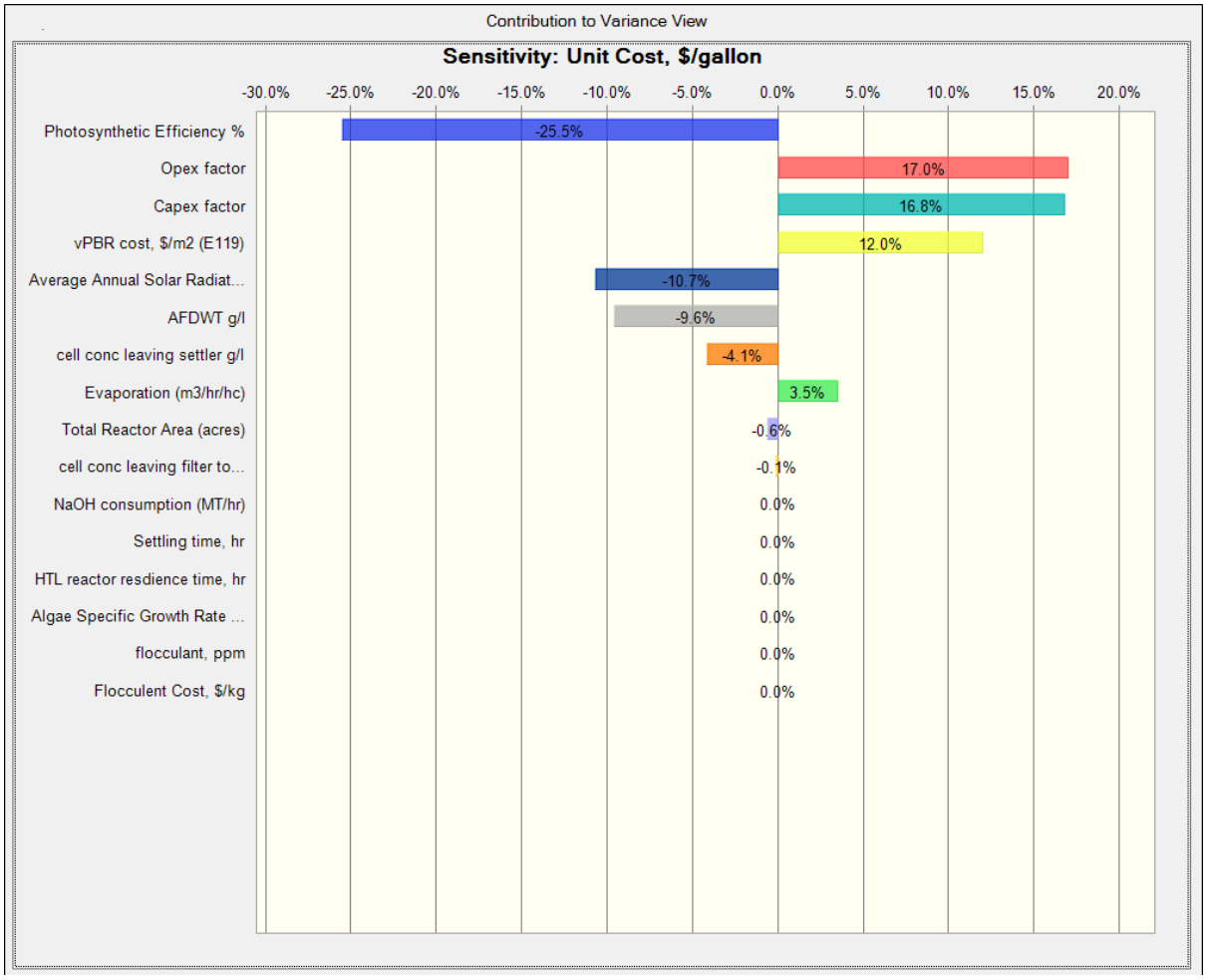

Figure 5.9-8 Sensitivity analysis (Contribution to Variance) of Monte Carlo results for one million simulations of REAP process.

A sensitivity analysis of the Monte Carlo results is presented in Figure 5.9-8. The list establishes the relative weightings of factors that contribute to the variance in cost distribution. It highlights that photosynthetic efficiency with a contribution of 25.5% dominates the cost followed by contributions of 17% for opex and 16.8% for capex. It is notable that it failed to identify the contribution of factors mostly associated with downstream processing and HTL that were subsequently found to be important. It overestimated the unit cost by two standard deviations. Nevertheless, it provided a useful reference point for subsequent work on the baseline model in Aspen.

5.9.3.3 Optimized REAP process flowsheet from Aspen model

This section discussed the stages of modeling development over the course of the project: cultivation, dewatering, DHTL, SEQHTL, water recycling, converter, and algae drying.

Overview of the end-to-end Aspen process model

The end-to-end Aspen models are set up for DHTL and SEQHTL separately. The Aspen models include the following sections: Cultivation, Dewatering, Conversion (DHTL or SEQHTL), water recycling and a converter model for converting the algae molecular from AFDW mode to DW mode. The block diagram of the end-to-end Aspen model is illustrated in Figure 5.9-9. Algae drying is modeled separately. The complete Aspen flowsheets are included in the spreadsheets for the different seasonal models submitted separately.

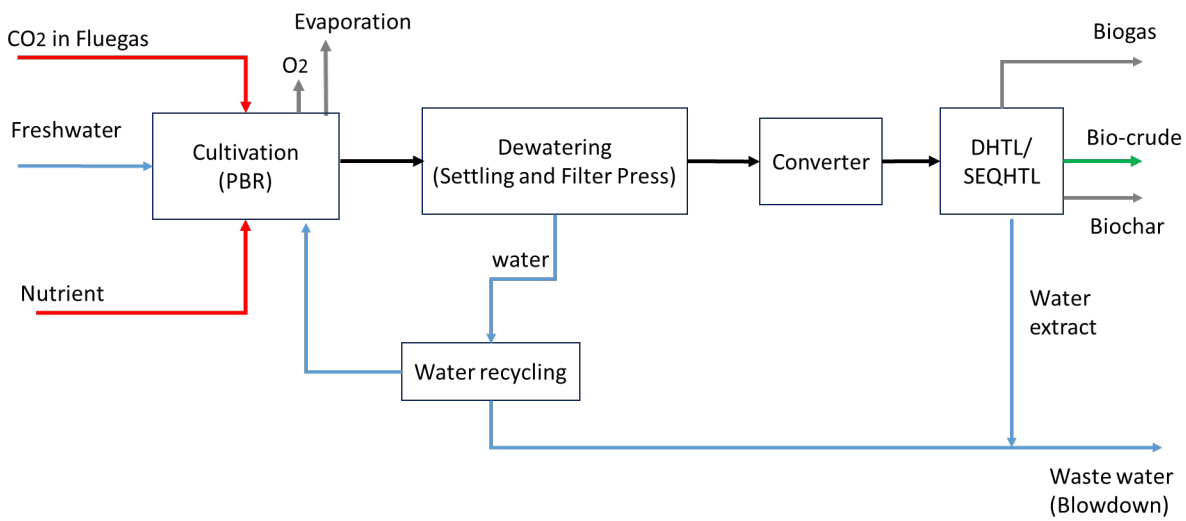

Figure 5.9-9 Block diagram of end-to-end Aspen model

Cultivation

The algal growth component was derived from the Aspen model developed by Pan Pacific for NAABB and is described in [5]. The cultivation model is illustrated in Figure 5.9-10. The cultivation unit uses information recycle loops. There are a series of blocks that account for solar energy input (E-sun1); estimate the conversion of the limiting reactant, the extent of reactions (HTX1), and the heat of the reactions (HTXRX1); account for energy losses due to the evaporation of water (HTXLH1). Evaporation is simulated at block Evap1. The nutrients urea and DAP are mixed with the prepared water then fed into the PBRs for algal growth. The fluegas as the CO2 source is mixed with the water then fed into the cultivation loop. The PBR setting used in the Aspen model is R-Stoic, meaning that the stoichiometric reactions are simulated in

the model. The algal productivity obtained from experimental data, together with evaporation rate and solar radiation data, is then used to reconcile the model to calculate the PBR area. The parameters for cultivation block will be discussed in Section 5.9.4.

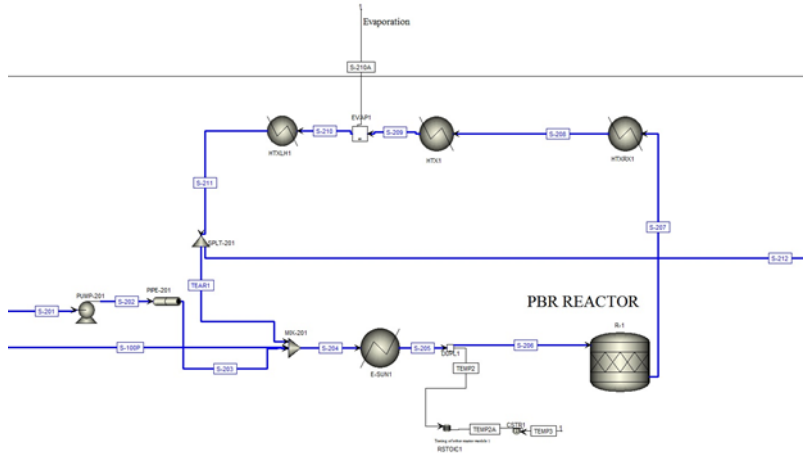

Figure 5.9-10 Cultivation flowsheet

Dewatering

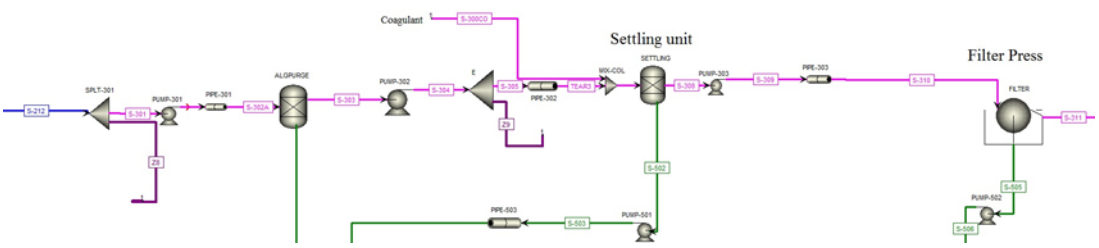

Figure 5.9-11 Dewatering flowsheet

Dewatering consists of the settling unit and filter press (see Figure 5.9-11). A coagulant reagent is mixed with the production stream from the cultivation area to let the algae flocculate and settle in the settling unit. After part of the water is separated, the slurry is filtered in the filter press to obtain 20 wt% algal slurry for the SEQHTL process. We are still missing information regarding the coagulant reagent and settling operation conditions so the settling unit is currently modeled as a cylinder.

DHTL

The flow diagram of DHTL process is shown in Figure 5.9-12. The DHTL flowsheet is derived from the literature [Case D of the NERL report 30352, the lowest capital cost and lowest operating cost case]. The 20 wt% algal slurry is pressurized to 100 bar and pre-heated by E-401 and E-402 to the given temperature, then the stream is fed into the DHTL reactor. In the DHTL

reactor, the algal biomass is converted to biogas, biochar and biocrude. The biogas is separated in the gas knock-out drum (SEPGAS-1), the biochar is separated in the filter, FIL-401. Then, the biocrude and water soluble products are separated from the water and oil separator; SEP-401. The HTL reactor setting used in the Aspen model is R-Yield, meaning that the conversion yield of the components are considered since the elemental analysis results of the experimental data are not satisfied by the stoichiometric settings in Aspen model. There are nutrients and other organic substances remaining in the water phase. The N and P recycle rate of the three algal strains, i.e. the ratio of the N and P of the water product to that of the algae, are obtained in a separate model, and discussed in Section 5.9.4.2. The organic substances remaining in the water phase can be converted, in a catalytic hydrogasification process to, for example, methane. However, this is beyond the current REAP scope of reporting. In this report, this water product stream will be treated as waste water and the estimated treatment cost will be detailed in variable operating costs. All the experimental conditions were optimized by the ASU group.

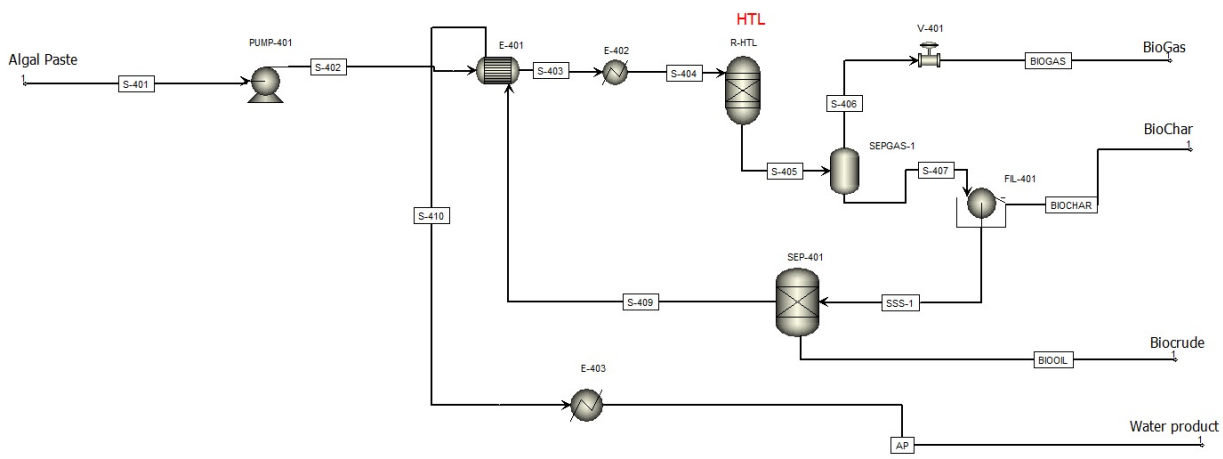

Figure 5.9-12: DHTL flow diagram

SEQHTL

The flow scheme of the energy integrated SEQHTL process is illustrated in Figure 5.9-13. The 20 wt% algal slurry is pressurized to 7 bar and pre-heated by E-401 and E-402 to a given temperature, then the stream is fed into the first HTL reactor. The treated algae (TA) is filtered out and the water phase is cooled by E-401. The TA slurry is then blended with water, adjusting the ratio of TA to water to 0.2, then pressurized to the required pressure and heated by E-403 and E-404 to the required temperature.

In the second HTL reactor, the TA is converted to bio-crude, bio-char, water-soluble residue and bio-gas. After several separation steps, the final product – bio-crude – is obtained. Water extract streams WE-1 and WE-2 containing nutrients, like the DHTL case, we have considered these

water streams to be waste water and their treatment costs as variable operating costs. All the experimental conditions are optimized in WSU and ASU groups. The process is optimized by the pinch analysis to obtain an energy efficiency process, which is discussed in Section 5.9.4 in this report.

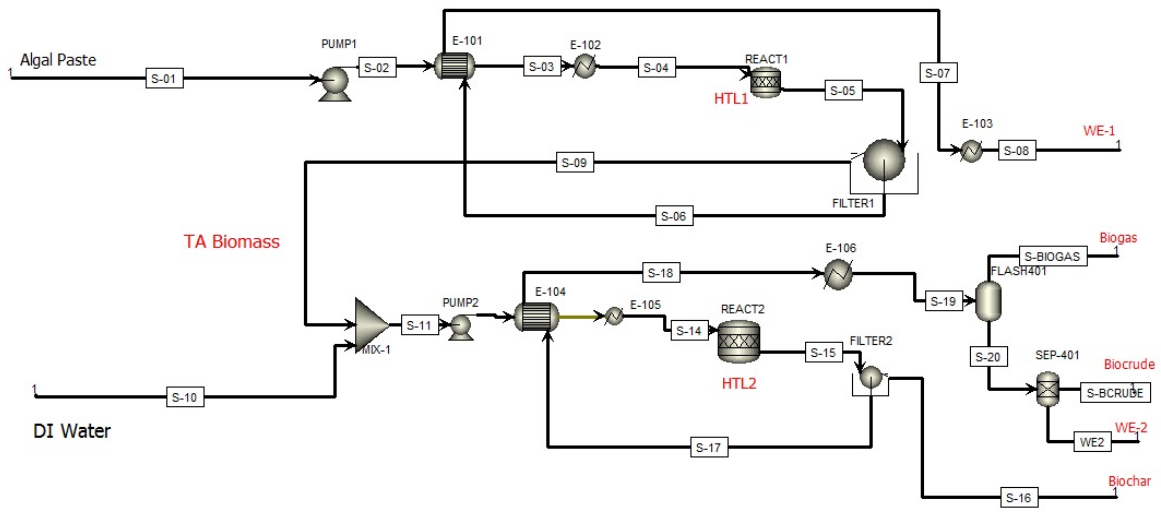

Figure 5.9-13: SEQHTL flow diagram

Water recycling and discharge

In this part of the process, the separated waters from the settling unit and filter press are combined (see Figure 5.9-14). 95% of the combined water is then recycled, with the rest discharged. The water phase stream of DHTL or SEQHTL process is mixed with the discharged stream to form the blowdown.

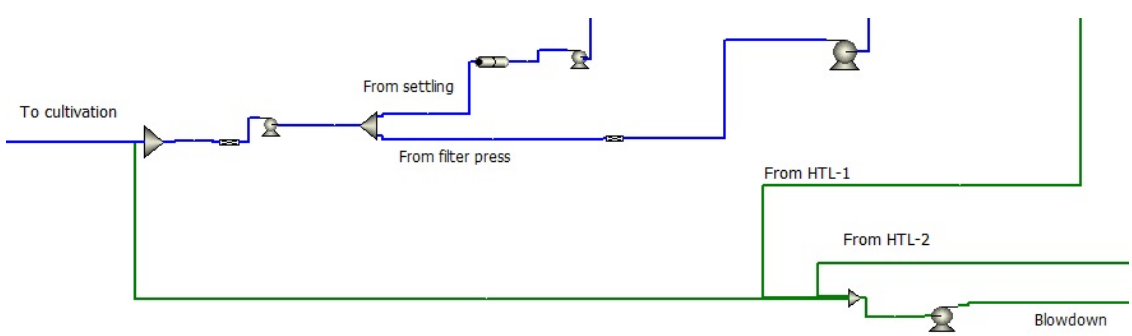

Figure 5.9-14: Water recycling and discharge flow diagram

Converter

The converter unit is only for modeling purpose. The empirical molecular of Algae used in the cultivation and dewatering units is $CH_{1.9}O_{0.4}N_{0.083}S_{0.002}P_{0.002}$, which is considered as the AFDW *Chlorella*. However, the elemental analysis for the DHTL and SEQHTL is DW basis. The converter unit is an R-Stoic model to reconcile the cultivation model and the conversion models of DHTL/SEQHTL. The converter model is presented in Figure 5.9-15.

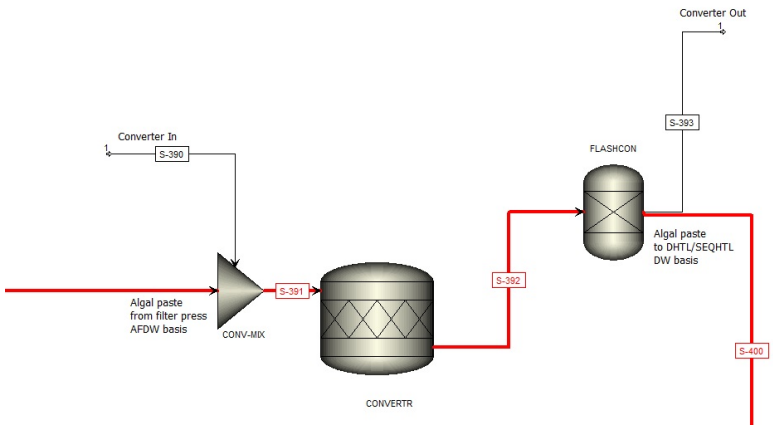

Figure 5.9-15: Converter flow diagram

Algae drying

The flow diagram of algae drying is shown in Figure 5.9-16. The Algae drying model insists dryer, furnace, air compressor and an air cooler. Air is pressurized by an air compressor through the furnace and is heated to 95 °C before fed into the dryer. The wet algae is dried by hot air in the dryer. The amount of air is controlled by the dew point of the vent.

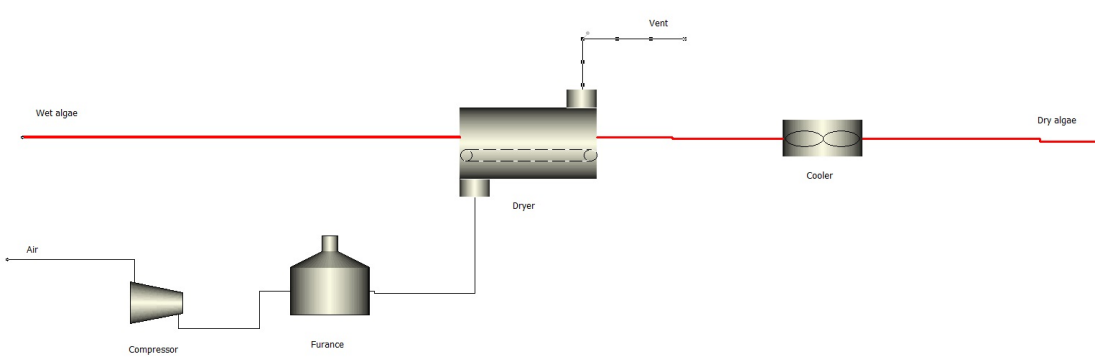

Figure 5.9-16: Algae drying flow diagram

5.9.4 Milestone 1.3.2 – Model of Integrated Unit Operations

Models of individual unit operations

Models of unit operations were set up in order to study the individual unit separately and optimize the unit operations for scaling up to commercial facilities. The parameters of the models are reconciled with the experimental data, which is the design basis of the individual models.

Model Assumptions:

Based on the algal organism rotation discussion in the Section 2, the end-to-end REAP Aspen models are each set up with slightly different parameters to reconcile the experimental data from the seasonal rotation. The model parameters for different organisms in the base case are summarized in Table 5.9-2.

Table 5.9-2 Model parameters for different organisms in the base case

		Kirschneriella	*Chlorella*	*Galdieria*
Cultivation	Operating period	Nov-Jan	Feb-Apr	May-Sept
	Algal biomass productivity (g/L/day)	0.16	0.11	0.15
	Algal biomass productivity [a] ($g/m^2/day$)	18.2	12.8	17.8
	CO_2 source	Flue gas, 20wt% CO_2	Flue gas, 20wt% CO_2	Flue gas, 20wt% CO_2
	N nutrient	Urea	Urea	Urea
	P nutrient	DAP	DAP	DAP
	Water supply	Freshwater	Freshwater	Freshwater
Dewatering and recycling	Harvesting efficiency	100%	100%	100%
	Solid content for DHTL	200±20 g/L	200±20 g/L	200±20 g/L
	Blowdown	5% of recycle rate	5% of recycle rate	5% of recycle rate
DHTL [b]	Biocrude yield (% DW algae)	41.0	24.9	31.2
	Biochar yield (% DW algae)	14.2	17.9	4.9
	Water product (% DW algae)	14.7	10.4	8.2
	Gas product by different	30.1	46.8	55.7
SEQHTL [c]	Biocrude yield (% DW algae)	26.3	29.4	35.0
	Biochar yield (% DW algae)	11.9	10.2	13.3
	Water product in stage 1 (% DW algae)	42.7	44.6	29.4

a. The net VPBR footprint is assumed to be 115 L/m^2, as discussed in Section 2.
b. The yield of DHTL process are from ASU
c. The yield of SEQHTL process of *Kirschneriella* is from WSU, Sept 2016, of *Chlorella* is from WSU, June 2015, and of *Galdieria* is from ASU, Aug 2016.

5.9.4.1 Area 100: Cultivation

Besides the parameters listed in the Table 5.9-2, other parameters for the modeling of cultivation in Aspen are set according to the location of AzCATI. These can be summarized as:

a. *Raw material feeding rate*:
   i. Fluegas flowrate set at 100 tonnes/hr, the nutrients and water feeding flowrate are adjusted to meet the design specifications

- Adjust the feeding rate of nutrients to control the remaining nutrients in the blowdown stream to less than 0.05 g/l
- Adjust the feeding rate of makeup water to control the algal concentration at 2-2.5 g/l in the PBR

b. *Growth parameters* (see Table 5.9.4-2):

i. The algal growth component was derived from the Aspen model developed by Pan Pacific for NAABB and is described in Dunlop et al. [5].
ii. Solar input is a key parameter in the algal growth model. We use the seasonal average solar radiation data from the experimental location, Mesa, AZ. Assume 15% solar energy lost due to the reflection and absorption of the PBRs.
iii. Assume the empirical molecular formula of the algal biomass is: $CH_{1.9}O_{0.4}N_{0.083}S_{0.002}P_{0.002}$. The HHV of the algae is 27 MJ/kg. The calorific value is then used to predict the photosynthetic efficiency of the strains.
iv. The photosynthetic efficiency of the strains in different seasons are reconciled with the areal productivity recorded in AzCATI Mesa, AZ and the seasonal solar radiation.
v. Growth data is obtained from the AzCATI MM VPBRs at 1m and 0.5m spacing (see Figure 5.9.1-xxx). The width of the MM VPBRs is 4cm. This occupies only a small amount of the PBR footprint. Therefore, 4% of the local evaporation rate is assumed for the Aspen model.

These assumptions are summarized in Table 5.9-3

Table 5.9-3 Growth parameters as applied in the Aspen model

	Kirschneriella	*Chlorella*	*Galdieria*
Operating period	Nov-Jan	Feb-Apr	May-Sept
Solar Input (kWh/m^2-day)*	2.95	5.83	6.52
Photosynthetic efficiency (%)**	4.63	1.64	2.05
Evaporation rate (m^3/hc/hr)***	0.046	0.121	0.175

* http://web.utk.edu/~archinfo/EcoDesign/escurriculum/CLIMATEDATA/CITYDATA/PHOENIX/PHOSolarRad.htm
** Photosynthetic efficiency =Areal Productivity*Area*(calorific of algae)/(Solar input)
*** Assumes 4% of the average local evaporation rate

vi. Stoichiometric reactions in PBR used in the Aspen model are presented in Table 5.9-4

Table 5.9-4 Stoichiometric reaction setting for PBR in the Aspen model

	Stoichiometric Reaction	ΔH (kcal/mol)
1	0.9585 HCO_3^- + 0.866 H_2O + 0.0415 urea + 0.0017 SO_4^{2-} + 0.002 HPO_4^{2-} --> Algae + 1.21965 O_2 + 0.9585 OH^-	133.44
1a*	0.9585 CO_2 + 0.865 H_2O + 0.0415 urea + 0.0017 SO_4^{2-} + 0.002 $H_2PO_4^-$ --> Algae + 1.21915 O_2	133.44
2	Algae + 1.2919 O_2 --> CO_2 + 0.0415 N_2 + 0.949 H_2O + 0.0017 SO_4^{2-} + 0.002 HPO_4^{2-}	-139.70
3**	6 Algae + 0.306 H_2O + 1.6914 O_2 --> 0.249 N_2 + SOLC + 0.0102 SO_4^{2-} + 0.012 HPO_4^{2-}	136.85

*1a: Setup when the solution is at pH 2.5

**SOLC (Soluble Carbon) is an aggregate of the metabolic of the by-products of the cell that spill out from the cell into the super natent and are not part of the product but in fact waste. It is composed of potentially thousands of unknown substance which we choose to lump together as a soluble carbon an chemically represent them as glucose.

Results from the Aspen model:

The results of the Aspen models of the strains are used for TEA and are discussed in the following sections 5.9.4 and 5.9.5. The economic data from the Aspen Economic Analyzer is used for capital cost estimation. The mass balance results of the raw materials and the energy consumption of the pumps and compressors taken from the Aspen models are used for the operation cost estimation. The utility demand of DHTL and SEQHTL process is obtained from separate models, since the elemental analysis results from laboratory are not satisfied in the end-to-end Aspen model, this study is discussed in Section 5.9.4. The water consumption of different strains at different season is obtained from the end-to-end Aspen models and listed in Table 5.9-5**.** The N and P recycle rate of DHTL is investigated in separate models and discussed in Section 5.9.4.

Some key mass and energy results are summarized in Table 5.9-5.

Table 5.9-5 Key results from the Aspen model

		Kirschneriella	*Chlorella*	*Galdieria*	*Annual result**
	Operating period	Nov-Jan	Feb-Apr	May-Sept	
	Bio-crude productivity (Gal/acre/yr)	2,767	1,565	2,286	2,208
	Water consumption (L/MJ biocrude)	2.24	4.74	4.58	3.97
SEQHTL	Bio-crude productivity (Gal/acre/yr)	1,877	1,530	2,444	2,009
	Water consumption (L/MJ biocrude)	2.87	4.50	3.41	3.55

* Productivity of the annual result are considered algae drying, which are discussed in the TEA section

Reactor Design: Comsol Multiphysics models of light integration and mass transfer in PBR

Comsol Multiphysics models the fluid dynamics of gas, liquid and their interfaces, and is able to compute sophisticated mass transfer equations. Horizontal photobioreactors are the simplest form of photobioreactor and hence were chosen in this study. By simultaneously solving light penetration, equilibrium, algae kinetics and mass transfer, a working model for horizontal photobioreactors has been established and validated against experimental data.

A horizontal photobioreactor was constructed in Comsol as a cuboid 3 m long, 1 m wide and 0.5 m high. The bottom layer was denoted as aqueous phase and the top as gas phase. Air with concentrated CO_2 was supplied through the center point from the bottom. The system was operating at 300 K and 1 bar. Ambient air composition was 21% (v/v) O_2 and 79% (v/v) N_2. Concentrated CO_2 was supplied at 4 L/min through a 0.1 m wide pipe at 5 bar. The species used of algae used was Chlorella.

The model consists of five domains (see Figure 5.9-17). The liquid phase domain represents the turbulent flowing algae culture. The Computational Fluid Dynamics (CFD) module calculates the full turbulent velocity profile from zero velocity at the bottom to velocity at the top which, when integrated, equals the average velocity observed in the real PBR. Similarly, a flowing gas phase domain is also modeled by the CFD module. A separate CO_2 top-up domain provides a simple mechanism by which CO_2 can be added to the reactor as required during the growth phase. Critically gas exchange between the gas phase and the liquid phase occurs. The dissolution of CO_2 from the gas phase into the liquid phase is dependent on the pH. There is thus a major mass transfer barrier between the gas phase and the liquid phase. A significant element of the model is devoted to calculating separately the gas phase and liquid phase for CO_2 and

combining them into an overall mass transfer for coefficient.

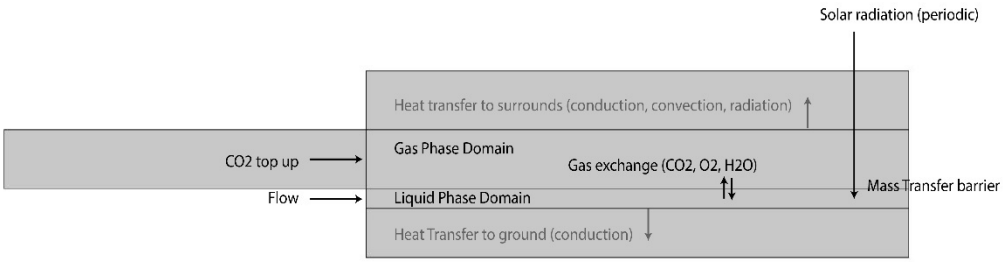

Figure 5.9-17 Comsol model schematic of REAP PBR

The solubility of the CO_2 and the O_2 in the liquid phase is governed by Henry's Law with data from Alberty (2003). The carbonate/bicarbonate equilibria are calculated from the classic study by Danckwerts (1970). The carbonate/bicarbonate kinetics are taken from Aspen's database while pH species diagrams are generated from within Aspen. Growth kinetics pf the algae as a function of light intensity and temperature were from Michael Huesemann studies (e.g. 2013), reinterpreted as a piecewise distribution of Michaelis-Menten kinetics followed by a period of photosaturation. Modeling the incoming solar addition involve setting up two models of light absorption: the traditional Beer-Lambert model and a model using the scattering equation from the literature [7]. Additionally, the model is set to calculate heat transfer from the liquid phase by conduction into the ground and from the gas phase to surrounding air by conduction, convection and radiation. Finally, Comsol is a finite element analysis (FEA) program so a mesh is applied to each domain. The equations for turbulent flow, mass transfer and light penetration are solved simultaneously as a function of time. The output is primarily predicted growth rate of the algae and CO_2, mass transfer (see Table 5.9-6) and subsequent depletion with accompanying pH changes.

Table 5.9-6: Example of basic mass transfer calculation for the Comsol model of REAP PBR

MASS_TRANSFER

Sc_water	nu0_water/D_CO2_water	Schmidt Number water	
Sc_air	nu0_gas/D_CO2_gas	Schmidt Number air	
hmd_water	4*(water_depth*width)/(2*water_depth+width)	hydraulic mean diameter	liquid
hmd_gas	4*(gas_space*width)/(2*gas_space+width)	hydraulic mean diameter	gas
Re_water	ubar*hmd_water/nu0_water	Reynolds Number water	
Re_gas	ubar_gas*hmd_gas/nu0_gas	Reynolds Number gas	
Sh_water	2+0.332*(Re_water)^0.5*(Sc_water)^0.333	Sherwood Number water	
Sh_gas	2+0.332*(Re_gas)^0.5*(Sc_air)^0.333	Sherwood Number gas	
k_mtc_water	Sh_water*D_CO2_water/hmd_water	mass transfer coefficient water side	
k_mtc_gas	Sh_gas*D_CO2_gas/hmd_gas	mass transfer coefficient gas side	
m_prime	1/(1[bar]/H_CO2/c_H2O)	slope of equilibrium line	
KL_overall	1/(1/(m_prime*k_mtc_gas)+1/k_mtc_water)	overall liquid-side mtc	
ratio	m_prime*k_mtc_gas/k_mtc_water	gas/liquid mass transfer coeff	
Sh_water_turb	0.029*Re_water^0.8*Sc_water^0.333	turbulent Sh number for water	
k_turb	Sh_water_turb*D_CO2_water/hmd_water	turbulent liquid side mtc	
KL_overall_turb	0.01/(1/(m_prime*k_mtc_gas)+1/k_turb)	overall mtc if turbulent	
t_clock	10[h]		
a_mtc	length*width/(length*width*water_depth)		
c_TotalC	comp1.cCO2L+comp1.cHCO3+c_CO3		
test_units	R_const*T_water/H_CO2*comp1.cCO2G		
KLa	KL_overall*a_mtc		
ratio2	KLa/kLa_CO2	ratio wrt Algenol	

The Comsol model currently works smoothly for simulations of several hundred hours until pH is introduced. This is a known problem in FEA and is referred to as the "scaling problem. FEA works best when all the numbers involved are of the same order of magnitude, e.g. 1 to 10. When pH is introduced numbers such as 10^{-7} can occur and numerical problems arise.

The Comsol model is also set up to incorporate a script of temperature and light for the duration of the simulation to represent observed experimental fluctuation in the test bed. In this respect, it is similar to Huesemann's model. An additional pH script has been written. The main way in which it differs from Huesemann's model is the emphasis on mass transfer limitation and particularly CO_2 in and out of water, but also O_2. The main difference relates to turbulent flow of the gas and liquid phases how vertical mixing, especially the liquid phase, will affect the growth rate.

Modeling of Horizontal PBR

In our previous work we established that we had the basis to investigate which factors were rate limiting in algal growth in horizontal reactors. As a new release of Comsol became available, we were able to extend the model substantially. We were able to dispense with empirical models of mass transfer and go for a direct solution of the turbulent Navier Stokes equation in the reactor. This resulted in a major increase in simulation time, but gave far more realistic solutions that were based on first principles in ways that had not been readily available until recently. The Mass Transfer Sub-model was rewritten to incorporate the change, with full interactions between turbulent flow, light, pH, and the complex CO2/bicarbonate/carbonate equilibrium.

We have previously demonstrated how mass transfer limitation could be diagnosed by - in essence - extrapolating the flow rate to infinity, when the boundary layer would disappear. In practice this is virtually impossible, so instead we plot the reciprocal of the mass transfer coefficient against the reciprocal of the velocity (actually the 0.8 power of the velocity, for reasons associated with the complex fluid dynamics) and extrapolate to zero.

We have also previously shown how the slope of the resulting straight line and its intercept on the Y-axis allowed us to quantify the resistances in the gas and liquid phases. In this study and the report, we further examine how the slope of the top (liquid side mass transfer resistance) line changes with time (see Figure 5.9-18). When the slope falls to zero, there is essentially no more mass transfer limitation. On logarithmic coordinates (Figure 5.9-19) we see that most of the mass transfer limitation is over within the first 50 hours in a 600 hour operation.

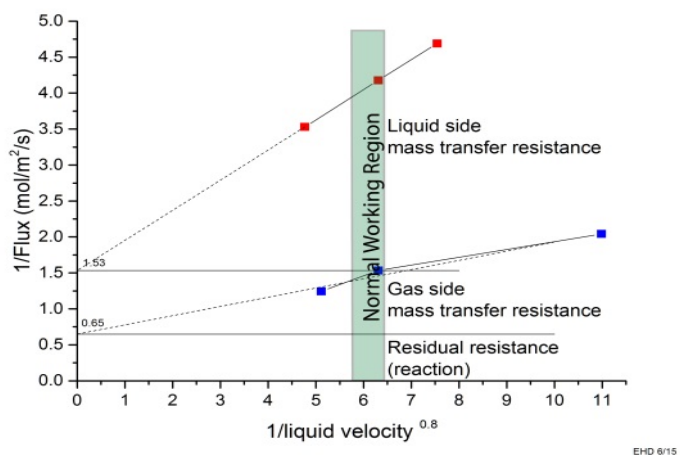

Figure 5.9-18: Quantifying the controlling mass transfer resistance in the horizontal PBR.

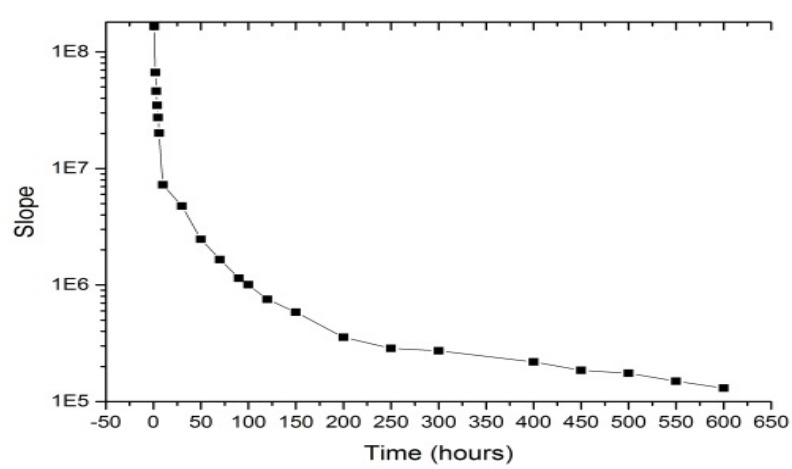

Figure 5.9-19: The slope of the Liquid Side line falls to zero as this resistance ceases to be dominant shown on a semi-logarithmic scale for clarity.

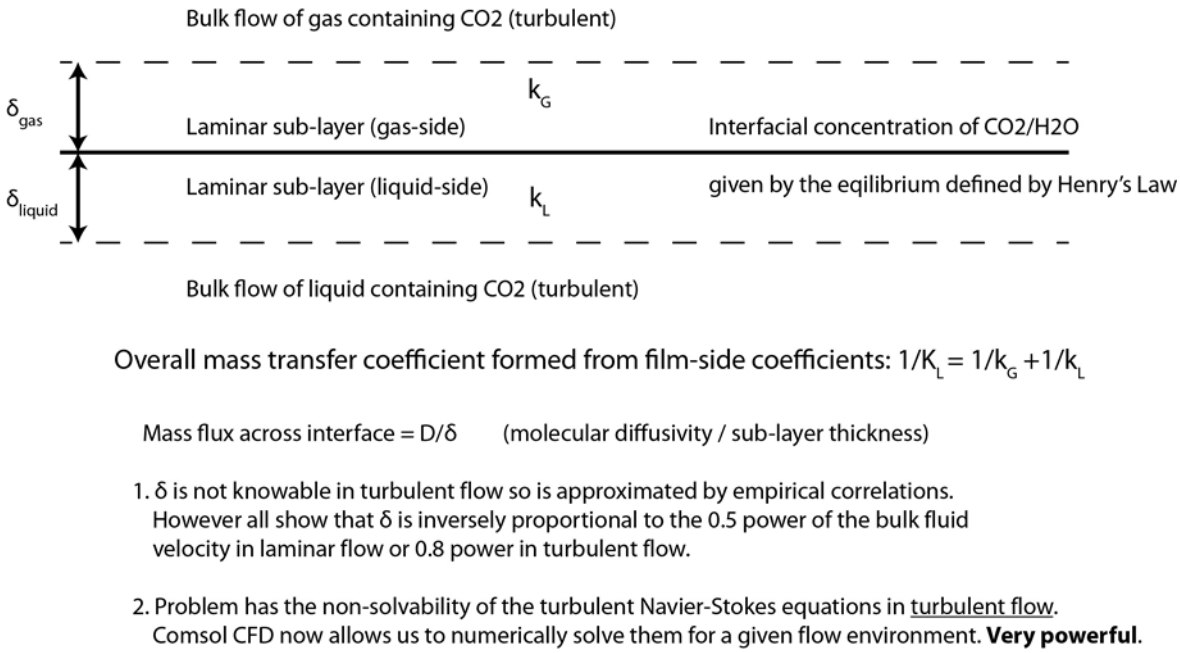

Figure 5.9-20: Finding the mass transfer coefficients in a photobioreactor.

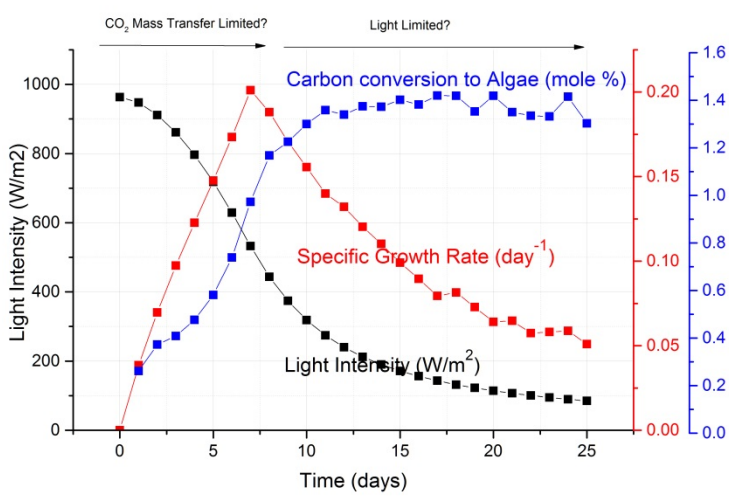

Figure 5.9-21: Evolution over time of the mass transfer coefficient, the specific growth rate, carbon conversion and light intensity.

Figure 5.9-21 allows us to look at the evolution of the apparent mass transfer coefficient, the specific growth rate, and the carbon conversion to algae. It behaves similarly to Figure 5.9.193 with the mass transfer coefficient at a minimum around five days, but more interestingly the specific growth rate peaks at around seven days. We saw that this coincides with the build-up of algal concentration causing light limitation. This leads us to conclude that there is a two-phase regime with mass transfer limitation in the first two days, followed by an abrupt transition to light limitation. This can be seen clearly in Figure 5.9-22, where light limitation takes over at approximately 500W/m^2.

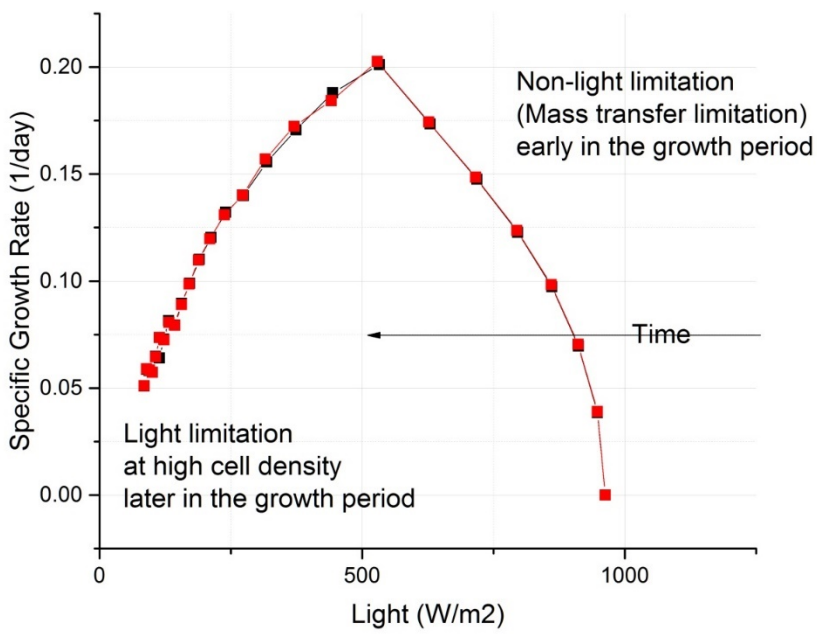

Figure 5.9-22: The transition from mass transfer limitation to light limitation around 500 W/m^2.

The model allows us to make this more explicit, as shown in Figure 5.9-23, by artificially varying the light intensity from a low of 10% of normal rate to ten times the normal rate. The resulting ash-free dry weight is initially unaffected by this, but rapidly shows major increases in accordance with the light limitation model. An interesting variant on Figure 5.9-23 is to plot the same data with a logarithmic Y-axis (see Figure 5.9-24). Major curvature of the lines can be seen, implying that the algae does not grow exponentially.

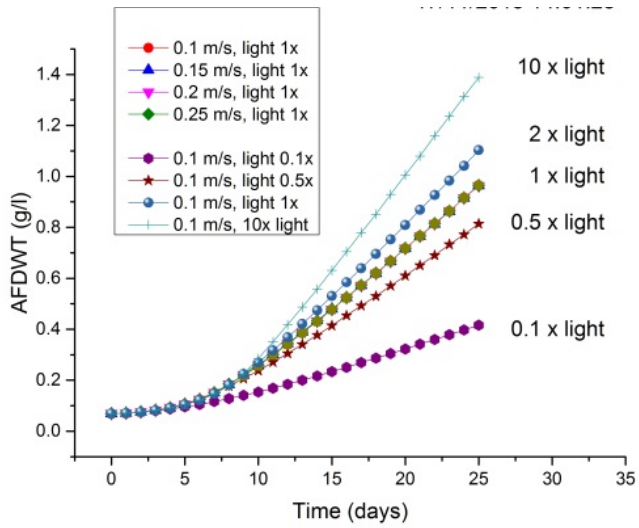

Figure 5.9-23: Artificial demonstration of light limitation as observed by varying light to the model from 0.1 times normal to 10 times normal light intensities.

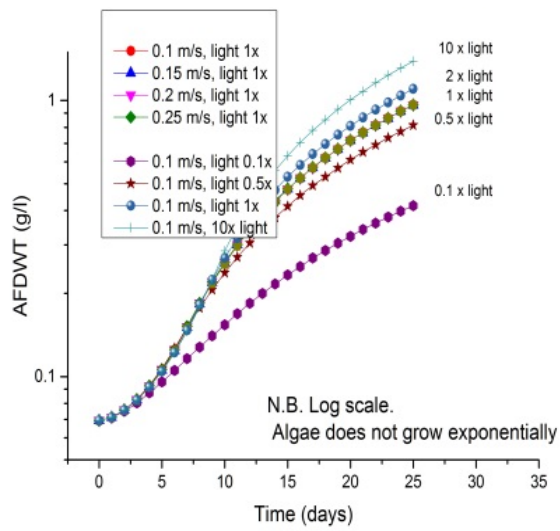

Figure 5.9-24: Figure 5.9-24 redrawn on semi-logarithmic coordinates showing that after light limitation sets in the algae do not grow logarithmically.

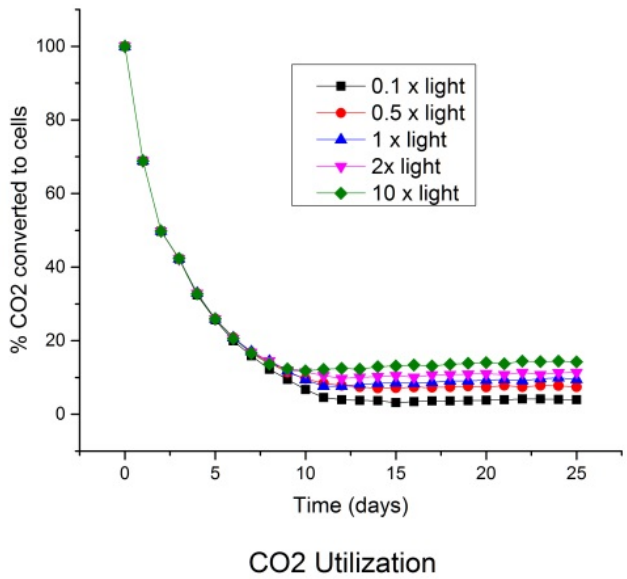

Figure 5.9-25: CO_2 utilization behaves similarly being increased as light is increased but only after light limitation sets in.

Figure 5.9-25 shows that CO_2 converted to cells as a function of the light intensity following the expectation of light limitation. However, more striking is that the CO_2 converted to cells never exceeds 20%, drawing attention to the major problems of CO_2 absorption even at pH 8.

Reactor Depth

The final study in this section was the effect of reactor depth on specific growth rate and productivity. The starting point of the study was a water depth of 25 centimeters. A series of studies, at both pH 2 and pH 8, are shown below in Figure 5.9-26. Depth was varied by reducing the norm of 25 cm down to an arbitrary minimum of 1 cm. It was observed that a pronounced peak in specific growth rate occurs as mass transfer limitation gives way to light limitation. Figure 5.9-27 shows that the ash-free algal dry weight at the peak rises sharply as the depth is decreased, as does the time to reach the peak. As depth decreased, both areal and volumetric productivity increased substantially. The reactor relative costs drop proportionately. Figure 5.9-28 shows this occurrence for pH 2 and pH 8. The situation is similar in both instances, but even more pronounced for pH 8. This is in line with our previous observations.

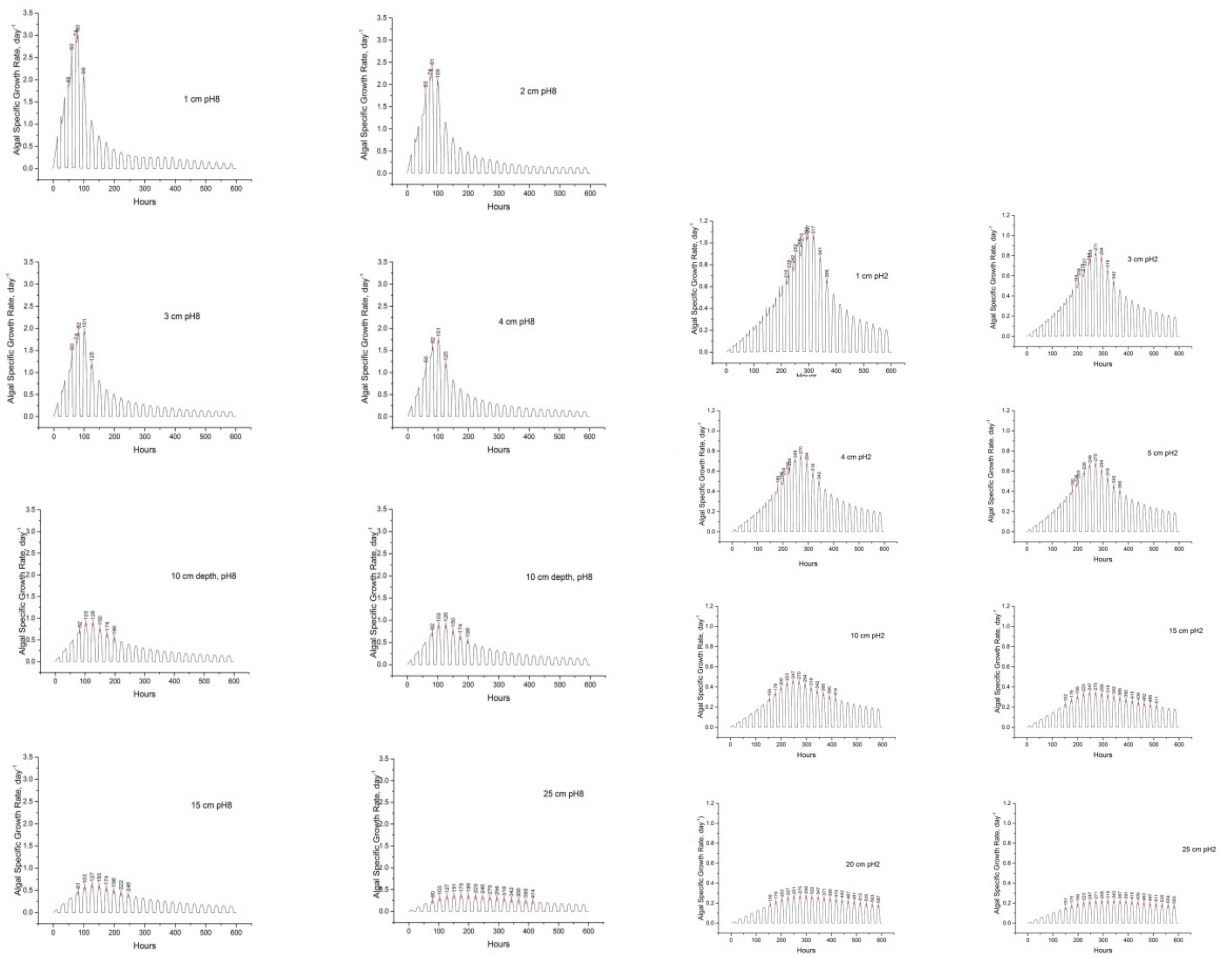

Figure 5.9-26: Specific Growth Rate with time for pH 2 and pH 8 for various reactor depths. A pronounced peak is observed. The peaks correspond to the daily light cycle.

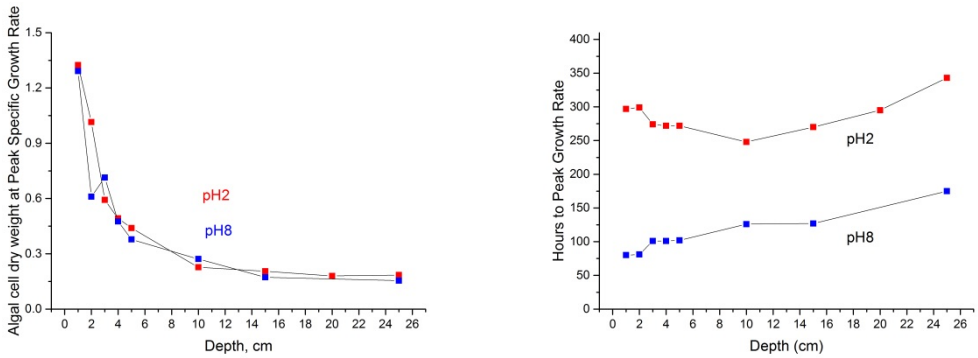

Figure 5.9-27: Algal dry weight at the peak rises rapidly as depth is decreased and time to the peak is likewise deceased.

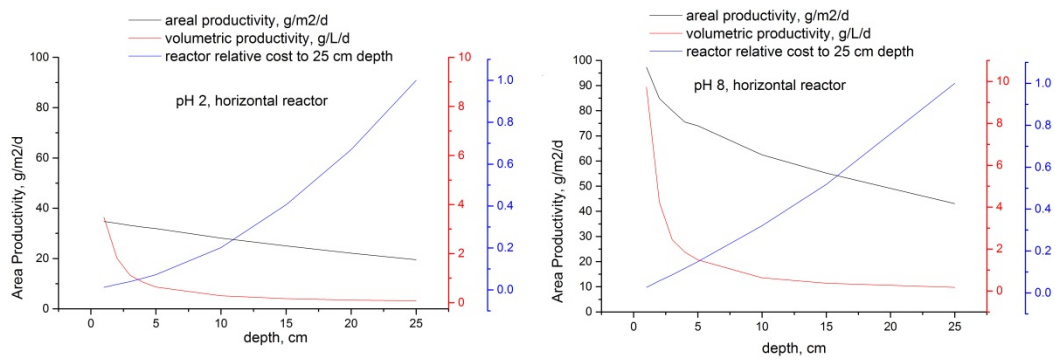

Figure 5.9-28: The effect of reactor depth at pH 2 and pH 8 on productivity and cost.

All factors favor the lower depths.

Conclusion

In conclusion, initially, algal growth is limited by the mass transfer of CO_2. The solution is to add an external CO_2 absorber and use the hydrostatic head to drive the circulation through the reactors. The second stage of the process is light limited. The solution here is to make the reactor as shallow as can be practically built and operated.

Modeling of Vertical PBR

REAP cultivation process was transferred to vertical PBR at AzCATI early in the Fall of 2015. This change necessitated the development of a Comsol model for the vertical PBR. The modeling of the horizontal PBR informed the development of the new model. The fluid mechanics however become exponentially more complicated in a vertical PBR model, and the interactions between rising bubbles and the liquid give rise to significant modeling challenges. For example, getting the interaction between the fluid dynamics and the biochemistry of the algal growth to converge in a reasonable timeframe.

Initial results from the vertical model reveal a number of important clues as to the challenges faced in reactor design of vertical PBR. The results of the Figure 5.9-29, for example, shows the wildly erratic circulation patterns until the algal solution moves from the bubble column to gas lift mode. It illustrates that the back mixing of the gas and the liquid will severely limit mass transfer to the equivalent of two theoretical absorption stages. In contrast, in the Aspen model we routinely require between five and eight theoretical stages to absorb the carbon dioxide necessary at ph 8. At pH 2 the number is indeterminate but large. This is a common problem throughput the history of chemical engineering. The solution is to introduce plates as found in a multi-stage distillation column. This is unlikely to be practicable in the case of the REAP process. The other common solution is a packed bed in which the column is packed with articles which may be spheres or proprietary shapes often made from ceramics, for example, the Raschig rings. This appears to be the preferable solution here.

These results, however, also interface with light absorption. This suggests splitting the reactor into two parts. : an absorption column packed with a ceramic tings into which carbon dioxide is passed and the algal solution fed to the cheapest form of reactor, and mitigate some of the problems of mixing in the vertical rectors. Another solution could also be to feed the solution to vertical reactors of arbitrary height (but as high as 30 feet/10 metres). This comes at a cost of pumping against the hydrostatic head but some of this is potentially recoverable. A gas lift reactor, Figure 5.9-30, or some variant is under development to determine a viable proposition.

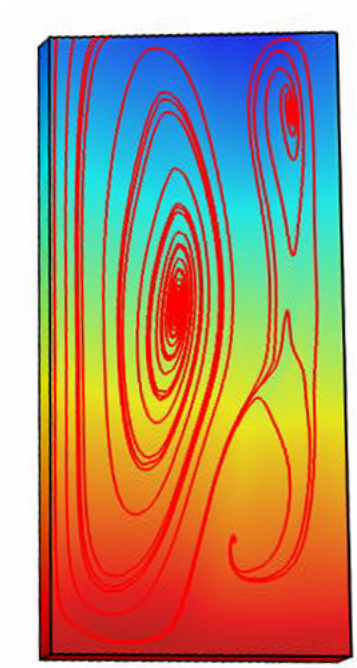

Figure 5.9-29: Circulation patterns calculated in the vertical reactor (LHS) are wildly erratic and limit operation to one theoretic absorption stage, which is a major limitation. Studies of variants involving the gas –lift (RHS) configuration are under way and are much more promising.

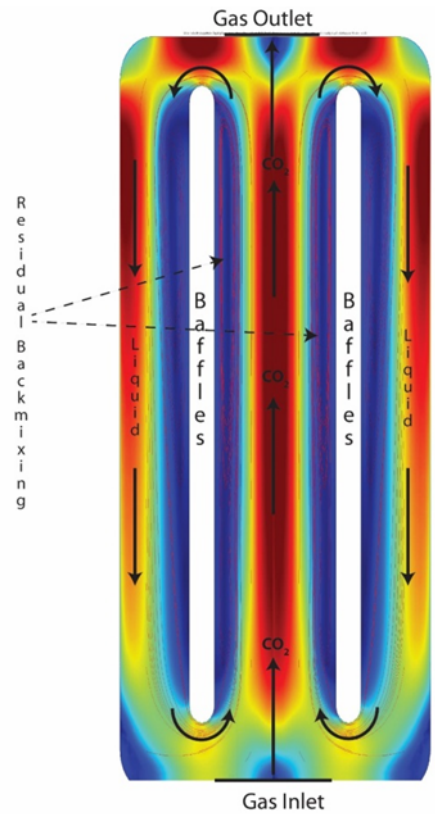

Figure 5.9-30: Model of gas lift reactor

With the low height still involved, this is still anticipated it will provide two theoretical stages (see Figure 5.9-31.) although many more are still required.

Figure 5.9-31 Gas lift reactor two stages

The pH and carbonate equilibria remain a challenge to the modeling of reactors and future work is required. There are also issues relating to resolving stiff partial differential equations. These are a mathematical description of a type of equation that is difficult to solve. Future work will need to address the high computing performance requirements of to solve these equations in the PBR models.

Spacing and light optimization using 3DS Max model

Overview

Recent research into growth modeling of microalgae for the production of biofuels in photobioreactors has concentrated on areas such as depth, photosynthetic efficiency, and mass transfer to improve growth rates and lipid production. Such predictive modeling has focused attention on light once it gets into the reactor. This study examines how light reaches vertical photobioreactors, and in particular the effect of shading caused by stacking reactors closely together. The objective of the study is to develop a method for the prediction of the effectiveness of vertical photobioreactors based on separation at a given location, date and time.

Method

Five reactors based on an existing experimental site for *Galdieria sp.* were modeled using a photometric sun in Autodesk 3DS Max Design 2016 (see Figure 5.9-32). The performance of the

reactor model was evaluated on the basis of the total illuminance for different orientations, and an apparent effectiveness factor for various separations was calculated then validated against the experimental data.

The reactor model was set up in Mesa, Arizona (33.304N, -111.673W) on 23rd June 2016 at 16:00:00. The construction material of the reactors was selected by comparing the total illuminance of reactors using black rough concrete and glass, with black rough concrete chosen. The optimal orientation was determined by evaluating the performance of the reactor model for reactors aligning along a north-south axis and an east-west axis. The model was then used to simulate the change in reactor effectiveness as they are more closely separated. The simulation was performed on 23rd June 16:00:00 and 26th January 08:30:00.

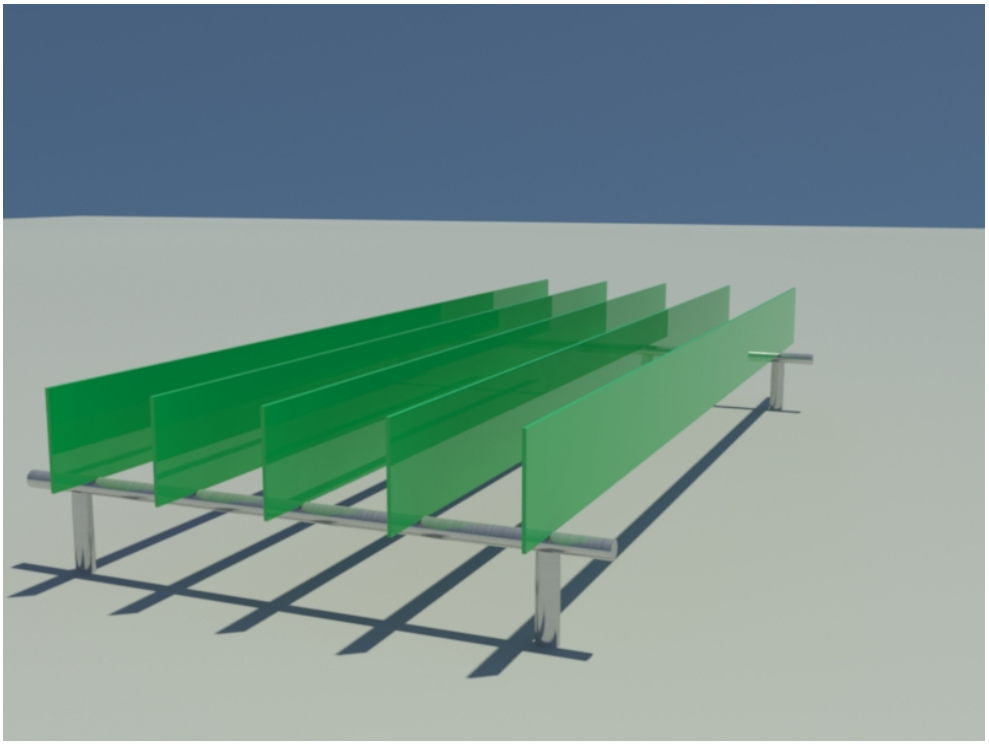

Figure 5.9-32: Representation of reactor set-up.

Results

Results show that reactors positioned on a north-south axis receive significantly more sunlight as compared to those placed on an east-west alignment (see Table 5.9-7). When reactors are positioned along the north-south axis, illuminance received on the front side tripled the value obtained with an east-west alignment. In both cases illuminance on the back side remained the same, leading to the total illuminance for reactors with a north-south alignment being more than twice the amount as the east-west alignment.

Table 5.9-7: Illuminance breakdowns for reactors positioned along north-south and west-east axes.

Parameters	North-South	East-West
Front illuminance (lux)	9.2×10^6	2.8×10^6
Back illuminance (lux)	1.9×10^6	1.9×10^6
Total illuminance (lux)	1.1×10^7	4.7×10^6

The results also show that the average effectiveness of the reactors rises steadily as separation increases. In the two examples studied, average effectiveness of the reactors decreased as they were stacked closer; however, the difference is highly dependent on the date and time of the modeling.

Case study 1 (23rd June 16:00:00) tested the apparent effectiveness factor for each reactor with a separation of 0.1 m, 0.2 m, 0.3 m, 0.4 m, 0.5 m and 1.0 m.

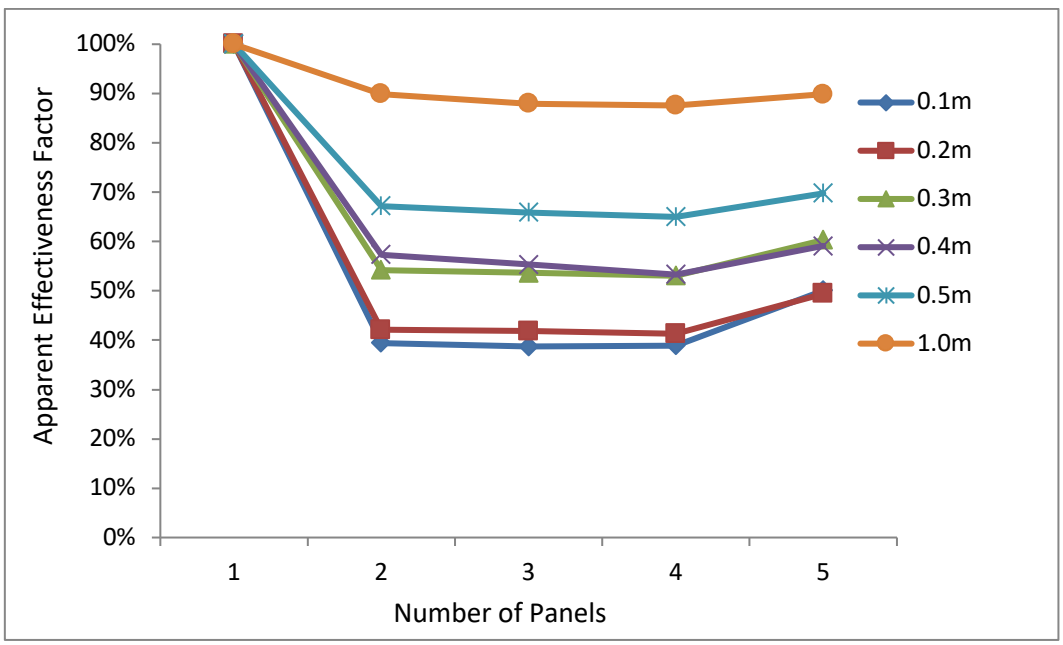

Figure 5.9-33: Apparent effectiveness factor for each reactor with a separation of 0.1 m, 0.2 m, 0.3 m, 0.4 m, 0.5 m and 1.0 m.

The results shown in Figure 5.9-33 highlight that the reactors become more effective as separation increases. In particular, the effectiveness with a separation of 0.3 m was found to be 64%, about 10% higher than 0.1 m and 0.2 m. Similarly, a spacing of 0.5 m gave rise to 74% effectiveness, 9% higher than 0.4 m. At 1.0 m the average effectiveness reached the highest value of 91% (see Figure 5.9-34).

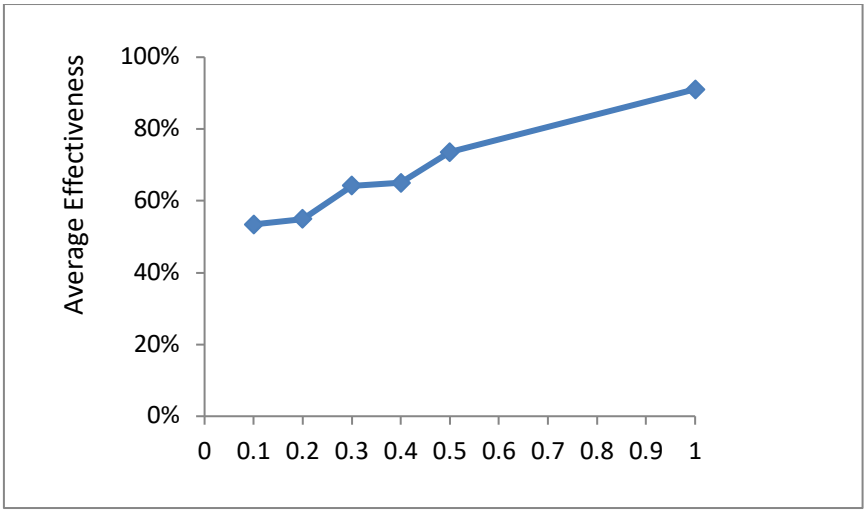

Figure 5.9-34: Average effectiveness of reactors at various separation distances.

Case study 2 (26th January 08:30:00) tested the apparent effectiveness factor for each reactor calculated with a separation of 0.3 m and 1.0 m.

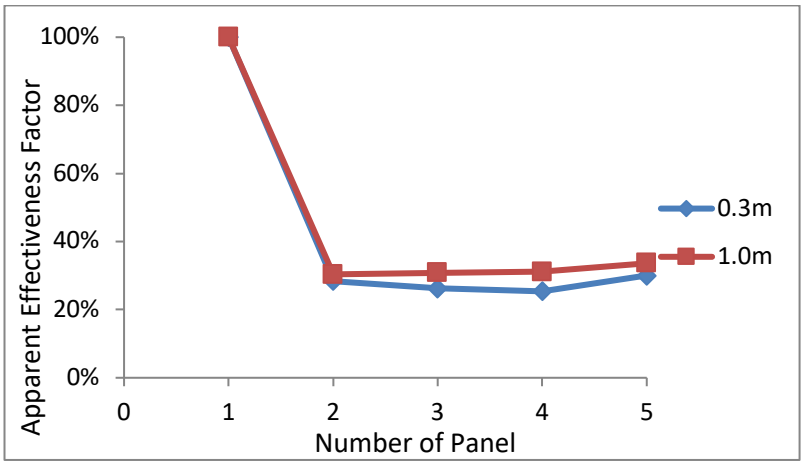

Figure 5.9-35: Apparent effectiveness factor for each reactor with a separation of 0.3 m and 1.0 m.

As shown in Figure 5.9-35, in this case the effect of shading is significant, as the effectiveness of the shaded reactors is only 30% even when the spacing is 1.0 m. The average effectiveness of the reactors at 0.3 m and at 1.0 m was 42% and 45% respectively. The significant shading is likely due to the shallow sunlight angle hitting the reactors.

The results from the light shading study (Figure 5.9-34 above) would imply that stacking the reactors closer together would reduce productivity. Figure 5.9-36 shows that this is not necessarly the case. Based on REAP data from AzCATI (Lammers et al.), the analysis shows

that there is surprisngly little differnce in productivity for different spacngs. The productivity on average is down from 0.17 g/L/day at 2.5 m spacing to 0.13 g/Lday at 0.5 spacing. A t-test of the data shows that the difference is just outside the level of statistical significance (at 6%).

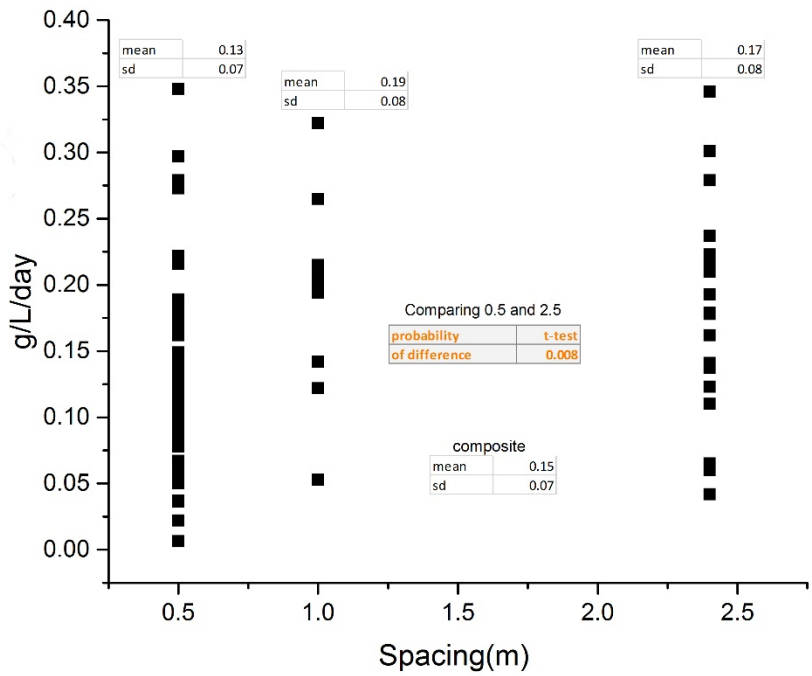

Figure 5.9-36 Analysis of productivity (g/L/Day) in terms of spacing based on REAP data at AzCATI (Lammers et al.)

To resolve this we neeed to examine Huesemann's graph of specific growth rate vs light intensity (Figure 5.9-37). It shows that halving the effective light intensity does not significantly reduce the growth rate. In fact it may even raise it slightly as photosaturation is reduced. It would take a very major reduction in light intensity before any effect is observed. This is in line with the observations of Slegers et al. [8].

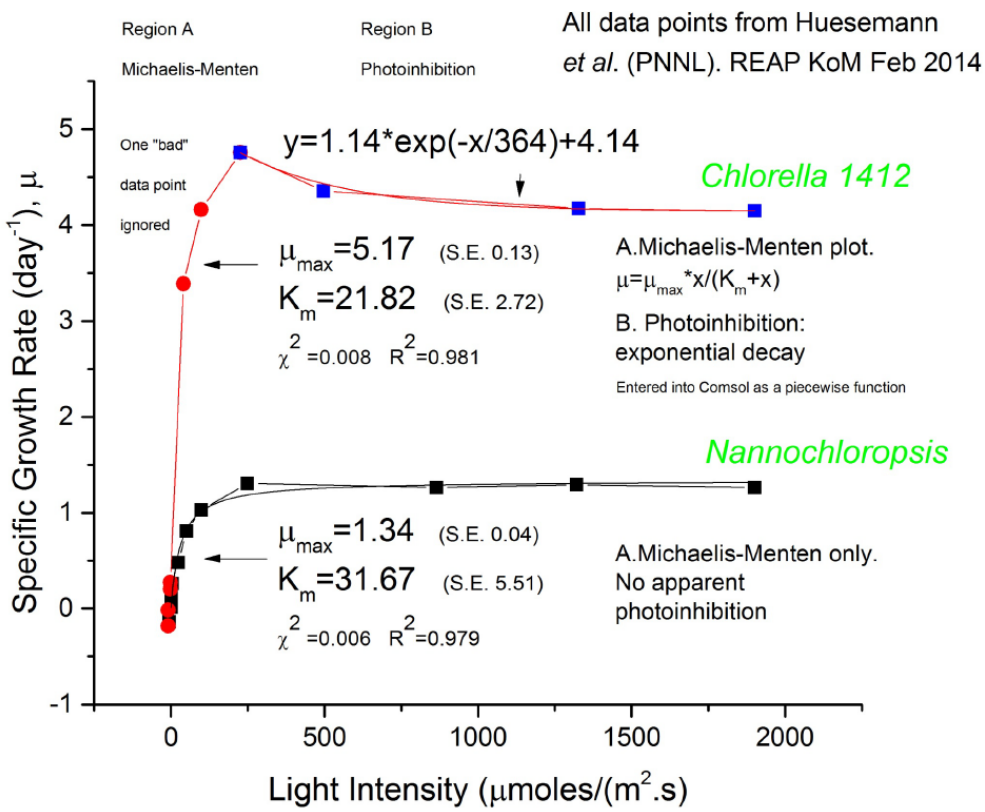

Figure 5.9-37 Huesemann's graph of specific growth rate vs light intensity

It is important to remember that Huesemann's light/growth rate curves were done at ultra-low, non-shading cell densities (starting OD750 ~ 0.002). We therefore cannot make a direct extrapolation of that data for the PBR cell densities (starting OD750 ~1.0).

Conclusion

Both case studies demonstrate that the average effectiveness of the reactors rises steadily as separation increases. These results allow the definition of an effectiveness factor due to spacing alone to be obtained as a function of separation. By introducing the effectiveness factor into a previously defined light-driven Comsol model of microalgae growth, the spacing effectiveness factor can then be converted to a growth effectiveness factor.

5.9.4.2 Area 400: Downstream biocrude conversion process

SEQHTL

Energy integration in SEQHTL using Pinch Analysis

The use of pinch analysis in SEQHTL process design

Recently, aligned with increased interest in biofuels, pinch analysis has been applied to various aspects of biofuel research including heat integration of bio-ethanol production [9], and heat integration of esterification process [10] [11]. The technique, which was developed in the late 1970s by Professor Bodo Linhoff, as a tool for engineers to design heat exchanger networks (HENs). It helps the engineers to set energy targets as part of process design, and identifies a range of design options to improve energy efficiency based on the inherent capabilities of the process. Our research shows that the application of pinch analysis to SEQHTL process design is of great interest and use to REAP TEA and LCA processes for algal biofuels.

Pan Pacific has prepared a work manual for the SEQHTL process. The work manual describes how to reconcile the raw data (elemental analyses and mass balance data for each stream) from experiments and how to calculate the Enthalpy of Formation (ΔH_f) for each biomass component. Based on the obtained thermodynamic data of the biomass compenents, then the stoichiometry for each reaction can be established and the heat of reaction can be calculated. With these data, the pinch analysis technique can be applied to optimize the process and integrate energy to finalize the process design.

General overview of pinch analysis

The overall steps within process design are represented by the onion diagram, Figure 5.9-38. Pinch analysis is an integral part of the overall strategy for process development and design. It helps the engineers to scope and screen major design options prior to simulations [12].

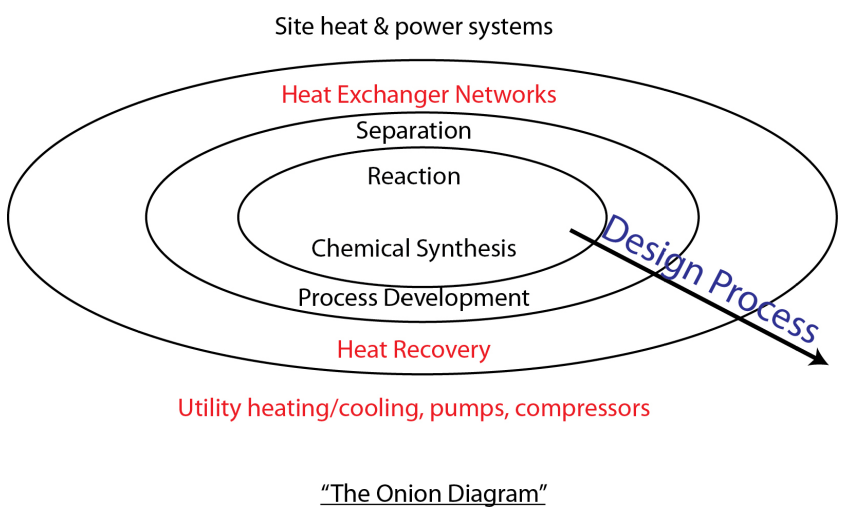

Figure 5.9-38 The onion diagram for process synthesis [12]

There are several important concepts of pinch analysis, among which Composite Curves, the Pinch, and the HEN Grid Diagram are the most important. The three concepts relate to the economic level of heat recovery that needs to be optimized.

Composite Curves are constructed from stream data derived from a process heat and material balance, and allow the designer to predict hot and cold utility targets ahead of design in order to understand driving forces for heat transfer and to locate the heat recovery Pinch. The HEN Grid Diagram enables the designer to develop heat recovery networks using the "Pinch Design Method" [13].

The design can only reach the targeted utility requirement if there is no Cross Pinch heat transfer from above the Pinch to below the Pinch:

A (Actual energy consumption) = T (Target) + XP (Cross-Pinch heat flow)

The Pinch principle allows the designer to keep the level of heat recovery optimized all through the evolution of even complex designs by ensuring that cross pinch heat transfer is avoided.

A systematic study method is required for pinch analysis. The stages of the process are as follows:

1. Obtain process flowsheet including temperature, flow and heat capacity data and a consistent heat and mass balance

2. Extract the stream data from the heat and mass balance

3. Select ΔT_{min}, calculate energy targets and the pinch temperature

4. Examine opportunities for process change, modify the stream data accordingly and recalculate the targets

5. Consider possibilities for integration with other plants on site, or restricting heat exchanger to a subset of the streams; compare new targets with the original one

6. Having decided whether to implement process changes and what utility levels will be used, design a heat exchanger network to recover heat within the process

7. Design the utility systems to supply the remaining heating and cooling requirements, modifying the heat exchanger network as necessary.

Defining the Base Case

The start basis of the pinch analysis of the SEQHTL process is the laboratory process, which illustrated in Fig 5.9-39. In this stage, only water is used to reduce the complexity of the optimization of the flowsheet.

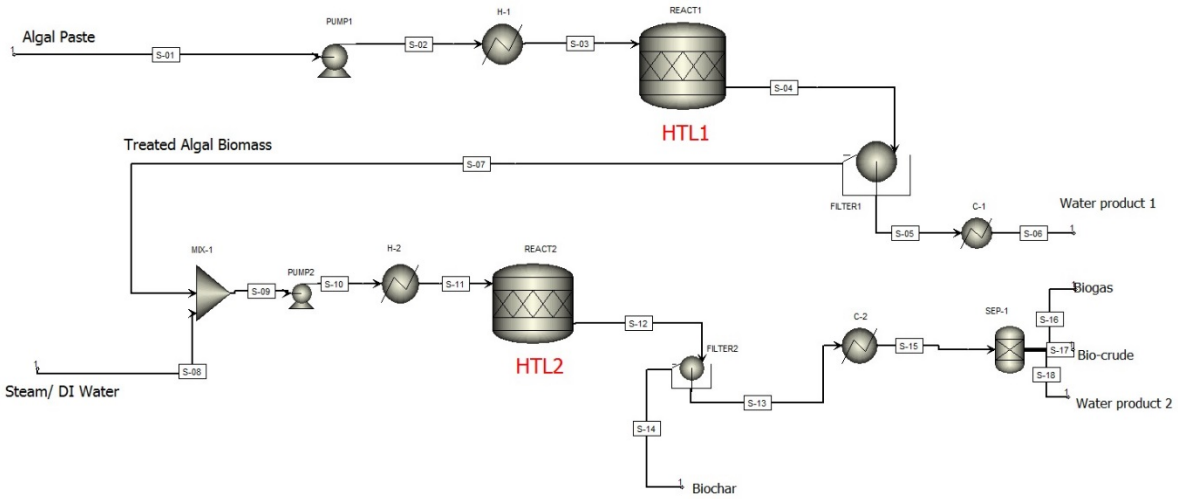

Figure 5.9-39 SEQHTL Base Case flowsheet

Figure 5.9-39 shows a lab flowsheet of SEQHTL process. Here we only focus on heat related units; others are omitted.

In this process, algal paste is pressurized to 7bar by PUMP1 and then heated to 160°C in heater H-1, before being fed into the first HTL reactor (REACT1, RStoic model). In the reactor, the algae is decomposed into Treated Algae (TA) and other water soluble components. After filtration in FILTER1, the water stream is cooled to 30°C in cooler C-1, for further treatment. The solid slurry is then mixed with water (stream S-08) in mixer MIX-1 to make the TA content to a specified concentration, then pressurized to 34bar by PUMP2 and heated up to 240°C in heater H-2 for the second reaction. The 240°C TA slurry is fed into the second HTL reactor (REACT2, RStoic model), where the TA continues to be decomposed to get a mixture of Biocrude, BioChar, BioGas and water soluble species. The mixture is filtrated in FILTER2 then the solid stream is collected as BioChar; after this, the liquid phase containing Biocrude is cooled to 30°C in cooler C-2, for further separations. In lab experiments, TA is totally separated and dried before mixing with water for the second stage reaction, while in continuous process design the high TA concentration stream (S-07) connects two stages and supposes no heat loss of this stream. This flowsheet becomes the Base Case of our study.

The network performance results extracted from AEA are listed in Table 5.9-8. The heating and cooling loads of the Base Case are much higher than the thermodynamic target. There is great potential for improvement.

Table 5.9-8: Results of Network Performance of Base Case

	Modeled	Thermodynamic Target
Heating [MW]	3.65	0.53
Cooling [MW]	3.39	0.27

Results of the optimized case

After two steps of the energy integrated optimization (details please refer to the supplementary material), the optimized flowsheet of the SEQHTL process is illustrated in Figure 5.9-40. In contrast to the Base Case flowsheet, there are two process heat exchangers, E-101 and E-103. The algal paste stream (in this model only water is used) is pressurized to 7bar then flows through E-101, in which the stream is heated to 138°C by the liquid stream from filter (FILTER1). The paste slurry is then heated by LP steam in E-102 to 160°C before being fed into reactor (REACT1). After filtration, the liquid stream heats the original algal paste, and the solid stream is mixed with water for the second HTL process. The slurry is pressurized to 34bar, flows through E-103, and is heated to 215°C by the liquid stream from Filter2. This is followed by another heater, E-104, to heat the stream to 240°C for the second HTL reaction.

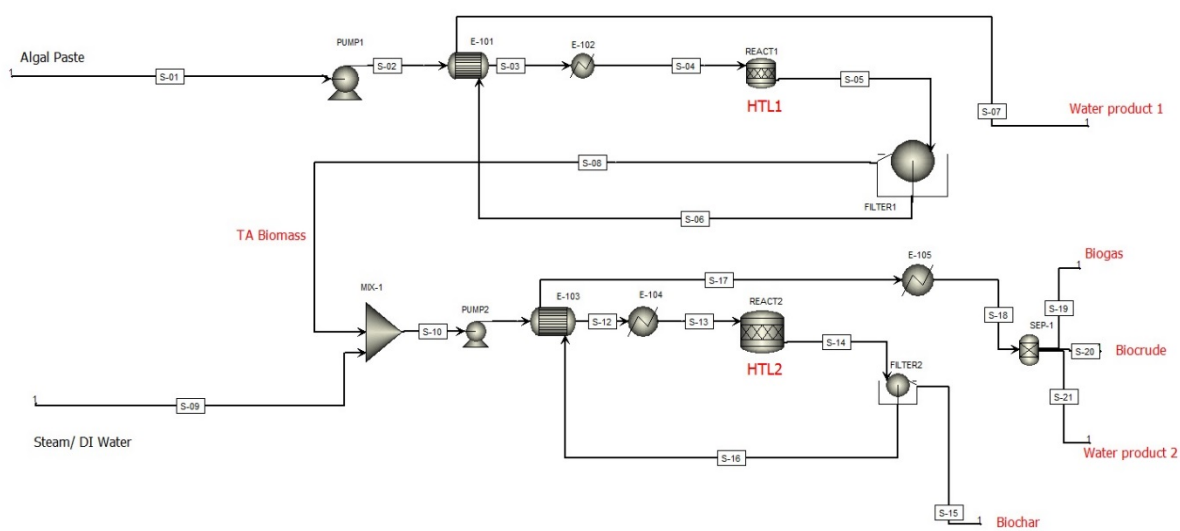

Figure 5.9-40: The flowsheet of the optimized case

Energy performance of the Optimized Case

The energy performance of the optimized case is listed in Table 5.9-9. The heating and cooling duties are ~ 10% to 15% above the target. However, they are greatly reduced compared to the performance of the base case. The heating and cooling loads are also close to their targets. Therefore, this design is selected for further modeling with biomass material.

Table 5.9-9: Comparison of performance of the Optimized Case and the Base Case

	Base Case	Optimized Case	Thermodynamic Target	Saving compared to the Base Case
Heating [MW]	3.65	0.57	0.53	84.3%
Cooling [MW]	3.39	0.31	0.27	90.8%

Energy performance with biomass in the optimized flowsheet

We now can use the Algae slurry as the feed (S-01) to run the Aspen model of the optimized flowsheet. The flowsheet with 10%wt and 20% wt algal feed is converged, the mass and energy data extracted and transferred to the Aspen Energy Analyzer. The energy performance is then analyzed.

Table 5.9-10 Summary of energy consumption of 10% and 20% wt Algae content cases

	10% Algae content		20% Algae content	
Energy consumption	Optimized flowsheet	Thermodynamic Target	Optimized flowsheet	Thermodynamic Target
Heating (MW)	3.64	3.31	2.26	1.98
Cooling (MW)	2.62	2.29	1.98	1.70
Energy Input (kJ/g BioCrude)	Optimized flowsheet	Thermodynamic Target	Optimized flowsheet	Thermodynamic Target
Heating (kJ/g BioCrude)	11.42	10.38	7.07	6.20
Cooling (kJ/g BioCrude)	8.22	7.18	6.20	5.33

Based on the pinch analysis, we are now able to compare the energy consumption between the 10 wt% and 20 wt% solid content algal slurries in the SEQHTL process. A comparison of the energy consumption of 10 wt% and 20 wt% algal slurries is found in Table 5.9-10. We see that more than 50% of the energy consumed in the SEQHTL process is heating. When the solid concentration increases, the energy consumption decreases. The total energy consumed in the SEQHTL process for the 20 wt% algal slurry case is much less than that of 10 wt% algal slurry case – that is, it is only 68% in the model and 66% in the target.

The energy performance of the optimized flowsheet is slightly higher than that of the thermodynamic target, indicating small potential to improve. It is acceptable at the concept

design phase. The thermodynamic target of the utility consumption is the energy limit of the SEQHTL process, i.e. the least load of the heating and cooling utilities. So this data is taken for estimating the operating cost of the SEQHTL process.

Shear-thinning viscosity study for algal suspension from SEQHTL

Accurate physical properties are essential for modeling most of the system, but become critical in the SEQ/HTL section. They are rarely available. Problems are known to be associated with pumping and with heat transfer in high concentration algal slurries and treated algal suspensions, primarily in the 10 to 20 wt% concentration range [14] [15] [16]. These problems arose during the course of these would be evident in the HTL experimental work at WSU and ASU. It seemed possible, indeed likely, that these suspensions would be pseudoplastic, i.e. show a shear thinning effect and. Some rapid tests were carried out at WSU and ASU to test this hypothesis. They confirmed the strong shear-thinning effect in the range 5 to 20% of *Chlorella* suspensions (see Figure 5.9-41). It indicated that a stirred vessel would not be suitable for the reactor design. Rather, a tube design acting as a plug flow vessel was strongly recommended.

Tests at WSU also examined the treated algae suspensions for Stage 1 of the SEQHTL process where problems had also arisen. The reported results (Figure 5.9-42) of the WSU tests showed a large amount of scatter, far beyond anything that could be associated with experimental error. This scatter was thought to be due to a high degree of structure existing in the TA (treated algae) that is unstable and depends on the mechanical history of the sample. If this was the case, then it could be expected to make filtration difficult. It could also give rise to significant heat transfer problems, as have been reported. The large degree of scatter on the other hand suggested that the mechanical strength of the structure was comparatively low and it would not take much to break it up. A simple mechanical stirrer was recommended to assist the WSU team to address their problems.

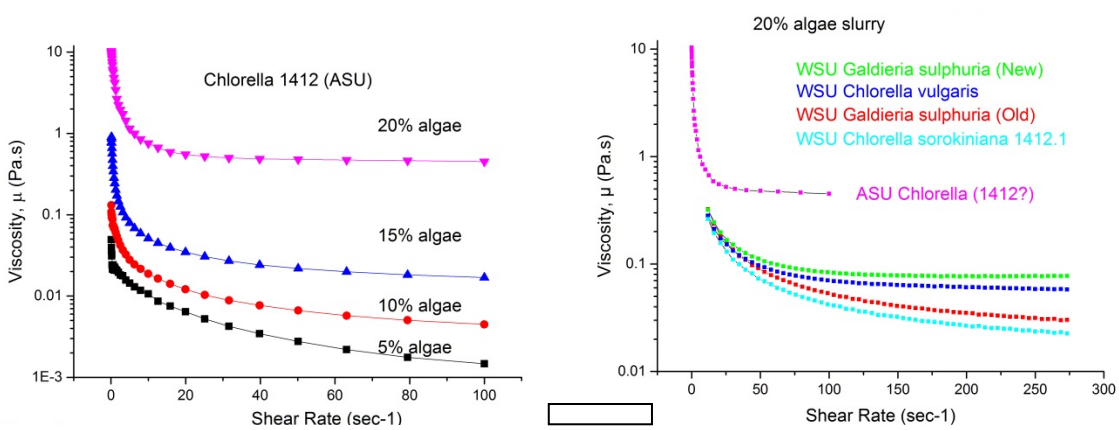

Figure 5.9-41: Results from ASU and WSU that confirm the strong shear-thinning effect in the range of 5 to 20% of the *Chlorella* suspensions. Note the logarithmic y-axis.

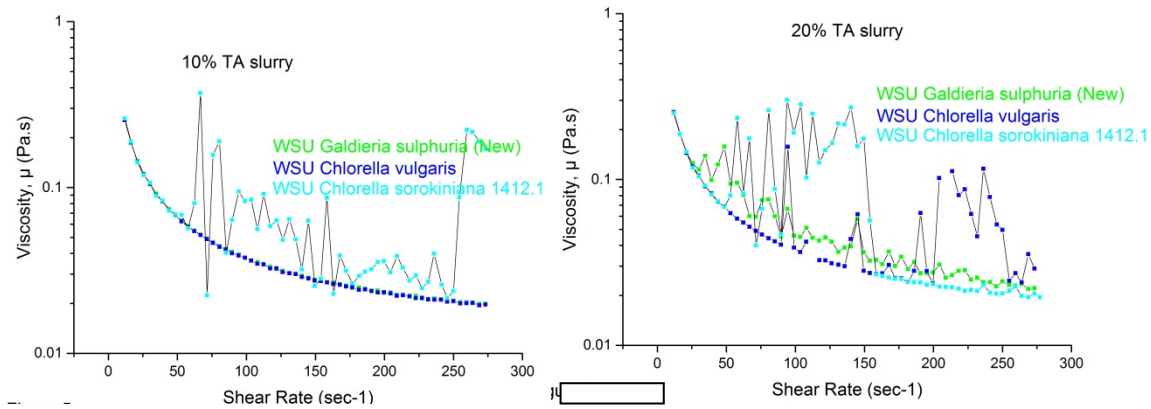

Figure 5.9-42: Results from WSU showing a large amount of scatter suggesting a high amount of structure in the treated algae (TA).

Manual for SEQHTL (supplementary material)

DHTL:

Aspen Plus models of DHTL to investigate the utility consumption of the DHTL process and the N and P recycle

Energy analysis of the DHTL process

Like the SEQHTL process, the energy performance of the DHTL process is also important for the TEA and LCA. The optimized DHTL flowsheet is referred to the literature [Case D of the NERL report 30352, the lowest capital cost and lowest operating cost case]. The biogas, biocrude, biochar are separated in the three phase separator (SEP-401) and the hot water stream heats the algal slurry in E-401. The preheated algal slurry is then heated by E-402 to 300ºC before entering into the DHTL reactor. Then the water products were cooled by E-403. The heating load is only for E-402, and the heating utility consumption is 7.66 kJ/g biocrude.

Nutrient recovery study in DHTL

The products of the DHTL process are the bio-crude, biochar, biogas and the water soluble species. The ASU group investigated the DHTL process water recycle to enhance the bio-crude yield as discussed in Section 5.7. The bio-crude yield was increased 5-10% when the water obtained in the initial HTL experiment was used as the water in the recycle run. The ASU group considered that this increase was due to the catalytic effect of the water soluble compounds such as acetic acid on the conversion process. Besides the catalytic species, there are some nutrients remains in the water product that need to be recycled or reused. The N and P recycle rate is defined as the fraction of the weight remains in the water product to that of the feed in algae. The nutrient recovery of the DHTL process is one of the important issues to consider as a means to

reduce the consumption of the nutrient and reduce the impact to the environment. The N and P recycle rate is one of the key performance areas in the Technical/Financial discussion.

The experimental and elemental analysis of the biomass components data are from ASU group. The DHTL flowsheet is shown in Fig 5.9-43. The yield for the algal biomass is shown in Table 5.9-12 and the elemental analysis results are summarized in Table 5.9-13. There are some missing data from the raw data and these data have to be adjusted and reconciled to fill into the Aspen model. The data reconciliation procedure is summarized in the supplementary material.

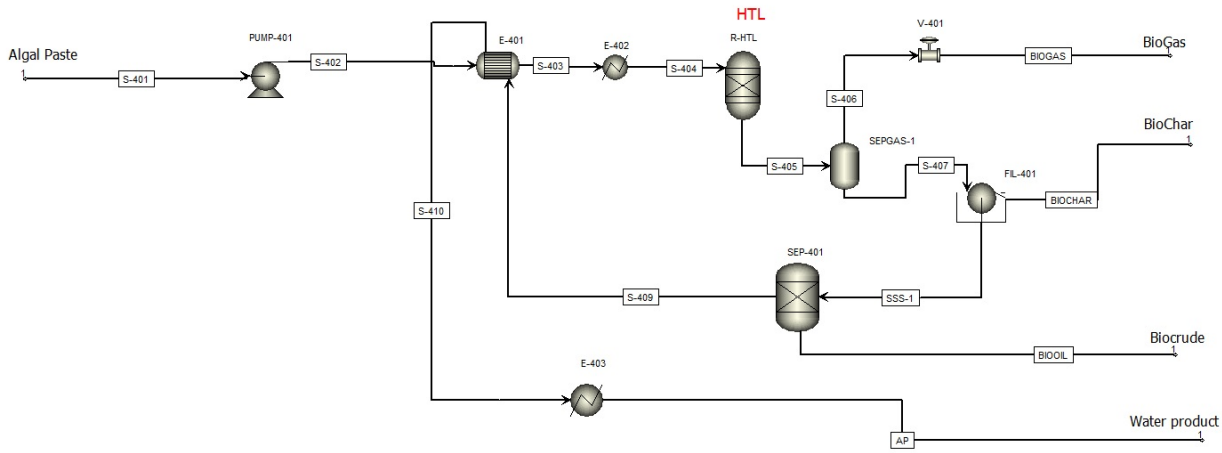

Figure 5.9-43: DHTL flow diagram

Table 5.9-12 DHTL yield*

		Kirschneriella	*Chlorella*	*Galdieria*
DHTL	Biocrude yield (% DW algae)	41.0	24.9	31.2
	Biochar yield (% DW algae)	14.2	17.9	4.9
	Water product (% DW algae)	14.7	10.4	8.2
	Gas product by different	30.1	46.8	55.7

*The yield of the DHTL process is obtained from ASU data

Table 5.9-13 Elemental analysis results of the DHTL experiments*

		C	H	N	S	O (by difference)	P (mg/g)
Kirchneriella	Algae	0.515	0.060	0.059	0.011	0.355	0.01402
	Biocrude	0.766	0.090	0.052	0.013	0.079	0.00011
	Biochar	0.660	0.039	0.042	0.007	0.252	0.03151
	Water product						0.08623
Galdieria	Algae	0.460	0.049	0.091	0.016	0.385	0.01410
	Biocrude	0.736	0.088	0.078	0.020	0.078	0.00013
	Biochar	0.586	0.064	0.077	0.015	0.258	0.03801
	Water product						0.10361
Chlorella	Algae	0.492	0.065	0.054	0.011	0.378	0.03006
	Biocrude	0.750	0.061	0.063	0.011	0.115	0.00051
	Biochar	0.651	0.053	0.058	0.007	0.232	0.05022
	Water product						0.16456

The bio-crude productivity is set at 4,300 kg/hr, which gives the annual productivity at 10 million gallons. The elemental flow of N and P for each strain can then be calculated by the Aspen model. The results are collected in Table 5.9-14.

Table 5.9-14 N and P flow rate and recycle rate of the DHTL process

			N flow rate (kg/hr)	P flow rate (kg/hr)
Kirschneriella	Feed in	Algae	805	192
	Out put	Biocrude	293	1
		Biochar	81	61
		Water product	430	130
		Biogas	0	0
	Recycle Rate		**53%**	**68%**
Chlorella	Feed in	Algae	1255	694
	Out put	Biocrude	361	3
		Biochar	238	207
		Water product	656	484
		Biogas	0	0
	Recycle Rate		**52%**	**70%**
Galdieria	Feed in	Algae	1699	264
	Out put	Biocrude	453	1
		Biochar	70	35
		Water product	803	229
		Biogas	373	0
	Recycle Rate		**47%**	**87%**

5.9.5 Milestone 1.3.3 – Techno-Economic Analysis (TEA)

TEA Modeling basic approach

One purpose of developing a process model of the REAP process in Aspen Plus is to provide the basis for the TEA. We therefore take the fully converged Aspen process model and collate data into an Excel spreadsheet.

Two steps are then used to analyze these outputs:

Step 1 – General Process Costing: We take a fully converged Aspen process model of the REAP and use the Aspen Economic Analyzer as the basis for the Capex and Opex estimations. The spreadsheet pulls data from disparate sections of the Aspen output of the REAP process, data checks them for mass and energy balance and internal consistency and then develops summary tables. The important tables in terms of the REAP TEA process are the costing routines particularly for piping and pumping, as well as factors pertaining to construction costs.

Step 2 – Financial Analysis: The outputs from Step 1 are collated into a different section of the spreadsheet for further detailed financial analysis. This financial analysis has three parts: 1. Estimated OPEX margins; 2. Cash flow analysis including DCF; and 3. Financial metrics including the use of tax shields in line with industry standards.

Financial model basis

This financial analysis is reported using the standard methods of NREL [1] and those based on industry standards developed by Pan Pacific as part of technical and financial modeling of algal biofuels.

There are a number of components used in the analysis. These are now described.

Capital cost estimation

The capital costs are gathered from a variety of sources:

- The mass and heat balance generated by the Aspen model are used to determine the size of the equipment needed. These are entered into the Aspen Economic Evaluation software to determine the installed capital cost.
- In addition, some selected equipment cost data is drawn from either budgetary estimates or from published literature

The scale is adjusted to match the appropriate scaling term by using the exponential law:

$$\text{Scaled equipment or plant cost } = \text{cost at orginal scale } \times \left(\frac{scale\ up\ capacity}{original\ capacity}\right)^n$$

Where 'n' is the scale factor and is normally 0.7. The exponential law is also applied to the scale-up or scale-down of the entire plant. In order to compare the costs for varying strains, bio-crude capacity is scaled to 10 million-gallon/yr for each model of the strains.

Cost-Year Indices

The cost-year 2011 is applied consistently across all DOE-BETO platforms for which similar "design case target" reports are being established during 2013-2015 efforts, and it is expected that performance goals and TEA outputs will remain in 2011 dollars through to 2017 to permit effective and accurate comparisons of future feedstock, conversion technologies, and other alternative scenarios. However, it is the cost-year of 2013, which provides the majority of equipment costs from the Aspen Economic Analyzer V8.4. Other equipment costs provided from literature are cost-years; 2011 (for the HTL equipment costs as published in 2013 [17]); and 2014 (for the majority of the cost estimation of the VPBRs and HPBRs).

Capital costs provided in years other than 2011 dollars were adjusted using the Plant Cost Indexes from chemical engineering published data [Chemical Engineering Plant Cost Index (CEPCI). Chemical Engineering, April 2015; 80] to the common basis year of 2011. Employee salaries were scaled using the labor indices provided by the US Department of Labor; Bureau of Labor Statistics Labor Indices Series ID CEU3232500008, available from http://data.bls.gov/cgi-bin/srgate]. The link details the general formulae for converting nominal values to real values and for adjusting dollars to a common basis and is as follows:

$$2011Cost = (Base\ Cost)(\frac{2011\ Cost\ Index}{Base\ Year\ Index})$$

Financial model estimation

The key assumptive parameters of the financial model are similar to other recently published design reports under DOE-BETO efforts [1] [17]. These parameters include:

1. Design and construction time: 36 months

2. Facility start-up time: 6 months

3. Cost-year dollar basis: 2011 dollars (Note* all cost results presented here will be in 2011 dollars)

4. Facility on-stream time: 90% (330 days/yr or 7,920 hours/yr). This is intended to represent an nth-plant facility and may be higher than can be realistically achieved today, particularly when considering the strain rotation of the cultivation system. This on-stream factor assumes year-round operation with approximately one month per year allocated to facility shut down, either for scheduled maintenance or other downtime factors.

Facility capacity definition and process capital cost estimation

Aspen Plus is the modeling software of the integrated REAP process. Wherever there is a lack of available data, for example, the physical property and thermodynamic data of the biomass, we systematically address these gaps by drawing on our expertise with major engineering groups in the area of bioprocess design [supplementary material methodology for computing the thermodynamic data of the SEQHTL process]. The raw data of the process is extracted from the converged end-to-end Aspen Plus model and then converted into useable engineering and financial data. Most of the equipment costs reported in this section are from the Aspen Economic Analyzer V8.4. The costs described in this Section are adjusted to the required equipment size and the cost-year is the 2011 dollar.

Definition of facility capacity

The REAP process begins with algal biomass grown and harvested from the PBRs under continuous steady-state conditions. The PBRs allow a high cell concentration to be harvested. In the design assumption, biomass is harvested at a culture density of 2.0 g/L AFDW for processing through to setting. Then the harvested algal biomass is dewatered and filtered to obtain a 20 wt% paste for a continuous DHTL process.

The product of this REAP project is the bio-fuel intermediate (bio-crude). The bio-crude productivity is a key parameter, with two important facets; the algal productivity and the DHTL conversion efficiency. In this report, the capacity of bio-crude is assumed to be 10 million gallons of bio-crude per year, and the PBR size (wetted area) is calculated by the bio-crude yield of the DHTL process and the average seasonal biomass productivity. In AzCATI several

different algal strains are cultivated in VPBRs in a natural environment to evaluate the productivity of each algal strain in different seasons. The seasonal strain rotation is a part of the REAP process design, however, in the conceptual design phase, the time gap of strain shifting in cultivation systems is ignored. A large quantity of selected algal strains are harvested, dried and sent to WSU and ASU for DHTL and SEQHTL investigation. In this report, DHTL is the baseline case and the SEQHTL process will be discussed as a case study in the later sections. Under optimized DHTL conditions, the yield of bio-crude for each selected strain is obtained.

The algal biomass productivity in VPBR system and the strain rotation are discussed in the previous Section 2. The algae yield is recorded in a volumetric basis in AzCATI, however, for the TEA study, the areal productivity of the algal biomass and the biocrude are interesting. To convert the volumetric productivity to an areal productivity of the biomass, the scaling up of the experimental VPBR system is taken into consideration.

The monthly strain rotation has also been discussed in Section 2.1. The organism selection is firstly based on the monthly average growth rate, then considers minimization of strain changes for a realizable crop rotation at scale. As a result, *Kirschneriella* is selected for winter, November to January, *Chlorella* for spring February to May and *Galdieria* for hot seasons May to September. In May, there are two algal strains with comparable performance for a smooth changeover. For TEA estimation, *Galdieria* is selected for May because of a higher biocrude conversion yield. The yearly operating hours of the TEA is 7920 hours, i.e. 330 days, therefore, the entire month of October and the last four days of September are allocated for maintenance.

Algenol Biofuel has developed the VIPER™ system, which is a vertical PBR system using hanging bags as its reactor unit. The hanging bag unit is typically a 10 feet long plastic bag with 3 feet of the fluid level containing 50L of slurry. Algenol Biofuel recommends 0.38m as the spacing of the VIPER™ system. The picture of the VIPERTM unit and the recommended array are shown in Figure 2-4. Based on the scaling up assumption, the footprint of the VIPER™ system is 115L/m2. The areal productivity of the algal biomass is converted by the volumetric productivity multiplying the footprint of the VIPER™ system, which is 115L/m^2.

The algal biomass productivity and bio-crude yield of related biomasses are listed in Table 5.9-15 for the integrated VPBR cultivation with DHTL conversion process.

Table 5.9-15 Productivity of algal strains in VPBRs and the bio-crude yield.

	Strain	Biomass volumetric productivity (g/l/day AFDW)	Biomass aerial productivity [a] (g/m^2/day AFDW)	Bio-crude yield (mass fraction)
Nov-Jan	*Kirschneriella*	0.16	18.2	0.41
Feb-Apr	*Chlorella*	0.11	12.8	0.25
May-Sept	*Galdieria*	0.15	17.8	0.31
Oct	-			

a: The aerial productivity is calculated by the volumetric productivity multiplied by the footprint of the VIPER™ system.

5.9.5.1 Techno-Economic Analysis of Unit Operations

Area 100: Cultivation

VPBR scale up design and cost estimation

VPBR area and biocrude productivity estimation

All the data in Table 5.9.3-1 is used to determine the area needed for the wetted area of the VPBRs. Assuming the total working hours per annum is 7940 hours, or 330 days, this equates to a 90% production efficiency of total available annual hours. Therefore, bio-crude productivity is 4302 kg/hr for a 10 million gallon/per year bio-crude facility. The days of operation are in keeping with the strain rotation plan. It is 92 days for *Kirschneriella* from November to January, 89 days for *Chlorella* from February to April and 149 days for *Galdieria* from May to September.

The DHTL and SEQHTL of the algal biomass are investigated in ASU and WSU, and the results are discussed in Section 5.6 and 5.7. Since the DHTL showed a higher biocrude conversion yield, the baseline of the TEA is chosen to be the DHTL process. The TEA of the integrated process with SEQHTL is discussed as a case study later. The different strains obtained different biocrude yields, the conversion yield of *Kirschneriella*, planned for November to January is 41%, the conversion yield of *Chlorella*, planned February to April is 25%, and the conversion yield of *Galdieria*, planned May to September is 31%.

Since the biomass productivity varies from month to month and the biocrude conversion yield is different amongst the strains, part of the algal biomass produced in the high seasons needs to be dried and stored for the low season. The *Kirschneriella* shows the highest areal productivity and the highest DHTL conversion yield, therefore, the dried *Kirschneriella* can be used in other months, when the biomass productivity and biocrude yield are low, for example, *Chlorella*, in February to April. In this instance, there is co-liquefaction of *Kirschneriella* and *Chlorella* from February to April. The investigation of the co-liquefaction of two algal species (*Coelastrella* and

Chlorella) is discussed in Section 5.7.3. The results of the co-liquefaction showed higher yields than any of the individual organisms. For TEA work, we assume that the biocrude yield of the co-liquefaction of *Kirschneriella* and *Chlorella* is the average of those two individual microalgae. This is a conservative estimation. From May to September, an additional 64kg/hr algal biomass is required to reach the target DHTL capacity, which is less compared to the *Galdieria* production target. (6,835 kg/hr). The DHTL conversion yield of *Galdieria* is chosen for months May to September.

Based on the above assumptions and the operating arrangement, 4,530 acres of wetted area is required for the VPBRs to reach the biocrude capacity of 10 million gallons per year. Table 5.9-16 shows a summary of the biocrude capacity estimation based on a wetted area of 4,530 acres and the strains rotation.

The quantity of *Kirschneriella* needed to be dried from November to January is calculated to be 3,424 kg/hr, which is listed in Table 5.9.3-3. Considering 90% usage of drying capacity, the capacity of the algae drying facility is then defined to be 3,800 kg/hr, and the quantity of dry *Kirschneriella* is 7,560 tonnes. These calculation result in an estimation of 2,208 gallons biocrude per acre per year productivity. Assume the density of the biocrude is 900 kg/m^3 and the LHV of the biocrude is 33 MJ/kg, the energy output of the baseline case is 248 GJ/acre/yr.

Table 5.9-16 Bio-crude capacity estimation of VPBR scenario based on a wetted area of 4,530 acres. The annual biocrude productivity is 2,208 gal/acre/yr.

Table 5.9-16 Bio-crude capacity estimation of VPBR scenario based on a wetted area of 4,530 acres. The annual biocrude productivity is 2,208 gal/acre/yr.

	Strain	Biomass productivity (g/m^2/day AFDW)	Bio-crude yield (mass fraction)	Operation days	Biomass produced (kg/hr)	Biocrude converted (kg/hr)	Gap to defined bio-crude productivity (kg/hr)*	Dry biomass required (kg/hr)**	Total dry biomass required (tonnes/season)	Biocrude produced (million gal/season)
Nov-Jan	*Kirschneriella*	18.2	0.41	92	13,916	5,705	1,404	-3,424	-7,560	2.79
Feb-Apr	*Chlorella*	12.8	0.33***	89	9,764	3,215	-1,087	3,301	7,052	2.70
May-Sept	*Galdieria*	17.8	0.31	149	13,621	4,252	-49	158	563	4.51
Annual Total				**330**						**10.00**

* a negative value means a less quantity of bio-crude converted than the defined DHTL capacity.
** a positive value means additional dry biomass is required
*** the biocrude conversion yield is estimated to be an average of *Kirschneriella* and *Chlorella*

Scale up the VPBR layout and cost estimation

PPT has modeled the orientation of the VPBR [3DMax model of panels in a 24 month report]. The North-South orientation is far better than the East-West orientation. All the VPBR panels should be orientated in the North-South position

Scale up Algenol VIPERS™ type reactors

VIPERS™ type reactor is a vertical bioreactor newly developed by Algenol Biofuel. The HB reactor used in AzCATI is the same unit as the VIPERS™ bioreactor. The unit (10 feet long, 36 inches high and has a 50L working volume) and recommended block placement by Algenol Biofuel are illustrated in Figure 5.9-44. Algenol has demonstrated a 2000-acre model for the VPBR layout. In that model, 4500 PBRs are placed in a block and 24 blocks are arrayed around a field process pad where gas and liquid management equipment serving the array of 24-blocks.

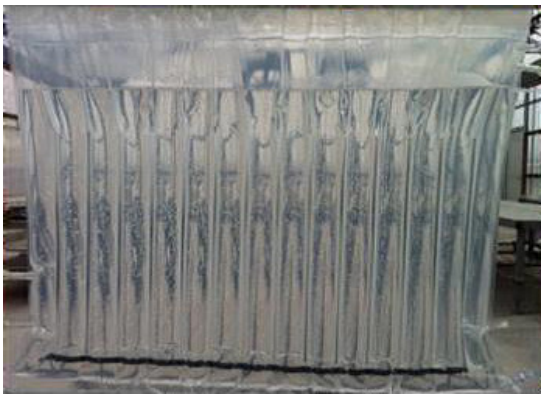

Figure 5.9-44 VIPERS™ vertical bioreactor unit (Left) and VIPERS™ system array (Right)

In Algenol's layout, the VIPER™ bags are hanging on a steel bar and supported by the wooden poles outside of the array. For convenient costing of the PBR system, we recommend using steel poles instead of wooden poles since the material and labor cost of light steel structure is available, and we suggest a 20-acre VIPERS™ system as a block and it is illustrated in Figure 5.9-45. The VIPERS™ units are placed at North-South orientation and the spacing is the same as the Algenol's recommendation, 0.38m spacing.

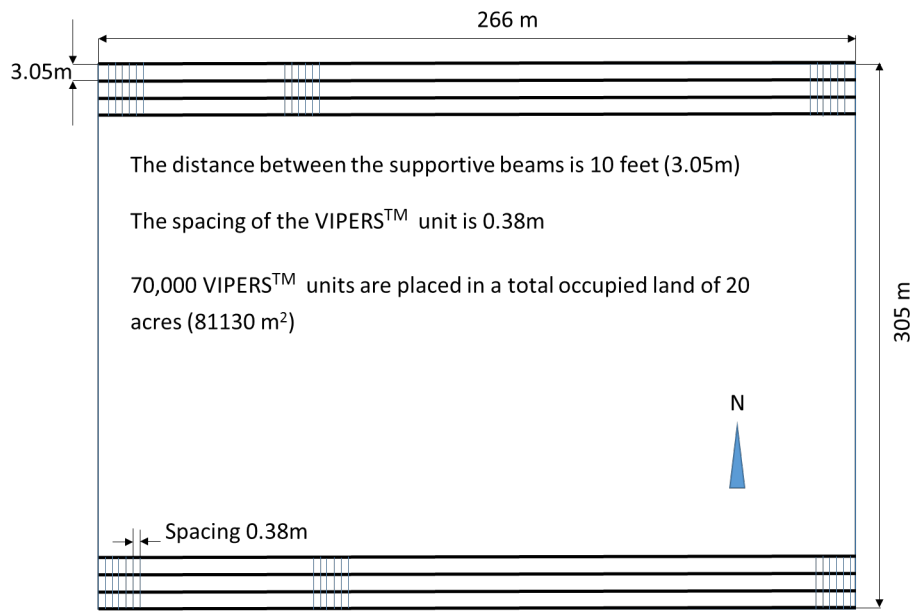

Figure 5.9-45 Illustration of 20-acre VIPERS™ type VPBR placement

The material and labor cost for the frame of the VIPERS™ type VPBR unit is estimated according to 2014 Front-End / Conceptual Estimating Yearbook (Compass International Consultants Inc., Morrisville, Pennsylvania, USA). For detailed estimation information refer to supplementary material. The breakdown of the capital costs of both VPBR systems for 4,530 acres is illustrated in Table 5.9-16. The overall capital cost for the VIPERS™ type VPBR system is $253,992,901, equivalent to $56k/acre. The range of the capital cost of the raceway pond is from $19k/acre to $48k/acre depending upon pond design. The cost of the VPBR is higher than that of the raceway pond, which is the biggest investment in the entire process. Increasing the productivity of the VPBR's is proving the biggest challenge to date.

Table 5.9-16 Breakdown capital cost for 4,530 acres of VPBR with VIPERS™ reactor design. (All the costs are in 2011 dollars)

Reactor type	Frame Material and labor	Plastic bags	Piping	Civil and others	Installed Cost
VIPERS™	$113,991,000	$31,710,000	$45,596,000	$62,695,000	$253,993,000

Other process capital cost estimation for cultivation

CO_2 delivery

This section describes the assumptions of CO_2 delivery to the site and injection to the cultivation system. In order to promote the high biomass growth rates required to achieve economical production of biocrude, supplementary CO_2 must be delivered to the cultivation system. In the REAP project, the CO_2 source is assumed to be the bulk flue gas delivered via low-pressure pipelines from a processing plant nearby. There is no off gas recirculation involved in the REAP integrated model.

The CO_2 capture is modelled by the Aspen Plus in the REAP integrated model. The average CO_2 capture rate is 85%. The conversion ratio of CO_2 to biomass is 6.7 kg CO_2/kg algal biomass. The average fluegas demand of the REAP facility is 4,800 tonnes/day. The modelled fluegas delivery system consists of a compressor and 5 mile (8 km) pipelines for flue gas delivery from a processing plant nearby.

For the base case, the cost of CO2 including compression and transportation via pipeline is set at \$45/tonne CO_2, which refers to the cost of captured CO_2 [18.]. The cost of compressors is from the Aspen Economic Analyzer, which is \$2.8MM installed (2011 dollars). The cost estimation of the HDPE pipelines is from consultation with senior engineers of a pipeline cooperation. The installed cost of the 8 km of pipelines for REAP CO_2 delivery is \$19.1MM (2011 dollars). Total installed equipment cost including civil, electric and instrumentation for this section is \$21.1MM (2011 dollars).

Make up water delivery

The strains used in REAP project are fresh water strains. The make up water is used mainly for compensating the evaporation and a minor amount is discharged as blowdown. The water is delivered from a nearby local water resource by pipelines. The acidity of the makeup water is adjusted by NaOH for pH8 or H_2SO_4 for pH2.5. This section consists of details of the pumps for make up water and a NaOH / H_2SO_4 solution and 5,000m of pipelines for water delivery to the cultivation system.

The peak flowrate of make up water in summer for growing enough algal biomass for a 10 million gallon per year bio-crude facility is 650 m^3/hr. Aspen Economic Analyzer calculates the installed cost for make up water pumps is \$116.9k and for the NaOH / H_2SO_4 pump is \$35.8k. The cost for an installed 5,000 m water pipeline is \$4.2MM. Total installed equipment cost including civil, electric and instrumentation for this section is \$5.1MM (2011 dollar).

Area 200: Dewatering and water recycle

Dewatering

Harvesting and dewatering algal biomass is always challenging due to the small size of algal cells, having a similar density to water and a low concentration. Typical cell concentration of a PBR system is 2-5 g/L. In the REAP model, the harvesting concentration of the algal biomass is set to be 2-2.5 g/L, because the algal biomass keeps a high growth rate in this concentration range. Many methods of harvesting and dewatering strategies have been investigated, include settling, membrane filtration, screen filtration, flocculation, centrifugation, filter press, and ultrasonic separation etc. This report describes the dewatering operations included in the Aspen Plus model and consists of settling and belt filter press operations. The design basis and capital cost estimation of the dewatering units are summarized in Table 5.9-17.

Table 5.9-17 Summary of performance and cost of dewatering units

	Inlet flowrate [a] M^3/day	Outlet concentration g/L AFDW	Installed Cost $MM	Energy Demand kWh/m^3
Settling	88,750	5	5.2	Negligible [b]
Belt Filter Press	35,448	200	2.5	0.05

a. Flow rates shown here are for peak summer season (May to September), which sets the design basis for equipment capacity.
b. Primary power demand for the settler is for inlet and outlet pumping, not reflected here for operational power of the settler.

Recently, Global Algae Innovations, Inc. demonstrated the Zobi Harvester, which is a membrane filtration system with high harvesting efficiency and as low as 0.04 kWh/m^3 energy demand (email communication). It is likely to become a competitive technology as the harvesting efficiency it demonstrated. The harvesting efficiency of the Zobi Harvester for the three algal strains need further investigation, in this report, the reference costs [1] [19] are used for the capital cost estimating of the dewatering facilities.

Water recycling and discharge

The clarified water from the dewatering facility is collected and routed back to the PBRs via a series of pumps and pipelines. During the peak summer season, the flow rate of the combined water for recycling is calculated at 4,900 m^3/hr (21,574 gal/min). Aspen then calculates the circulation pumping power needed to recycle the clarified water through the pipeline network. Aspen models the pump efficiency for the facility pipelines at 85%, with the total power demand being 105 kW for the overall facility.

Only a single pipeline network is considered in the facility design for normal water circulation. No additional pipeline systems are included to allow for such events as a PBR leakage / disposal. It is assumed that each individual PBR will be isolated by regulatory valves on both the feed and harvest lines and a damaged PBR would be drained, assessed and repaired or replaced as necessary by a maintenance team. To mitigate a buildup of salts and other inorganics, 5% of the combined clarified water is discharged as blowdown.

The breakdown costing of the estimated equipment cost for this section is summarized in Table 5.9-18. All the equipment cost estimation is from Aspen Economic Analyzer. The total installed equipment cost is $7.9MM (2011 dollar-cost).

Table 5.9-18 Breakdown capital cost of the dewatering, water recycling and discharge facilities. (all costs are in 2011 dollar-costs.)

Operation unit	Equipment Cost	Installed Cost
Settling	$655,662	$655,662
Filter press	$3,214,801	$3,214,801
Harvesting pump	$339,423	$1,583,660
Recycling pump	$202,366	$1,059,171
Discharge pump	$99,239	$462,398
Discharge pipe	$921,476	$921,476
Total	**$5,432,967**	**$7,897,169**

Area 300: Algae drying and storing

As discussed in the previous sections, the algae drying operations are important for keeping a stable operation of the entire DHTL process. The drying capacity for the baseline case is 3,800 kg/hr, and storage capacity is 7,560 tonnes/yr. The algae is dried using hot air from a spray dryer at 95 degree C. It is then cooled on a moving conveyer belt, and then the dry algae is stored in silos. The drying and storage capacities are the basis for estimating the equipment costs. The power for the compressor is 3.85kW, and the utility demand of the furnace for heating air is 1.77MW, all the energy data are given by the Aspen model.

The equipment list of this section and costs estimated by the Aspen Economic Analyzer are summarized in Table 5.9-19.

Table 5.9-19 Breakdown of capital costs of the algae drying facility, 3,800 kg/hr drying capacity, 7,560 tonnes/yr storage capacity, all costs are in 2011 dollars.

Operation unit	Equipment Cost	Installed Cost
Dryer	$647,158	$970,737
Furnace	$146,983	$587,931
Cooler	$34,136	$102,407
Silo *8	$960,143	$1,632,243
Compressor	$556,258	$742,130
Total	**$2,344,678**	**$4,035,448**

Area 400: Downstream biocrude conversion process - DHTL

The DHTL process is the algae biomass conversion procedure involved in the REAP design. The investigation of the reaction conditions in the process have been undertaken by Dr. Deng of ASU. The laboratory process is the design modeling basis of the DHTL process.

The capacity of the DHTL facility is 10 million gallons per year, i.e. 4,302 kg bio-crude/hr (1,263 gal/hr). The material and energy balance of the optimized Aspen Plus model for *Galdieria* is the cost estimating basis of the DHTL process. The capital cost for the DHTL process is based on vendor budgetary estimates from the National Advanced Biofuels Consortium (NABC) for wood based HTL systems [17]. The original NABC costing data were scaled to the whole algae HTL rate. The HTL reactor used in batch mode in ASU is a stirrer autoclave and used a plug flow reactor in the continuous HTL investigation. The HTL reactors are a jacketed serpentine pipe with a heating medium in the annular space. This is similar to a double pipe heat exchanger or the serpentine reactors used for low density polyethylene manufacturing [Exxon 2014]. In the batch experiment, the optimized reaction time is 30 minutes, therefore, when scaled up, 30 minutes is assumed to be the retention time of the material in the continuous plug flow reactor. This retention time is equal to the LHSV (Liquid Hourly Space Velocity) of 2 L/L/h. In PNNL' report [17], the LHSV chosen has been discussed, because it affects the size of the reactor. In that report, 4 L/L/h is the baseline design of PNNL's assumption. However, in the continuous DHTL experiments in ASU, low biocrude yield is recorded at the retention time of 20 minutes, i.e. 3 L/L/h of the LHSV. Therefore, in this section, 2 L/L/h of the LHSV is chosen for estimating the capital cost of the HTL reactor assuming the same yield of the batch mode.

The electricity energy for pumping the 20%wt algal biomass slurry to 100 bar is estimated to be 198kW by the Aspen model and the heating utility of the DHTL process is 7.66 kJ/g biocrude by the Aspen Energy Analyzer.

The metallurgy of the NABC costing data (316 stainless) is the same as that used in the algae experimental work. The scaling assumptions and the installation factors used are the same as those discussed in the literature [17]. The equipment list of this section and the costs estimated are summarized in Table 5.9-20.

Table 5.9-20 Breakdown of capital costs of the DHTL process, all costs are in 2011 dollar

Operation unit	Equipment Cost	Installed Cost
R-HTL	$2,397,919	$4,795,838
E-401	$2,160,897	$4,753,974
E-402	$9,906,615	$21,794,554
E-403	$5,515,324	$12,133,712
Filter-401	$1,720,999	$2,925,698
Sep-401	$1,712,360	$3,424,720
Pump-401	$363,031	$834,972
Total	**$23,777,146**	**$50,663,468**

5.9.5.2 Techno-Economic Analysis of REAP Process

A fundamental rule of chemical engineering design is to start with the analysis of a fully converged mass and energy balance. This is especially true for the financial analysis. This approach is used as the starting point for the REAP Techno-economic Analysis (TEA). The method for this analysis is based on a proprietary analytical tool in the form of an industry-validated spreadsheet developed by Pan Pacific. This spreadsheet includes sections for costing and financial analysis for TEA based on the harmonized model used by the Department of Energy as the benchmark for TEA of algal processes. This method is therefore used in the initial analyses.

The output data of the integrated system model is used as the key input data of the REAP TEA. Information for the REAP TEA is also drawn from Aspen Economics Analyzer and other public literature [Compass 2014 Front-end/Conceptual Estimating Yearbook], [17] [1] when other databases are insufficient, especially in the early stages of a project.

The purpose of developing a process model of the REAP process in Aspen Plus is to provide a basis for the TEA, that in turn will provide the basis for the Capex and Opex estimations for the process.

In previous sections, we took the Aspen model and use the Aspen Economic Analyzer and other literature to determine the size of the major equipment needed. In this section, the equipment costs are summarized and then calculated to the total capital investment (TCI). The variable and fixed operating costs are then calculated. These results are then collated to determine the minimum biocrude selling price (MBSP) by a discounted cash flow analysis. The MBSP is required to obtain a zero net present value (NPV) with a finite internal rate of return (IRR), i.e. for the given IRR target, NPV is zero after the end of the 30-year facility lifetime. The following section summarizes the assumptions made in completing the discounted cash flow analysis.

Total capital investment (TCI)

The equipment costs and installed costs of individual processing areas are described in Section 5.9.3 of this report. All the costs provided in Section 5.9.3 have been adjusted to actual size by an exponential scaling expression.

Once the total equipment cost has been determined in the year under review, direct and indirect costs are added to determine the total capital investment (TCI).

Firstly, direct cost factors are applied relative to installed costs to determine total direct costs (TDC). These include warehouse allowances, site development and additional piping. Indirect cost factors including field expenses, office, engineering and construction activities, contingency and other related costs are calculated relative to TDC and summarized to obtain the fixed capital investment (FCI).

Finally, the FCI is combined with working capital (5% of the FCI). Then land costs are added to give the TCI. In NREL biorefinery design reports [17] [20] [21], the direct and indirect costing

factors were based on separating the costs attributed to the process areas falling inside battery limits (ISBL) and those falling outside battery limits (OSBL) of the facility. The new NREL report [1] about the process design and economics of algal biomass used three categories of factors to estimate the TCI. The REAP project has a similar situation. Category One includes cultivation facility (PBRs). Category Two consists of dewatering, algae drying and DHTL facilities. Category Three is the OSBL facilities (flue gas delivery and make-up water delivery). The factors of the three facility categories are summarized in Table 5.9-21

Table 5.9-21: Additional direct costs and indirect costs for determining TCI

Item	Description	Dewatering, Algae drying and DHTL	PBRs	OSBL (flue gas delivery and make up water delivery)
Additional Direct Costs				
Warehouse	On-site storage of equipment and supplies	4% of installed cost	1.2% of installed cost of PBRs	0%
Site development	Fencing, curbing, parking lot, roads, drainage, general paving. This allows for minimum site development assuming a clear site with no unusual problems.	9% of installed cost	Included in PBR cost estimation	$1,534/acre (roads and fences)
Additional piping	To connect ISBL equipment to storage and utilities	4.5% of installed cost	Included in PBR cost estimation	0%
Indirect Costs		% of TDC of the three areas	% of TDC of PBRs	% of OSBL TDC
Pro-ratable expenses	This includes fringe benefits, burdens, and insurances of the construction contractors.	10% of TDC	4% of TDC	1% of TDC
Field expenses	Consumables, small tool and equipment rental, field services, temporary construction facilities, and field construction supervision	10% of TDC	4.5% of TDC	1% of TDC
Operating and construction expenses	Engineering plus incidentals, purchasing, and construction	20% of TDC	10.3% of TDC	1% of TDC
Project contingency	Extra cash on hand for unexpected expenses arising	10% of TDC	10% of TDC	10% of TDC

	during construction			
Other costs	Start-up, commissioning costs. Land acquisition costs, rights of way, permits, fees, statutory charges. Piling, soil compaction, unusual foundations. Sales, usage and other taxes. Freight, insurance in transit, and import duties on equipment. Overtime wages during construction. Field insurance. Project team costs. Transportation equipment, bulk shipping containers, plant vehicles, etc.	10% of TDC	2.6% of TDC	1% of TDC

Table 5.9-22 Project cost worksheet including Total Direct Costs and Total Capital

Process Area	Purchased Cost	Installed Cost PBR	Installed Cost Dewatering, Algae drying, DHTL	Installed Cost OSBL	Total Installed Cost
Cultivation PBR($MM)	$114.0	$254.0			$254.0
Flue gas delivery ($MM)	$19.9			$21.1	$21.1
Water delivery ($MM)	$4.4			$5.1	$5.1
Dewatering ($MM)	$5.4		$7.9		$7.9
Algae drying ($MM)	$2.3		$4.0		$4.0
DHTL ($MM)	$23.8		$50.7		$50.7
Totals ($MM)	**$169.9**	**$127.4**	**$62.6**	**$26.2**	**$342.8**
Site Development ($MM)		NA	$5.6	$2.8	$8.4
Warehouse ($MM)		$3.0	$2.5	NA	$5.6
Additional Piping ($MM)		NA	$2.8	NA	$2.8
Total Direct Costs (TDC) ($MM)		**$257.0**	**$73.6**	**$29.0**	**$359.6**
Pro-rateable Costs ($MM)		$10.2	$6.3	$0.3	$16.7
Field Expenses ($MM)		$11.4	$6.3	$0.3	$18.0
Office and Construction Fees ($MM)		$26.2	$12.5	$0.3	$38.9
Project Contingency ($MM)		$25.4	$6.3	$2.6	$34.3
Other Costs (Start-Up, Permits, etc) ($MM)		$6.6	$6.3	$0.3	$13.1
Total Indirect Costs ($MM)		**$79.8**	**$37.6**	**$3.7**	**$121.0**
Fixed Capital Investment (FCI) ($MM)		**$336.8**	**$111.1**	**$32.6**	**$480.5**
Land ($MM)					$17.7
Working Capital ($MM)					$24.0
Total Capital Investment (TCI) ($MM)					**$522.2**
Lang Factor (FCI/Installed Cost)					1.4
TCI per Annual Gallon Biocrude					$52.22/Gal
TCI per annual energy of biocrude					$0.470/MJ biocrude

Applying the direct and indirect cost factors listed in Table 5.9-21 to the capital cost of the facilities as discussed previously, the Total Capital Investment (TCI) of the integrated process of REAP is currently estimated at $ 522.2 MM. Assume the density of biocrude is 900kg/m^3 and the LHV of the biocrude is 33MJ/kg, the TCI per annual energy of the produced biocrude is $0.470 per MJ of biocrude. From Table 5.9.4-2, the major capital investment is the VPBRs, half of the total FCI. The resulting ratios: FCI to installed costs are 1.3 for the PBRs: 1.8 for dewatering, algae drying and DHTL: and 1.3 for OSBL: The total FCI to total installed cost ratios are 1.4 for dewatering. Algae drying and DHTL process ratio is 1.8, which is similar to a typical biorefinery design. However, the resulting FCI to installed cost ratios of PBRs and OSBL are lower. The main reason is most of the piping and civil costs are already contained in the cost

estimations of PBRs and OBSL, and the smaller direct and indirect cost factors of the PBRs and OSBL are already included in the TCI estimates.

Total operating expenses

Variable Operating Costs

Variable operating costs: include flue gas, nutrients, other raw materials, power demand and utilities, which are incurred only when the process is operating. For the algal cultivation facility modeled in this report, variable operating costs of raw material consumption vary with algal biomass production. The algae drying facility operates only in the high season, therefore the power demand of this unit is only calculated for the high season. Quantities of raw materials used for cultivation are determined by the Aspen Plus material balance, based on running individual Aspen models for each algal biomass rotation, then scaled to the area of 4,530 acre and summarizing the operating hours in each rotation period and then determining the net annual raw material costs, power demands and utility demands. The power demands and utility demands of the DHTL facility are estimated based on the separate 10 MGY biocrude DHTL model then adding in the total annual variable operating cost summary. Additional energy for the gas management of the PBRs has been determined by Algenol. The gas management includes the compressors and piping required for aerating the PBRs. The aeration energy consumption is discussed in the LCA in Section 5.8, which is 9.6Wh/PBR/day at 0.034 vvm aeration rate. For the base case, there are 1.6×10^7 PBRs in the 4,530 acre of the wetted land, the hourly average electricity consumption is 6,342 kW. The additional energy consumptions of gas management is involved in the utility use.

Table 5.9-23 shows the hourly usage of the raw materials and the utilities.

=

Table 5.9-23 Hourly usage of the materials and utilities

Operating period	*Kirschneriella* Nov-Jan	*Chlorella* Feb-Apr	*Galdieria* May-Sept
CO_2 (kg/hr)*	32,102	22,475	29,372
Urea (kg/hr)	1,893	1,324	1,756
DAP (kg/hr)	397	278	349
$NaOH/H_2SO_4$ (kg/hr)	232	166	205
Makeup water (kg/hr)	397,014	455,853	653,851
Power for algal biomass (kW)	2,140	1,626	2,030
Power for algae drying (kW)	6	0	0
Power for DHTL (kW)	244	220	268
Power for gas management (kW)	6,342	6,342	6,342
BOD (kg/hr)	832	658	914
Utility for algae drying (GJ/hr)	6	0	0
Utility for DHTL (GJ/hr)	33	33	33

- Only the CO_2 weight in flue gas

BG-11 is used in the most cultivation experiments in AzCATI as the media, the concentration of the chemicals in the media are listed in Table 5.9.4-4. The cost of individual chemicals in the media is obtained from http://www.alibaba.com and it is then assumed that the cost of the chemicals in year 2011 remains the same as that in year 2016. The annual cost of media is then determined by the amount of make up water and listed in the Table 5.9-24.

Table 5.9-24 Summary of Chemicals and Cost of Media BG-11

Chemical Compound	g/L	Cost ($/tonne)*	Cost $/M^3 water
Sodium carbonate	0.02	200	4.0E-03
Sodium nitrate	1.50	400	6.0E-01
Magnesium sulphate heptahydrate	0.75	100	7.5E-02
Potassium phosphate dibasic	0.04	2500	1.0E-01
Calcium chloride dihydrate	0.36	120	4.3E-02
Citric acid	0.06	585	3.5E-02
Ferric ammonium citrate	0.06	600	3.6E-02
EDTA Disodium hydrate	0.02	2900	5.2E-02
Manganese(II) chloride tetrahydrate	1.8E-03	1500	2.7E-03
Zinc sulfate heptahydrate	2.2E-04	630	1.4E-04
Boric acid	2.9E-03	850	2.4E-03
Copper(II) sulfate pentahydrate	7.9E-05	1750	1.4E-04
Sodium molybdate dihydrate	3.9E-04	6000	2.3E-03
Cobalt(II) nitrate hexahydrate	5.0E-05	10000	5.0E-04
Cyanocobalamin (Vitamin B12)	6.8E-08	20000	1.4E-06
Total ($/M^3 water)			**0.95**

* Cost of the chemicals from http://www.alibaba.com

Table 5.9-25 shows the annual usage and annual variable costs. Annual CO_2 consumption listed in Table 5.9-25 is the actual CO_2 weight in the fluegas and the unit cost refers to the captured CO_2 cost [Gerdes,K., Cost and performance of PC and IGCC plants for a range of carbon dioxide capture. DOE/NETL-2011/1498. NREL 2011. http//www.netl.doe.gov/file%20library/research/energy%20analysis/publications/gerdes-08022011.pd*f*]

In total, the annual variable operating cost is $34.8 MM for producing 10 million gallons of biocrude, which results $3.48/Gal variable operating cost. Assume the density of the biocrude is 900 kg/m^3 and the LHV of the biocrude is 33 MJ/kg, the operating cost for biocrude energy is $0.031/MJ biocrude.

Table 5.9-25 Summary of Variable Operating Costs

Component	Annual usage	Unit Cost (2011$)	Annual Cost ($MM)
CO_2 (tonnes)	225,582	$45 /tonne	10.2
Urea (tonnes)	13,386	$450 /tonne	6.0
DAP (tonnes)	2,737	$710 /tonne	1.9
$NaOH/H_2SO_4$ (tonnes)	1,611	$300 /tonne	0.5
Makeup water (tonnes)	4,225,488	$0 /tonne	0.0
Power (MWh)	67,663	$0.0685 /kWh	4.6
Utility (GJ)	277,004	$23/GJ	6.5
BOD treatment (tonnes)	6,509	$656 / tonne	4.3
Media			4.3
Total variable operating costs			**38.2**
Variable operating cost per gallon biocurde			3.82 $/Gal
Variable operating cost per MJ biocurde			0.034 $/MJ biocrude

From the Table 5.9-25, the biggest operating cost is for CO_2. The cost estimation of CO_2 is referred to the captured price. If a free of charge fluegas source is available, then the variable operating cost per gallon biocrude would be reduced to $2.46/Gal, and the variable operating cost per MJ biocrude would be $0.022/MJ biocrude. The utility cost occupied the second biggest portion of the variable operating cost, because the high temperature of the DHTL reactor. Therefore, reducing utility consumption is the big challenge.

The total annual makeup water is 4.23 million tonnes per year, which is 112 gallons per gallon biocrude, i.e. 3.76 L/MJ biocrude. Compared to the water usage level of 195 gallons of water per gallon of biodiesel as reported in the harmonization report [2010], the water usage of the baseline case is greatly reduced.

In the VIPER™ system, algal biomass is grown in disposable plastic hanging bags. The current useable life of a hanging bag is 5 years, therefore, replacement of the plastic hanging bags is one of the operating expenses to be considered. The initial installation of plastic hanging bags is a set factor in the capital cost of a PBR system and therefore will an ongoing operating cost incurred every five years, replacing the plastic hanging bags, occurring in year 6, 11,16, 21 and 26.

Fixed Operating Costs

The fixed operating costs include labor and fixed overhead costs, which are incurred in full when the plant is operating, regardless of output capacity. Staffing requirements and labor costs are modified for the REAP project relative to standard assumptions used in recent biorefinery design reports [22] [1]. A number of fixed labor costs are assumed in the prior report, including: plant manager, lab manager, maintenance supervisor, shift supervisor, cultivation operator, downstream operator and clerks / secretaries. The salaries and number of the operators are taken from the literature [1] [22] and converted to the 2011 dollar-cost. Maintenance, insurance and taxes are all standard cost assumptions used for BETO design [20]. The fixed costs are shown in Table 5.9-26.

Table 5.9-26 Fixed Operating Costs

Position	Number	Total Cost (2011) million $/year
Plant Manager	1	0.15
Plant Engineer (cultivation)	1	0.07
Plant Engineer (downstream conversion)	1	0.07
Maintenance Supervisor	1	0.06
Maintenance Technician	7	0.28
Lab Manager	1	0.06
Lab Technician	4	0.16
Shift Supervisor (cultivation)	4	0.19
Shift Operators (cultivation)	32	1.28
Shift Supervisor (downstream conversion)	4	0.19
Shift Operators (downstream conversion)	20	0.80
Yard Employees	4	0.11
Clerks & Secretaries	3	0.12
Labor total	**83**	**3.54**
Labor Burden (90%)		3.19
Maintenance (3% TIC)		10.28
Insurance and taxes (0.7% of FCI)		3.36
Total Fixed Operating Costs		**20.37**

The total annual operating cost for the baseline case is the sum of variable cost and fixed operating cost, which is $55.1 MM, i.e. $0.049/MJ biocrude.

Minimum biocrude selling price (MBSP)

The discounted cash flow analysis is used for estimating the minimum selling price of biocrude. In this report, the assumption of the parameters used in the discounted cash flow analysis is taken from a recently published NERL design report [1] and is summarized in Table 5.9-27.

Table 5.9-27 Discounted Cash Flow Analysis Parameters

Plant life	30 years
Discount rate	10%
General plant depreciation	200% declining balance (DB)
General plant recovery period	7 years
Federal tax rate	35%
Financing	40% equity
Loan terms	10-year loan at 8% APR
Construction period	3 years
First 12 months' expenditures	8%
Next 12 months' expenditures	60%
Last 12 months' expenditures	32%
Working capital	5% of fixed capital investment
Start-up time	6 months
Revenues during start-up	50%
Variable costs incurred during start-up	75%
Fixed costs incurred during start-up	100%

Using the parameters in Table 5.9-27 and the capital costs and operating costs information in Table 5.9-23 to Table 5.9-26, the resulting minimum biocrude selling price (MBSP) for the VPBR scenario with VIPER type PBR system and DHTL facility is $15.19/Gal (2011 dollar-cost). The 10% IRR and other economic inputs noted above are used to distinguish the MBSP. Table 5.9-28 summarizes the yield, rates and processing costs for the baseline case. If the IRR is set to be zero, the MBSP is reduced to $13.08/Gal (2011 dollar-costs). The complete discounted cash flow summary worksheet is shown in the Appendix. If a free fluegas source is available, then the biocrude selling price could be reduced to $14.14/Gal, additional, if the IRR is set to zero, the MBSP is only $12.05/Gal.

Table 5.9-28 Summary of Yields, Rates and MBSP of the baseline case

	VPBR (VIPER type)
Facility size	4,530 acre wet area
On-line time	7,920 hr/yr
Biocrude production rate	10.0 MM gallons/yr
Biocrude yield	2,208 gallons/acre/yr
Total installed equipment cost	$342.8 MM
Total capital investment (TCI)	$522.2 MM
TCI per annual gallon biocrude	$52.2
Minimum Biocrude Selling Price	$15.19/gallon

Case studies

Case study I:Mixotrophic cultivation conditions in summer

In AzCATI, the cultivation group investigated the mixotrophic cultivation conditions in the VPBRs in summer, and the results of *Galdieria* show that with an additional 25mM of sucrose, the average productivity was recorded at 0.43 g/L/day in the MM type PBR with a 0.5m spacing. Considering the PBR layout and the spacing between panels, this per aerial algal productivity is equivalent to 49.6 g/m^2/day. If we assume that 50% of the footprint is autotrophic and 50% is mixotrophic then the net aerial productivity would be 33.7 g/m^2/day which is nearly double the capacity of the autotrophic cultivation condition. In this section, the mixotrophic growth results will be applied to the model and will illustrate the significant benefits to the capital and operating costs.

The same principle for the wetted area estimates explained in Section 5.9.3 are applied for predicting the wetted area required for a mixotrophic cultivation in summer. For 10 MGY biocrude capacity, the total wetted area required for the mixotrophic case is 3,320 acre. In the mixotrophic cultivation condition, part of the *Galdieria* harvested in May to September is dried and used during the other months. Like the baseline case, from February to April, there is co-liquefaction of *Galdieria* and *Chlorella*, and the DHTL yield of the co-liquefaction is assumed to be the average of individual organisms, which is 0.28. From November to January, the DHTL yield of *Kirschneriella* is chosen for the wetted area estimation.

The quantity of *Galdieria* cultivated in mixotrophic conditions and needed to be dried from May to September is calculated to be 5,091 kg/hr, which is listed in Table 5.9-29. Considering the 95% usage of the drying capacity, the capacity of the algae drying facility is then defined to be 5,300 kg/hr, and the quantity of dry *Galdieria* produced is 18,205 tonnes. These calculations result in an estimate of 3,009 gallons biocrude per acre per year productivity. The energy output of the mixotrophic case is 338GJ/acre/yr.

Table 5.9-29 Bio-crude capacity estimation of mixotrophic scenario based on a wetted area of 3,320 acres. The annual biocrude productivity is 3,009 gal/acre/yr.

	Strain	Biomass productivity (g/m^2/day AFDW)	Bio-crude yield (mass fraction)	Operation days	Biomass produced (kg/hr)	Biocrude converted (kg/hr)	Gap to defined bio-crude productivity (kg/hr)*	Dry biomass required (kg/hr)**	Total dry biomass required (tonnes/season)	Biocrude produced (million gal/season)
Nov-Jan	*Kirschneriella*	18.2	0.41	92	10,199	4,181	-120	385	850	2.8
Feb-Apr	*Chlorella*	12.8	0.28***	89	7,156	2,006	-2,296	8,188	17,490	2.7
May-Sept	*Galdieria*	33.7	0.31	149	18,869	5,891	1,589	-5,091	-18,205	4.5
Annual Total				**330**						**10.0**

* a negative value means a less quantity of bio-crude converted than the defined DHTL capacity.
** a positive value means additional dry biomass is required
*** the biocrude conversion yield is estimated to be an average of *Galdieria* and *Chlorella*

Since the wetted area is reduced to 3,320 acres for the mixotrophic case, the capital cost of the VPBR and the drying facility are re-calculated to the new conditions and summarized in Table 5.9-30.

Table 5.9-30 Breakdown of capital costs for 3,320 acres of VPBR with VIPERS™ reactor design, all costs in 2011 dollars.

Reactor type	Frame Material and labor	Plastic bags	Piping	Civil and others	Installed Cost
VIPERS™	$83,543,242	$23,240,000	$33,417,297	$45,948,783	$186,149,322

The cost estimate of the VIPERS™ VPBR system is $56k per acre, which is the same as the autotrophic case, the baseline case. The total cost of 3,320 acres of wetted area is $186,149,322.

The drying capacity of the mixotrophic case is estimated to be 5,300 kg/hr, therefore the capital cost of the drying facility is adjusted and collated in Table 5.9-31. The installed cost of the drying facility is $8.4MM. The power consumption of the compressor in this case is 7.3 kW and the heating utility for the furnace in this case is 8.3 GJ/hr. These adjustments of the power and utility consumption are then included into the operating cost estimation of the mixotrophic case.

Table 5.9-31 The breakdown of capital costs of the algae drying facility for the VPBR with mixotrophic cultivation in summer, 5,300 kg/hr drying capacity, 18,205 tonnes/yr storage capacity. All costs in 2011 dollars

Operation unit	Equipment Cost	Installed Cost
Dryer	$851,544	$1,277,317
Furnace	$1,241,760	$4,967,042
Cooler	$36,386	$109,158
Silo *4	$741,422	$1,260,418
Compressor	$599,948	$798,072
Total	**$3,471,061**	**$8,412,006**

Assuming other operational units are the same as discussed in Section 5.9.3, the total investment costs of the mixotrophic case are summarized in Table 5.9-32. The total installed cost of the mixotrophic case is $279.3 MM, 81% of the baseline case. The total capital investment is $431.2 MM, which is 82% of the TCI of the baseline case.

Table 5.9-32 Project cost worksheet including Total Direct Costs and Total Capital Investment in the case of mixotrophic cultivation in summer.

Process Area	Purchased Cost	Installed Cost PBR	Installed Cost Dewatering, Algae drying, DHTL	Installed Cost OSBL	Total Installed Cost
Cultivation PBR($MM)	$83.5	$186.1			$186.1
Flue gas delivery ($MM)	$19.9			$21.1	$21.1
Water delivery ($MM)	$4.4			$5.1	$5.1
Dewatering ($MM)	$5.4		$7.9		$7.9
Algae drying ($MM)	$3.5		$8.4		$8.4
DHTL ($MM)	$23.8		$50.7		$50.7
Totals ($MM)	**$140.5**	**$186.1**	**$67.0**	**$26.2**	**$279.3**
Site Development ($MM)		NA	$6.0	$2.8	$8.8
Warehouse ($MM)		$2.2	$2.7	NA	$4.9
Additional Piping ($MM)		NA	$3.0	NA	$3.0
Total Direct Costs (TDC) ($MM)		**$188.4**	**$78.7**	**$29.0**	**$296.1**
Pro-rateable Costs ($MM)		$7.4	$6.7	$0.3	$14.4
Field Expenses ($MM)		$8.4	$6.7	$0.3	$15.3
Office and Construction Fees ($MM)		$19.2	$13.4	$0.3	$32.8
Project Contingency ($MM)		$18.6	$6.7	$2.6	$27.9
Other Costs (Start-Up, Permits, etc) ($MM)		$4.8	$6.7	$0.3	$11.8
Total Indirect Costs ($MM)		**$58.5**	**$40.2**	**$3.7**	**$102.3**
Fixed Capital Investment (FCI) ($MM)		**$246.8**	**$118.9**	**$32.6**	**$398.4**
Land ($MM)					$12.9
Working Capital ($MM)					$19.9
Total Capital Investment (TCI) ($MM)					**$431.2**
		Lang Factor (FCI/Installed Cost)			1.4
		TCI per Annual Gallon Biocrude			$43.1/Gal
TCI per annual energy of biocrude					$0.384/MJ biocrude

The additional sugar to be used in the mixotrophic cultivation experiments is 25mM as reported by the AzCATI group, which is 2,288 kg/hr consumption for the modeled 10 MGY biocurde facility. The operating cost estimation of the mixotrophic period need to be adjusted to follow the changes. The material consumptions of the mixotrophic cultivation of *Galdieria* in summer are shown in Table 5.9-33, and the amended annual variable operating cost estimation of the mixotrophic case is summarized in Table 5.9-34.

Table 5.9-33 Hourly usage of the materials and utilities of *Galdieria* in mixotrophic condition

Operating period	*Galdieria* May-Sept
CO_2 (kg/hr)*	29,369
Urea (kg/hr)	1,731
DAP (kg/hr)	378
$NaOH/H_2SO_4$ (kg/hr)	251
Makeup water (kg/hr)	508,515
Sugar (kg/hr)	2,288
Power for algal biomass (kW)	1,989
Power for algae drying (kW)	7
Power for DHTL (kW)	264
Power for gas management (kW)	6,342
BOD (kg/hr)	909
Utility for algae drying (GJ/hr)	8
Utility for DHTL (GJ/hr)	33

* Only the CO_2 weight in flue gas

Table 5.9-34 Summary of Variable Operating Costs of the mixotrophic case

Component	Annual usage	Unit Cost (2011$)	Annual Cost ($MM)
CO_2 (tonnes)	223,912	$45 /tonne	10.0
Urea (tonnes)	13,200	$450 /tonne	5.9
DAP (tonnes)	2,821	$700 /tonne	2.0
$NaOH/H_2SO_4$ (tonnes)	1,764	$300 /tonne	0.5
Makeup water (tonnes)	4,225,488	$0 /tonne	0.0
Power (MWh)	54,100	$0.0685 /kWh	3.7
Utility (GJ)	290,755	$23/GJ	6.8
BOD treatment (tonnes)	6,493	$656 / tonne	4.3
Media			4.3
Sugar (tonnes)	8,183	$600 / tonne*	4.9
Total variable operating costs			**42.4**
Variable operating cost per gallon biocurde			4.24 $/Gal
Variable operating cost per MJ biocurde			0.038 $/MJ biocrude

* Cellobiose is planned to be used as the sugar source in the commercial facility, the price range of cellobiose is $0.6 – 20 /kg [alibaba.com], we use the lower end to predict the operating cost.

Compared to the base case, the utility cost increases by approximately 5% from $6.5 MM/yr to $6.8 MM/yr and the cost of sugar ($4.9 MM/yr) becomes the third largest material cost of the

variable operating cost. The total variable cost per gallon biocrude is then estimated to be $4.34 /Gal, 15% higher than that of the autotrophic case.

The same discounted cash flow analysis parameters from Section 5.9.3 are used for predicting the MBSP for the mixotrophic case. The MBSP for the VPBR scenario with the mixotrophic case is $13.76/Gal (2011 dollar values), 10% less than the autotrophic case. Table 5.9-35 summarizes the yield, rates and processing costs for the mixotrophic cultivation case. The complete discounted cash flow summary worksheet is shown in the Appendix XXX.

Table 5.9-35 Summary of Yields, Rates and MBSP of the mixotrophic case with VIPER™ type VPBRs

	Mixotrophic case (VIPER type PBR)
Facility size	3,320 acre wet area
On-line time	7,920 hr/yr
Biocrude production rate	5.0 MM gallons/yr
Biocrude yield	3,009 gallons/acre/yr
Total installed equipment cost	$279.3 MM
Total capital investment (TCI)	$431.2 MM
TCI per annual gallon biocrude	$43.1
Minimum Biocrude Selling Price	$13.66 /gallon

Case study II: SEQHTL as the biocrude conversion process

The SEQHTL process is the algae biomass conversion procedure involved in the REAP design. The investigation of the reaction conditions in the process have been undertaken by Dr. Chen of WSU and Dr. Deng of ASU. The laboratory process is the design modeling basis of the SEQHTL process. The algal slurry is treated under mild conditions in the first stage hydrothermal liquefaction reactor and is converted to treated algae (TA) and the water soluble species. Then the TA slurry is blended with water to adjust the ratio of TA to water to 0.2. Under high temperature and high pressure conditions, the TA slurry is converted to bio-crude, bio-char, bio-gas and water soluble residue.

The energy involved in the heating and cooling of the streams is immense. The pinch analysis applied in the laboratory process is optimized to maximize energy efficiencies throughout the process, the optimized process flowsheet is illustrated in Figure 5.9-40. When 20 wt% *Chlorella* is applied to the optimized flowsheet, the heating utility demand is 6.20 kJ/g bio-crude. The heating duty of SEQHTL process is 20% less than that of the DHTL process, which results in a lower operating cost.

As seen in the case of DHTL, the three algal biomass showed different conversion yields in the SEQHTL process. The conversion yield of the algal biomass is summarized in Table 5.9-36.

Table 5.9-36 Productivity of algal strains in VPBRs and the bio-crude yield of SEQHTL process.

	Strain	Biomass volumetric productivity (g/l/day AFDW)	Biomass aerial productivity [a] (g/m^2/day AFDW)	Bio-crude yield of SEQHTL (mass fraction)
Nov-Jan	*Kirschneriella*	0.16	18.2	0.26[b]
Feb-Apr	*Chlorella*	0.11	12.8	0.31[c]
May-Sept	*Galdieria*	0.15	17.8	0.35[d]
Oct	-			

a: The aerial productivity is calculated by the volumetric productivity multiplied by the footprint of the VIPER™ system.

b: From WSU result in September 2016

c: From WSU result in June 2015

d: From ASU result in August 2016

Like the DHTL scenario, the wetted area for the VPBRs needs to be re-calculated for producing enough biomass for the SEQHTL facility. The same principle is applied to the estimates of the wetted areas needed, these being 4,980 acres for the autotrophic case and 3,480 acres for the mixotrophic case. Algae drying is only required for *Galdieria* in summer. Consider 95% of the capacity usage, then the drying capacity for the autotrophic case is 2,800 kg/hr and for the mixotrophic case is 8,300 kg/hr. The results are summarized in Table 5.9-37 for the autotrophic case and in Table 5.9-38 for the mixotrophic case.

Table 5.9-37 Biocrude capacity optimization with autotrophic cultivation and SEQHTL process based on a wetted area of 4,980 acres. The annual biocrude productivity is 2,009 gal/acre/yr.

	Strain	Biomass productivity (g/m^2/day AFDW)	SEQHTL Bio-crude yield (mass fraction)	Operation days	Biomass produced (kg/hr)	Biocrude converted (kg/hr)	Gap to defined bio-crude productivity (kg/hr)*	Dry biomass required (kg/hr)**	Total dry biomass required (tonnes/season)	Biocrude produced (million gal/season)
Nov-Jan	*Kirschneriella*	18.2	26%	92	15,298	4,022	-280	1,064	-2,350	2.79
Feb-Apr	*Chlorella*	12.8	31%	89	10,734	3,278	-1,024	3,352	-7,159	2.70
May-Sept	*Galdieria*	17.8	35%	149	14,974	5,235	933	-2,670	9,546	4.52
Annual Total				**330**						**10.00**

* a negative value means a less quantity of bio-crude converted than the defined SEQHTL capacity.
** a positive value means additional dry biomass is required

Table 5.9-38 Biocrude capacity optimization with mixotrophic cultivation and SEQHTL process based on a wetted area of 3,480 acres. The annual biocrude productivity is 2,877 gal/acre/yr.

	Strain	Biomass productivity (g/m^2/day AFDW)	SEQHTL Bio-crude yield (mass fraction)	Operation days	Biomass produced (kg/hr)	Biocrude converted (kg/hr)	Gap to defined bio-crude productivity (kg/hr)*	Dry biomass required (kg/hr)**	Total dry biomass required (tonnes/season)	Biocrude produced (million gal/season)
Nov-Jan	*Kirschneriella*	18.2	26%	92	10,690	2,810	-1,491	5,672	-12,524	2.79
Feb-Apr	*Chlorella*	12.8	31%	89	7,501	2,291	-2,011	6,585	-14,065	2.70
May-Sept	*Galdieria*	33.7	35%	149	19,779	6,915	2,613	-7,474	26,728	4.52
Annual Total				**330**						**10.00**

* a negative value means a less quantity of bio-crude converted than the defined SEQHTL capacity.
** a positive value means additional dry biomass is required

The capacity of the SEQHTL facility is forecast to be 10 million gallons per year, i.e. 4,302 kg bio-crude/hr (1,263 gal/hr). The material and energy balance of the optimized Aspen Plus model is the basis for the cost estimates of the SEQHTL process. The equipment cost scaling factors are referred to in the literature [17]. The equipment list of the SEQHTL process and the cost estimates are summarized in Table 5.9-39. The total installed capital cost of a 10MGY SEQHTL facility is $63.2 MM, which is 20% higher than the DHTL estimation.

Table 5.9-39 Breakdown of capital costs of the SEQHTL process (all costs are in 2011 dollars)

Operation unit	Equipment Cost	Installed Cost
REACT1	$2,108,729	$4,217,459
REACT2	$1,393,846	$2,787,692
E-401	$1,390,803	$3,059,768
E-402	$1,977,859	$4,351,289
E-403	$465,489	$1,024,075
E-404	$7,142,065	$15,712,542
E-405	$1,963,017	$4,318,637
E-406	$1,658,039	$3,647,685
Filter-401	$907,447	$1,814,893
Filter-402	$1,283,071	$2,566,143
Sep-401	$3,567,192	$7,134,384
FLASH-401	$4,336,517	$8,673,035
FLASH-402	$1,509,519	$3,019,038
PUMP401	$247,903	$570,177
PUMP402	$150,858	$346,974
Total	**$30,102,354**	**$63,243,791**

The drying capacity of the autotrophic case is 2,800 kg/hr and of the mixotrophic case is 8,300 kg/hr. The capital cost of these facilities are adjusted to the given capacity and summarized in Table 5.9-40.

Table 5.9-40 Breakdown of capital costs of the algae drying facilities (all costs are in 2011 dollars)

	Autotrophic case		Mixotrophic case	
Operation unit	Equipment Cost	Installed Cost	Equipment Cost	Installed Cost
Dryer	$522,604	$783,905	$1,118,192	$1,677,288
Furnace	$118,694	$474,776	$253,965	$1,015,857
Cooler	$27,566	$82,697	$58,982	$176,944
Silo *8	$775,350	$1,318,096	$1,658,984	$2,820,272
Compressor	$449,199	$599,297	$961,131	$1,282,290
Total	**$1,893,413**	**$3,258,771**	**$4,051,253**	**$6,972,651**

With the amended wetted area for the VPBR system and with the capital cost of the SEQHTL facility, the TCI of the integrated process with SEQHTL can be estimated, based on the same assumptions and parameters used for the DHTL scenario. The TCI for the autotrophic case is summarized in Table 5.9-41 and for mixotrophic case is summarized in Table 5.9-42.

Table 5.9-41 Total Capital Investment in the case of SEQHTL with autotrophic cultivation in summer.

Process Area	Purchased Cost	Installed Cost PBR	Installed Cost Dewatering, Algae drying, SEQHTL	Installed Cost OSBL	Total Installed Cost
Cultivation PBR($MM)	$125.3	$279.2			$279.2
Flue gas delivery ($MM)	$19.9			$21.1	$21.1
Water delivery ($MM)	$4.4			$5.1	$5.1
Dewatering ($MM)	$5.4		$7.9		$7.9
Algae drying ($MM)	$1.9		$3.3		$3.3
SEQHTL ($MM)	$30.1		$63.2		$63.2
Totals ($MM)	**$187.1**	**$279.2**	**$74.4**	**$26.2**	**$379.8**
Site Development ($MM)		NA	$6.7	$2.8	$9.5
Warehouse ($MM)		$3.4	$3.0	NA	$6.3
Additional Piping ($MM)		NA	$3.3	NA	$3.3
Total Direct Costs (TDC) ($MM)		**$282.6**	**$87.4**	**$29.0**	**$399.0**
Pro-rateable Costs ($MM)		$11.2	$7.4	$0.3	$18.9
Field Expenses ($MM)		$12.6	$7.4	$0.3	$20.3
Office and Construction Fees ($MM)		$28.8	$14.9	$0.3	$43.9
Project Contingency ($MM)		$27.9	$7.4	$2.6	$38.0
Other Costs (Start-Up, Permits, etc) ($MM)		$7.3	$7.4	$0.3	$15.0
Total Indirect Costs ($MM)		**$87.7**	**$44.6**	**$3.7**	**$136.0**
Fixed Capital Investment (FCI) ($MM)		**$370.3**	**$132.1**	**$32.6**	**$535.0**
Land ($MM)					$19.4
Working Capital ($MM)					$26.7
Total Capital Investment (TCI) ($MM)					**$581.1**
Lang Factor (FCI/Installed Cost)					1.4
TCI per Annual Gallon Biocrude					$58.1/Gal
TCI per annual energy of biocrude					$0.523/MJ biocrude

Table 5.9-42 Total Capital Investment in the case of SEQHTL with mixotrophic cultivation in summer.

Process Area	Purchased Cost	PBR	Installed Cost Dewatering, Algae drying, SEQHTL	OSBL	Total Installed Cost
Cultivation PBR($MM)	$87.6	$195.1			$195.1
Flue gas delivery ($MM)	$19.9			$21.1	$21.1
Water delivery ($MM)	$4.4			$5.1	$5.1
Dewatering ($MM)	$5.4		$7.9		$7.9
Algae drying ($MM)	$4.1		$7.0		$7.0
SEQHTL ($MM)	$30.1		$63.2		$63.2
Totals ($MM)	$151.5	$195.1	$78.1	$26.2	$299.4
Site Development ($MM)		NA	$7.0	$2.8	$9.8
Warehouse ($MM)		$2.3	$3.1	NA	$5.5
Additional Piping ($MM)		NA	$3.5	NA	$3.5
Total Direct Costs (TDC) ($MM)		**$197.5**	**$91.8**	**$29.0**	**$318.2**
Pro-rateable Costs ($MM)		$7.8	$7.8	$0.3	$15.9
Field Expenses ($MM)		$8.8	$7.8	$0.3	$16.9
Office and Construction Fees ($MM)		$20.1	$15.6	$0.3	$36.0
Project Contingency ($MM)		$19.5	$7.8	$2.6	$29.9
Other Costs (Start-Up, Permits, etc) ($MM)		$5.1	$7.8	$0.3	$13.1
Total Indirect Costs ($MM)		**$61.3**	**$46.9**	**$3.7**	**$111.8**
Fixed Capital Investment (FCI) ($MM)		**$258.7**	**$138.7**	**$32.6**	**$430.0**
Land ($MM)					$13.6
Working Capital ($MM)					$21.5
Total Capital Investment (TCI) ($MM)					**$465.1**
Lang Factor (FCI/Installed Cost)					1.4
TCI per Annual Gallon Biocrude					$46.5/Gal
TCI per annual energy of biocrude					$0.419/MJ biocrude

The operating cost estimate of SEQHTL uses the same method as the DHTL scenario with the variable operating cost estimates for the autotrophic and mixotrophic conditions summarized in Table 5.9-43. The utility cost of SEQHTL is not the biggest variable operating cost, because the energy analysis for these two processes show that the heating duty for the DHTL process is 7.66 kJ/g biocrude and for the SEQHTL process is 6.20 kJ/g biocrude, which equates to a 24% reduction in the heating utility consumption. The BOD treatment is the highest variable operating cost. The reason is the carbohydrate of the algal cell is extracted in the first stage DHTL operation and remains in the water phase. At this stage the extracted water soluble components are discharged as blowdown, the highest organic carbon concentration of the first stage extract fraction is 80,150 mg/L (WSU result for *Galdieria*, 180C for 1st stage). This carbohydrate component is considered to be purified or reused in other investigations, which obtains valuable

by-products and offsets the overall cost of biocrude. However, the additional investment and revenue of by-products are not involved in the TEA of this report. All the components in the water phase are considered as BOD in the blowdown stream.

Table 5.9-43 Summary of Variable Operating Costs of SEQHTL scenarios

Component	Unit Cost (2011$)	Annual usage (autotrophic)	Annual Cost ($MM) (autotrophic)	Annual usage (mixotrophic)	Annual Cost ($MM) (mixotrophic)
tonnes)	$45 /tonne	243,841	11.0	243,843	11.0
(tonnes)	$450 /tonne	14,294	6.4	14,296	6.4
(tonnes)	$700 /tonne	2,879	2.0	2,879	2.0
I/H_2SO_4 (tonnes)	$300 /tonne	1,927	0.6	1,911	0.6
up water (tonnes)	$0 /tonne	4,194,545	0.0	4,496,995	0.0
r (MWh)	$0.0685 /kWh	75,490	4.8	58,910	4.0
y (GJ)	$23/GJ	211,245	4.9	211,245	4.9
treatment (tonnes)	$656 / tonne	46,453	30.5	46,308	30.4
a			4.0		4.3
	$600 / tonne	0	0.0	10,887	6.5
variable operating costs			**64.2**		**65.4**
ble operating cost per gallon biocurde			6.42		6.54
ble operating cost per MJ biocurde			0.057		0.058

Using the same financial assumptions as the DHTL scenarios, the biocrude selling price for the SEQHTL scenario are predicted based on the capital cost and operating cost estimates above, with the results summarized in Table 5.9-44. The MBSP for autotrophic and mixotrophic conditions are calculated to be $19.10/Gal and $16.20/Gal, respectively, which are about 20-25% higher than the DHTL cases.

Table 5.9-44 Summary of Yields, Rates and MBSP of the process with SEQHTL

	Autotrophic condition	Mixotrophic condition
Facility size	4,580 acre wet area	3,480 acre wet area
On-line time	7,920 hr/yr	7,920 hr/yr
Biocrude production rate	10.0 MM gallons/yr	10.0 MM gallons/yr
Biocrude yield	2,009 gallons/acre/yr	2,878 gallons/acre/yr
Total installed equipment cost	$379.8 MM	$299.4 MM
Total capital investment (TCI)	$581.1 MM	$465.1 MM
TCI per annual gallon biocrude	$58.1	$46.5
Minimum Biocrude Selling Price	$19.10 /gallon	$16.20 /gallon

Comparison of the DHTL and SEQHTL scenarios

The DHTL and SEQHTL are the two conversion processes involved in the REAP project. It is worthwhile comparing the capital cost and utility consumption of the two processes for ongoing investigation.

Capital cost comparison

The biocrude yield of both conversion processes have been discussed in previous sections, where the DHTL shows a higher biocrude yield. Two different samples of GS were studied. The yield ratio of DHTL/SEQHTL for biocrude production was 1.6, 1.3, 0.83, and 1.8 for KC, GS, GS, and CS respectively. Subsequently, the higher the biocrude yield, the smaller the area required for producing sufficient algal biomass. For a 10 million gallon per year biocrude facility, the DHTL process requires 4,530 acres of wetted land and the SEQHTL process needs 4,980 acres of wetted land. The capital cost of the VPBR occupies the biggest portion of the total capital investment, therefore, the DHTL process shows an advantage because of a higher conversion yield.

The capital costs for both processes are discussed in the previous sections. Figure 5.9.6-1 illustrates the summary of the DHTL/SEQHTL installed costs, PBR costs and total capital investment for a 10 million gallon per year biocrude facility for both scenarios. The installed equipment cost of DHTL and SEQHTL as discussed in Section 5.9.3 and Section 5.9.5, are $50.7 MM for the DHTL facility and $63.2 MM for the SEQHTL facility. The capital cost of the SEQHTL process is 20% higher than the DHTL.

The capital cost of DHTL and SEQHTL scenarios are summarized in Figure 5.9-46.

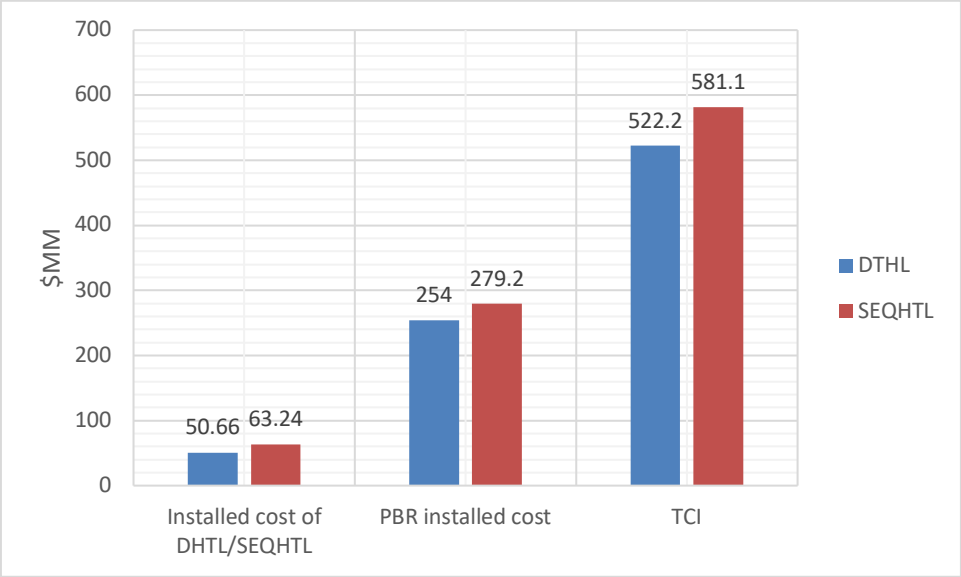

Figure 5.9-46 Capital cost comparison of DHTL and SEQHTL scenarios

Operating cost comparison

However, the pinch analysis of both processes showed about a 20% lower utility consumption for the SEQHTL process (6.20kJ/g biocrude) than the DHTL process (7.66 kJ/g biocrude). The pinch analysis results will be discussed in the following section. The variable operating cost

comparisons of DHTL and SEQHTL are illustrated in Figure 5.9-47. The utility cost of the SEQHTL case is lower than the DHTL case, however, the BOD of SEQHTL is much higher than the DHTL case, because of the high amount of carbohydrate remaining in the water phase in the first stage of treatment. Therefore, effective recovery or reuse of this valuable water-soluble species is one of the ongoing challenges. Due to the high BOD treatment cost, the total variable operating cost of SEQHTL is about 75% higher than that of the DHTL scenario.

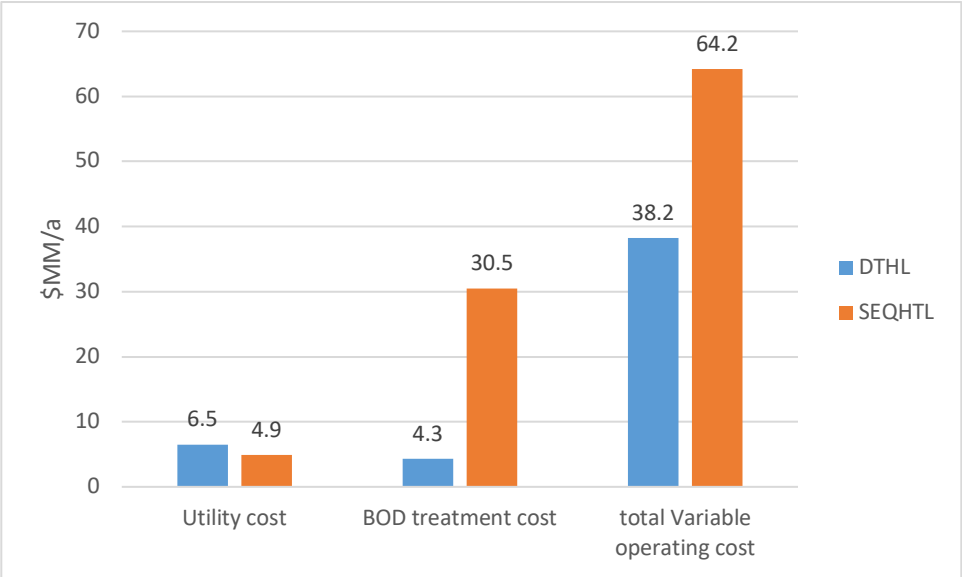

Figure 5.9-47 Variable operating cost comparison of DHTL and SEQHTL scenarios

Suggestions for future investigation

From the comparison discussion above, there are two aspects of the SEQHTL process needing improvement and these are the conversion yield and the reuse of the carbohydrate dissolved in the first stage water phase. For DHTL, due to the high temperature reaction condition, the biggest barrier to this technology is the high utility demand. Coupling with other facilities to maximize utility energy usage is currently under investigation.

5.9.7 References

[1] Davis, R., Markham, J., Kinchin, C., Grundl, N., Tan, E. C. C., Humbird, D. Process design and economics for the production of algal biomass: algal biomass production in open pond systems and processing through dewatering for downstream conversion. Feb 2016, NREL 64772

[2] Huesemann, M. H., Crowe, B. J., Waller, P., Chavis, A.R., Hobbs, S. J., Edmundson, S. J., Wigmosta, M. J. A Validated Model to Predict Microalgae Growth in Outdoor Pond Cultures Subjected to Fluctuating Light Intensities and Water Temperatures. *Algal Research,* 13 (2016) 195–206

[3] Edmundson, S. J., Huesemann, M. H. The Dark Side of Algae Cultivation: characterizing night biomass loss in three photosynthetic algae, Chlorella sorokiniana, Nannochloropsis salina and Picochlorum sp."*Algal Research*, 12 (2015) 470–476

[4] Huesemann, M. H., van Wagenen, J. M., Miller, T. W., Chavis, A. R., Hobbs Jr, W. B., Crowe, B. J. A Screening Model to Predict Microalgae Biomass Growth in Photobioreactors and Raceway Ponds. *Biotechnology and Bioengineering*, 110:6 (2013) 1583–1594.

[5] Dunlop, E.H., Coaldrake, A.K., Silva, C.S., and Seider, W.D. 2013. An Energy–limited Model of Algal Biofuels Production: Towards the Next Generation of Advanced Biofuels. *AIChE Journal*, 59:12 (2013), 4641–54

[6] Davis, R., Fishman, D., Frank, E. D., Wigmosten, M. S. Renewable diesel from algal lipids: an integrated baseline for cost, emissions, and resource potential from a harmonized model, ANL, NREL, PNNL; June 2012

[7] Suh, I.S., Lee, S.B. A Light Distribution Model for an Internally Radiating Photobioreactor. *Biotechnology and Bioengineering*, 82:2 (2003) 180–189.

[8] Slegers, P. M., Wijffels, R. H., van Straten, R. H., van Boxtel, A. J. B. Design scenarios for flat panel photobioreactors. *Applied Energy,* 88:10 (2011) 3342–3353.

[9] Kravarja, P., Modarresi, A., Friedl, A. Heat integration of biochemical ethanol production from straw. *Applied Engineering* 102 (2013) 32–43.

[10] Sánchez, E., Ojeda, K., El–Halwagi, M., Kaforov, V. Biodiesel from microalgae oil production in two sequential esterification/transesterification reactors: pinch analysis of heat integration. *Chemical Engineering Journal* 176–177 (2011) 211–216.

[11] Pokoo–Aikins, G., Nadim, A., El–Halwagi, M., Mahalec, V. Design and analysis of biodiesel production from algae grown through carbon sequestration. *Clean Technologies and Environmental Policy* 12 (2010) 239–254.

[12] Kemp, I. Pinch Analysis and Process Integration. Butterworth–Heinemann, 2nd edition, 2007.

[13] Linhoff, B., Hindmarsh, E. The Pinch design method of heat exchanger networks. *Chemical Engineering Science* 38:5 (1983), 745–763.

[14] Petrov, G.D., G. Bratkova. Viscosity of algal cultures and estimation of turbulency in devices for the mass culture of microalgae. *Algological Studies*, 81 (1996) 99–104.

[15] Wileman, A., Ozkan, A., Berberoglu, H. Rheological properties of algae slurries for minimizing harvesting energy requirements in biofuel production. *Bioresource Technology*, 104 (2012) 432–439.

[16] Yap, B. H.J., Martin, G. J.O., Scales, P. J. Rheological manipulation of flocculated algal slurries to achieve high solids processing. *Algal Research*, 14 (2016) 1–8.

[17] Knorr, D., Lukas, J., Schoen, P. Production of Advanced biofuels via liquefaction, hydrothermal liquefaction reactor design. April 5, 2013 NREL 60462

[18] Gerdes, K., Cost and performance of PC and IGCC plants for a range of carbon dioxide capture. DOE/NETL–2011/1498. National Energy Technology Laboratory, 2011.

[19] Beal, C. M., Gerber, L. N., Sills, D. L., Huntley, M. E., Machesky, S. C., Walsh, M. J., Tester, J. W., Archibald, I., Granados, J., Greene, C. H. Algal biofuel production for fuels and feed in a 100–ha facility: A comprehensive techno–economic analysis and life cycle assessment. *Algal Research*, 10 (2015) 266–279.

[20] Dutta, A. et al. Process design and economics for conversion of lignocellulisic biomass to ethanol: thermochemical pathway by indirect gasification and mixed alcohol synthesis. NREL/TP–5100–51400. NREL, 2011

[21] Humbird, d. et al. Process design and economics for conversion of lignocellulosic biomass to ethanol: Dilute-Acid Pretreatment and Enzymatic Hydrolysis of Corn Stover. May 2011, NREL 47764.

[22] Jones, S., Davis, R., Zhu, Y., Kinchin, C., Anderson, D., Hallen, R., Elliott, D., Schmidt, A., Albrecht, K., Hart, T., Butcher, M., Drennan, C., Snowden–Swan, L. Process Design and Economics for the Conversion of Algal Biomass to Hydrocarbons: Whole Algae Hydrothermal Liquefaction and Upgrading. PNNL, March 2014.

[23] Albrecht, K. O., Zhu, Y., Schmidt, A. J., Billing, J. M., Hart, T. R., Jones, S. B., Maupin G., Hallen, R., Ahrens, T., Anderson, D. Impact of heterotrophically stressed algae for biofuel production via hydrothermal liquefaction and catalytic hydrotreating in continuous–flow reactors. *Algal Research*, 14 (2016) 17–27.

[24] Baer, S., Heining, M., Schwerna, P., Buchholz, R., Hübner, H. Optimization of spectral light quality for growth and product formation in different microalgae using a continuous photobioreactor. *Algal Research*, 14 (2016) 109–115.

[25] Barros, A., Tiago Guerra, L., Simões, M., Santos, E., Fonseca, D., Silva, J., Costa, L., Navalho, J. Mass balance analysis of carbon and nitrogen in industrial scale mixotrophic microalgae cultures. *Algal Research*, 21 (2017) 23–41.

[26] Brindley, C., Jiménez–Ruíz, N., Acién, F.G., Fernández–Sevilla, J.M. Light regime optimization in photobioreactors using a dynamic photosynthesis model. *Algal Research*, 16 (2016) 399–408.

[27] Chakraborty, M., Miao, C., McDonald, A., Chen, S. Concomitant extraction of bio–oil and value added polysaccharides from Chlorella sorokiniana using a unique sequential hydrothermal extraction technology. *Fuel*, 95 (2012) 63–70.

[28] Deschênes, J., Boudreau, A., Tremblay, R. Mixotrophic production of microalgae in pilot–scale photobioreactors: Practicability and process considerations. *Algal Research*, 10 (2015) 80–86.

[29] Dong, T., Knoshaug, E. P., Davis, R., Laurens, L. M.L., Van Wychen, S., Pienkos, P. T., Nagle, N. Combined algal processing: A novel integrated biorefinery process to produce algal biofuels and Bioproducts. *Algal Research*, 19 (2016) 316–323.

[30] Du, W., Jongbloets, J. A., Pineda Hernández, H., Bruggemab, F. J., Hellingwerf, K. J., dos Santos, F. B. Photonfluxostat: A method for light–limited batch cultivation of cyanobacteria at different, yet constant, growth rates. *Algal Research*, 20 (2016) 118–125.

[31] Dutta, S., Neto, F., Coelho, M. C. Microalgae biofuels: A comparative study on techno–economic analysis & life–cycle assessment. *Algal Research*, 20 (2016) 44–52.

[32] Gómez–Pérez, C.A., Espinosa, J., Montenegro Ruiz, L.C., van Boxtel, A.J.B. CFD simulation for reduced energy costs in tubular photobioreactors using wall turbulence promoters. *Algal Research*, 12 (2015) 1–9.

[33] Harvind Reddy, K., Muppaneni, T., Ponnusamy, S., Sudasinghe, N., Pegallapati, A., Selvaratnam, T., Seger, M., Dungan, B., Nirmalakhandan, N., Schaub, T., Holguin, F. O., Lammers, P., Voorhies, W., Deng, S. Temperature effect on hydrothermal liquefaction of Nannochloropsis gaditana and Chlorella sp. *Applied Energy*, 165 (2016) 943–951.

[34] He, Y., Liang, X., Jazrawi, C., Montoya, A., Yuen, A., Cole, A. J., Neveux, N., Paul, N. A., de Nys, R., Maschmeyer, T., Haynes, B. S. Continuous hydrothermal liquefaction of macroalgae in the presence of organic co–solvents. *Algal Research*, 17 (2016) 185–195.

[35] Khoo, C. G., Lam, M. K., Lee, K. T. Pilot–scale semi–continuous cultivation of microalgae Chlorella vulgaris in bubble column photobioreactor (BC–PBR): Hydrodynamics and gas–liquid mass transfer study. *Algal Research*, 15 (2016) 65–76.

[36] Miao, C., Chakraborty, M., Chen, S. Impact of reaction conditions on the simultaneous production of polysaccharides and bio–oil from heterotrophically grown Chlorella sorokiniana by a unique sequential hydrothermal liquefaction process. *Bioresource Technology*, 110 (2012) 617–627.

[37] Mitra, D., van Leeuwen, J., Lamsal, B. Heterotrophic/mixotrophic cultivation of oleaginous Chlorella vulgaris on industrial co–products. *Algal Research*, 1 (2012) 40–48.

[38] Novoveská, L., Zapata, A. K.M., Zabolotney, J. B., Atwood, M. C., Sundstrom, E. R. Optimizing microalgae cultivation and wastewater treatment in large–scale offshore photobioreactors. *Algal Research*, 18 (2016) 86–94.

[39] Perrine, Z., Negi, S., Sayre, R. T. Optimization of photosynthetic light energy utilization by microalgae. *Algal Research*, 1(2012) 134–142.

[40] Posada, J. A., Brentner, L. B., Ramirea, A., Patel, M. K. Conceptual design of sustainable integrated microalgae biorefineries: Parametric analysis of energy use, greenhouse gas emissions and techno–economics. *Algal Research*, 17 (2016) 113–131.

[41] Quinn, J. C., Smith, T. G., Downes, C. M., Quinn, C. Microalgae to biofuels lifecycle assessment — Multiple pathway evaluation. *Algal Research*, 4 (2014) 116–122.

[42] Selvaratnam, T., Reddy, H., Muppaneni, T., Holguin, F.O., Nirmalakhandan, N., Lammers, P. J., Deng, S. Optimizing energy yields from nutrient recycling using sequential hydrothermal liquefaction with Galdieria sulphuraria. *Algal Research*, 12 (2015) 74–79.

[43] Skorupskaite, V., Makareviciene, V., Levisauskas, D.. Optimization of mixotrophic cultivation of microalgae Chlorellasp. for biofuel production using response surface methodology. *Algal Research*, 7 (2015) 45–50.

[44] Solimeno, A., Samsó, R., García, J. Parameter sensitivity analysis of a mechanistic model to simulate microalgae growth. *Algal Research*, 15 (2016) 217–223.

[45] Solimeno, A., Samsó, R., Uggetti, E., Sialve, B., Steyer, J., Gabarró, A., García, J. New mechanistic model to simulate microalgae growth. *Algal Research*, 12 (2015) 350–358.